Availability of Metal Cations in Aquatic Systems from DGT Measurements

Ramiro Uribe Kaffure

Dipòsit Legal: L.1221-2012
http://hdl.handle.net/10803/94522

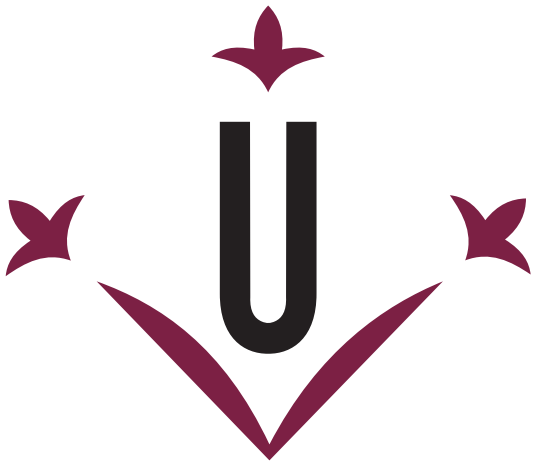

Universitat de Lleida

Departament de Química

Doctoral Thesis

Availability of Metal Cations in Aquatic Systems from DGT Measurements

A thesis submitted by Ramiro Uribe Kaffure to the University of Lleida in fulfilment of the requirements for the degree of Doctor

---

Supervised by:
Dr. Jaume Puy Llorens and Dr. Joan Cecilia Averós

A mis padres Ines, Susana y Aldemar

A mi esposa Lorena

A mis hijos Santiago, Esteban y Mafe

Agradecimientos

La culminación de esta tesis no hubiese sido posible sin la adecuada guía, colaboración, paciencia y comprensión de mis tutores, mis amigos y mi familia. A ellos, y a las personas e instituciones que de alguna forma aportaron a la realización de este trabajo, quiero expresar mis agradecimientos.

A la Universidad del Tolima, la Universitat de Lleida, la Fundación Carolina y al grupo de investigación en Físico-Química de Sistemas Macromoleculares de Interés Ambiental, por proveerme los recursos físicos y financieros para completar mi formación doctoral.

A los Drs. Jaume Puy y Joan Cecilia, mis tutores, de quienes recibí apoyo académico permanente y oportuno mucho más allá de los aspectos meramente formales. Su generosidad sobrepasó lo académico y me brindaron un excelente ambiente de trabajo en todos los ámbitos. Me considero afortunado por haber tenido la oportunidad de trabajar con ellos.

A todos los miembros del grupo de investigación por su constante apoyo. En particular a los Drs. José Salvador, Josep Galceran, Encarna Companys y Carlos Rey, por su valiosa y desinteresada ayuda, la cual contribuyó, indudablemente, a la culminación exitosa de esta tesis.

A los Drs. Ramón Canela y Jordi Eras, por su permanente motivación y colaboración.

A los profesores, los estudiantes de doctorado, el personal técnico y administrativo, en general a todos los integrantes del Departament de Química de la Universitat de Lleida, quienes amablemente me acogieron y me facilitaron la integración a las costumbres catalanas.

A los compañeros y amigos con quienes compartí la mayor parte del tiempo aquí en Cataluña: Mireia, Calin, Sandrine, David, Diana y Sara. Gracias a la desinteresada amistad que me ofrecieron, en ellos encontré siempre un apoyo en los momentos más difíciles. Adicionalmente, agradezco a Sandrine y Calin todo lo aprendido a través de las numerosas discusiones académicas.

A los amigos con quienes compartí por un tiempo la vivienda: Paola, Edinson y Miguel. Siempre me sentí muy a gusto y en un ambiente familiar junto a ellos.

A Irache, Leo, Karina y José, a quienes tuve la oportunidad de conocer aquí en Lleida. Sin predisposición alguna me acogieron como un miembro más de su familia y por ello les estaré siempre inmensamente agradecido.

A mis más cercanos amigos en Colombia: Luis, Fernando, Martín, John, Mario, Ramón, Héctor y Herman. Más allá de la inmensa amistad, su colaboración, apoyo y comprensión han sido invaluables.

A mi esposa Lorena, quien siempre estuvo dispuesta para acompañarme y animarme en toda eventualidad. Así mismo, a toda su familia, incluido Miguel, por apoyarme y acogerme sin reparos.

A Santiago y a Esteban por su paciencia y por darme las fuerzas para seguir adelante cada día.

A mis hermanos por su apoyo y comprensión y, principalmente, por cuidar a Santiago.

Finalmente, mis agradecimientos más profundos van para mis padres. A Inés, Susana y Aldemar, además de su permanente y desinteresado apoyo en todos los ámbitos, les agradezco el haber sido siempre un ejemplo de honestidad, perseverancia, dedicación y sacrificio. Nada de esto habría sido posible sin su ayuda. ¡Muchas Gracias!

Abstract

The uptake (bioavailability) of contaminants by living organisms mostly occurs by exposure to dissolved species. Plants are exposed to pollutants in the soil by their roots and animals mainly by drinking contaminated water or indirectly by eating contaminated plants or other animals.

Of principal significance is the potential for heavy metals to enter the aquatic and soil solution phase where their associated environmental risk increase. Understanding the bioavailability is key to the assessment of the potential toxicity or nutritional properties of trace metals and their compounds in natural media.

Diffusive Gradient in Thin Films (DGT) are simple devices developed for in situ measurement of the bioavailability of trace metals in aquatic environments. DGT is now widely used to measure a range of determinands in waters, soils and sediments. In most cases the mass accumulated is interpreted in terms of a labile form of the component being measured using a simple equation that applies to steady-state conditions. However, detailed interpretation of the results of DGT-based measurements is associated to a range of uncertainties and questions that need further investigation.

Our analysis of the dynamic features of (DGT) devices indicates that the penetration of complexes into the resin layer dramatically increases their lability. We report approximate analytical expressions for the metal flux, the lability degree and the concentration profiles in a DGT when complexes penetration is considered. The experimental accumulation of Cd by DGT sensors in Cd-NTA systems confirmed these theoretical analyses.

These results indicate that the resin disc thickness plays a key role in the metal accumulation in DGT. For complexes that are partially labile to the DGT measurement, their dissociation inside the resin domain is the main source of metal accumulation. This phenomenon explains the practical independence of the lability degree of a complex in a DGT device with respect to the ligand concentration. This also helps to understand the reduce mixture effect predicted in DGT.

In the same theoretical framework, we propose a simple analytical model to assess the influence of low ionic strengths in the DGT metal accumulation of charged complexes.

Finally, we introduce the kinetic conditional spectrum (KCS) methodology for the description of metal-macromolecular binding in multicomponent systems.

Resum

L'absorció de substàncies contaminants per organismes vius, es dóna principalment per l'exposició a les espècies dissoltes. Les plantes estan exposades, en les seves arrels, als contaminants en el sòl i els animals (principalment) per beure aigua contaminada, o pel consum de plantes contaminades o d'altres animals.

A causa del potencial dels metalls pesats per barrejar-se en les aigües i els sòls, on el seu risc ambiental associat i el dels seus compostos augmenta, la comprensió de la seva biodisponibilitat és clau per a l'avaluació de la toxicitat o dels seus potencials propietats nutritives en mitjans naturals.

La tècnica analítica anomenada *Diffusive Gradient in Thin Films* (DGT) consisteix en dispositius senzills desenvolupats per al mesurament *in situ* de la biodisponibilitat de metalls pesants en mitjans aquosos. Els sensors DGT són àmpliament utilitzats per mesurar la concentració d'una gran varietat d'espècies en aigües, sòls i sediments. En la majoria dels casos, la concentració mesurada (o la massa acumulada en el dispositiu) s'interpreta en termes de la forma làbil de l'espècie que es va mesurar, usant una equació simple que s'aplica en condicions d'estat estacionari. No obstant això, la interpretació detallada dels resultats dels mesuraments basades en DGT està associada a fenòmens complexos i, per tant, es requereix més investigació.

Un Anàlisi detallada de les característiques dinàmiques dels sensors (DGT), ens indica que la penetració dels complexos en la capa de resina augmenta dramàticament la seva labilitat. Aquí, presentem expressions analítiques aproximades per calcular el flux de metall, el grau de labilitat i els perfils de concentració en un DGT, quan es considera que els complexos poden penetrar en la resina. L'acumulació experimental de Cd en sensors DGT al sistema Cd-NTA, confirma les anàlisis teòrics.

Els nostres resultats indiquen que el gruix del disc de resina juga un paper fonamental en l'acumulació de metalls en sensors DGT. Per complexos parcialment làbils, la seva dissociació a l'interior del domini de resina és la principal font de metall acumulat. Aquest fenomen explica la independència del grau de labilitat amb respecte a la concentració de lligand d'un complex en DGT. Així mateix, ajuda a comprendre el reduït efecte barreja que es preveu amb els sensors DGT.

Dins el mateix esquema teòric, proposem un model analític simple per avaluar (en DGT) la influència de la força iònica en l'acumulació de metalls que formin complexos amb càrrega neta diferent de zero.

Finalment, introduïm el concepte d'espectre cinètic condicional (KCS, per les seves sigles en anglès), com una metodologia per a la descripció de l'enllaç metall-macromolècula en sistemes amb múltiples components.

Resumen

La absorción de sustancias contaminantes por organismos vivos, se da principalmente por la exposición a las especies disueltas. Las plantas están expuestas, en sus raíces, a los contaminantes en el suelo y los animales (principalmente) por beber agua contaminada, o por el consumo de plantas contaminadas o de otros animales.

Debido al potencial de los metales pesados para mezclarse en las aguas y los suelos, donde su riesgo ambiental asociado y el de sus compuestos aumenta, la comprensión de su biodisponibilidad es clave para la evaluación de su toxicidad o de sus potenciales propiedades nutritivas en medios naturales.

La técnica analítica denominada *Diffusive Gradient in Thin Films* (DGT) consiste en dispositivos sencillos desarrollados para la medición *in situ* de la biodisponibilidad de metales pesados en medios acuosos. Los sensores DGT son ampliamente utilizados para medir la concentración de una gran variedad de especies en aguas, suelos y sedimentos. En la mayoría de los casos, la concentración medida (o la masa acumulada en el dispositivo) se interpreta en términos de la forma lábil de la especie que se midió, usando una ecuación simple que se aplica en condiciones de estado estacionario. Sin embargo, la interpretación detallada de los resultados de las mediciones basadas en DGT esta asociada a fenómenos complejos y, por lo tanto, se requiere más investigación.

Un Análisis detallado de las características dinámicas de los sensores (DGT), nos indica que la penetración de los complejos en la capa de resina aumenta dramáticamente su labilidad. Aquí, presentamos expresiones analíticas aproximadas para calcular el flujo de metal, el grado de labilidad y los perfiles de concentración en un DGT, cuando se considera que los complejos pueden penetrar en la resina. La acumulación experimental de Cd en sensores DGT en el sistema Cd-NTA, confirma los análisis teóricos.

Nuestros resultados indican que el espesor del disco de resina juega un papel fundamental en la acumulación de metales en sensores DGT. Para complejos parcialmente lábiles, su disociación en el interior del dominio de resina es la principal fuente de metal acumulado. Este fenómeno explica la independencia del grado de labilidad con respecto a la concentración de ligando de un complejo en DGT. Así mismo, ayuda a comprender el reducido efecto mezcla que se prevé con los sensores DGT.

Dentro del mismo esquema teórico, proponemos un modelo analítico simple para evaluar (en DGT) la influencia de la fuerza iónica en la acumulación de metales que formen complejos con carga neta distinta de cero.

Por último, introducimos el concepto de espectro cinético condicional (KCS, por sus siglas en inglés), como una metodología para la descripción del enlace metal-macromolécula en sistemas con múltiples componentes.

Contents

1 Introduction

1.1 Heavy Metals in Environment

Despite of many different definitions have been proposed to the term "heavy metal", some based on density, some on atomic number or atomic weight, and some on chemical properties [1], the term is often used to denote a group of metals and semimetals (metalloids) that have been associated with contamination and potential toxicity or ecotoxicity.

Heavy (or trace) metals are elements present naturally in the Earth's crust. They are therefore found naturally in soils and rocks with a subsequent range of natural background concentrations in soils, sediments, waters and organisms. However, anthropogenic releases can give rise to higher concentrations of the metals relative to the normal background values.

The amounts of most heavy metals deposited to the surface of the Earth are many times greater than depositions from natural background sources. Among many others sources (metalliferous mining, atmospheric pollution, agricultural materials, sewage sludges, electronics, cosmetics, dyestuffs, pesticides, chemical industries etc.), combustion processes as power generation, smelting, incineration and the internal combustion engine, are the most important sources of heavy metals [2–6].

Due to its toxic nature and wide spread use, the contamination by the heavy metals has become a significant environmental problem. In order to understand and minimize the hazardous effects of such elements on the environment and human health, there is a particular need for the development of an analytical capability for determining the heavy metal concentrations

in environment both accurately and rapidly.

1.2 Bioavailability and Speciation

The uptake (bioavailability) of contaminants by living organisms mostly occurs by exposure to dissolved species. Plants are exposed to pollutants in the soil by their roots and animals mainly by drinking contaminated water or indirectly by eating contaminated plants or other animals. Thus the concentration of contaminants in the aqueous phase is of great importance. Suspended particles such as colloidal or dissolved organic matter can immobilise toxic elements by complexation, precipitation, adsorption and biotransformation, so the particles act as a sort of buffer for these elements. The buffer capacity of the natural environment strongly influences the impact of toxic chemicals.

It has been generally recognised that it is not the overall concentration of a pollutant which controls the toxicity of a contaminated site, but rather the concentration of the different physico-chemical forms of this pollutant, i.e., the bioavailability of each one of the different species has to be considered.

In the simplest case, the biological response consistently varies as a function of the free metal concentration. This behaviour had lead to the formulation of the Free Ion Activity Model (FIAM) [7]. However, as reported by Campbell [8], there is experimental evidence of systems in which the FIAM model poorly explains the bioaccumulation.

Actually, the FIAM model applies when internalization process are so slow in comparison with transport that no concentration gradients arise close to the internalization surface. However, when this condition is not fulfilled, i.e., when internalization is faster than transport, a concentration gradient appears and all the equilibrium processes in which the metal participates tend to shift toward dissociation. The arriving of metal to the surface can be controlled by the transport, by kinetics of the processes or for both of them. Thus, bioaccumulation is a dynamic process that depends not only on the transport but also on the interconversion of metal ions over different chemical and/or physico-chemical forms (speciation).

Of principal significance is the potential for heavy metals to enter the aquatic and soil solution phase where their mobility and bioavailability increases their associated environmental risk. So, knowledge of its speciation is of great importance, both from the point of view of their essentiality for various life forms, and with respect to their toxicity.

For instance, in aquatic systems, physico-chemical forms of metal ions include: the free hydrated metal ion; complexes of metal with simple or-

ganic species (such us chloride and carbonate); complexes of metal with macromolecular ligands (like humic and fulvic acids); metal ions adsorbed on a variety of colloidal particles (for example clay minerals and oxides of iron, manganese or aluminium); and precipitated metal compounds (such as heavy metal sulphides). All these species can co-exist and, hence, the prediction of the metal ion distribution in these systems may be quite complicated.

It is well-known that toxic effects of heavy metals may be modified in the presence of complexing agents [9, 10], depending also on the transport phenomena. In cases with lower complex mobility, metals will be less available for uptake by organisms. In general, many chemical and biological properties of metals in natural waters can hardly be explained on the basis of total metal concentrations. The understanding of these properties greatly improves by taking into account the actual speciation of the metals [11].

1.3 Dynamic Speciation

As it has been pointed out, the serious pollution hazard of heavy metals demands reliable analytical techniques able to measure the flux of metal that reaches micro-organisms, algae, plants, and living organisms present in the media [12]. The analysis of this flux is called dynamic speciation since it depends on the time scale and on the kinetic parameters of the undergoing processes, as well as on the spatial scale and geometry of the sensor or micro-organism.

The metal flux toward a consuming interface, for example, an analytical sensor or an accumulating organism in an aquatic ecosystem, results from the coupled diffusion and kinetics of interconversion between M and its various species in the medium, as schematized in Figure 1.1. The prediction of the process that controls the metal flux is embodied in the concept of lability [13]. A system is labile when, for $(k_a + k_d)t > 1$, the mass transport process to the surface is the limiting one, so that the kinetics of the complex association/dissociation processes are, in comparison, fast enough to reach quasi equilibrium conditions at any relevant spatial scale and time scale of the experiment. At the other limit, a system is denoted as nonlabile (or inert) when the dissociation processes limit the metal flux. Lability is influenced by a range of factors including the kinetics of the complexation processes, the transport phenomena present in the system, the size of the sensor, the processes at the surface leading to consumption of the target species, and the mixture of ligands present in the system.

A quantitative evaluation of the contribution of the complexes to the metal flux for a general case requires the rigorous solution of the resulting system of

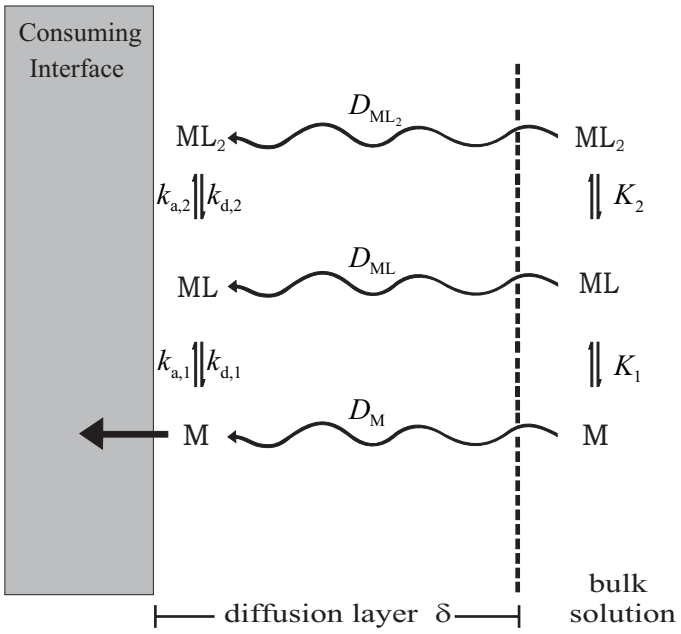

Figure 1.1: Schematic representation of coupled reaction-diffusion processes of successive metal complexes ML_i, at a consuming interface. D_j = diffusion coefficient of species j (j = M, L, ML, ML_2, ...). K_i, $k_{a,i}$, $k_{d,i}$ are respectively the equilibrium constant, formation and dissociation rate constants of ML_i.

transport and reaction equations. However, in almost all cases of practical interest, the resulting system of coupled partial differential equations can not be analytically solved. Then, the numerical solutions may be the only way we can get solutions for this system.

1.4 Diffusive Gradient in Thin Films (DGT)

Diffusive Gradient in Thin Films (DGT) are simple devices developed for *in situ* measurement of the availability of trace metals in aquatic environments [14, 15]. DGT have been also used in sediment [16] and soils [17].

The DGT is composed of three layers (see Figure 1.2): a binding-impregnated hydrogel layer (or resin layer), a hydrogel as a diffusion layer, and a membrane filter. These three layers are mounted in a plastic holder device with a window exposed to the sampling medium [15]. The hydrogels consist of a hydrophilic network made of acrylamide-polymer chains, linked with agarose cross-linkers. The membrane filter (pore size 0.45 μm) protects the hydrogel surface.

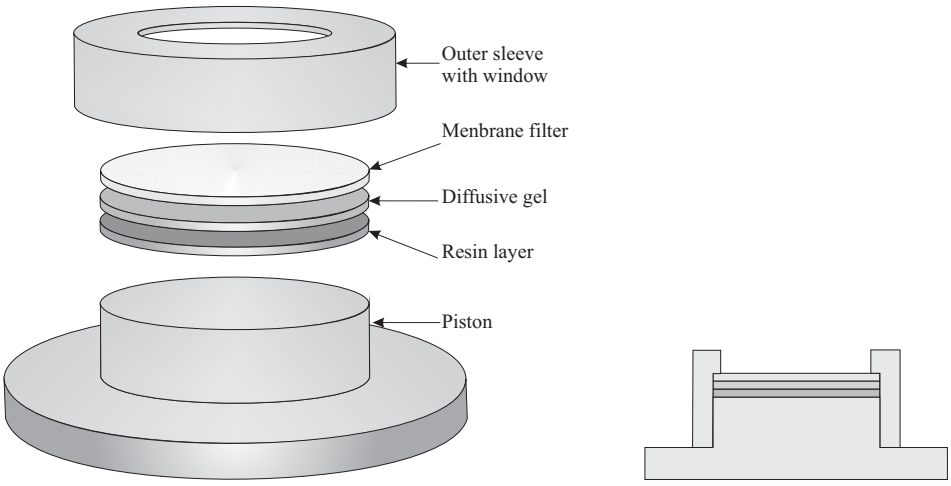

(a) 3D view **(b)** Cross section view

Figure 1.2: Scheme of a DGT device.

When the DGT is deployed in a sampling solution, species diffuse through the diffusive boundary layer DBL[1], the membrane filter and hydrogel to finally accumulate in the binding layer. Thereby, a concentration gradient is developed in the diffusion layer, which is maintained as long as the binding layer is not saturated. The flux of each specie i, J_i, through the diffusive layer, can be described by Fick first law of diffusion:

$$J_i = D_i \frac{\mathrm{d}c_i}{\mathrm{d}x}, \tag{1.1}$$

where D_i is the diffusion coefficient, c_i is the concentration and $\mathrm{d}c_i/\mathrm{d}x$ is the spacial concentration gradient of specie i.

The DGT device is exposed to the target solution for a known time, t. After retrieval, the DGT is opened and the analytes are desorbed/eluted from the binding layer and quantified using a suitable analytical technique. For the normal Chelex-DGT, nitric acid is recommended as eluent. Knowing the accumulated moles and diffusion coefficient of the analyte, as well as the deployment time and temperature, the average concentration during the time of exposure can be calculated. DGT measurements generate time-weighted average concentrations during deployment time. Longer deployment times will improve the detection limit since greater analyte amounts will be accumulated.

[1]Between any solid and a liquid there is a zone of laminar flow in which the process of molecular diffusion dominates solute transport. This zone (which typically ranges in thickness between 0.1 and 1 mm, depending on the interfacial flow velocity) is referred to as the diffusive boundary layer, DBL.

In principle, the DGT technique is quite simple, but detailed interpretation of the results of DGT-based measurements is associated to a range of uncertainties and questions that need further investigation. These questions are discussed in the following chapters.

1.5 Outline of this Thesis

The aim of this thesis is to contribute to the development of the analytical capability for determining the bioavailability of trace metals in natural waters. For this, we have focused our analysis on the DGT as a dynamic speciation technique. Special care has been given to the study of lability degree of complexes in single ligand systems and in a mixture of complexes.

The content of the different chapters is given below

Chapter 2 introduces a new strategy for numerical solution of systems of coupled partial differential equations (PDE) which describe the reaction-diffusion processes of a mixture of metal complexes, being adsorbed at a consuming interface. The solutions obtained here are used in the next chapters both for understanding the physico-chemical processes and for testing approximated analytical solutions.

In Chapter 3 we use the rigorous digital simulation (Chapter 2) to solve the diffusion-reaction processes in the gel and resin layers of a DGT deployed in a solution that contains a metal (M) and a single ligand (L). The results show an important effect of the complex penetration into the resin layer on the lability degree. The experimental accumulation of Cd by DGT sensors in Cd-NTA systems confirm these theoretical analyses.

In Chapter 4 simple approximate analytical expressions for the metal flux, the lability degree and the concentration profiles in a DGT experiment are reported. These results highlighted the key role of the thickness of the resin layer in determining the lability and the metal flux. A general procedure for estimating the lability of any complex in a standard DGT configuration is provided.

Chapter 5 studies the metal accumulation identifying two sources: free metal arriving at the resin layer and metal released by complex dissociation inside the resin disc. Simple analytical expressions for the lability criteria are also reported in this chapter. Additionally, using the rigourous numerical solution, we explore the transient DGT regimes in order to assess the time scale of the technique.

In Chapter 6 we discus the effect of negative charge of resin due to the

metal binding sites. Thus, while at high ionic strength electrostatic effects of these charged sites are screened by the background electrolyte, at low ionic strength there will be an additional influence on the metal accumulation from the charge of the resin disc. Analytical expressions to assess the influence of low ionic strengths in the DGT metal accumulation of charged complexes, are reported.

Chapter 7 deals with the mixture effect, that is, the change in the lability degree (or in the flux) of a complex in a mixture with respect to the lability degree of the same complex in a single ligand system. Here, we assess the mixture effect for a DGT sensor.

Chapter 8 introduces the conditional kinetic spectrum (CKS) methodology for the description of metal-macromolecular binding in multicomponent systems. We use this methodology to compute the lability degree of Pb-fulvic acid system at different pH values.

References

[1] Duffus, J. 'Heavy metals' – A meaningless term? *Pure and Applied Chemistry* 75, **2003**: 1357.

[2] Battarbee, R., Anderson, N., Appleby, P., Flower, R., Fritz, S., Haworth, E., Higgitt, S., Jones, V., Kreiser, A., Munro, M., Natkanski, J., Oldfield, F., Patrick, S., Richardson, N., Rippey, B. and Stevenson, A. *Lake Acidification in the United Kingdom 1800–1986.* ENSIS Publishing, London, **1988**.

[3] Duce, R. and Tindale, N. Atmospheric transport of iron and its deposition in the ocean. *Llimnology and Oceanography* 36(8), **1991**: 1715–1726.

[4] Galloway, J., Thornton, J., Norton, S., Volchok, H. and Mclean, R. Trace-metals in atmospheric deposition – A review and assessment. *Atmospheric Environment* 16(7), **1982**: 1677–1700.

[5] Nriagu, J. A global assessment of natural sources of atmospheric trace metals. *Nature* 338, **1989**: 47–49.

[6] Nriagu, J. and Pacyna, J. Quantitative assessment of worldwide contamination of air, water, and soils by trace metals. *Nature* 333, **1988**: 134–139.

[7] Morel, F. *Principles of Aquatic Chemistry.* John Wiley, New York, **1993**.

[8] Campbell, P. *Interactions Between Trace Metal and Aquatic Organisms: A Critique of the Free-ion Activity Model.* John Wiley and Sons, Chichester, **1995**.

[9] Khangarot, B. and Ray, P. Investigation of correlation between physicochemical properties of metals and their toxicity to the water flea daphnia-magna straus. *Eecotoxicology and Environmental Safety* 18(2), **1989**: 109–120.

[10] Corp, N. and Morgan, A. Accumulation of heavy-metals from polluted soils by the earthworm, lumbricus-rubellus – Can laboratory exposure of control worms reduce biomonitoring problems? *Environmental Pollution* 74(1), **1991**: 39–52.

[11] Buffle, J. *Complexation Reactions in Aquatic Systems. An Analytical Approach.* Chichester, UK, **1988**.

[12] Buffle, J. and Horvai, G. *In situ Monitoring of Aquatic Systems: Chemical Analysis and Speciation*, volume 6. John Wiley and Sons, Chichester, UK, **2000**.

[13] van Leeuwen, H. Revisited: the conception of lability of metal complexes. *Electroanalysis* 13(10), **2001**: 826–830.

[14] Davison, W. and Zhang, H. In situ speciation measurements of trace components in natural-waters using thin-film gels. *Nature* 367(6463), **1994**: 546–548.

[15] Zhang, H. and Davison, W. Performance characteristics of diffusion gradients in thin films for the in situ measurement of trace metals in aqueous solution. *Analytical Chemistry* 67(19), **1995**: 3391–3400.

[16] Zhang, H., Davison, W., Miller, S. and Tych, W. In-situ high-resolution measurements of fluxes of Ni, Cu, Fe, and Mn and concentrations of Zn and Cd in porewaters by DGT. *Geochimica et Cosmochimica Acta* 59(20), **1995**: 4181–4192.

[17] Zhang, H., Zhao, F., Sun, B., Davison, W. and McGrath, S. A new method to measure effective soil solution concentration predicts copper availability to plants. *Environmental Science and Technology* 35(12), **2001**: 2602–2607.

2

Simulación numérica de modelos no lineales de reacción-difusión en una dimensión espacial

2.1 Introducción

Los modelos matemáticos que describen procesos de reacción-difusión consisten en sistemas de ecuaciones diferenciales en derivadas parciales (EDP) con términos de reacción polinómicos [1].

La forma de resolución más común de estos sistemas consiste, en una primera fase, en la discretización de las ecuaciones, lo que transforma el sistema diferencial en un sistema algebraico distinto para cada incremento de tiempo. A continuación, cuando es no lineal, el sistema resultante se resuelve mediante técnicas tipo Newton [2]. Es decir, iterativamente, se aproximan las ecuaciones algebraicas con el desarrollo de primer orden y se resuelve el sistema lineal resultante.

En esta segunda etapa cabe destacar dos dificultades. La menor de ellas es la falta de robustez del método, cosa que obliga a la introducción de estrategias tipo Armijo o de minimización de la norma [3,4], que mejoren la convergencia del proceso iterativo. No obstante, el mayor obstáculo es consecuencia de la dimensión n del sistema lineal. En estos problemas el número de incógnitas n, es igual al producto del número de especies por el número de nodos de

la discretización espacial. Teniendo en cuenta que n puede ser grande y que el tiempo de resolución de un sistema de ecuaciones lineales es del orden de $n^3/3$ [3], el coste computacional puede ser prohibitivo en un ordenador de propósito general.

En este trabajo se ha desarrollado un conjunto de algoritmos que permiten la simulación de sistemas con un gran número de especies químicas y con un coste computacional que admite la simulación de procesos de cierta complejidad en un tiempo razonablemente corto. Para ello es necesario imponer una única condición: todas las reacciones deben expresarse en etapas de la forma $\mathrm{A} + \mathrm{B} \rightleftharpoons \mathrm{C}$.

Bajo esta condición se construye una estructura de datos sencilla que, a partir de una indexación arbitraria de las especies, asigna todo el conjunto de parámetros físicos, tanto los referidos a las sustancias como los que afectan a las reacciones químicas presentes. Así mismo, la algorítmica también incorpora la resolución del problema no lineal de equilibrio necesario para inicializar todas las concentraciones.

2.2 El modelo

Consideremos la complejación en equilibrio de diferentes metales y ligandos en solución, que reaccionan de acuerdo al esquema elemental representado en la ecuación 2.1.

$$\mathrm{A} + \mathrm{B} \underset{k_\mathrm{d}}{\overset{k_\mathrm{a}}{\rightleftharpoons}} \mathrm{C}, \tag{2.1}$$

donde A, B y C pueden representar un metal, un ligando o cualquier combinación entre ellos, y k_a y k_d representan las constantes cinéticas de asociación y disociación respectivamente. Las condiciones de equilibrio para esta reacción se expresan en la forma

$$K = \frac{k_\mathrm{a}}{k_\mathrm{d}} = \frac{c^*_\mathrm{AB}}{c^*_\mathrm{A} c^*_\mathrm{B}}, \tag{2.2}$$

donde K es la constante de equilibrio y c^*_i indica la concentración de la especie i en la solución.

Cuando se introduce un sensor DGT en la solución, las especies allí presentes se difunden hacia la resina (localizada entre $0 < x < r$), a través de la capa de gel comprendida entre $r < x < r + g$ (ver Figura 2.1). En el interior del DGT, la concentración $c(x, t)$ de cada especie se ve modificada por la difusión, por la reacción con las otras especies presentes en la solución y por la posible reacción con la resina.

Antes de formular matemáticamente las ecuaciones de balance para las especies del sistema, haremos algunas suposiciones.

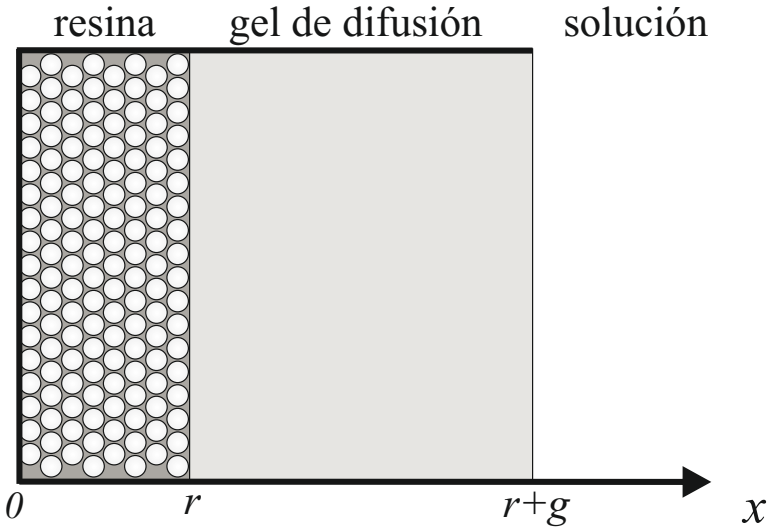

Figura 2.1: Diagrama esquemático de un dispositivo DGT en una solución.

- Debido a que los discos de resina están hechos de material complejante embebido en el mismo tipo de gel que compone la capa difusiva, es razonable considerar que las especies que se difunden a través del gel, pueden penetrar en la resina [5].

- Las especies que, después de difundirse a través del gel, pueden unirse a la resina, lo hacen mediante el esquema descrito en la ecuación 2.3.

$$\mathrm{A} + \mathrm{R} \underset{k_{\mathrm{d,R}}}{\overset{k_{\mathrm{a,R}}}{\rightleftharpoons}} \mathrm{AR}, \tag{2.3}$$

  donde R denota los sitios libres en el interior de la resina y $k_{\mathrm{a,R}}$, $k_{\mathrm{d,R}}$ y $K_{\mathrm{R}} = k_{\mathrm{a,R}}/k_{\mathrm{d,R}}$ representan las constantes cinéticas y de equilibrio, respectivamente

- Cuando el material usado para la resina es Chelex, los granos de resina se localizan principalmente en la capa adyacente al gel de difusión [6]. Sin embargo, en una primera aproximación, consideramos que la resina esta uniformemente distribuida en el dominio $0 < x < r$. Así mismo, consideramos que los sitios libres de la resina (R) y todos los complejos que se formen con estos sitios, son inmóviles.

- Por simplicidad, y debido a que, en general, los coeficientes de difusión en el gel, el filtro y la DBL son similares, la capa difusiva de ancho g en la Figura 2.1, que se extiende desde la resina hasta la interfaz entre filtro y la solución, incluye el tamaño de estas tres capas.

- No se consideran efectos electrostáticos, fuerzas de migración, etc., originados por las cargas de los grupos funcionales de la resina, debido a que hay suficiente exceso del electrolito de fondo

Bajo estas condiciones, la difusión es el mecanismo de transporte más relevante en el sistema y, por lo tanto, las ecuaciones de transporte, para cada especie i, pueden escribirse mediante expresiones de la forma

$$\begin{aligned} \frac{\partial c_i}{\partial t} &= D_i^{\mathrm{R}} \frac{\partial^2 c_i}{\partial x^2} + \text{«términos de reacción»} \quad 0 < x < r, \\ \frac{\partial c_i}{\partial t} &= D_i \frac{\partial^2 c_i}{\partial x^2} \ + \text{«términos de reacción»} \quad r < x < r + g, \end{aligned} \tag{2.4}$$

donde D_i^{R} y D_i son los coeficientes de difusión de la especie i en la resina y el gel, respectivamente y los denominados «términos de reacción» hacen referencia a los términos cinéticos correspondientes a la reacción de la especie i con otras sustancias de la solución.

Técnicamente, las expresiones mostradas en 2.4 son ecuaciones diferenciales en derivadas parciales de segundo orden, de tipo parabólico, que sólo pueden ser solucionadas analíticamente bajo condiciones muy particulares.

En general, en los casos de interés práctico, estos sistemas de ecuaciones no tienen una solución analítica. Entonces, las soluciones numéricas pueden ser la mejor (o la única) forma de obtener los valores de concentración para cada punto del espacio en cada instante de tiempo.

Como se describió en la introducción, la estrategia más utilizada para resolver estos sistemas numéricamente, consiste en discretizar las ecuaciones y posteriormente resolver iterativamente el sistema de ecuaciones algebraicas. En las siguientes secciones se describe una estrategia novedosa para solucionar numéricamente los sistemas de ecuaciones de la forma 2.4.

2.3 Planteamiento del problema

Consideremos un conjunto de reacciones elementales, en número igual a *numreac*, de la forma,

$$\begin{array}{lll}
\mathrm{c_{L_{11}}} + \mathrm{c_{L_{12}}} \underset{\mathrm{k_{d,1}}}{\overset{\mathrm{k_{a,1}}}{\rightleftharpoons}} \mathrm{c_{L_{13}}} & & \text{Reacción 1} \\
\mathrm{c_{L_{21}}} + \mathrm{c_{L_{22}}} \underset{\mathrm{k_{d,2}}}{\overset{\mathrm{k_{a,2}}}{\rightleftharpoons}} \mathrm{c_{L_{23}}} & & \text{Reacción 2} \\
\vdots & & \vdots \\
\mathrm{c_{L_{j1}}} + \mathrm{c_{L_{j2}}} \underset{k_{\mathrm{d},j}}{\overset{k_{\mathrm{a},j}}{\rightleftharpoons}} \mathrm{c_{L_{j3}}} & & \text{Reacción } j \\
\vdots & & \vdots
\end{array} \tag{2.5}$$

donde $k_{\mathrm{a},j}$, $k_{\mathrm{d},j}$ y $K_j = k_{\mathrm{a},j}/k_{\mathrm{d},j}$, con $j = 1, 2, \ldots, numreac$, representan las constantes cinéticas y de equilibrio, respectivamente

El sistema se codifica de acuerdo a la indexación utilizada en 2.5, en principio totalmente arbitraria, de las especies presentes, sin ningún tipo de restricción sobre el número de metales o de ligandos. Como ya se ha dicho, la única restricción impuesta consiste en que todas las reacciones químicas presentes deben escribirse en etapas de la forma $\mathrm{A} + \mathrm{B} \rightleftharpoons \mathrm{C}$.

Dado que en general los datos de partida acostumbran a ser las concentraciones totales de las sustancias puras (aquellas que no son el resultado de alguna reacción), en primer lugar hay que resolver el problema de equilibrio, es decir, se debe encontrar el valor de la concentración en solución (o valor de concentración bulk) para cada una de las especies de sistema.

Para ello construimos las matrices *mreac* y *kreac*, que permiten introducir la información referente a las reacciones químicas que deben considerarse en $x = r + g$. La primera de estas matrices, *mreac*, es la matriz de índices que contiene tres columnas y un número de filas igual al número de reacciones *numreac*,

$$mreac = \begin{pmatrix} L_{11} & L_{12} & L_{13} \\ L_{21} & L_{22} & L_{23} \\ \vdots & \vdots & \vdots \\ L_{j1} & L_{j2} & L_{j3} \\ \vdots & \vdots & \vdots \end{pmatrix}. \tag{2.6}$$

La matriz *mreac* se construye de manera que, si en la reacción j-ésima la sustancia 5 se combina con la 7 para dar 8, los índices de la fila j serán 5 7 8; esto es, las dos primeras columnas contienen los componentes y la tercera indica el compuesto formado.

La matriz *kreac* contiene el mismo número de filas que la matriz *mreac*, pero solo dos columnas. La primera columna indica los valores de la constante

de asociación ($k_{\mathrm{a},j}$) y la segunda los de la constante de disociación ($k_{\mathrm{d},j}$) de cada reacción j, con $j = 1, 2, \ldots, numreac$,

$$kreac = \begin{pmatrix} k_{\mathrm{a}1} & k_{\mathrm{d}1} \\ k_{\mathrm{a}2} & k_{\mathrm{d}2} \\ \vdots & \vdots \\ k_{\mathrm{a}j} & k_{\mathrm{d}j} \\ \vdots & \vdots \end{pmatrix}. \tag{2.7}$$

La estrategia para resolver el problema de equilibrio, consiste en expresar la concentración de las especies no puras (es decir, las especies que aparecen en la tercera columna de *mreac*), como combinación de las concentraciones totales de las sustancias puras, que son conocidas en el sistema. El resultado es un sistema de ecuaciones no lineales, que se resuelve utilizando una variación del método de Newton-Raphson. La estructura del programa y la solución detallada del problema de equilibrio se encuentran contenidas en la Sección 2.A (página 29).

Una vez resuelto el problema de equilibrio, es decir, una vez obtenidos valores de concentración bulk para cada especie en $t = 0$ y en $x = r + g$, se procede a plantear el problema de transporte de forma genérica para un número arbitrario de especies químicas.

Sea *numeq* el número de especies del problema, el cual, evidentemente, coincide con el número de ecuaciones diferenciales. En primer lugar se consideran dos vectores de coeficientes de difusión, uno para la región $(0, r)$, denominado $\vec{D}^{\mathrm{R}} = (D_1^{\mathrm{R}}, D_2^{\mathrm{R}}, \ldots, D_{numeq}^{\mathrm{R}})$, que contiene los coeficientes de difusión para cada especie en el interior de la fase resina, y el otro denotado por $\vec{D} = (D_1, D_2, \ldots, D_{numeq})$, que corresponde a los coeficientes de difusión en el interior del gel ($r < x < r + g$). Los coeficientes de difusión de la resina y sus derivados son nulos puesto que se consideran fijos en la matriz de gel del disco de resina.

Las matrices *mreac* y *kreac* que se utilizaron en la solución del problema de equilibrio, deben ampliarse con la incorporación de las reacciones correspondientes a la resina y a los compuestos que la contienen.

Estas dos nuevas matrices contienen la información para expresar el problema general. Para cada especie i, donde $i = 1, \ldots, numeq$, la correspondiente ecuación de reacción-difusión será de la forma

$$\frac{\partial c_i}{\partial t} = \begin{Bmatrix} D_i^{\mathrm{R}} \\ D_i \end{Bmatrix} \frac{\partial^2 c_i}{\partial x^2} + \sum_{j=1}^{numreac} \left(A_{i,j} c_{mreac(j,1)} c_{mreac(j,2)} + B_{i,j} c_{mreac(j,3)} \right), \tag{2.8}$$

donde D_i^{R} actúa como coeficiente de difusión en $(0, r)$ y D_i en $(r, r+g)$.

Para un valor determinado del índice i, los coeficientes $A_{i,j}$ y $B_{i,j}$ se pueden calcular mediante el siguiente algoritmo: si en la reacción j no interviene la especie i, $A_{i,j} = B_{i,j} = 0$. En caso contrario, el valor absoluto de $A_{i,j}$ es igual a $k_{\mathrm{a},j}$ y el de $B_{i,j}$ vale $k_{\mathrm{d},j}$. Finalmente se debe tener en cuenta que el coeficiente del término que contiene a la sustancia i-ésima debe ser negativo.

El algoritmo anterior escrito en términos programables es el siguiente:

para $j = 1, numreac$
  $ipos = 0$
  para $l = 1, 3$
    si $(mreac(j, l) = i)$ **entonces**
      $ipos = l$
    finsi
  finpara
  si $(ipos = 0)$ **entonces**
    $A_{i,j} = 0$
    $B_{i,j} = 0$
  si no
    $A_{i,j} = k_{\mathrm{a},j}$ $(= kreac(j, 1))$
    $B_{i,j} = k_{\mathrm{d},j}$ $(= kreac(j, 2))$
    si $(ipos = 3)$**entonces**
      $B_{i,j} = -B_{i,j}$
    si no
      $A_{i,j} = -A_{i,j}$
    finsi
  finsi
finpara

2.3.1 Condiciones iniciales y de contorno

En el tiempo $t = 0$, la concentración de cada una de las especies i en el dominio espacial $(0, r+g)$ es cero, es decir $c_i(x, 0) = 0$, excepto para los sitios libres de la resina cuya concentración inicial es $c_{\mathrm{R}}(x, 0) = c_{\mathrm{TR}}$ en el dominio $(0, r)$ –ó $c_{\mathrm{R},j}(x, 0) = c_{\mathrm{TR},j}$ para el caso en que tengamos diferentes resinas– y cero para $r < x < r + g$.

Para las especies con $D_i \neq 0$, se deben considerar, además, la condición de contorno en $x = r + g$,

$$c_i(r + g, t) = c_i^*;$$

la correspondiente en $x = 0$,

$$\left.\frac{\partial c_i}{\partial x}\right|_{x=0} = 0;$$

y las relaciones de continuidad en $x = r$,

$$c_i(r^-, t) = c_i(r^+, t)\ ; \qquad D_i^{\mathrm{R}} \left.\frac{\partial c_i}{\partial x}\right|_{x=r^-} = D_i \left.\frac{\partial c_i}{\partial x}\right|_{x=r^+}.$$

2.4 Adimensionalización del problema

Para adecuar las escalas al orden de magnitud de los datos, a continuación se describen los cambios de variable que conducen al problema adimensional.

- Para todas las especies en solución, es decir, para todas las especies de las que se dispone de un valor de concentración bulk, obtenido de la solución del problema de equilibrio, definimos las concentraciones normalizadas,
$$q_i = \frac{c_i}{c_i^*}.$$
- Para el resto, es decir, la resina y sus compuestos,
$$q_j = \frac{c_j}{c_{\mathrm{TR}}}.$$
- Para la coordenada espacial, en lugar de adimensionalizar, se usa el cambio de escala,
$$z = \frac{x}{\sqrt{D_{\max}}},$$
donde $D_{\max}$ es el mayor coeficiente de difusión. Esto obliga a definir $r^* = r/\sqrt{D_{\max}}$; $g^* = g/\sqrt{D_{\max}}$; $d_i = D_i/D_{\max}$; y $d_i^{\mathrm{R}} = D_i^{\mathrm{R}}/D_{\max}$.
- Dado que se pretende simular experimentos en los que intervienen distintas escalas temporales, el eje de tiempos no se adimensionaliza.

Con estas nuevas variables, las ecuaciones de reacción-difusión descritas en la expresión 2.8 se reescriben como

$$\frac{\partial q_i}{\partial t} = \begin{Bmatrix} d_i^{\mathrm{R}} \\ d_i \end{Bmatrix} \frac{\partial^2 q_i}{\partial z^2} + \sum_{j=1}^{numreac} \left(\hat{A}_{i,j} q_{mreac(j,1)} q_{mreac(j,2)} + \hat{B}_{i,j} q_{mreac(j,3)} \right), \tag{2.9}$$

donde d_i^{R} actúa como coeficiente de difusión en $(0, r^*)$ y d_i en $(r^*, r^* + g^*)$, y donde los nuevos coeficientes $\hat{A}_{i,j}$ y $\hat{B}_{i,j}$ se calculan como

$$\hat{A}_{i,j} = A_{i,j} \frac{c^*_{mreac(j,1)} c^*_{mreac(j,2)}}{c_i^*}; \quad \hat{B}_{i,j} = B_{i,j} \frac{c^*_{mreac(j,3)}}{c_i^*}. \tag{2.10}$$

Para las concentraciones de la resina y sus derivados, c_i^* debe ser sustituida por c_{TR}.

Las condiciones iniciales y de contorno para todas las sustancias que no contienen resina, es decir, para todas aquellas cuyo coeficiente de difusión es distinto de cero, son ahora

$$q_i(z,0) = 0; \quad q_i(r^* + g^*, t) = 1 \tag{2.11}$$

y

$$\left.\frac{\partial q_i}{\partial z}\right|_{z=0} = 0\,; \quad q_i(r^{*-}, t) = q_i(r^{*+}, t); \quad \left.\frac{\partial q_i}{\partial z}\right|_{z=r^{*-}} = \frac{d_i}{d_i^R} \left.\frac{\partial q_i}{\partial z}\right|_{z=r^{*+}}. \tag{2.12}$$

Las sustancias restantes solo necesitan una condición inicial: para la resina

$$q_{\mathrm{R}}(z,0) = \begin{cases} 1 & \text{si} \quad 0 < z < r^* \\ 0 & \text{si} \quad r^* < z < r^* + g^* \end{cases},$$

para los derivados de la resina $q_i(x,0) = 0$ en $(0, r^* + g^*)$.

2.5 Discretización

El eje espacial se discretiza en segmentos iguales de longitud Δz y el temporal en intervalos iguales Δt (ver Figura 2.2).

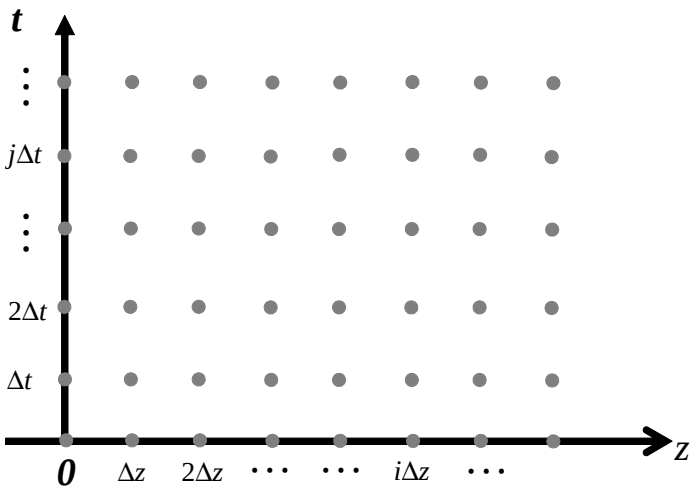

Figura 2.2: Esquema de discretización espacio temporal.

Sea $F(z,t)$ una función que puede contener derivadas espaciales, de distintos ordenes, de la función $f(z,t)$. Si

$$\frac{\partial f(z,t)}{\partial t} = F(z,t), \tag{2.13}$$

se puede discretizar 2.13 como una combinación lineal de la forma

$$\frac{f(z_i,t+\Delta t)-f(z_i,t)}{\Delta t} \simeq \sigma F(z_i,t+\Delta t)+(1-\sigma)F(z_i,t), \tag{2.14}$$

donde, $0 \leq \sigma \leq 1$.

En general, para las EDP del tipo parabólico, el esquema de discretización de Euler inverso (es decir, tomando $\sigma = 1$ en la ecuación 2.14), permite escoger incrementos de z y de t arbitrarios, sin comprometer la estabilidad ni introducir oscilaciones espurias en el proceso iterativo [2].

A continuación, para cada sustancia i, discretizaremos la ecuación diferencial 2.9 usando el esquema de Euler inverso para obtener un sistema de ecuaciones algebraicas.

Para las especies con coeficiente de difusión diferente de cero, la ecuación 2.9 se transforma en

$$\frac{q_i(z,t+\Delta t)-q_i(z,t)}{\Delta t} = \begin{Bmatrix} d_i^{\mathrm{R}} \\ d_i \end{Bmatrix} \frac{q_i(z+\Delta z,t+\Delta t)-2q_i(z,t+\Delta t)+q_i(z-\Delta z,t+\Delta t)}{\Delta z^2} + \sum_{j=1}^{numreac} \hat{A}_{i,j} q_{mreac(j,1)}(z,t+\Delta t) q_{mreac(j,2)}(z,t+\Delta t) + \hat{B}_{i,j} q_{mreac(j,3)}(z,t+\Delta t). \tag{2.15}$$

En este caso, las condiciones de contorno descritas en las ecuaciones 2.11 y 2.12 se transforman en

$$q_i(\Delta z,t+\Delta t)-q_i(0,t+\Delta t)=0, \quad q_i(r^*+g^*,t+\Delta t)=1 \tag{2.16}$$

y

$$q_i(r,t+\Delta t)-q_i(r-\Delta z,t+\Delta t) = \frac{d_i}{d_i^R}\left[q_i(r+\Delta z,t+\Delta t)-q_i(r,t+\Delta t)\right]. \tag{2.17}$$

No se escribe ninguna expresión para la continuidad de la solución para $z = r^*$. Simplemente, de ahora en adelante se considerará que, para dicha

posición, cada sustancia tiene un valor de concentración único (una manera sencilla de decir que es continua, debido a la ausencia de efectos electrostáticos).

Debido a que la resina y sus componentes se consideran inmóviles, las ecuaciones diferenciales para estas sustancias no contienen derivadas espaciales. De este modo las ecuaciones descritas en 2.9 para las especies con coeficiente de difusión nulo, se reescriben en forma discreta como

$$\frac{q_i(z,t+\Delta t)-q_i(z,t)}{\Delta t}=$$

$$\sum_{j=1}^{numreac} \hat{A}^{\mathrm{R}}_{i,j} q_{mreac(j,1)}(z,t+\Delta t) q_{mreac(j,2)}(z,t+\Delta t)+\hat{B}^{\mathrm{R}}_{i,j} q_{mreac(j,3)}(z,t+\Delta t), \tag{2.18}$$

para $(0,r^*)$ y

$$q_i(z,t+\Delta t)=0, \quad \forall\ z\in(r^*,r^*+g^*). \tag{2.19}$$

2.6 Resolución iterativa del sistema de ecuaciones resultante

En las expresiones 2.15 y 2.18, los términos derivados de las reacciones homogéneas acoplan el sistema de ecuaciones algebraicas resultante, al involucrar términos de segundo orden como productos de concentraciones de especies distintas. Como se mencionó en la introducción, éste tipo de sistemas no lineales se resuelve, generalmente, utilizando técnicas iterativas del tipo Newton. La novedad introducida en esta tesis, consistió en utilizar un esquema de iteración directa, lo que nos permitió la construcción de algoritmos sencillos, veloces y eficientes.

La idea básica de estos algoritmos consiste en, suponiendo conocida la solución para todas las especies en el instante t, obtener la solución en el instante $t+\Delta t$ según el esquema siguiente:

1.- Inicializar todas las concentraciones en $t+\Delta t$ con la solución en el instante t.

2.-

para $i=1, numeq$

Resolver el problema discreto i-ésimo (para la especie i-ésima) considerando las especies j-ésimas ($i\neq j$) constantes en esta etapa y cuyo valor en $t+\Delta t$ es el

correspondiente al de su cómputo más reciente.
finpara

3.- Repetir el paso 2 hasta que la norma de la diferencia entre dos iteraciones consecutivas sea inferior a un valor pequeño prefijado.

La estructura iterativa descrita tiene la ventaja de que la resolución, para cada sustancia i con coeficiente de difusión diferente de cero, se reduce a un sistema tridiagonal, en el cual la diagonal es fuertemente dominante debido al signo negativo de los términos de reacción de la ecuación de c_i que contienen a c_i. Aún mejor, para la resina y sus compuestos, especies para las cuales el coeficiente de difusión es cero, el sistema es diagonal. Todo esto redunda en un gran aumento de la velocidad de cálculo, ya que resulta mucho más económico resolver unas decenas o unos centenares de veces los sistemas mencionados (cada uno de ellos se resuelve en tiempo de orden n), que resolver el sistema no lineal completo descrito en 2.15 y 2.18. En este último caso, aunque se resuelva en un número de iteraciones pequeño, cada iteración involucra un tiempo de cálculo del orden de n^3. Teniendo en cuenta que n es igual al producto del número de especies multiplicado por la cantidad de intervalos en que se discretiza el dominio espacial, cualquier intento de resolución directa puede resultar prohibitivo.

Implícitamente, al describir las discretizaciones, se ha considerado que el dominio completo $(0, r^* + g^*)$ se discretiza en intervalos de igual longitud Δz en ambos subdominios. Entonces, para cada especie, se usarán distintos vectores que representarán la solución en cada posición de la malla de puntos, en un instante dado y para un determinado estado k del proceso iterativo.

Si se representa el vector de concentraciones para una especie en la forma

$$\vec{q}_i^{\,k}(t) = \Big(q_i^k(0,t)\ ,\ q_i^k(\Delta z,t)\ ,\ q_i^k(2\Delta z,t)\ ,\ \ \ldots, q_i^k(nint\times\Delta z,t)\Big)\,, \quad (2.20)$$

donde *nint* indica el número de intervalos en que se divide el dominio (ver Figura 2.3), los vectores que intervienen en los algoritmos estarán formados por la yuxtaposición de los vectores de cada especie para distintos tiempos y niveles de iteración. Fundamentalmente se usan

$$\begin{aligned}
\vec{q}_{ant} &\equiv (\vec{q}_1(t), \vec{q}_2(t), \ldots, \vec{q}_{numeq}(t)),\\
\vec{q}_{aux} &\equiv (\vec{q}_1^{\,k}(t+\Delta t), \vec{q}_2^{\,k}(t+\Delta t), \ldots, \vec{q}_{numeq}^{\,k}(t+\Delta t)),\\
\vec{q}_{sig} &\equiv (\vec{q}_1^{\,k+1}(t+\Delta t), \vec{q}_2^{\,k+1}(t+\Delta t), \ldots, \vec{q}_{numeq}^{\,k+1}(t+\Delta t)). \quad (2.21)
\end{aligned}$$

Dado que la solución en $z = r^* + g^*$ es conocida, su valor no se incluye dentro de la resolución. Entonces, el punto de índice l es el extremo izquierdo del

subintervalo l, es decir, corresponde a la posición $z = (l-1)\Delta z$. Con el índice nr se indica el correspondiente al último intervalo del subdominio resina de manera que, el punto $z = r^*$ se corresponde al índice $nr + 1$.

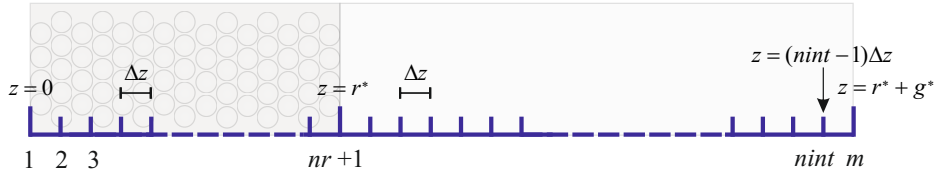

Figura 2.3: Esquema de discretización espacial.

La longitud de los vectores $\vec{q}_{ant}$, $\vec{q}_{aux}$ y $\vec{q}_{sig}$ es igual a $ntot = numeq \times nint$. Todo esto implica que, para acceder a la posición j-ésima de algún vector correspondiente a la sustancia i-ésima debe calcuarse $l = (i-1) * nint + j$. Esta relación se utilizará repetidamente en los algoritmos que se describen a continuación.

2.7 Algoritmo general de resolución

A continuación se procede a la construcción descendente del algoritmo general de resolución.

Algoritmo

Inicialización de $\vec{q}_{ant}$ con las condiciones iniciales
para $t = \Delta t,\ tfin,\ \Delta t$ (bucle de tiempo)
    $test = 100000$
    $\vec{q}_{aux} = \vec{q}_{ant}$
    $\vec{q}_{sig} = \vec{q}_{aux}$
    mientras $(test > ...)$
        para $i = 1, numeq$ (resolver para la especie i)
            $ii = (i-1) * nint$
            si $(d_i \neq 0)$
                BLOQUE 1
            si no
                BLOQUE 2
            finsi
        finpara
        $test = ||\vec{q}_{sig} - \vec{q}_{aux}||$
        $\vec{q}_{aux} = \vec{q}_{sig}$
    finmientras
    $\vec{q}_{ant} = \vec{q}_{sig}$
finpara

Bloque 1: Resolución para especies con coeficiente de difusión distinto de cero

$ddR = d_i^R \Delta t / \Delta z^2$
$dd = d_i \Delta t / \Delta z^2$
$subd(1) = 0$
$supd(1) = 1$
$subd(nr+1) = -1$
$supd(nr+1) = -d_i / d_i^R$

para $l = 2, nr$
    $subd(l) = -ddR$
    $supd(l) = -ddR$
finpara

para $l = nr+2, nint$
    $subd(l) = -dd$
    $supd(l) = -dd$
finpara

$diag(1) = -1$
$diag(nr+1) = 1 + d_i / d_i^R$
$ti(1) = 0$
$ti(nr+1) = 0$
para $l = 2, nr$
    $diag(l) = 1 + 2 * ddR$
    $ti(l) = q_{ant}(ii + l)$
    para $j = 1, numreac$
        si $(A_{i,j} \neq 0)$ **entonces**
            $i1 = (mreac(j,1) - 1) * nint$
            $i2 = (mreac(j,2) - 1) * nint$
            $i3 = (mreac(j,3) - 1) * nint$
            si $(A_{i,j} < 0)$
                $\sigma = -A_{i,j} \Delta t$
                si $(i1 \neq ii)$
                    $\sigma = \sigma * q_{sig}(i1 + l)$
                finsi
                si $(i2 \neq ii)$
                    $\sigma = \sigma * q_{sig}(i2 + l)$
                finsi
                $\mu = B_{i,j} q_{sig}(i3 + l) \Delta t$
                $diag(l) = diag(l) + \sigma$
                $ti(l) = ti(l) + \mu$

si no
$\sigma = A_{i,j} q_{sig}(i1 + l) q_{sig}(i2 + l) \Delta t$
$\mu = -B_{i,j} \Delta t$
$diag(l) = diag(l) + \mu$
$ti(l) = ti(l) + \sigma$
finsi
finsi
finpara
finpara
para $l = nr + 2, nint$
$diag(l) = 1 + 2 * dd$
$ti(l) = q_{ant}(ii + l)$
para $j = 1, numreac$
si $(A_{i,j} \neq 0)$ **entonces**
$i1 = (mreac(j, 1) - 1) * nint$
$i2 = (mreac(j, 2) - 1) * nint$
$i3 = (mreac(j, 3) - 1) * nint$
si $(A_{i,j} < 0)$
$\sigma = -A_{i,j} \Delta t$
si $(i1 \neq ii)$
$\sigma = \sigma * q_{sig}(i1 + l)$
finsi
si $(i2 \neq ii)$
$\sigma = \sigma * q_{sig}(i2 + l)$
finsi
$\mu = B_{i,j} q_{sig}(i3 + l) \Delta t$
$diag(l) = diag(l) + \sigma$
$ti(l) = ti(l) + \mu$
si no
$\sigma = A_{i,j} q_{sig}(i1 + l) q_{sig}(i2 + l) \Delta t$
$\mu = -B_{i,j} \Delta t$
$diag(l) = diag(l) + \mu$
$ti(l) = ti(l) + \sigma$
finsi
finsi
finpara
finpara
call **tridag**$(subd, diag, supd, ti, res, nint)$
para $l = 1, nint$
$q_{sig}(ii + l) = res(l)$
finpara

Bloque 2: Resolución para especies con coeficiente de difusión igual a cero

para $l = 1, nr + 1$
  $\alpha = 1/\Delta t$
  $\beta = q_{ant}(ii + l)$
  para $j = 1, numreac$
    si $(A_{i,j} \neq 0)$
      $i1 = (mreac(j, 1) - 1) * nint$
      $i2 = (mreac(j, 2) - 1) * nint$
      $i3 = (mreac(j, 3) - 1) * nint$
      si $(A_{i,j} < 0)$
        $\sigma = -A_{i,j}\Delta t$
        si $(i1 \neq ii)$
          $\sigma = \sigma * q_{sig}(i1 + l)$
        finsi
        si $(i2 \neq ii)$
          $\sigma = \sigma * q_{sig}(i2 + l)$
        finsi
        $\mu = B_{i,j}q_{sig}(i3 + l)\Delta t$
        $\alpha = \alpha + \sigma$
        $\beta = \beta + \mu$
      si no
        $\sigma = A_{i,j}q_{sig}(i1 + l)q_{sig}(i2 + l)\Delta t$
        $\mu = -B_{i,j}\Delta t$
        $\alpha = \alpha + \sigma$
        $\beta = \beta + \mu$
      finsi
    finsi
  finpara
  $q_{sig}(ii + l) = \beta/\alpha$
finpara

para $l = nr + 2, nint$
  $q_{sig}(ii + l) = 0$
finpara

La discretización espacial de un modelo de EDP se puede llevar a cabo usando diversas técnicas. Las más utilizadas son las de diferencias finitas, las de elementos finitos en todas sus variantes o las de volúmenes finitos [2, 7]. Cada una de estas técnicas tiene sus ventajas e inconvenientes. Así, por ejemplo, la discretización mediante diferencias finitas conduce a algoritmos sencillos de programación muy fácil. Sin embargo, exigen el uso de redes espaciales de paso fijo, lo que implica un número de puntos grande y, en consecuencia, tiempos de cálculo que tienden a ser importantes.

Por otra parte, el método de los elementos finitos permite trabajar con distribuciones de puntos arbitrarias, usando intervalos espaciales pequeños donde se presume que el error va a ser mayor y anchuras mayores allí donde se sabe que el error será inferior [8]. Esta flexibilidad, aunque se traduce en un coste computacional menor al del caso de las diferencias finitas, conlleva un esfuerzo algorítmico y de programación que puede ser significativo.

Sin embargo, en este trabajo, la manera de discretizar la parte espacial no es esencial. Tal como ya se ha explicado, la novedad algorítmica que se propone consiste en la resolución iterativa del sistema no lineal especie a especie para cada paso temporal. En una simulación que pueda considerarse estándar, esto implica la resolución de unos centenares de sistemas tridiagonales, de coste computacional proporcional al número de puntos n, en lugar de unos pocos sistemas de ecuaciones lineales completos, cuya dimensión es igual a n multiplicado por el número de especies $numeq$, y de tiempo de CPU proporcional al cubo, no de n, si no al de $n \times numeq$. La ganancia en tiempo de ejecución es evidente. Basta considerar $n = 1000$ para darse cuenta de ello sea cual sea el número de especies químicas involucrado. Por supuesto que el método de los elementos finitos aumentaría un poco más la velocidad de las simulaciones y no debe rechazarse la posibilidad de usarlo, pero el esquema iterativo propuesto ha demostrado ser eficiente incluso en el peor de los escenarios posibles como es el uso de un esquema de diferencias finitas.

En honor a la verdad y teniendo en cuenta el carácter más físico-químico que matemático de esta tesis, hay que señalar que no se lleva a cabo el estudio de la convergencia del método iterativo. A pesar de todo, cabe decir que se ha constatado que, excepto en condiciones muy adversas, el cálculo resulta ser convergente y, por lo tanto, aproxima la solución deseada. En general, dichas condiciones adversas suelen ser consecuencia de una mala inicialización y, tal como se comentará más adelante, se ha invertido cierto esfuerzo en la obtención de inicializaciones adecuadas.

En general, la calidad de las simulaciones numéricas de problemas de reacción-difusión suele verse comprometida a medida que los valores de las constantes cinéticas de reacción aumentan. Es más, tal como se ha dicho, a partir de ciertos valores los procesos iterativos dejan de converger si no se dispo-

ne de inicializaciones excelentes. No obstante, a medida que aumentan las constantes de velocidad manteniendo su cociente constante, los perfiles de concentración tienden a los que se obtendrían en el caso totalmente lábil ($\xi = 1$), esto es, cuando las constantes de velocidad son infintas pero con límite del cociente igual a la constante de equilibrio. Esto ha sido de gran utilidad en algun sistema sencillo en el que es posible obtener la solución del mencionado caso totalmente lábil. El uso de esta solución conduce a buenas inicializaciones para valores de k_d grandes. Desgraciadamente, no es posible obtener la solución totalmente lábil en el caso general. Por esta razón se han desarrollado técnicas específicas de inicialización para estos casos. La estrategia general consiste en resolver el sistema, en cada paso de tiempo, para un conjunto de constantes cinéticas menores que las deseadas pero que proporcionan una solución. Con este resultado se inicializa el problema para un valor más grande de las constantes de reacción. El procedimiento se repite hasta alcanzar los valores de las constantes requeridas. El algoritmo descrito deja de funcionar cuando las constantes son enormes, pero aun así, permiten explorar un rango de valores suficientemente grande para obtener conclusiones acerca de la labilidad.

Por último, vale la pena destacar que aunque el dominio completo $(0, r^* + g^*)$ se ha dividido en intervalos de igual longitud Δz en cada uno de los dos subdominios, esta discretización no es esencial. De hecho, si se requiere, el problema se puede dividir fácilmente en varios subdominios, cada uno con su propia discretización. Esto proporciona dos grandes ventajas: por un lado, permite escoger intervalos pequeños donde las funciones varían rápidamente (usualmente cerca de la superficie de adsorción) e intervalos grandes en el resto del dominio, aumentando, aún más, la velocidad del cálculo. Por otro lado, permite resolver configuraciones diferentes a la de un sensor DGT. Es decir, con la condición que las reacciones se puedan expresar siempre en la forma elemental $\mathrm{A} + \mathrm{B} \rightleftharpoons \mathrm{C}$, se puede adecuar el algoritmo para resolver arreglos diferentes, simplemente modificando las condiciones iniciales y de contorno. Por ejemplo, en este trabajo hemos explorado sensores DGT con resinas de poca anchura y, en particular, el límite de los detectores voltamétricos ($r \to 0$)

2.A Resolución del problema de equilibrio

En esta sección se detalla el programa construido en FORTRAN para resolver el problema de equilibrio.

Nos guiaremos por un ejemplo sencillo para comprender mejor el programa. Sean las reacciones:

$$\begin{aligned} c_1 + c_2 &\underset{k_2}{\overset{k_1}{\rightleftharpoons}} c_3 \qquad \text{reacción 1} \\ c_1 + c_4 &\underset{k_4}{\overset{k_3}{\rightleftharpoons}} c_2 \qquad \text{reacción 2} \\ c_3 + c_4 &\underset{k_6}{\overset{k_5}{\rightleftharpoons}} c_5 \qquad \text{reacción 3} \end{aligned} \tag{2.22}$$

Como primer paso, introducimos los datos del problema mediante un fichero de texto plano (*reacciones.txt*), que tendrá la siguiente forma:

$$\begin{array}{ccccc} 3 & & & & \\ k_1 & k_2 & 1 & 2 & 3 \\ k_3 & k_4 & 1 & 4 & 2 \\ k_5 & k_6 & 3 & 4 & 5 \end{array} \tag{2.23}$$

La primera línea del fichero contiene el número total de reacciones (esto facilita le lectura del fichero). Cada una de las siguientes líneas contiene las constantes cinéticas y los índices asignados a las especies en cada una de las reacciones involucradas.

El fichero *reacciones.txt* contiene toda la información necesaria para resolver el problema de equilibrio. A continuación transcribimos el programa en FORTRAN que resuelve dicho sistema.

El programa

program *Equilibrium*
implicit double precision $(a-h, o-z)$
parameter $(nreacmax = 200, numeqmax = 400)$
parameter $(ncolmax = 20, numspmax = 20)$
dimension $mreac(nreacmax, 3), meq(numeqmax, ncolmax)$
dimension $ipos(nreacmax), maux(numeqmax, 3 * ncolmax)$
dimension $ivecsp(numspmax), icontaux(numeqmax)$
dimension $iveceq(numeqmax)$
dimension $ct(numspmax), c(numeqmax), csp(numspmax)$
double precision $kreac(nreacmax, 2), keq(numeqmax)$
dimension $fun(numspmax), ajac(numspmax, numspmax)$

Definiciones generales.

Construcción de las matrices *kreac* y *mreac*

open(1, *file* = *'reacciones.txt'*,*status* = *'old'*)
read(1,*) *numreac*
do $i = 1, numreac$
  read(1,*) $kreac(i,1), kreac(i,2), mreac(i,1),$
  $mreac(i,2), mreac(i,3)$
enddo

Se lee el fichero *reacciones.txt* para construir las matrices

$$kreac = \begin{pmatrix} k_1 & k_2 \\ k_3 & k_4 \\ k_5 & k_6 \end{pmatrix}$$

$$mreac = \begin{pmatrix} 1 & 2 & 3 \\ 1 & 4 & 2 \\ 3 & 4 & 5 \end{pmatrix}.$$

A continuación, se construye la matriz de ecuaciones (*meq*), de *numeqmax* filas y *ncolmax* columnas:

$$meq = \begin{pmatrix} 2 & 1 & 2 & \cdots \\ 2 & 1 & 2 & \cdots \\ 2 & 1 & 3 & \cdots \\ 2 & 2 & 3 & \cdots \\ 1 & 3 & & \cdots \end{pmatrix}.$$

Esta matriz contiene en su primera columna el número de reacciones en las que aparece cada sustancia. Las columnas siguientes nos indican el número de la reacción.

Construcción de las matriz de ecuaciones *meq*

$numeq = 1$
do $i = 1, numreac$
  do $j = 1, 3$
    if($mreac(i,j)$.**gt**.$numeq$) $numeq = mreac(i,j)$
  enddo
enddo

Primero se obtiene *numeq* (número de ecuaciones), como el máximo en la matriz *mreac*.

Construcción de la primera columna de meq

```
do i = 1, numeq
  do j = 1, ncolmax
    meq(i, j) = 0
  enddo
enddo
do i = 1, numreac
  do j = 1, 3
    index = mreac(i, j)
    meq(index, 1) = meq(index, 1) + 1
  enddo
enddo
```

Para construir la primera columna, se barre la matriz *mreac*. Cada vez que se encuentra una sustancia se suma un uno, a la fila correspondiente a esa sustancia, en la primera columna de la matriz *meq*,

$$meq = \begin{pmatrix} 2 & 0 & 0 & \cdots \\ 2 & 0 & 0 & \cdots \\ 2 & 0 & 0 & \cdots \\ 2 & 0 & 0 & \cdots \\ 1 & 0 & 0 & \cdots \end{pmatrix}.$$

Construcción del resto de meq

```
do i = 1, numeq
  ipos(i) = 2
enddo
do i = 1, numreac
  do j = 1, 3
    index = mreac(i, j)
    meq(index, ipos(index)) = i
    ipos(index) = ipos(index) + 1
  enddo
enddo
```

En la matriz de reacciones *mreac* cada fila corresponde a una reacción. En este bloque se barre la matriz *mreac* por filas. Cada vez que encuentra una sustancia, se asigna en la correspondiente fila de *meq* (a partir de la segunda columna), el número de la reacción en la que aparece dicha especie,

$$meq = \begin{pmatrix} 2 & 1 & 2 & \cdots \\ 2 & 1 & 2 & \cdots \\ 2 & 1 & 3 & \cdots \\ 2 & 2 & 3 & \cdots \\ 1 & 3 & & \cdots \end{pmatrix}.$$

Búsqueda de las sustancias puras

```
numsp = 0
do i = 1, numeq
  ipura = 1
  do j = 1, numreac
    if(i.eq.mreac(j, 3)) ipura = 0
  enddo
  if (ipura.eq.1) then
    numsp = numsp + 1
    ivecsp(numsp) = i
  endif
enddo
```

Si una sustancia es pura, no debe aparecer en la tercera columna de *mreac*. La variable *numsp* contiene el total de sustancias puras y el vector ivecsp nos indica cuales especies son: $numsp = 2$,

$$ivecsp = \begin{pmatrix} 1 \\ 4 \end{pmatrix}.$$

Ahora, en equilibrio se cumplen las siguientes relaciones:

$$\begin{aligned} c_2^* &= \frac{k_3}{k_4} c_1^* c_4^* \\ c_3^* &= \frac{k_1}{k_2} c_1^* c_2^* = \frac{k_1}{k_2}\frac{k_3}{k_4} c_1^* c_1^* c_4^* \\ c_5^* &= \frac{k_5}{k_6} c_2^* c_4^* = \frac{k_1}{k_2}\frac{k_3}{k_4}\frac{k_5}{k_6} c_1^* c_1^* c_4^* c_4^* \\ c_{\mathrm{T},1} &= c_1^* + c_2^* + 2c_3^* + 2c_5^* \\ c_{\mathrm{T},4} &= c_4^* + c_2^* + c_3^* + 2c_5^* \end{aligned} \tag{2.24}$$

Para resolver éste conjunto de ecuaciones construimos las matrices *maux* y *keq*, que contendrán la información del sistema. En nuestro ejemplo serán:

$$maux = \begin{pmatrix} 1 & 0 & 0 & 0 & 0 & \cdots \\ 1 & 4 & 0 & 0 & 0 & \cdots \\ 1 & 1 & 4 & 0 & 0 & \cdots \\ 4 & 0 & 0 & 0 & 0 & \cdots \\ 1 & 1 & 4 & 4 & 0 & \cdots \end{pmatrix} \tag{2.25}$$

y

$$keq = \begin{pmatrix} 1 \\ \frac{k_3}{k_4} \\ \frac{k_1}{k_2}\frac{k_3}{k_4} \\ 1 \\ \frac{k_1}{k_2}\frac{k_3}{k_4}\frac{k_5}{k_6} \end{pmatrix}. \tag{2.26}$$

Construcción de la matriz auxiliar ($maux$)

do $i = 1, numeq$
  do $j = 1, 3 * ncolmax$
    $maux(i, j) = 0$ — Inicialización de *maux*.
  enddo
enddo

do $i = 1, numsp$
  $index = ivecsp(i)$
  $maux(index, 1) = index$
  $icontaux(index) = 1$
  $keq(index) = 1.\text{d}0$
enddo

A partir de la información obtenida en *ivecsp*, llenamos la primera columna de *maux*, en las filas correspondientes a las sustancias puras. Además, construimos el contador auxiliar *icontaux* que indica cuantas columnas diferentes de cero hay en cada fila de *maux*,

$$maux = \begin{pmatrix} 1 & 0 & 0 & 0 & 0 & \cdots \\ 0 & 0 & 0 & 0 & 0 & \cdots \\ 0 & 0 & 0 & 0 & 0 & \cdots \\ 4 & 0 & 0 & 0 & 0 & \cdots \\ 0 & 0 & 0 & 0 & 0 & \cdots \end{pmatrix} \quad keq = \begin{pmatrix} 1 \\ 0 \\ 0 \\ 1 \\ 0 \end{pmatrix}$$

$$icontaux = \begin{pmatrix} 1 \\ 0 \\ 0 \\ 1 \\ 0 \end{pmatrix}.$$

do $i = 1, numreac$
  $index = mreac(i, 3)$
  $maux(index, 1) = mreac(i, 1)$
  $maux(index, 2) = mreac(i, 2)$
  $icontaux(index) = 2$
  $keq(index) = kreac(i, 1)/kreac(i, 2)$
enddo

Para las sustancias no puras copiamos la primera y segunda columna de *mreac*, en la correspondiente fila de *maux*,

$$maux = \begin{pmatrix} 1 & 0 & 0 & 0 & 0 & \cdots \\ 1 & 4 & 0 & 0 & 0 & \cdots \\ 1 & 1 & 0 & 0 & 0 & \cdots \\ 4 & 0 & 0 & 0 & 0 & \cdots \\ 1 & 1 & 0 & 0 & 0 & \cdots \end{pmatrix}.$$

Situamos el contador en la segunda columna y actualizamos *keq*,

$$keq = \begin{pmatrix} 1 \\ \frac{k_3}{k_4} \\ \frac{k_1}{k_2} \\ 1 \\ \frac{k_5}{k_6} \end{pmatrix} \quad icontaux = \begin{pmatrix} 1 \\ 2 \\ 2 \\ 1 \\ 2 \end{pmatrix}.$$

```
do i = 1, numeq
  ip = 1
  do while (ip.le.icontaux(i))
    index = maux(i, ip)
    if (isp(index, mreac, numreac).eq.1) then
      ip = ip + 1
    else
      icorr = icontaux(index) − 1
      if (ip.lt.icontaux(i)) then
        do j = icontaux(i), ip + 1, −1
          maux(i, j + icorr) = maux(i, j)
        enddo
      endif
      do j = ip, ip + icorr
        maux(i, j) = maux(index, j − ip + 1)
      enddo
      icontaux(i) = icontaux(i)
      +icontaux(index) − 1
      keq(i) = keq(i) ∗ keq(index)
    endif
  enddo
enddo
```

En este bloque se barre la matriz *maux* construida hasta el momento. Cada vez que encuentra una sustancia no pura (subrutina *isp*), se remplaza por la combinación de sustancias puras equivalente (ver 2.24). Así, mismo, cada vez que realiza un cambio, se actualizan los vectores *keq* e *icontaux* en las filas correspondientes. En nuestro ejemplo el resultado se muestra en 2.25 y 2.26 para *maux* y *keq*, respectivamente. La matriz *icontaux* quedará:

$$icontaux = \begin{pmatrix} 1 \\ 2 \\ 3 \\ 1 \\ 4 \end{pmatrix}.$$

Cálculo del vector de índices de ecuaciones

```
do i = 1, numeq
  iveceq(i) = 0
enddo
do i = 1, numeq
  do j = 1, numsp
    if(ivecsp(j).eq.i)iveceq(i) = j
  enddo
enddo
```

El sistema de ecuaciones de equilibrio es de dimensión igual al número de sustancias puras. Dado que los índices de las sustancias puras pueden ser arbitrarios, el vector $iveceq(i)$, partiendo del índice i de una sustancia, devuelve el índice de la ecuación de equilibrio correspondiente a la sustancia i-ésima. Si la sustancia i no es pura devuelve el valor cero,

$$ivecsp = \begin{pmatrix} 1 \\ 4 \end{pmatrix} \Rightarrow iveceq = \begin{pmatrix} 1 \\ 0 \\ 0 \\ 2 \\ 0 \end{pmatrix}.$$

Construcción de los vectores ct y csp

open$(2, file =$*'ct.txt'*,$status =$*'old'*$)$
do $i = 1, numsp$
  read$(2, *)$ $ct(i)$
enddo
do $i = 1, numsp$
  $csp(i) = float(i)/10.$
enddo
call *calfjeq*$(ct, csp, numeq, keq, icontaux, maux, iveceq,$
$numsp, fun, ajac)$
end

Se leen los valores de las concentraciones totales iniciales y se resuelve el sistema invocando la función *calfjeq*, que se detallará en el siguiente apartado.

Funciones y subrutinas

Función *isp*

integer function $isp(index, mreac, numreac)$
parameter $(nreacmax = 200)$
dimension $mreac(nreacmax, 3)$
$isp = 1$
do $j = 1, numreac$
  if$(index$.**eq**.$mreac(j, 3))isp = 0$
enddo
return
end

La función *isp* nos devuelve un 1 si la sustancia contenida en *index* es pura; o un 0 si no lo es.

Subrutina *calfjeq*

A partir de los vectores $\overrightarrow{ct}$ de concentraciones totales de las sustancias puras y de un vector de concentraciones $\overrightarrow{csp}$, la subrutina *calfjeq* proporciona el vector de funciones de equilibrio $fun(i)$ y la matriz jacobiana $ajac(i, j)$.

$\overrightarrow{fun} = -\overrightarrow{ct}$
$(ajac) = (0)$

para $i = 1$, $numeq$
  $prod = keq(i)$
  para $j = 1, icontaux(i)$ (para todos los elementos de la fila i de $maux$)
    $indexi = iveceq(maux(i, j))$ (qué ecuación corresponde a la sustancia $maux(i, j)$)
    $prod = prod * csp(indexi)$ (producto de keq por las concentraciones de la fila i de $maux$)
  finpara

  para $j = 1, icontaux(i)$ (se recorren todos los elementos de la fila i de $maux$)
    $indexi = iveceq(maux(i, j))$
    $fun(index(i)) = fun(index(i)) + prod$
    para $l = 1, icontaux(i)$
      $indexj = iveceq(maux(i, l))$
      $sum = prod/csp(indexj)$ (equivale a derivar el término)
      $ajac(indexi, indexj) = ajac(indexi, indexj) + sum$ (se actualiza el elemento de $ajac$)
    finpara
  finpara
finpara

Se resuelve el sistema mediante una modificación del método de Newton-Raphson que controla el vector de actualizaciones en cada iteración.

Calcular $(ajac)$ y $\overrightarrow{fun}$ a partir de $\overrightarrow{csp}$ mediante CALFJEQ
$fant = ||\overrightarrow{fun}||$
$test = 1.$

mientras $(test > valor)$
  resolver $(ajac)\overrightarrow{zz} = -\overrightarrow{fun}$
  $\overrightarrow{caux} = \overrightarrow{csp} + \overrightarrow{zz}$
  calcular $\overrightarrow{fsig} = \overrightarrow{fun}(\overrightarrow{caux})$
  mientras $(fsig > fant,$ o algún $caux(i) < 0,$ o algún $caux(i) > ct(i))$
    $\overrightarrow{zz} = \overrightarrow{zz}/2$
    $\overrightarrow{caux} = \overrightarrow{csp} + \overrightarrow{zz}$
    recalcular $\overrightarrow{fsig} = \overrightarrow{fun}(\overrightarrow{caux})$
  finmientras
  $\overrightarrow{csp} = \overrightarrow{caux}$
  $test = ||\overrightarrow{zz}||$
  $fant = fsig$
finmientras

El algoritmo anterior, se encuentra traducido en FORTRAN a continuación.

```
subroutine calfjeq(ct,csp,numeq,keq,icontaux,maux, iveceq,numsp,fun,ajac)
parameter (numeqmax = 400, ncolmax = 20, numspmax = 20)
implicit double precision (a − h, o − z)
dimension ct(numspmax), csp(numspmax)
dimension icontaux(numeqmax), iveceq(numeqmax)
dimension maux(numeqmax, 3 ∗ ncolmax)
dimension fun(numspmax), ajac(numspmax, numspmax)
double precision keq(numeqmax)


do i = 1, numsp
   fun(i) = −ct(i)
enddo
do i = 1, numsp
   do j = 1, numsp
      ajac(i, j) = 0.d0
   enddo
enddo
do i = 1, numeq
   prod = keq(i)
   do j = 1, icontaux(i)
      indexi = iveceq(maux(i, j))
      prod = prod ∗ csp(indexi)
   enddo
   do j = 1, icontaux(i)
      indexi = iveceq(maux(i, j))
      fun(indexi) = fun(indexi) + prod
      do l = 1, icontaux(i)
         indexj = iveceq(maux(i, l))
         sum = prod/csp(indexj)
         ajac(indexi, indexj) =
         ajac(indexi, indexj) + sum
      enddo
   enddo
enddo
return
end
```

Referencias

[1] Crank, J. *The Mathematics of Diffusion.* Clarendon Press, Oxford, **1975**.

[2] Ames, W. F. *Numerical Methods for Partial Differential Equations.* Academic Press, London, **1992**.

[3] Hager, W. W. *Applied Numerical Linear Algebra.* Prentice-Hall, **1988**.

[4] Press, W., Flannery, B., Teukolsky, S. and Vetterling, W. *Numerical Recipes. The Art of Scientific Computing.* Cambridge University Press, **1987**.

[5] Garmo, O., Lehto, N., Zhang, H., Davison, W., Royset, O. and Steinnes, E. Dynamic aspects of DGT as demonstrated by experiments with lanthanide complexes of a multidentate ligand. *Environmental Science and Technology* 40(15), **2006**: 4754–4760.

[6] Zhang, H. and Davison, W. Direct in situ measurements of labile inorganically and organically bound metal species in synthetic solutions and natural waters ussing diffusive gradients in thin films. *Analytical Chemistry* 72, **2000**: 4447–4457.

[7] Mitchell, A. and Griffiths, D. *The Finite Difference Method in Partial Differential.* John Wiley and Sons, **1980**.

[8] Hughes, T. J. *The Finite Element Method: Linear Static and Dynamic Finite Element Analysis.* Prentice-Hall, **1987**.

3

Key Role of the Resin Layer Thickness in the Lability of Complexes Measured by DGT

Part of the content of this chapter has been published in:
***Environmental Science and Technology* 45(11), 2011: 4869–4875.**

3.1 Introduction

The uptake of metal cations from water by biota induces a flux. When the uptake is fast compared to the possible rate of supply from solution, complexes with the ligands present in natural waters may affect the flux by modifying the mobility of the metal species or kinetically limiting the dissociation processes [1, 2]. The concept of lability is useful to indicate the ability of complexes to contribute to the metal flux. Lability criteria are simple inequalities aimed at deciding whether the metal flux is limited by the dissociation processes, in which case the system is called partially labile, or by the transport of the species to the limiting surface, in which case the system is termed (fully) labile [3–7]. A quantitative evaluation of the complex contribution to the metal flux is provided by the lability degree, ξ. This parameter is the ratio of the actual contribution of the complex to the metal flux, to the maximum contribution reached if the complex was labile.

Thus, ξ is defined [6] as

$$\xi = \frac{J - J_{\text{free}}}{J_{\text{labile}} - J_{\text{free}}} \tag{3.1}$$

where J denotes the actual metal flux, J_{free} the metal flux due to the free metal in the system if there was no contribution from the complex (i.e. inert case, also labelled J_{inert}) and J_{labile} is the metal flux expected in the system if the complex was fully labile. The lability degree has been evaluated under different conditions and analytical expressions have been reported for limiting situations such as excess of ligand and steady-state conditions [1, 8–15]

DGT [16–18] has emerged as a powerful technique for in situ measurement of metal fluxes. It comprises a resin layer that strongly binds the metal ions, covered with a gel and filter layer that defines a diffusion domain. DGT has successfully been applied to the measurement of metals [16], radionuclides [19] and anions, including phosphate [20], in waters, as well as a range of determinands in sediments [21] and soils [22]. The measurement of the accumulated moles n, allows the computation of an "effective" concentration c_{DGT}, via $c_{\text{DGT}} = ng/ADt$, where g is the thickness of the DGT gel and filter layer, A is the sensor exposed area, D is the metal diffusion coefficient and t the accumulation time.

Discussion of the lability information conveyed by DGT measurements has so far always involved assumptions [18, 23–25]. According to the simplest interpretation, the metal concentration at the resin surface has been assumed to be zero and expressions for the lability degree derived for voltammetry have been applied [18]. This is a very good approximation for labile complexes, as they fully dissociate at the resin surface where, because of strong and rapid binding, the concentration of uncomplexed metal is reasonably assumed to be zero. However, since partially labile complexes do not fully dissociate at the resin surface and can diffuse within the resin layer, the approximation cannot be used generally to study the lability of complexes.

It was the aim of this work to:

- develop a detailed numerical model of the DGT measurement for quantifying the contribution of the complexes to the metal flux;
- assess the impact of the resin layer on the lability of complexes; and
- compare the model predictions with experimental data for the Cd-NTA system.

3.2 Mathematical Formulation

Let us consider, in solution, the complexation of a metal M with a ligand L according to the scheme

$$\mathrm{M} + \mathrm{L} \underset{k_\mathrm{d}}{\overset{k_\mathrm{a}}{\rightleftharpoons}} \mathrm{ML}, \tag{3.2}$$

with corresponding equilibrium conditions

$$K = \frac{k_\mathrm{a}}{k_\mathrm{d}} = \frac{c^*_\mathrm{ML}}{c^*_\mathrm{M} c^*_\mathrm{L}}, \tag{3.3}$$

where K, k_a and k_d are respectively the equilibrium, and the association and dissociation rate constants of the complexation process, whereas c^*_i labels the concentration of species i in the bulk solution.

The model is similar to that used previously [24, 25]. The diffusion domain is considered to comprise two layers, the resin layer ($0 < x < r$) and the gel layer ($r < x < r + g$), where r and g are the thickness of the resin and gel layers respectively. Species M, L, and ML can diffuse through these layers. Thus, we assume that metal can penetrate into the resin layer and bind to the resin sites according to the scheme

$$\mathrm{M} + \mathrm{R} \underset{k_\mathrm{d,R}}{\overset{k_\mathrm{a,R}}{\rightleftharpoons}} \mathrm{MR}, \tag{3.4}$$

with $k_\mathrm{a,R}$, $k_\mathrm{d,R}$ and $K_\mathrm{R} = k_\mathrm{a}/k_\mathrm{d}$, labelling the corresponding kinetic and stability constants. We assume that the complex also penetrates into the resin gel, but does not form ternary complexes with the resin, so that metal has to dissociate previously to bind to the resin sites [26].

When Chelex is used as the resin, the beads are mainly present near to the diffusive gel side of the resin gel [17]; however, as a first approximation, resin sites are here assumed to be evenly distributed. Excluded volume or Donnan effects of the resin beads are neglected [27]. Penetration of complexes in the resin gel has been demonstrated [28] and is reasonable considering that the resin disc comprises binding agent dispersed in the same gel used for the gel layer. There is evidence that the diffusion domain extends into the adjoining solution. For deployments in solution, the thickness of this extra layer is called the diffusive boundary layer (DBL) [18]. Here it will not be explicitly considered since, if the difference between the respective diffusion coefficients of M, L and ML in the solution and the gel layer is negligible, the existence of the DBL can be accounted for by simply increasing the effective value of g. The diffusion coefficients of metal ions in the filter commonly used to cover the gel layer have been shown to be similar to the values in the gel layer. Therefore this layer can also be considered by extending g.

The mathematical formulation of the schemes 3.2 and 3.4 leads to diffusion equations including kinetic source terms for M, L and ML in both gel and resin domains, while extra reacting terms with the resin sites have to be included for the metal in the resin layer. For the resin, we consider a reaction involving metal, free sites (R) and sites occupied by metal (MR), with the corresponding kinetic and stability constants. No diffusion of the resin beads or their sites is considered.

The boundary value problem is defined by bulk equilibrium concentrations at the gel/solution interface, while null flux of all the diffusive species is assumed at the plane $x = 0$, the side of the resin layer opposite to that contacting the gel. At the interface between gel and resin layers, continuity of the concentrations and fluxes is assumed.

Initial conditions are defined by equilibrium concentrations in the solution, while the concentrations of M, L and ML are zero in the gel phase. The numerical solution is achieved by means of the fast iterative procedure described in Chapter 2. Details of both, the mathematical formulation and numerical solution can be found in Section 3.A.1 and Chapter 2.

3.3 Lability of Complexes as Measured by DGT

Let us denote by J the flux of metal that is binding to the resin beads. At time, t, the number of moles of metal bound to the resin is then given by

$$n = A \int_0^t J \mathrm{d}t. \tag{3.5}$$

Notice that, in the transient regime, J differs from the metal flux crossing the plane $x = r$,

$$J_r = D_{\mathrm{M}} \frac{\partial c_{\mathrm{M}}}{\partial x}\bigg|_{x=r} + D_{\mathrm{ML}} \frac{\partial c_{\mathrm{ML}}}{\partial x}\bigg|_{x=r},$$

since part of the metal and complex crossing this surface can accumulate in the resin layer. Instead,

$$J = D_{\mathrm{M}} \frac{\partial c_{\mathrm{M}}}{\partial x}\bigg|_{x=r} + D_{\mathrm{ML}} \frac{\partial c_{\mathrm{ML}}}{\partial x}\bigg|_{x=r} - \int_0^r \frac{\partial c_{\mathrm{M}}}{\partial t} \mathrm{d}x - \int_0^r \frac{\partial c_{\mathrm{ML}}}{\partial t} \mathrm{d}x. \tag{3.6}$$

A numerical simulation tool of the DGT system was developed and used to calculate J and the lability degree, ξ (see Chapter 2 for details). Results of

the flux and the lability degree as a function of kinetic dissociation constant, in a system with only a metal and a single ligand, are shown in Figure 3.1.

The continuous line with triangles in Figure 3.1 shows an increase in both the flux received by the resin (panel a) and the lability degree (panel b) as the dissociation constants increase (keeping a fixed stability constant). The increase of the metal flux reflects the increasing contribution of the complex as the dissociation process becomes faster. This contribution reaches an upper limit (the labile situation) when dissociation proceeds so quickly that a local equilibrium is essentially reached at any time and spacial position. The flux is then solely limited by transport. In the numerical simulation J_{labile} is obtained as

$$J_{\text{labile}} = \lim_{\substack{k_a, k_d \to \infty \\ k_a/k_d \to K}} J$$

while

$$J_{\text{free}} = \lim_{\substack{k_a, k_d \to 0 \\ k_a/k_d \to K}} J$$

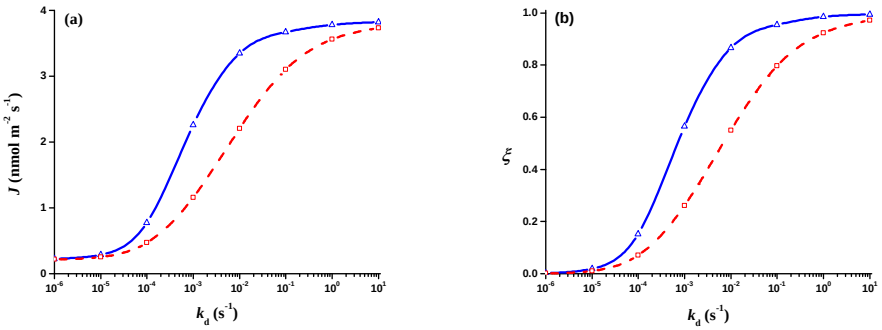

Figure 3.1: (a) Metal flux received by the DGT sensor versus dissociation constant of the complex (k_d). (b) Lability degree of a complex in terms of k_d. Triangles and blue continuous line: values obtained by numerical simulation with $r = 4 \times 10^{-4}$ m . Squares and red dashed line: values obtained by numerical simulation with $r = 0$. Numerical simulation results for 4, 7 and 15 hours coincide. Parameters: $K = 10^2$ m^3 mol^{-1}; $g = 1.13 \times 10^{-3}$ m; $D_M = D_{M,R} = 6.09 \times 10^{-10}$ m^2 s^{-1}; $D_L = D_{L,R} = 4.26 \times 10^{-10}$ m^2 s^{-1}; $c_{T,M} = 10^{-2}$ mol m^{-3}; $c_{T,L} = 0.249$ mol m^{-3}; $k_{a,R} = 10^{15}$ m^3 mol^{-1} s^{-1}; $k_{d,R} = 10^{-6}$ s^{-1}; and $c_{T,R} = 10^{-2}$ mol m^{-3}.

Both panels in Figure 3.1 represent the system after it has reached a *quasi steady-state* regime with practically time-independent concentration profiles of M, ML and L. We denote this situation as quasi steady state because the profiles of MR and R do change continuously. The time to reach this quasi steady state can be estimated as the time needed for the flux (calculated via

numerical simulation) to reach 95% of the steady-state flux. Although this time depends also on the gel thickness, we highlight here its dependence on the kinetic constants. For the data of Figure 3.1, it increases from a value close to 19 min for non labile or fully labile complexes (in agreement with the expression $t \approx g^2/2D_{\mathrm{M}}$) up to 86 min for partially labile complexes ($\xi \approx 0.5$). So, especially for both extreme kinetic situations, this time is negligible relative to the typical deployment times.

As indicated in the caption of Figure 3.1, the flux to the resin at 4, 7 or 15 hours superimpose. In this situation, all the metal and complex transported gets bound to the resin without saturation, while the ligand arising in the resin layer from the complex dissociation diffuses towards the bulk solution. In agreement with the flux results, the lability degree also becomes time independent.

We now consider the influence of the resin layer on the lability degree. Figure 3.1 also depicts the flux and the lability degree of the complex assuming that it was unable to penetrate into the resin layer (discontinuous line with squares). These values have been computed with the numerical simulation using $r = 0$ and coincide with those obtained from Eqns 14 and 22 of Salvador *et al.* [9] that were developed for a planar voltammetric sensor and an electro-inactive complex under diffusion limited conditions.

As seen in Figure 3.1, the penetration of the complex into the resin layer increases both the metal flux and the lability degree. The importance of this effect on the dynamic properties of DGT behaviour is clear. For the parameters of Figure 3.1, the lability degree of a complex with $\xi = 0.6$ according to a standard DGT set up, is halved to $\xi = 0.3$ if it is unable to penetrate into the resin layer. Figure 3.1 indicates that the relevance of this phenomenon vanishes for inert or fully labile complexes, since in the first case the complex never dissociates, whereas in the second one it is fully dissociated at the resin-gel interface (i.e. at $x = r$). Accordingly, continuous and discontinuous lines merge in the rightmost and leftmost parts of Figure 3.1.

Figure 3.2 aids understanding of the influence of the resin on the lability degree by plotting the concentration profiles with and without penetration of the complex into the resin layer. The complex concentration profile is more depleted when it can penetrate into the resin layer, since net dissociation takes place not only in the reaction layer of the gel domain, but also in the resin domain.

From an environmental point of view, the present results indicate that in a DGT sensor, complexes are more labile than could be expected if the penetration of the complex into the resin was not considered. Consequently,

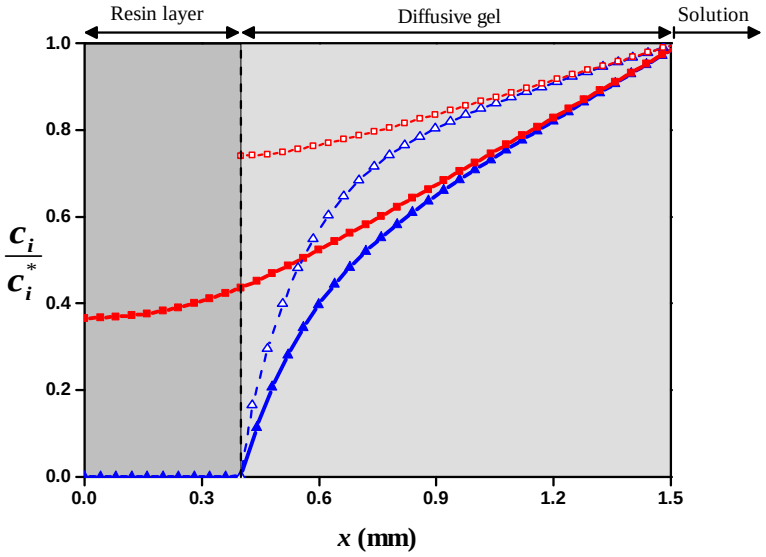

Figure 3.2: Normalized concentration profiles of M (triangles) and ML (squares). Blue continuous line with blue triangles and red continuous line with red squares depict profiles obtained by the numerical simulation for $r = 4 \times 10^{-4}$ m. Blue dashed line with blue open triangle and red dashed line with red open square show numerical simulation results for $r = 0$. Parameters: $k_a = 10^{-1}$ m^3 mol^{-1} s^{-1} and $k_d = 10^{-3}$ s^{-1}. The rest of parameters as in Figure 3.1.

lability and flux expressions that do not explicitly consider the complex penetration into the resin layer can fail in their predictions.

3.4 The Cd-NTA Experimental System

Nitrilotriacetic acid (NTA), an organic ligand that forms strong complexes with metal ions, has been used as a model of natural organic ligands. Previous studies, see Diaz *et al.* [29] and references therein, have shown that Cd(II) and NTA^{3-} form a stable 1:1 ML complex and that the 1:2 ML_2 form is produced only in the presence of a large excess of ligand. The association-dissociation kinetics of the ML complex renders it voltammetrically partially labile, with a strong dependence on pH; low pH values decrease its inert character by increasing ML dissociation, whereas at higher pH values the system approaches totally inert behavior [29]. As time scales for dissociation are larger in DGT than in voltammetry and even larger when penetration of the complexes into the resin layer is considered, a more labile behaviour of the Cd-NTA with DGT is expected [5]. NTA is involved in four protonation

processes, but, to our knowledge, no other complexes between Cd and other protonated forms of NTA have been reported, so a more elaborate scheme than a simple metal ligand is not required [30]. From now on, electric charges will be omitted for simplicity and NTA will refer to the species NTA^{3-}, while NTA_T will be used to refer to the total NTA concentration, including NTA bound to Cd and the free species, regardless of their protonation state.

Experiments to measure the Cd accumulation in a DGT sensor from a solution of Cd-NTA at different pH and concentrations have been conducted. See Section 3.A.3 for experimental details.

Figure 3.3 depicts the normalized Cd accumulation for a reference system where just Cd is present (i.e., without NTA). The ratio of accumulated moles to total Cd concentration, $n/c_{T,Cd}$, is used as ordinate axis to include in the same figure the results obtained for different Cd concentrations.

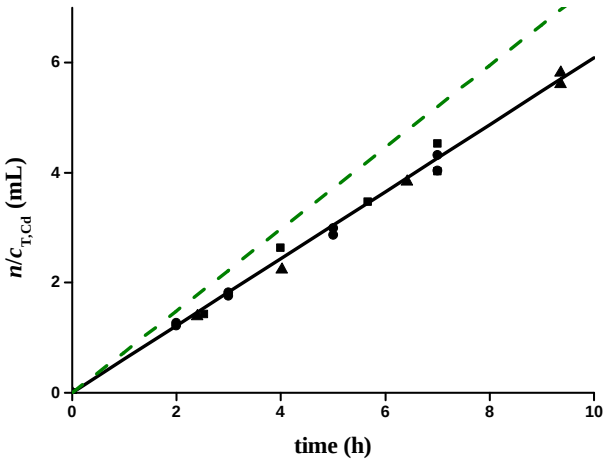

Figure 3.3: DGT accumulation in a system with only Cd present. Markers: experimental measurements with different Cd concentrations: 1.11×10^{-2} mol m^{-3} (▲); 1.06×10^{-2} mol m^{-3} (●); and 9.96×10^{-3} mol m^{-3} (■). Cd accumulation expected according to Eqn 3.7 for a diffusion domain whose thickness is $g = 0.925 \times 10^{-3}$ m (green dashed line) and $g = 1.13 \times 10^{-3}$ m (black line) . Other parameters: $D_{Cd} = 6.09 \times 10^{-10}$ m^2 s^{-1}, $r = 4 \times 10^{-4}$ m and $I = 0.05$ M.

The good linearity observed in Figure 3.3 indicates that quasi steady-state conditions are quickly reached (after 13 min, the transient regime has practically finished since, then, the flux is already 95% of the steady-state one).

Using the simplest interpretation,

$$\frac{n}{c_{\mathrm{T,Cd}}} = \frac{JA}{c_{\mathrm{T,Cd}}}t = \frac{D_{\mathrm{Cd}}A}{g}t, \tag{3.7}$$

so the slope of Figure 3.3 can be used to fit an effective thickness of the diffusion domain. Using $D_{\mathrm{Cd}} = 6.09 \times 10^{-10}$ m^2 s^{-1} (DGT Research Ltd., http://www.dgtresearch.com), the effective thickness of the diffusion layer is 1.13×10^{-3} m. The difference between this value and the nominal g of the DGT devices of 0.925×10^{-3} m provides a measure of the DBL thickness of 205 μm, similar to other reported values in well-stirred systems [18, 23, 28, 31, 32]. Notice that, by using the total Cd concentration in Eqn 3.7 we are assuming that any species in solution that contain Cd (ionic pairs like $CdNO_3^+$, for instance) are labile and have the same diffusion coefficient as free Cd.

The accumulation of Cd in the presence of NTA at different pH and $\mathrm{NTA_T}$ concentrations is depicted in Figure 3.4 (and also in Figures 3.7 and 3.8 of the Supporting Information, page 59). Speciation calculations for all the conditions of these figures with Visual MINTEQ [33] indicate that the free Cd concentration is negligible (0.028% of total Cd) in these systems, since almost all Cd is complexed to the NTA (Cd-NTA, 98.65%). As Cd-$(\mathrm{NTA})_2$ is only 1.3% of total Cd, it can be neglected and only free Cd and Cd-NTA will be considered. Dividing the accumulated mass reported in Figures 3.4, 3.7 or 3.8 by the total Cd concentration yields an almost common accumulation factor ($n/c_{\mathrm{T,Cd}}$ versus t for all the different figures superimpose), with a value 0.7 lower than the accumulation factor found when only Cd was present in the system (Figure 3.3). The diffusion coefficient of the complex has been reported to be 0.7 times that of the free metal, that is $\epsilon = D_{\mathrm{ML}}/D_{\mathrm{M}} = 0.7$ [34]. Therefore, the results of Figure 3.4 indicate that the system is fully labile.

Let us now estimate the rest of parameters of the Cd-NTA system under the conditions of Figure 3.4 in order to compare the experimental measurements with the corresponding predictions derived from the numerical simulation.

Due to the protonation processes, the complexation of NTA with Cd may shift the H-NTA species towards dissociation and in this way modify all the protonation equilibria. Thus, balance equations for the ligand concentration (NTA) have to include protonation kinetic terms. Considering that protonation processes are much faster than metal complexation, this problem can be rewritten as formally identical to a problem with only one ligand [35] with an effective ligand concentration, stability constant and kinetic association

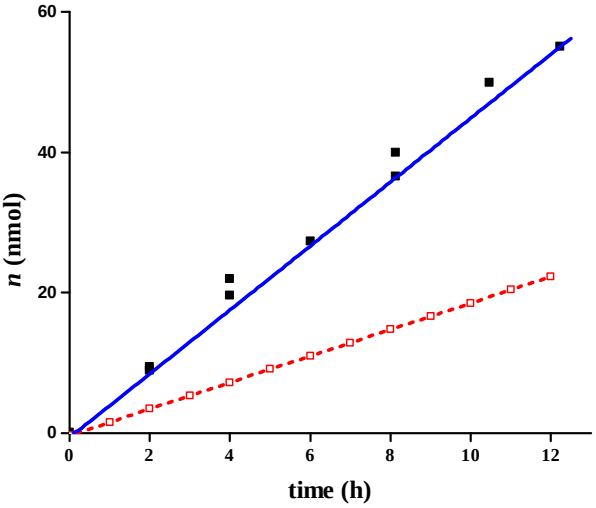

Figure 3.4: Moles of Cd accumulated by DGT in presence of NTA. Marker (■): experimental measurements. Blue line: theoretical accumulation predicted by numerical simulation when there is penetration of the complex into the resin layer ($r = 4 \times 10^{-4}$ m). Red dashed line plus (□): theoretical accumulation predicted by numerical simulation when there is not penetration of the complex into the resin layer ($r = 0$). Parameters: total NTA concentration, $c_{\mathrm{T,NTA}} = 0.249$ mol m^{-3}; Total Cd concentration, $c_{\mathrm{TC_d}} = 1.08 \times 10^{-2}$ mol m^{-3}; pH = 7.50; $I = 0.05$ M; $k_{\mathrm{a}}^{\mathrm{eff}} = 2.58 \times 10^{5}$ m^3 mol^{-1} s^{-1}; $k_{\mathrm{d}}^{\mathrm{eff}} = 2.76$ s^{-1}. The rest of parameters as in Figure 3.1.

constant given by (see Section 3.A.5 for details)

$$c_{\mathrm{NTA}}^{\mathrm{eff}} = c_{\mathrm{NTA^{3-}}}(1 + \beta_{\mathrm{H},1}c_{\mathrm{H^+}} + \beta_{\mathrm{H},2}c_{\mathrm{H^+}}^2 + \beta_{\mathrm{H},3}c_{\mathrm{H^+}}^3 + \beta_{\mathrm{H},4}c_{\mathrm{H^+}}^4), \tag{3.8}$$

$$K_{\mathrm{CdNTA}}^{\mathrm{eff}} = \frac{K_{\mathrm{CdNTA}}}{(1 + \beta_{\mathrm{H},1}c_{\mathrm{H^+}} + \beta_{\mathrm{H},2}c_{\mathrm{H^+}}^2 + \beta_{\mathrm{H},3}c_{\mathrm{H^+}}^3 + \beta_{\mathrm{H},4}c_{\mathrm{H^+}}^4)}, \tag{3.9}$$

$$k_{\mathrm{a}}^{\mathrm{eff}} = \frac{k_{\mathrm{a}}}{(1 + \beta_{\mathrm{H},1}c_{\mathrm{H^+}} + \beta_{\mathrm{H},2}c_{\mathrm{H^+}}^2 + \beta_{\mathrm{H},3}c_{\mathrm{H^+}}^3 + \beta_{\mathrm{H},4}c_{\mathrm{H^+}}^4)}. \tag{3.10}$$

A common diffusion coefficient is assumed for all the protonated NTA species as well as for Cd-NTA, so that this common diffusion coefficient also applies to NTA$^{\mathrm{eff}}$. With these definitions the effective ligand concentration is just the addition of all the protonated NTA species. Since almost all Cd is bound as Cd-NTA, a good approximation for $c_{\mathrm{NTA}}^{\mathrm{eff}}$ is

$$c_{\mathrm{NTA}}^{\mathrm{eff}} \approx c_{\mathrm{T,NTA}} - c_{\mathrm{T,Cd}}.$$

The association kinetic constant for Cd-NTA is estimated from the Eigen

mechanism [35, 36]. According to Eigen ideas, the association kinetic constant is given by the product of the stability constant for the outer sphere complex, K^{os}_{CdNTA}, times the kinetic constant for the release of a water molecule from the inner hydration sphere of the metal, k_w. With $K^{os}_{CdNTA} = 2.22\ m^3\ mol^{-1}$ for a ionic strength of 0.05 M and $k_w = 3 \times 10^8\ s^{-1}$ [37], k_a is estimated to be $4.96 \times 10^7\ m^3\ mol^{-1}\ s^{-1}$, so that with the data of Figure 3.4, $k^{eff}_a = 2.58 \times 10^5\ m^3\ mol^{-1}\ s^{-1}$. Since $K^{eff}_{CdNTA} = 1.5 \times 10^4\ m^3\ mol^{-1}$ for the conditions of Figure 3.4, k^{eff}_d is then given by

$$k^{eff}_d = \frac{k^{eff}_a}{K_{CdNTA}} = 2.76\ s^{-1}. \tag{3.11}$$

With these parameters, the simulation tool described in Chapter 2 that takes into account the thickness of the resin layer produces the continuous line depicted in Figure 3.4, in good agreement with the experimental data. However, if the condition $r = 0$ is used to simulate the experiment, the accumulation predicted with the above parameters underestimates the accumulation experimentally obtained (dashed line in Figure 3.4).

Accordingly, for the conditions of Figure 3.4, the model predicts a lability degree of only 50% without considering penetration of the complex into the resin layer, while the simulation of a DGT sensor that considers this penetration predicts $\xi = 0.99$, as observed experimentally. These results clearly demonstrate the important effect of the resin layer, which increases the lability degree of the complexes in comparison to the lability degree expected when this layer is not considered.

Notice that the simulation requires a value for the kinetic and stability constants of the metal-resin complex, as well as a capacity of the resin for binding metal. The dependence of the simulation results on these particular values is negligible provided the kinetic association constant and stability constant for metal binding to resin are high enough to deplete the metal concentration at the resin-gel interface to a very small fraction of its total concentration, and the maximum capacity (of the resin) is high enough to avoid saturation effects. These conditions are fulfilled in typical DGT applications.

3.5 General Implications

For complexes that diffuse into the resin layer, the thickness of the resin layer has a huge influence on their lability degree. If the free metal concentration is negligible inside the resin layer, the dissociation of the complexes which penetrate into the resin layer adds to the measured metal and dramatically

increases the lability degree. Expressions for the lability degree deduced in the context of voltammetric techniques are, in general, inapplicable to the DGT measurements, as they neglect the complex penetration into the resin layer.

Experimental results for the Cd-NTA system obtained at different pH and NTA concentrations were consistent with fully labile behaviour. The results were accurately simulated using a dynamic numerical model that included penetration of complexes into the resin layer, but the simulated accumulations were substantially lower than measured when complexes were excluded from the resin layer.

According to these findings, DGT can be expected to measure a greater proportion of the metal in a natural water than previously thought, because most metal complexes can be expected to be labile. Field measurements support this suggestion. In situ measurements of Zn, Cu and Mn by DGT agree well with total filterable concentrations for a wide range of waters [38–40]. Lower DGT values for Cu and Ni at low concentrations have been attributed to the partial lability of their complexes with humic substances, consistent with the very strong complexes with Cu and the known slow dissociation of Ni complexes. The consistently higher concentrations of Cu in natural waters measured by DGT compared to voltammetry [39] probably reflects the increased lability associated with the resin layer, rather than simply reflecting a larger dissociation region given by the diffusive layer.

Some studies have indicated that labile complexes are the main source of bioaccumulated metal [41, 42]. The high degree of lability that the DGT measurement confers on a system suggests that DGT measurements can be well suited to assess biouptake in these cases. Detailed interpretation of the DGT measurements in terms of equilibrium speciation in solution and rates of complex dissociation needs to consider fully the effect of the penetration of complexes into the resin layer. Measurements that vary this thickness are therefore likely to be informative, while they do not suffer the disadvantages of markedly reducing the measured mass, as occurs as the diffusive layer thickness is increased.

3.A Supporting Information

3.A.1 Numerical Simulation of a DGT Sensor

3.A.1.1 The Model

The model formulation coincides with that of Tusseau-Vuillemin *et al.* [24] and Lehto *et al.* [25].

Let D_i and $D_{i,\mathrm{R}}$ stand for the diffusion coefficients of species i in the diffusive gel or in the resin domain, respectively and let c_i stand for the concentration of species i at a given spatial position x and time t. Total concentrations are denoted as $c_{\mathrm{T},i}$.

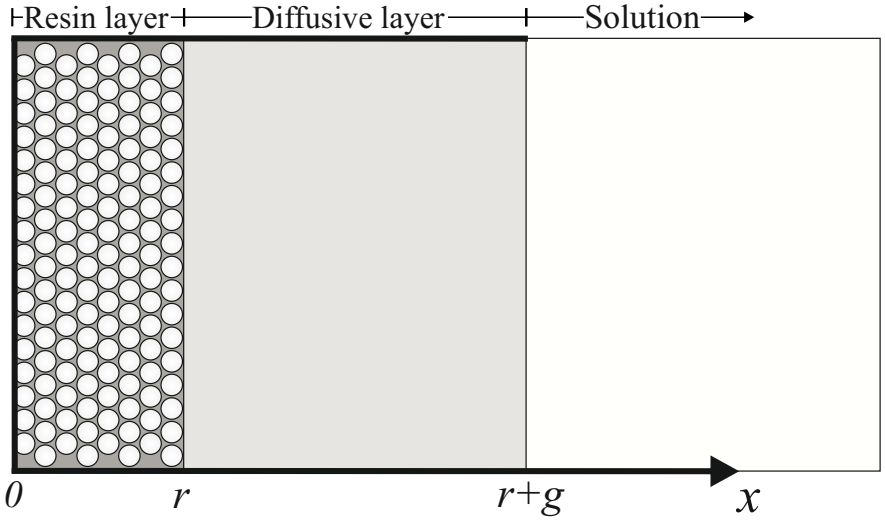

Figure 3.5: DGT Scheme.

According to the scheme in Figure 3.5, we can write the transport equations for the different species inside the domain $(0, r+g)$.

- **For Free Metal (M)**

$$\frac{\partial c_{\mathrm{M}}}{\partial t} = D_{\mathrm{M,R}} \frac{\partial^2 c_{\mathrm{M}}}{\partial x^2} - k_{\mathrm{a}} c_{\mathrm{M}} c_{\mathrm{L}} + k_{\mathrm{d}} c_{\mathrm{ML}} - k_{\mathrm{a,R}} c_{\mathrm{M}} c_{\mathrm{R}} + k_{\mathrm{d,R}} c_{\mathrm{MR}}, \quad (3.12)$$

for $0 < x < r$ and

$$\frac{\partial c_{\mathrm{M}}}{\partial t} = D_{\mathrm{M}} \frac{\partial^2 c_{\mathrm{M}}}{\partial x^2} - k_{\mathrm{a}} c_{\mathrm{M}} c_{\mathrm{L}} + k_{\mathrm{d}} c_{\mathrm{ML}}, \quad (3.13)$$

if $r < x < r + g$.

- **For Ligand (L)**

$$\frac{\partial c_{\mathrm{L}}}{\partial t} = \begin{Bmatrix} D_{\mathrm{L,R}} \\ D_{\mathrm{L}} \end{Bmatrix} \frac{\partial^2 c_{\mathrm{L}}}{\partial x^2} - k_{\mathrm{a}} c_{\mathrm{M}} c_{\mathrm{L}} + k_{\mathrm{d}} c_{\mathrm{ML}}, \tag{3.14}$$

where the curly bracket indicates that $D_{\mathrm{L,R}}$ applies when $0 < x < r$, and D_{L} applies for $r < x < r + g$.

- **For Complex (ML)**

Assuming the same diffusion coefficient for complex and ligand,

$$\frac{\partial c_{\mathrm{ML}}}{\partial t} = \begin{Bmatrix} D_{\mathrm{L,R}} \\ D_{\mathrm{L}} \end{Bmatrix} \frac{\partial^2 c_{\mathrm{ML}}}{\partial x^2} + k_{\mathrm{a}} c_{\mathrm{M}} c_{\mathrm{L}} - k_{\mathrm{d}} c_{\mathrm{ML}}, \tag{3.15}$$

for $0 < x < r + g$.

- **For Resin Free (R) and Occupied (MR) sites**

$$\frac{\partial c_{\mathrm{R}}}{\partial t} = -k_{\mathrm{a,R}} c_{\mathrm{M}} c_{\mathrm{R}} + k_{\mathrm{d,R}} c_{\mathrm{MR}}, \tag{3.16}$$

and

$$\frac{\partial c_{\mathrm{MR}}}{\partial t} = k_{\mathrm{a,R}} c_{\mathrm{M}} c_{\mathrm{R}} - k_{\mathrm{d,R}} c_{\mathrm{MR}}, \tag{3.17}$$

for $0 < x \leq r$. There is no resin in the gel domain so $c_{\mathrm{R}}(x,t) = c_{\mathrm{MR}}(x,t) = 0$ for $r < x < r + g$.

3.A.1.2 Initial and Boundary Conditions

Initial conditions correspond to the absence of metal and ligand in the sensor,

$$\begin{aligned} c_{\mathrm{M}}(x,0) = c_{\mathrm{L}}(x,0) = c_{\mathrm{ML}}(x,0) &= 0 \qquad \text{if} \quad 0 < x < r + g \\ c_{\mathrm{MR}}(x,0) &= 0 \qquad \text{if} \quad 0 < x < r \\ c_{\mathrm{R}}(x,0) &= c_{\mathrm{T,R}} \qquad \text{if} \quad 0 < x < r, \end{aligned} \tag{3.18}$$

where c_{TR} denotes the total concentration of resin sites (free or occupied).

Boundary conditions at $x = r + g$ correspond to bulk concentrations,

$$\begin{aligned} c_{\mathrm{M}}(r+g,t) &= c_{\mathrm{M}}^{*} \\ c_{\mathrm{L}}(r+g,t) &= c_{\mathrm{L}}^{*} \\ c_{\mathrm{ML}}(r+g,t) &= c_{\mathrm{ML}}^{*}. \end{aligned} \tag{3.19}$$

At the gel-resin interface ($x = r$) the M, L and ML concentrations and their fluxes must be continuous, that is,

$$\begin{aligned} c_{\mathrm{M}}(r^{-},t) &= c_{\mathrm{M}}(r^{+},t); & D_{\mathrm{M,R}} \left.\frac{\partial c_{\mathrm{M}}}{\partial x}\right|_{r^{-}} &= D_{\mathrm{M}} \left.\frac{\partial c_{\mathrm{M}}}{\partial x}\right|_{r^{+}} \\ c_{\mathrm{L}}(r^{-},t) &= c_{\mathrm{L}}(r^{+},t); & D_{\mathrm{L,R}} \left.\frac{\partial c_{\mathrm{L}}}{\partial x}\right|_{r^{-}} &= D_{\mathrm{L}} \left.\frac{\partial c_{\mathrm{L}}}{\partial x}\right|_{r^{+}} \\ c_{\mathrm{ML}}(r^{-},t) &= c_{\mathrm{ML}}(r^{+},t); & D_{\mathrm{L,R}} \left.\frac{\partial c_{\mathrm{ML}}}{\partial x}\right|_{r^{-}} &= D_{\mathrm{L}} \left.\frac{\partial c_{\mathrm{ML}}}{\partial x}\right|_{r^{+}}. \end{aligned} \tag{3.20}$$

The continuity of the concentrations indicates that no Donnan effects are considered, so that charge effects of the resin are screened by the supporting electrolyte.

Equations 3.12 to 3.17 with the conditions 3.18 to 3.20 form a coupled system of equations for $c_{\mathrm{M}}(x,t)$, $c_{\mathrm{L}}(x,t)$, $c_{\mathrm{ML}}(x,t)$, $c_{\mathrm{R}}(x,t)$ and $c_{\mathrm{MR}}(x,t)$. The procedure to numerically solve this system is described in Chapter 2.

3.A.2 Concentration Profiles in a DGT Experiment

Let us consider a DGT experiment using the numerical simulation in Chapter 2.

Figure 3.6 depicts the concentration profiles of metal and complex through the DGT layers and adjoining solution for different values of the kinetic complexation constants. With the parameters used in this figure, the metal concentration drops to almost zero at the resin interface due to the strong and fast resin binding. For low values of the dissociation rate constants (see panel a), the complex concentration profile is flat and equal to the complex concentration in solution, while the metal concentration profile is linear. This indicates the inert behaviour of the complex, which does not contribute to the flux received by DGT in the quasi steady-state regime reached (the linear metal concentration profile indicates a time independent metal flux). On increasing the kinetic complexation constants (see panel b), the complex is depleted and its contribution to the metal flux through dissociation is apparent. Notice that the metal concentrations do not increase linearly with distance and their values at a given x are greater than those of the inert case, due to the complex dissociation contributing to a higher local metal

concentration. A further increase of the kinetic constants leads to a more depleted complex concentration profile. Metal and complex concentration profiles increasingly coincide in the gel domain (see panel c). When both normalised profiles coincide, metal and complex are in local equilibrium, indicating that the complex is able to dissociate sufficiently rapidly to maintain equilibrium conditions with the metal. The thickness of the layer where both profiles diverge, can be related to the reaction layer. As expected, the thickness of the reaction layer decreases as the kinetic constants increase. Notice that at the interface between the resin and gel layers the slope of the complex concentration profile is not zero and the complex penetrates into the resin layer. The decrease in the complex concentration as the back plastic wall of the device is approached continues inside the resin, indicating that the dissociation process does not cease at the resin interface. A further increase of the kinetic constants (see panel d) leads to linear metal and complex concentration profiles superimposed throughout the entire gel domain. This corresponds to the labile situation where the dissociation of the complex is so fast that local equilibrium with the metal is reached at each relevant spatial and time position.

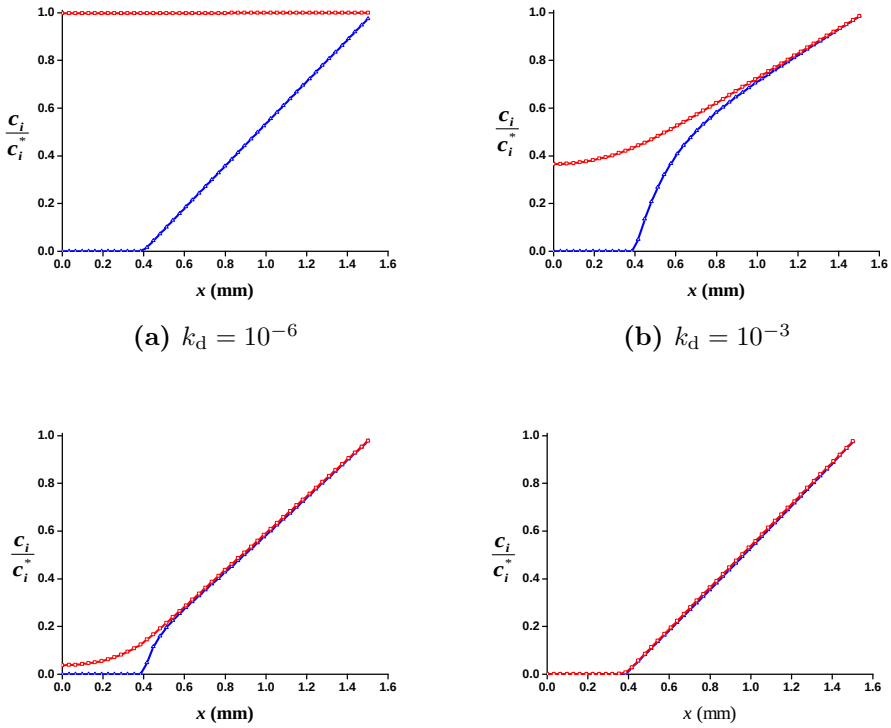

(a) $k_\mathrm{d} = 10^{-6}$ **(b)** $k_\mathrm{d} = 10^{-3}$

(c) $k_\mathrm{d} = 10^{-2}$ **(d)** $k_\mathrm{d} = 10^{0}$

Figure 3.6: Normalized concentration profiles of M (Blue line with blue triangle markers) and ML (red line with red square markers). Profiles are obtained by numerical simulation described in Chapter 2. Parameters: $r = 4 \times 10^{-4}$ m, $K = 10^{2}$ m^3 mol^{-1}. Panel (a): $k_\mathrm{d} = 10^{-6}$ s^{-1}; panel (b): $k_\mathrm{d} = 10^{-3}$ s^{-1}; panel (c): $k_\mathrm{d} = 10^{-2}$ s^{-1}; and panel (d): $k_\mathrm{d} = 10^{0}$ s^{-1}. The rest of parameters as in Figure 3.1.

3.A.3 Experimental Section

3.A.3.1 DGT Sensors

All DGT sensors were purchased from DGT Research Ltd. (Lancaster, U.K.). Commercially available DGT deployment mouldings made of ABS polymer, based on a simple, tight-fitting piston design with a 2 cm diameter window, were used for all measurements. A 0.4 mm thick Chelex-gel was placed on the piston surface with the side packed with resin beads facing upward (i.e., in close contact with the diffusive layer). On the top of the Chelex-gel, a 0.8 mm thick diffusive agarose polyacrylamide gel and a cellulose nitrate membrane (Whatman, pore size 0.45 μm, thickness 0.125 mm) were placed. A more detailed description is found at DGT Research's homepage (http//:www.dgtresearch.com).

3.A.3.2 DGT Experiments

A series of experiments were performed to determine the mass of cadmium accumulated at different times by DGT devices deployed in solutions containing Cd (prepared from the solid nitrate product, Merck, analytical grade) at a concentration close to 10^{-2} mol m^{-3} and NTA (Fluka, analytical grade) at concentrations of 0.249 and 1.8 mol m^{-3}. The pH value was adjusted, by means of small additions of NaOH or HNO_3, to 7 or 7.5 before and during the deployment. Ionic strength of the solution was adjusted to 0.05 mol L^{-1} with $NaNO_3$ (Merck, suprapur). Ultra-pure water (Mill-Q plus 185 System, Millipore) was employed in all the experiments.

3.A.3.3 DGT Exposure Chamber

A 5 L polyethylene bucket was used as the exposure chamber. Eleven DGTs were fixed by press-stud. The pH value was monitored continuously with a glass electrode. A reference electrode Ag/AgCl/3 mol L^{-1} KCl, with a 0.05 mol L^{-1} $NaNO_3$ jacket was used. The exposure chamber was placed in a thermostated bath to keep the deployment solution at constant temperature of 25 ± 0.1 °C. The solution was stirred during deployment using an overhead stirrer.

3.A.3.4 Retrieval and Analysis

For all experiments, aliquots of the solution were collected at regular intervals to check the total Cd concentration. DGT devices, once removed from solution, were rinsed with ultrapure water and opened for removal of the resin gels, which were then eluted in 1 mL of concentrated nitric acid

for at least 24 h. The number of moles of metal in the form of non dissociated complex due to the complex penetration into the resin domain is negligible in comparison with those bound to the resin beads. All solutions were analysed by inductively coupled plasma-optical emission spectroscopy (ICP-OES) (Activa-S, Horiba Scientific).

3.A.4 Additional Figures

Additional figures that verified the influence of the thickness of the DGT resin layer on the accumulated mass for the Cd-NTA system are shown.

Conditional stability constants and kinetic parameters for the Cd-NTA system at a given pH, ionic strength and total metal and total ligand concentration were estimated as reported in Section 3.4. Values used in the numerical simulations for the kinetic association and dissociation constants of the metal to the resin sites are $k_{a,R} = 10^{15}$ m^3 mol^{-1} s^{-1} and $k_{d,R} = 10^{-6}$ s^{-1} while the total concentration of resin sites in the resin layer is $c_{TR} = 10^{-2}$ mol m^{-3}. These values are high enough to neglect saturation effects and to reach an almost null metal concentration at the resin interface.

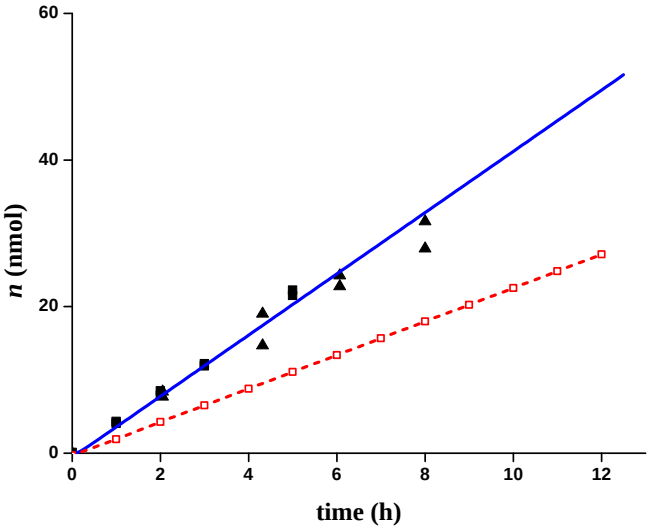

Figure 3.7: Moles of Cd accumulated by DGT in presence of NTA. Markers: experimental measurements for two deployments (■) and (▲). Blue continuous line: theoretical accumulation predicted by numerical simulation when penetration of the complex into the resin layer is considered ($r = 4 \times 10^{-4}$ m). Red dashed line with red empty squares: theoretical accumulation predicted by numerical simulation when penetration of the complex into the resin layer is not allowed ($r = 0$). Parameters: total NTA concentration $c_{\mathrm{T,NTA}} = 0.249$ mol m^{-3}; total Cd concentration $c_{\mathrm{T,Cd}} = 9.96 \times 10^{-3}$ mol m^{-3}; $k_{\mathrm{a}}^{\mathrm{eff}} = 8.87 \times 10^{4}$ m^3 mol^{-1} s^{-1}; $k_{\mathrm{d}} = k_{\mathrm{d}}^{\mathrm{eff}} = 2.76$ s^{-1}; pH = 7.03; $I = 0.05$ M. The rest of parameters as in Figure 3.4.

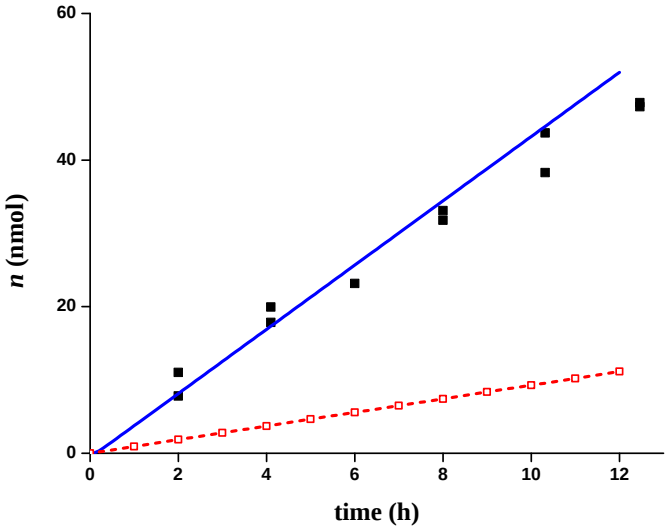

Figure 3.8: Moles of Cd accumulated by DGT in presence of NTA. Markers: experimental measurements (■). Blue continuous line: theoretical accumulation predicted by numerical simulation when penetration of the complex into the resin layer is considered ($r = 4 \times 10^{-4}$ m). Red dashed line with red empty squares markers: theoretical accumulation predicted by numerical simulation when penetration of the complex into the resin layer is not allowed ($r = 0$). Parameters: total NTA concentration $c_{\mathrm{T,NTA}} = 1.8$ mol m^{-3}; total Cd concentration $c_{\mathrm{TCd}} = 1.08 \times 10^{-2}$ mol m^{-3}; $k_{\mathrm{a}}^{\mathrm{eff}} = 2.58 \times 10^{5}$ mol^{-1} m^3 s^{-1}; $k_{\mathrm{d}} = k_{\mathrm{d}}^{\mathrm{eff}} = 2.76$ s^{-1}; pH = 7.50; $I = 0.05$ M. The rest of parameters as in Figure 3.4.

3.A.5 Formulation of the Cd-NTA Speciation in a DGT Sensor as a System with Only One Complex and Ligand Species.

NTA is involved in four acid-base equilibria. Among all these species only NTA^{3-} is known to interact with Cd to give the complex species Cd-NTA and Cd-$(NTA)_2$. Thus, only NTA^{3-} is the ligand in the Cd-NTA system. However, the concentration of NTA^{3-} is not only modified by the presence of Cd, but also by the pH of the system. The formulation of the Cd-NTA system as

$$\mathrm{M} + \mathrm{L} \underset{k_\mathrm{d}}{\overset{k_\mathrm{a}}{\rightleftharpoons}} \mathrm{ML}, \tag{3.21}$$

with a fixed total ligand concentration, c_{TL}, computed as $c_{\mathrm{TL}} = c_{\mathrm{L}} + c_{\mathrm{ML}}$ is then not valid. It is the aim of this section to show that the Cd-NTA system (involving all protonated an unprotonated species) can be reformulated so that equation equivalent to the system represented with scheme 3.21 can be applied.

Let us assume that:

- Protonated and unprotonated NTA species have the same diffusion coefficient, D_{L}.

- The kinetics of interconversion between the protonated/unprotonated NTA species is considered instantaneous (i.e., they are always at equilibrium), so that all the protonated and unprotonated species diffuse and react as one "single species".

A scheme of the processes in solution is:

$$\begin{aligned}
\mathrm{M} + \mathrm{L} &\underset{k_{\mathrm{d,L}}}{\overset{k_{\mathrm{a,L}}}{\rightleftharpoons}} \mathrm{ML} \\
\mathrm{L} + \mathrm{H} &\underset{k_{\mathrm{d1,H}}}{\overset{k_{\mathrm{a1,H}}}{\rightleftharpoons}} \mathrm{HL} \\
\mathrm{HL} + \mathrm{H} &\underset{k_{\mathrm{d2,H}}}{\overset{k_{\mathrm{a2,H}}}{\rightleftharpoons}} \mathrm{H_2L} \\
&\vdots \\
\mathrm{H_3L} + \mathrm{H} &\underset{k_{\mathrm{d4,H}}}{\overset{k_{\mathrm{a4,H}}}{\rightleftharpoons}} \mathrm{H_4L}.
\end{aligned} \tag{3.22}$$

The transport problem can be stated as

$$\frac{\partial c_{\mathrm{M}}}{\partial t} = D_{\mathrm{M}}\frac{\partial^2 c_{\mathrm{M}}}{\partial x^2} - k_{\mathrm{a,L}}c_{\mathrm{M}}c_{\mathrm{L}} + k_{\mathrm{d,L}}c_{\mathrm{ML}}, \tag{3.23}$$

$$\frac{\partial c_{\mathrm{ML}}}{\partial t} = D_{\mathrm{L}}\frac{\partial^2 c_{\mathrm{ML}}}{\partial x^2} + k_{\mathrm{a,L}}c_{\mathrm{M}}c_{\mathrm{L}} - k_{\mathrm{d,L}}c_{\mathrm{ML}}, \tag{3.24}$$

$$\frac{\partial c_{\mathrm{L}}}{\partial t} = D_{\mathrm{L}}\frac{\partial^2 c_{\mathrm{L}}}{\partial x^2} - k_{\mathrm{a,L}}c_{\mathrm{M}}c_{\mathrm{L}} + k_{\mathrm{d,L}}c_{\mathrm{ML}} - k_{\mathrm{a1,H}}c_{\mathrm{H}}c_{\mathrm{L}} + k_{\mathrm{d1,H}}c_{\mathrm{HL}}, \tag{3.25}$$

$$\frac{\partial c_{\mathrm{HL}}}{\partial t} = D_{\mathrm{L}}\frac{\partial^2 c_{\mathrm{HL}}}{\partial x^2} - k_{\mathrm{a2,H}}c_{\mathrm{H}}c_{\mathrm{HL}} + k_{\mathrm{d2,H}}c_{\mathrm{H_2L}} + k_{\mathrm{a1,H}}c_{\mathrm{H}}c_{\mathrm{L}} - k_{\mathrm{d1,H}}c_{\mathrm{HL}}, \tag{3.26}$$

$$\vdots$$

$$\frac{\partial c_{\mathrm{H_4L}}}{\partial t} = D_{\mathrm{L}}\frac{\partial^2 c_{\mathrm{H_4L}}}{\partial x^2} + k_{\mathrm{a4,H}}c_{\mathrm{H}}c_{\mathrm{H_3L}} - k_{\mathrm{d4,H}}c_{\mathrm{H_3L}}. \tag{3.27}$$

Adding the transport equations of all the protonated ligand forms (Eqns 3.25 to 3.27,

$$\frac{\partial c_{\mathrm{LP}}}{\partial t} = D_{\mathrm{L}}\frac{\partial^2 c_{\mathrm{LP}}}{\partial x^2} - k_{\mathrm{a,L}}c_{\mathrm{M}}c_{\mathrm{L}} + k_{\mathrm{d,L}}c_{\mathrm{ML}}, \tag{3.28}$$

where c_{LP} stand for

$$c_{\mathrm{LP}} = c_{\mathrm{L}} + c_{\mathrm{HL}} + c_{\mathrm{H_2L}} + c_{\mathrm{H_3L}} + c_{\mathrm{H_4L}}. \tag{3.29}$$

Since protonation is instantaneous, acid-base equilibria relationship apply:

$$\beta_{i,\mathrm{H}} = \frac{c_{\mathrm{H}_i\mathrm{L}}}{c_{\mathrm{H}}^i c_{\mathrm{L}}},$$

and c_{L} can be rewritten as

$$c_{\mathrm{L}} = \frac{c_{\mathrm{LP}}}{1 + \sum_{i=1}^{4} \beta_{i,\mathrm{H}} c_{\mathrm{H}}^i}.$$

In terms of c_{LP}, Eqns 3.23, 3.24 and 3.28 become

$$\frac{\partial c_{\mathrm{M}}}{\partial t} = D_{\mathrm{M}}\frac{\partial^2 c_{\mathrm{M}}}{\partial x^2} - \frac{k_{\mathrm{a,L}}}{1 + \sum_{i=1}^{4} \beta_{i,\mathrm{H}} c_{\mathrm{H}}^i} c_{\mathrm{M}}c_{\mathrm{LP}} + k_{\mathrm{d,L}}c_{\mathrm{ML}}, \tag{3.30}$$

$$\frac{\partial c_{\mathrm{ML}}}{\partial t} = D_{\mathrm{L}}\frac{\partial^2 c_{\mathrm{ML}}}{\partial x^2} + \frac{k_{\mathrm{a,L}}}{1 + \sum_{i=1}^{4} \beta_{i,\mathrm{H}} c_{\mathrm{H}}^i} c_{\mathrm{M}}c_{\mathrm{LP}} - k_{\mathrm{d,L}}c_{\mathrm{ML}}, \tag{3.31}$$

and

$$\frac{\partial c_{\mathrm{LP}}}{\partial t} = D_{\mathrm{L}} \frac{\partial^2 c_{\mathrm{LP}}}{\partial x^2} - \frac{k_{\mathrm{a,L}}}{1 + \sum_{i=1}^{4} \beta_{i,\mathrm{H}} c_{\mathrm{H}}^i} c_{\mathrm{M}} c_{\mathrm{LP}} + k_{\mathrm{d,L}} c_{\mathrm{ML}}. \tag{3.32}$$

Equations 3.30 to 3.32 are formally identical to a system with one ligand with concentration c_{LP} that is not involved in any protonation equilibria. The effective association and dissociation constants of this ligand with the metal are

$$k_{\mathrm{d}}^{\mathrm{eff}} = k_{\mathrm{d,L}}, \tag{3.33}$$

and

$$k_{\mathrm{a}}^{\mathrm{eff}} = \frac{k_{\mathrm{a,L}}}{1 + \sum_{i=1}^{4} \beta_{i,\mathrm{H}} c_{\mathrm{H}}^i}. \tag{3.34}$$

The effective stability constant of the metal complexation with this formal ligand c_{LP}, of concentration given by Eqn 3.29, is

$$K^{\mathrm{eff}} = \frac{k_{\mathrm{a}}^{\mathrm{eff}}}{k_{\mathrm{d}}^{\mathrm{eff}}} = \frac{K}{1 + \sum_{i=1}^{4} \beta_{i,\mathrm{H}} c_{\mathrm{H}}^i}.$$

References

[1] Galceran, J. and van Leeuwen, H. P. *IUPAC Series on Analytical and Physical Chemistry of Environmental Systems*, chapter Physicochemical kinetics and transport at chemical-biological surfaces. John Wiley, **2004**, 147–203.

[2] Wilkinson, K. J. and Buffle, J. *Physicochemical Kinetics and Transport at Chemical-biological Surfaces*. John Wiley, Chichester, UK, **2004**, 445–533.

[3] Davison, W. Defining the electroanalyticallly measured species in a natural water sample. *Journal of Electroanalytical Chemistry* 87, **1978**: 395–404.

[4] Whitfield, M. and Turner, D. R. *Chemical Modeling in Aqueous Systems*. American Chemical Society, Washington DC, **1979**, 657–680.

[5] De Jong, H. and Van Leeuwen, H. Voltammetry of metal complex systems with different diffusion coefficients of the species involved. *Journal of Electroanalytical Chemistry* 234, **1987**.

[6] Galceran, J., Puy, J., Salvador, J., Cecilia, J. and van Leeuwen, H. Voltammetric lability of metal complexes at spherical microelectrodes with various radii. *Journal of Electroanalytical Chemistry* 505(1-2), **2001**: 85–94.

[7] van Leeuwen, H. Revisited: the conception of lability of metal complexes. *Electroanalysis* 13(10), **2001**: 826–830.

[8] Galceran, J., Puy, J., Salvador, J., Cecilia, J., Mas, F. and Garces, J. Lability and mobility effects on mixtures of ligands under steady-state conditions. *Physical Chemistry Chemical Physics* 5(22), **2003**: 5091–5100.

[9] Salvador, J., Puy, J., Cecilia, J. and Galceran, J. Lability of complexes in steady-state finite planar diffusion. *Journal of Electroanalytical Chemistry* 588(2), **2006**: 303–313.

[10] Salvador, J., Puy, J., Galceran, J., J., Cecilia, J., Town, R. and van Leeuwen, H. Lability criteria for successive metal complexes in steady-state planar diffusion. *Journal of Physical Chemistry B* 110(2), **2006**: 891–899.

[11] Salvador, J., Garces, J., Galceran, J. and Puy, J. Lability of a mixture of metal complexes under steady-state planar diffusion in a finite domain. *Journal of Physical Chemistry B* 110, **2006**: 13661–13669.

[12] Buffle, J., Startchev, K. and Galceran, J. Computing steady-state metal flux at microorganism and bioanalogical sensor interfaces in multiligand systems. A reaction layer approximation and its comparison with the rigorous solution. *Physical Chemistry Chemical Physics* 9, **2007**: 2844–2855.

[13] Salvador, J., Garces, J., Companys, E., Cecilia, J., Galceran, J., Puy, J. and Town, R. Ligand mixture effects in metal complex lability. *Journal of Physical Chemistry A* 111, **2007**: 4304–4311.

[14] Pinheiro, J. P., Salvador, J., Companys, E., Galceran, J. and Puy, J. Experimental verification of the metal flux enhancement in a mixture of two metal complexes: the Cd/NTA/glycine and Cd/NTA/citric acid systems. *Physical Chemistry Chemical Physics* 12(5), **2010**: 1131–1138.

[15] Degryse, F., Smolders, E. and Merckx, R. Labile Cd complexes increase Cd availability to plants. *Environmental Science and Technology* 40(3), **2006**: 830–836.

[16] Davison, W. and Zhang, H. In situ speciation measurements of trace components in natural-waters using thin-film gels. *Nature* 367(6463), **1994**: 546–548.

[17] Zhang, H. and Davison, W. Direct in situ measurements of labile inorganically and organically bound metal species in synthetic solutions and natural waters ussing diffusive gradients in thin films. *Analytical Chemistry* 72, **2000**: 4447–4457.

[18] Warnken, K., Davison, W., Zhang, H., Galceran, J. and Puy, J. In situ measurements of metal complex exchange kinetics in freshwater. *Environmental Science and Technology* 41(9), **2007**: 3179–3185.

[19] Chang, L. Y., Davison, W., Zhang, H. and Kelly, M. Performance characteristics for the measurement of Cs and Sr by diffusive gradients in thin films (DGT). *Analytica Chimica Acta* 368(3), **1998**: 243–253.

[20] Zhang, H., Davison, W., Gadi, R. and Kobayashi, T. In situ measurement of dissolved phosphorus in natural water using DGT. *Analytica Chimica Acta* 370(1), **1998**: 29–38.

[21] Tankere-Muller, S., Zhang, H., Davison, W., Finke, N., Larsen, O., Stahl, H. and Glud, R. Fine scale remobilisation of Fe, Mn, Co, Ni, Cu and Cd in contaminated marine sediment. *Marine Chemistry* 106, **2007**: 192–207.

[22] Degryse, F., Smolders, E., Zhang, H. and Davison, W. Predicting availability of mineral elements to plants with the DGT technique: a review of experimental data and interpretation by modelling. *Environmental Chemistry* 6(3), **2009**: 198–218.

[23] Scally, S., Davison, W. and Zhang, H. In situ measurements of dissociation kinetics and labilities of metals complexes in solution using DGT. *Environmental Science and Technology* 37, **2003**: 1379–1384.

[24] Tusseau-Vuillemin, M. H., Gilbin, R. and Taillefert, M. A dynamic numerical model to characterize labile metal complexes collected with diffusion gradient in thin films devices. *Environmental Science and Technology* 37(8), **2003**: 1645–1652.

[25] Lehto, N., Davison, W., Zhang, H. and Tych, W. An evaluation of DGT performance using a dynamic numerical model. *Environmental Science and Technology* 40(20), **2006**: 6368–6376.

[26] Chakrabarti, C., Lu, Y., Gregoire, D., Back, M. and Schroeder, W. Kinetic-studies of metal speciation using chelex cation-exchange resin – Application to cadmium, copper, and lead speciation in river water and snow. *Environmental Science and Technology* 28(11), **1994**: 1957–1967.

[27] Yezek, L., van der Veeken, P. and van Leeuwen, H. Donnan effects in metal speciation analysis by DET/DGT. *Environmental Science and Technology* 42(24), **2008**: 9250–9254.

[28] Garmo, O., Lehto, N., Zhang, H., Davison, W., Royset, O. and Steinnes, E. Dynamic aspects of DGT as demonstrated by experiments with lanthanide complexes of a multidentate ligand. *Environmental Science and Technology* 40(15), **2006**: 4754–4760.

[29] Diaz, J., Sanchis, J., Chekmeneva, E., Arino, C. and Esteban, M. Non-linear multivariate curve resolution analysis of voltammetric pH titrations. *Analyst* 135(7), **2010**: 1653–1662.

[30] Van Leeuwen, H. P. and Town, R. M. Outer-sphere and inner-sphere ligand protonation in metal complexation kinetics: The lability of EDTA complexes. *Environmental Science and Technology* 43(1), **2009**: 88–93.

[31] Garmo, O., Royset, O., Steinnes, E. and Flaten, T. Performance study of diffusive gradients in thin films for 55 elements. *Analytical Chemistry* 75(14), **2003**: 3573–3580.

[32] Warnken, K., Zhang, H. and Davison, W. Accuracy of the diffusive gradients in thin-films technique: Diffusive boundary layer and effective sampling area considerations. *Analytical Chemistry* 78(11), **2006**: 3780–3787.

[33] Gustafsson, J. Visual Minteq version 3.0, **1991**.

[34] Unsworth, E. R., Zhang, H. and Davison, W. Use of diffusive gradients in thin films to measure cadmium speciation in solutions with synthetic and natural ligands: Comparison with model predictions. *Environmental Science and Technology* 39(2), **2005**: 624–630.

[35] van Leeuwen, H., Town, R. and Buffle, J. Impact of ligand protonation on eigen-type metal complexation kinetics in aqueous systems. *Journal of Physical Chemistry A* 111(11), **2007**: 2115–2121.

[36] van Leeuwen, H. and Town, R. Stripping chronopotentiometry at scanned deposition potential (SSCP). Part 4. The kinetic current regime. *Journal of Electroanalytical Chemistry* 561(1-2), **2004**: 67–74.

[37] Buffle, J., Zhang, Z. and Startchev, K. Metal flux and dynamic speciation at (bio)interfaces. Part 1: Critical evaluation and compilation of physicochemical parameters for complexes with simple ligands and fulvic/humic substances. *Environmental Science and Technology* 41(22), **2007**: 7609–7620.

[38] Gimpel, J., Zhang, H., Davison, W. and Edwards, A. In situ trace metal speciation in lake surface waters using DGT, dialysis, and filtration. *Environmental Science and Technology* 37(1), **2003**: 138–146.

[39] Unsworth, E., Warnken, K., Zhang, H., Davison, W., Black, F., Buffle, J., Cao, J., Cleven, R., Galceran, J., Gunkel, P., Kalis, E., Kistler, D., van Leeuwen, H., Martin, M., Noel, S., Nur, Y., Odzak, N., Puy, J., van Riemsdijk, W., Sigg, L., Temminghoff, E., Tercier-Waeber, M., Toepperwien, S., Town, R., Weng, L. and Xue, H. Model predictions of metal speciation in freshwaters compared measurements by in situ techniques. *Environ Sci Technol* 40, **2006**: 1942–1949.

[40] Warnken, K., Lawlor, A., Lofts, S., Tipping, E., Davison, W. and Zhang, H. In situ speciation measurements of trace metals in headwater streams. *Environmental Science and Technology* 43(19), **2009**: 7230–7236.

[41] Meylan, S., Behra, R. and Sigg, L. Influence of metal speciation in natural freshwater on bioaccumulation of copper and zinc in periphyton: A microcosm study. *Environmental Science and Technology* 38(11), **2004**: 3104–3111.

[42] Ferreira, D., Tousset, N., Ridame, C. and Tusseau-Vuillemin, M. More than inorganic copper is bioavailable to aquatic mosses at environmentally relevant concentrations. *Environmental Toxicology and Chemistry* 27(10), **2008**: 2108–2116.

4

Contribution of Partially Labile Complexes to the DGT Metal Flux

Part of the content of this chapter has been published in:
***Environmental Science and Technology* 45(12), 2011: 5317–5322.**

4.1 Introduction

DGT (Diffusive Gradients in Thin Films) [1–6] is a powerful technique for the in situ measurement of metal fluxes (moles of metal arriving at the sensor per unit area and time), which are relevant to the availability of metals and to gain understanding of ecotoxicological properties of natural media.

Metal availability is influenced by the interactions of metal cations with ligands present in the natural media, and, in particular, by the lability of the complex. Here, we use the term "lability" in its dynamic sense, rather than its thermodynamic one. If we have a sensor or organism that strongly extracts a species (a metal cation, in the present case) from a solution, the resulting flux (uptake/biouptake) could be limited either by diffusion of the complex (the transport due to the free metal is negligible in comparison to that of the complex when $\epsilon K' \gg 1$, a typical condition of interest) or by the kinetics of dissociation. The comparison of the observed metal flux when kinetics of dissociation contribute, with the metal flux when diffusion is the limiting step, gives rise to the lability criteria. A system is termed (fully) labile when kinetics are so fast that the metal flux is limited by diffusion of

the complex. A system is inert when dissociation is so slow that the metal flux is limited by dissociation.

Lability can be quantified [7] with the lability degree, ξ: the ratio of the actual contribution of the complex to the metal flux to the maximum contribution reached if the complex was fully labile.

Details of the most commonly used DGT device are reported elsewhere [8]. The penetration of partially labile complexes into the resin layer is expected for complexes able to diffuse through the gel layer, since the resin disc and the gel disc are usually made with the same polymer. Recently, it was shown that in a DGT measurement, the penetration of the complex into the resin layer greatly affects the metal flux and the lability degree of the complex [8]. It was also shown that expressions reported for the lability of complexes in voltammetric sensors (where penetration of complexes into the electrode is not allowed) were, in general, not applicable to DGT, since the resin layer is a characteristic feature of DGT. Accumulations of Cd in the resin layer of DGT deployed in various Cd-nitrilotriacetic acid (NTA) solutions were successfully predicted using a numerical simulation considering complex penetration into the resin layer, while expressions derived for voltammetry underestimated the accumulated Cd.

It was the aim of this work to:

- develop analytical expressions for quantifying the contribution of the complexes to the metal flux for typical DGT configurations;
- compare these expressions with numerical simulations and experimental data for the Cd-NTA experimental system;
- advance the conceptual understanding of the factors impacting on the DGT response and their relevance to natural systems; and
- provide general diagrams to assess the lability of any complex in a standard DGT configuration.

4.2 The Model

Let us consider, in solution, the complexation of a metal M with a ligand L to form a complex ML according to the scheme

$$\mathrm{M} + \mathrm{L} \underset{k_\mathrm{d}}{\overset{k_\mathrm{a}}{\rightleftharpoons}} \mathrm{ML}, \tag{4.1}$$

We make several assumptions:

(i) Only free metal ions, M, bind rapidly and strongly to the resin, so that the free metal concentration c_{M} inside the resin layer is negligible,

$$\mathrm{M} + \mathrm{R} \rightharpoonup \mathrm{MR}. \tag{4.2}$$

(ii) The complex, ML, can penetrate inside the resin layer, of thickness r, where its dissociation still proceeds, but direct binding of the complex to the resin sites via ternary complexes is not considered [9]. Thus, the complex inside the resin layer acts as a source of metal that gets bound to the resin. Binding sites in the resin are evenly distributed in the resin domain and are immobile.

(iii) Saturation effects of the resin are negligible, i.e. there is a large excess of resin sites.

(iv) There is an excess of ligand with respect to metal in solution, so that the free ligand concentration can be taken as constant regardless of the formed ML. The excess equilibrium constant is

$$K' = \frac{k'_{\mathrm{a}}}{k_{\mathrm{d}}} = \frac{c^*_{\mathrm{ML}}}{c^*_{\mathrm{M}}} = K c^*_{\mathrm{L}}, \tag{4.3}$$

and the excess association kinetic constant is

$$k'_{\mathrm{a}} = k_{\mathrm{a}} c^*_{\mathrm{L}},$$

where K, k_{a} and k_{d} are, respectively, the equilibrium, the association and dissociation kinetic constants of the complexation process, and c^*_i labels the concentration of species i in the bulk solution

(v) For simplicity, the diffusion layer extending from the resin layer to the bulk solution is considered to be solely represented by the gel layer of thickness g (see Figure 3.5, page 53). The filter membrane and/or a diffusive boundary layer can optionally be included as part of g when diffusion coefficients of the complex are similar in each of these layers.

Under these conditions, the system reaches a quasi steady state in which the complex diffusing into the resin layer dissociates and the resulting free metal ion binds to the resin. We aim to find an analytical solution for the metal flux, the lability degree and the concentration profiles, corresponding to this quasi steady state.

An extension of the expressions here reported for the metal flux and lability degree when the diffusion domain extends into the solution (with different diffusion coefficients for metal and complex in the DBL and in the gel layer) is reported in Section 4.A.3 (Supporting Information, page 100).

4.3 Analytical Solution

4.3.1 Expression for the Flux

The steady-state metal flux, J, is the total metal flux entering the resin layer both as free metal and complex,

$$J = D_{\mathrm{M}} \frac{\mathrm{d}c_{\mathrm{M}}}{\mathrm{d}x}\bigg|_{x=r} + D_{\mathrm{ML}} \frac{\mathrm{d}c_{\mathrm{ML}}}{\mathrm{d}x}\bigg|_{x=r} \tag{4.4}$$

The flux (J) times the area of the resin-gel interface is also the number of moles of M that are binding to the resin per unit time.

Under the conditions stated in the previous section, the steady-state concentration profiles can be obtained from the solutions of simple ordinary second order differential equations with constant coefficients. From the analytical solution of the concentration profiles, the metal flux measured by a DGT can be written as (see Section 4.A.1 on page 84)

$$J = \frac{D_{\mathrm{M}} c^*_{\mathrm{M}}}{g} + \frac{D_{\mathrm{ML}} c^*_{\mathrm{ML}}}{g} \left[1 - \frac{1 + \epsilon K'}{\epsilon K' + \frac{g}{m} \coth\left(\frac{g}{m}\right) + \frac{g}{\lambda_{\mathrm{ML}}} (1 + \epsilon K') \tanh\left(\frac{r}{\lambda_{\mathrm{ML}}}\right)} \right], \tag{4.5}$$

where $\epsilon = D_{\mathrm{ML}}/D_{\mathrm{M}}$,

$$\frac{1}{m^2} = \frac{1}{\lambda^2_{\mathrm{ML}}} + \frac{1}{\mu^2}, \tag{4.6}$$

$$\lambda^2_{\mathrm{ML}} = \sqrt{\frac{D_{\mathrm{ML}}}{k_{\mathrm{d}}}} = \sqrt{\epsilon K'} \mu, \tag{4.7}$$

and

$$\mu = \sqrt{\frac{D_{\mathrm{M}}}{k'_{\mathrm{a}}}}. \tag{4.8}$$

λ_{ML}, m and μ have dimensions of a distance. λ_{ML} can be seen as a "penetration parameter" related to the distance required for a complex to dissociate fully as it diffuses into the resin layer; m can be seen as a distance related to the thickness of the layer in the gel domain where equilibrium between

metal and complex is not achieved and μ is the reaction layer parameter introduced by Koutecky in planar semi-infinite diffusion [10]. See below for a detailed physical interpretation.

4.3.2 The Lability Degree

The lability degree, ξ, is defined [7] as

$$\xi = \frac{J - J_{\text{free}}}{J_{\text{labile}} - J_{\text{free}}}, \tag{4.9}$$

where J denotes the actual metal flux, J_{free} the metal flux due to the free metal in the system without any contribution of the complex (also denoted as J_{inert} to indicate the flux if the complex was totally inert) and J_{labile}, the metal flux expected in the system if the complex was fully labile. The lability degree increases as the complex dissociates so that, as it is shown in Section 4.A.1,

$$\xi = 1 - \frac{c_{\text{ML}}(x = r)}{c^*_{\text{ML}}}. \tag{4.10}$$

In terms of the system parameters, ξ can be expressed as

$$\xi = 1 - \frac{1 + \epsilon K'}{\epsilon K' + \dfrac{g}{m}\coth\left(\dfrac{g}{m}\right) + \dfrac{g}{\lambda_{\text{ML}}}(1 + \epsilon K')\tanh\left(\dfrac{r}{\lambda_{\text{ML}}}\right)}, \tag{4.11}$$

which also indicates that an equivalent expression for the metal flux is

$$J = \frac{D_{\text{M}} c^*_{\text{M}}}{g} + \frac{D_{\text{ML}} c^*_{\text{ML}}}{g}\xi = \frac{D_{\text{M}} c^*_{\text{M}}(1 + \epsilon K')}{g}. \tag{4.12}$$

Equation 4.11 indicates that the lability degree of a complex increases with increasing resin thickness. This finding demonstrates that the resin layer influences the lability of complexes, as well as facilitates the accumulation of the metal. However, the increase of the lability degree due to the increase of the resin layer thickness is limited. Indeed, ξ tends asymptotically to a maximum when $r \gg \lambda_{\text{ML}}$ because $\tanh(r/\lambda_{\text{ML}}) \to 1$.

4.3.3 Physical Meaning of m and λ_{ML}

Due to the consumption of free metal within the resin phase (see Figure 4.1), the concentration profiles of both free metal and complex decrease when going from the solution interface towards the resin/gel interface. Close to the bulk solution, the decrease in free metal concentration induces the

dissociation of the complex, which occurs until local equilibrium between the species is reached. Under these conditions, M and ML normalised profiles coincide.

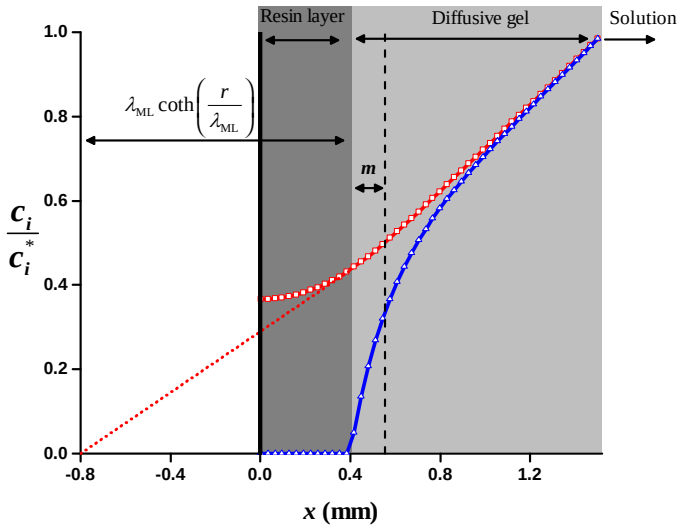

Figure 4.1: Normalized concentration profiles of M and ML. Markers: red squares (ML) and blue triangles (M) have been calculated with the numerical simulation described in Chapter 2. Continuous lines depict the approximate analytical expressions reported in the Supporting Information as solutions of the present model. The effective thickness of the complex penetration into the resin layer ($\lambda_{ML}\tanh(r/\lambda_{ML})$) and the effective thickness of the reaction layer ($m\tanh(g/m)$) in the gel domain (with the parameters of this figure $m\tanh(g/m)\approx m$) are also depicted. Parameters: $K = 10^2$ m^3 mol^{-1}; $k_a = 10^{-1}$ m^3 mol^{-1} s^{-1}; $k_d = 10^{-3}$ s^{-1}; $r = 4\times10^{-4}$ m; $g = 1.13\times10^{-3}$ m; $D_M = D_{M,R} = 6.09\times10^{-10}$ m^2 s^{-1}; $D_L = D_{L,R} = 4.26\times10^{-10}$ m^2 s^{-1}; $c_{T,M} = 10^{-2}$ mol m^{-3}; $c_{T,L} = 0.249$ mol m^{-3}. For the numerical simulation: kinetic association and dissociation constants of the metal to the resin sites are $k_{a,R} = 10^{15}$ m^3 mol^{-1} s^{-1} and $k_{d,R} = 10^{-6}$ s^{-1}; total concentration of resin sites in the resin layer, $c_{T,R} = 50$ mol m^{-3} and time $t = 10$ h.

For complexes that are not fully labile, close to the resin-layer surface there is a region where dissociation is not fast enough to maintain equilibrium. This is the classical reaction layer introduced in the context of a voltammetric experiment involving a metal that forms an electroinactive complex in solution. It can also be regarded as a disequilibration layer. However, the present problem has some specific characteristics, since disequilibration not only occurs in this layer of the gel, but also extends into the resin domain. Complexes that are not fully labile can penetrate into the resin layer,

because their concentration at $x = r$ (the gel layer/resin layer interface) differs from 0. Within the resin layer, dissociation of the complex does not cease, as equilibrium with free metal is impossible due to the absence of M. The "total reaction layer" or "disequilibration layer", understood as the full domain where there is not equilibrium, then comprises a layer in the gel domain (similar to the voltammetric reaction layer) plus another one in the resin domain which corresponds to the smaller between the effective distance for the complex concentration dropping to zero or the resin-layer thickness (when this full dissociation distance is greater than r).

Let us estimate the effective thickness of the reaction layer in the gel domain. When equilibrium is not established, $\phi = c_{\mathrm{ML}} - K'c_{\mathrm{M}}$ [11, 12] differs from zero. The effective thickness of the reaction layer in the gel domain can be obtained by constructing a tangent to the profile of ϕ at the resin/gel interface ($x = r$); it is then the distance necessary for ϕ to drop to zero. As shown in Section 4.A.1.8 of the Supporting Information (page 91), this distance becomes $m\tanh(g/m)$. When $g \gg m$, $\tanh(g/m) \approx 1$ and the effective thickness of the reaction layer is given by m (which can also be called the disequilibration parameter).

Let us now consider the disequilibration layer inside the resin domain. This is the layer where the complex concentration is not zero. An effective penetration distance of the complex into the resin layer is estimated by representing the complex concentration profile by a straight line that is a tangent to the complex concentration profile at $x = r$, and finding the distance at which this straight line becomes zero. As shown in the Supporting Information (see Section 4.A.1.7), the penetration distance that would be required for full dissociation of the complex is $\lambda_{\mathrm{ML}}\coth(r/\lambda_{\mathrm{ML}})$. For $r \gg \lambda_{\mathrm{ML}}$, $\coth(r/\lambda_{\mathrm{ML}}) \approx 1$ and the distance is just λ_{ML} (which can be called the penetration parameter).

Figure 4.1 shows that concentration profiles of free and complexed metal, calculated using the analytical expressions reported in the Supporting Information (Eqns 4.49 to 4.51, page 89), agree well with results from the rigorous numerical simulation of the system of differential equations described in [8]. Normalized concentration profiles of metal and complex are used to allow their direct comparison. The thickness of the gel layer where both normalized profiles diverge is given by $m\tanh(g/m)$. For the data of Figure 4.1, $g \gg m$ and $\tanh(g/m) \approx 1$, so that m is the effective thickness of the reaction layer in the gel domain, which is indicated by the vertical dashed line in Figure 4.1. At the interface between the resin and gel layers, the slope of the complex concentration profile is not zero and the complex penetrates into the resin layer. Figure 4.1 also depicts (see the point at which the dotted line cut the horizontal axis) the effective penetration distance of the complex necessary for full dissociation, $\lambda_{\mathrm{ML}}\coth(r/\lambda_{\mathrm{ML}})$. In the case of the

figure, this distance lies outside the domain of the DGT sensor, indicating that the complex does not fully dissociate.

4.3.4 Accuracy of the Analytical Solution

A check of the accuracy of equations 4.5 and 4.11 in reproducing the metal flux and the lability degree was performed by considering experimental results for the Cd-NTA system (see Figure 4.2). Due to proton and Cd competition in the binding to NTA, some transformations are required to convert the formulation of this system into one formally identical to a system with only one complex being present, so that Eqn 4.11 can be applied [8, 13].

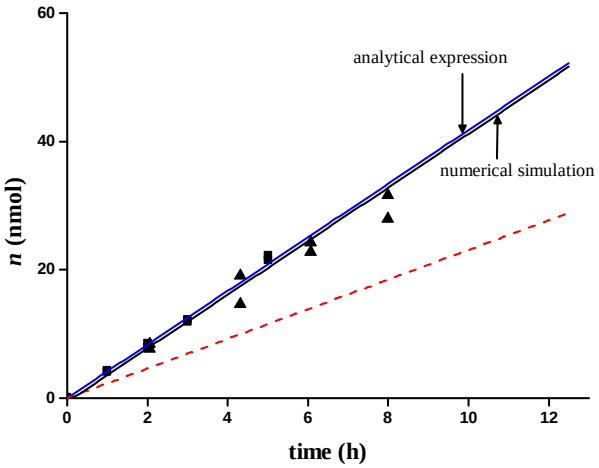

Figure 4.2: Moles of Cd accumulated by DGT in the presence of NTA. Markers: experimental measurements corresponding to two different deployments (■) and (▲). Black continuous line: theoretical accumulation predicted from numerical simulation when there is penetration of the complex into the resin layer ($r = 4 \times 10^{-4}$ m). Blue continuous line: theoretical accumulation predicted from the approximate analytical expression 4.5 with $r = 4 \times 10^{-4}$ m. Red dashed line: theoretical accumulation predicted from the analytical expression 4.5 with $r = 0$, i.e., when the complex is not able to penetrate into the resin. Parameters: total NTA concentration $c_{\mathrm{T,NTA}} = 0.249$ mol m^{-3}; total Cd concentration $c_{\mathrm{TCd}} = 9.96 \times 10^{-3}$ mol m^{-3}; $k_{\mathrm{a}}^{\mathrm{eff}} = 8.77 \times 10^{4}$ m^3 mol^{-1} s^{-1}; $k_{\mathrm{d}} = k_{\mathrm{d}}^{\mathrm{eff}} = 2.76$ s^{-1}; pH = 7.03; $I = 0.05$ M. Remaining parameters as in Figure 4.1.

Conditional stability and kinetic parameters used correspond to those reported in Mongin *et al.* [8]. By using these parameters (see caption of Figure 4.2), the analytical expression 4.5 produces the blue continuous line

depicted in the figure, in good agreement with the numerical and experimental results. Likewise, Eqn 4.11 predicts a lability degree of 0.98, in good agreement with the experimental results, which were indistinguishable from 1.0. However, if Eqn 4.5, together with the condition $r = 0$ (or the voltammetric expression derived in Salvador *et al.* [14]), is used to simulate the experiment, the accumulated mass predicted with the above parameters underestimates the experimentally obtained mass (red dashed line in Figure 4.2) and the lability degree is just 0.55. Additional results from simulation and experimental measurements for other pH values or concentrations of the Cd-NTA system can be found in the Supporting Information (see Figures 4.8 to 4.11, pages 95–98). In all cases, for the conditions of these figures, the penetration of the complex into the resin layer plays a key role in facilitating the fully labile behaviour of the Cd-NTA complex. Expressions 4.5 and 4.11 predict these results with good accuracy.

4.3.5 Impact of the Resin Thickness on the Lability Degree

We now analyse the influence of the resin thickness in more detail. Figure 4.3 depicts the dependence of the lability degree of the Cd-NTA complex on the thickness of the resin layer for the conditions of Figure 4.2. The

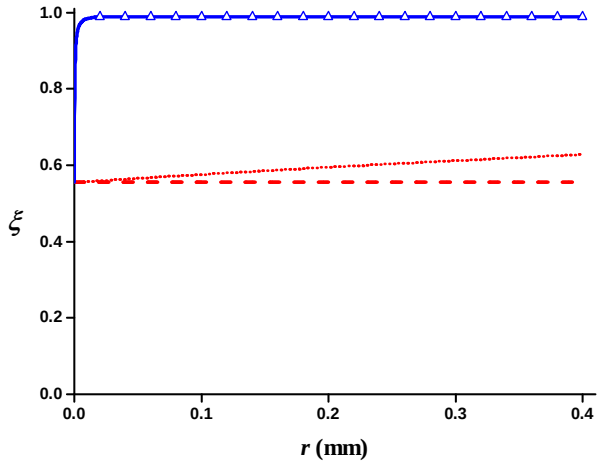

Figure 4.3: Dependence of the lability degree ξ on the thickness of the resin layer. Markers: Blue triangles indicate values from numerical simulation. Blue continuous line depicts the values from the analytical expression 4.11. Red dashed line represents ξ given by Eqn 4.11 with $r = 0$. Red dotted line represents ξ from Eqn 4.11 with thickness of the gel domain given by $g' = g + r$ and no penetration inside the resin. Remaining parameters as in Figure 4.2.

blue continuous line depicts the lability degree as given by Eqn 4.11 for the standard gel thickness of a DGT sensor with variable resin thickness. If $r \to 0$, the blue continuous line tends to the red dashed one, which depicts the lability degree of a complex that is unable to penetrate the resin layer (obtained from Eqn 4.11 with $r = 0$), so that it is, obviously, not influenced by r . Notice the marked increase in the lability degree (blue line) when r takes values of the order of λ_{ML} (~ 0.01 mm). When $r \gg \lambda_{\mathrm{ML}}$, $\coth(r/\lambda_{\mathrm{ML}})$ tends to unity and further increases of r do not modify the lability degree.

Figure 4.3 also depicts with a red dotted line the lability degree (computed with Eqn 4.11) of a virtual DGT sensor whose thickness of the gel layer was $g' = g + r$ and r' was 0. As seen in the red dotted line, the lability degree increases as the thickness of the gel layer increases, since the effective time for dissociation (time used by the complex to cross the gel layer) increases. However, the figure shows a dramatic difference between the effect of increasing either the resin or gel layer thicknesses. This distinctive behaviour can be conceptually appreciated if we recall that an increase of the thickness of r leads to an increase in the thickness of the zone where the complex can approach full dissociation, provided that $r \ll \lambda_{\mathrm{ML}}$ (see previous paragraph). When $r \gg \lambda_{\mathrm{ML}}$, the resin is thick enough for the complex to reach full dissociation in the resin layer (in the distance λ_{ML}) and further increases of r do not modify the lability degree. In contrast, the same increase of the thickness of the sensor in g does not imply an increase of the reaction layer, given by $m \tanh(g/m)$, unless $g \ll m$ which is not the case in Figure 4.3 ($g = 1.13 \times 10^{-3}$ m; $m = 1.7 \times 10^{-7}$ m; $\lambda_{\mathrm{ML}} = 1.04 \times 10^{-5}$ m; $\mu = 1.7 \times 10^{-7}$ m).

The influence of the resin thickness on the lability degree is still more noticeable if the kinetic dissociation constant is decreased by one order of magnitude (see Figure 4.10, page 97). Notice the dramatic error in the interpretation of the DGT measurement if penetration into the resin layer was not taken into account: from a lability degree of 0.1 we go to a lability degree close to 1 when the penetration of the complex into the resin domain is considered. Keeping K fixed (see Figure 4.11, page 98), when both kinetic constants are decreased by 4 orders of magnitude with respect to Figure 4.3, λ_{ML} is of the order of 1 mm; the increase of the lability takes place for r values of the order of millimeters and the highest lability degree reached is close to 0.5. Notice that in this case, the lability degree and the metal flux obtained can be selected by choosing a convenient resin thickness.

We now focus on the usual case of non-negligible complex contribution to the metal flux ($\epsilon K' \gg 1$), and $g > r$ (typical standard DGT sensor). Under these conditions, it can be shown from Eqn 4.11 that a complex is fully labile, $\xi \to 1$, when $r > \lambda_{\mathrm{ML}}$ (see Section 4.A.1.9 of the Supporting Information for details, page 91). Accordingly, in the standard DGT arrangement where

$g > r$, the lability of a complex with $\xi < 1$ could be increased by increasing the resin layer thickness, while an increase of the gel layer thickness will show a much less pronounced effect. The increase of the resin layer thickness will also lead to an increase of the metal flux and of the accumulated moles, in contrast to an increase of the gel layer thickness, which, while increasing moderately the lability degree, will decrease the amount of accumulated metal (due to the decrease of the metal flux).

As Eigen ideas indicate that k_a for any complex of a given cation can be estimated from $k_a = K^{os} k_w$, where K^{os} and k_w stand respectively for the stability constant of the outer sphere ML complex and the dehydration rate constant of M, Eqn 4.11 can also be used to estimate the highest value of the stability constant (K') compatible with a complex with $D_{ML} = 0.7 D_M$ being still fully labile. Figure 4.4 shows these curves for different cations. k_a-values for each cation have been estimated using Eigen relationship with k_w values reported in the literature [15] and K^{os}-values obtained using the electrostatic model for a ligand of charge -2.

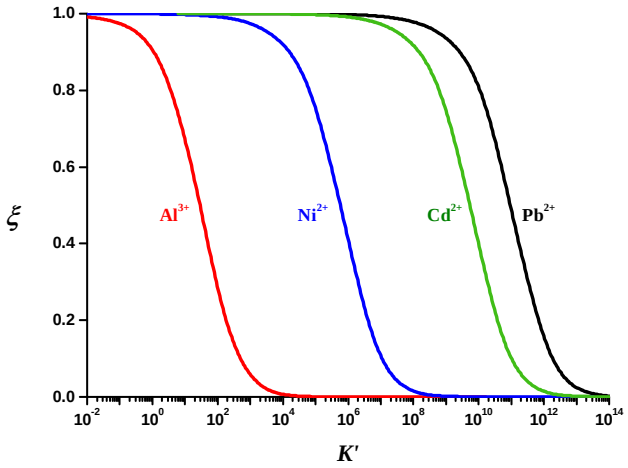

Figure 4.4: Dependence of the lability degree on K' for complexes of different cations in a standard DGT sensor, computed with Eqn 4.11. Parameters: $k_a(\mathrm{Al}) = 2 \times 10^{-2}$ m^3 mol^{-1} s^{-1}; $k_a(\mathrm{Ni}) = 6.15 \times 10^2$ m^3 mol^{-1} s^{-1}; $k_a(\mathrm{Cd}) = 6.15 \times 10^6$ m^3 mol^{-1} s^{-1}; $k_a(\mathrm{Pb}) = 1.43 \times 10^8$ m^3 mol^{-1} s^{-1}; $D_{\mathrm{Al}} = 4.75 \times 10^{-9}$ m^2 s^{-1}; $D_{\mathrm{Ni}} = 5.77 \times 10^{-10}$ m^2 s^{-1}; $D_{\mathrm{Cd}} = 6.09 \times 10^{-10}$ m^2 s^{-1}; $D_{\mathrm{Pb}} = 8.03 \times 10^{-10}$ m^2 s^{-1}. The rest of parameters as in Figure 4.1.

According to the results shown in Figure 4.4, Cd complexes with effective stability constant (K') lower than 10^8 are expected to be fully labile in a standard DGT sensor. The figure gives also information for Pb, Ni and Al

complexes. The different metals have similar curves, but the transition of lability occurs at different K' values.

We can further simplify Eqn 4.11 for the usual case when $\epsilon K' \gg 1$ and $g \geq 2r$ (the "standard" DGT sensor). As $\lambda_{\mathrm{ML}} = \sqrt{\epsilon K' m}$, $\lambda_{\mathrm{ML}} > m$ and, if $r > \lambda_{\mathrm{ML}}$, then $g > r > \lambda_{\mathrm{ML}} > m$, i.e., $g > m$. Thus, the condition $r > \lambda_{\mathrm{ML}}$ implies $g > m$ and fully labile behaviour (see, as before, Section 4.A.1.9, page 91). However, the opposite implication is not true, i.e., $g > m$ does not imply $r > \lambda_{\mathrm{ML}}$. When $g > m$ we have at least a partially labile complex, since this condition indicates that at least in some region of the gel layer (whose thickness is $g - m$) metal and complex are in equilibrium. The condition $g > m$ applied in Eqn 4.11 leads to

$$\xi = 1 - \frac{1}{1 + \dfrac{g}{\lambda_{\mathrm{ML}}} \tanh\left(\dfrac{r}{\lambda_{\mathrm{ML}}}\right)}, \tag{4.13}$$

an expression which indicates that for given values of r and g, ξ is independent from k_{a}, $c_{\mathrm{T,L}}$ and D_{M} and only dependent on D_{ML} and k_{d}. Conceptually, the dependence of the lability degree on D_{ML} and on k_{d} is consistent with the fact that only dissociation and diffusion of the complex takes place in the resin layer. In this case ($g > m$), D_{ML} and k_{d} are the only relevant parameters determining the lability degree in a standard DGT sensor.

The independence of ξ on pH and ligand concentration predicted by the approximate Eqn 4.13 is a special feature of DGT sensors, since these factors have been recognized to affect the lability degree for measurements made using voltammetric sensors [16]. However, due to the approximate character of Eqn 4.13, some slight dependence may be encountered practically.

Expression 4.13 is depicted in Figure 4.5 which shows the lability degree versus the kinetic dissociation constant for different D_{ML}-values. It can be used to estimate the lability degree of any complex independently of the ligand and metal cation. For example, complexes with $D_{\mathrm{ML}} = 6 \times 10^{-10}$ m^2 s^{-1} will start loosing lability for $k_{\mathrm{d}} < 0.1$ s^{-1}. As said before, lability compares the maximum diffusive flux with the maximum kinetic contribution. Since the maximum diffusive flux increases as D_{ML} increases, the loss of lability starts at higher k_{d} values (which determines the kinetic flux) as D_{ML} increases, as can be seen in Figure 4.5. Particular values of the lability degree of NTA complexes with Cd, Co and Ni are depicted in the figure for two pH values. Notice the small dependence of the lability degree as pH changes from 6 to 9. Additional values for different metal and total NTA concentrations are reported in Table 4.1 of Supporting Information, page 99.

This good agreement between DGT measurements of the Cd-NTA system

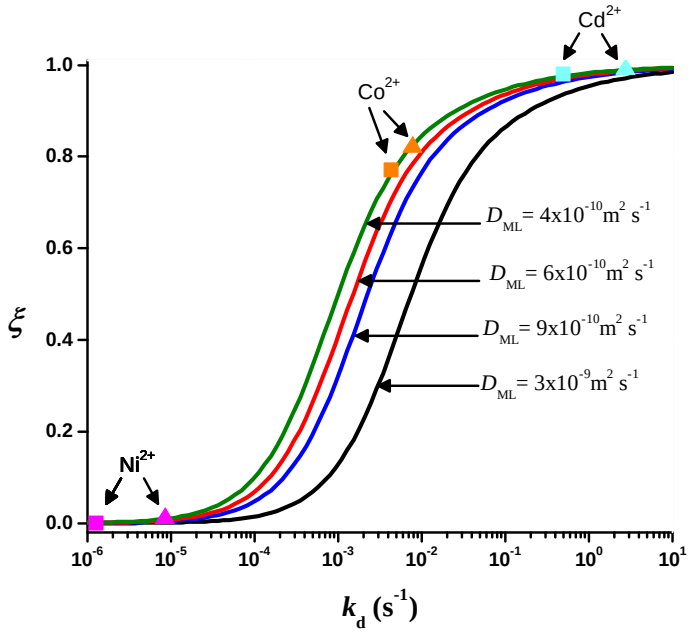

Figure 4.5: Dependence of the lability degree on k_{d} in a standard DGT sensor as given by Eqn 4.13. $D_{\mathrm{ML}} = 3 \times 10^{-9}$ m^2 s^{-1} (black line); $D_{\mathrm{ML}} = 9 \times 10^{-10}$ m^2 s^{-1} (blue line); $D_{\mathrm{ML}} = 6 \times 10^{-10}$ m^2 s^{-1} (red line); $D_{\mathrm{ML}} = 4 \times 10^{-10}$ m^2 s^{-1} (green line); values of g and r as in Figure 4.1. Square (pH=9) and triangle (pH=6) markers indicate the theoretical lability degree calculated with Eqn 4.13 for M-NTA complexes when total metal concentration $c_{\mathrm{T,M}} = 10^{-7}$ M, $c_{\mathrm{T,NTA}} = 10^{-3}$ M, $\epsilon = 0.7$ (for all complexes), ionic strength 0.05 M and speciation parameters from NIST 46.6.

and predictions made using the analytical equations provides confidence in the latter and their use more generally for predicting metal accumulated by DGT and associated lability, as shown in Figures 4.4 and 4.5. Further measurements in the presence of other metals and ligands are required to provide more exhaustive validation. This new understanding represents an important step in the direction of quantitative interpretation of in situ DGT measurements in natural waters. However, the complexities of accommodating heterogeneous ligands will need to be tackled.

4.A Supporting Information

4.A.1 Steady State Approximate Analytical Solution for the Metal Flux, Lability Degree and Concentration Profiles Under Typical DGT Conditions in Systems with Dynamic Complexes

4.A.1.1 The Model

We make the following assumptions:

- There is fast and strong free metal ion binding to the resin, so that the free metal concentration inside the resin layer is negligible.
- Saturation effects of the resin are negligible, i.e. there is a large excess of resin sites (R) with respect to the metal bound (MR) throughout the deployment time of interest.
- Free metal (M) interacts with the ligand (L) to form a complex (ML) and there is an excess of ligand with respect to metal in solution, so that the free ligand concentration can be taken as constant regardless of ML formation.
- The complex can penetrate and diffuse within the resin layer, where its dissociation still applies. Thus, the complex inside the resin layer acts as a source of free metal that then becomes bound to the resin.

Under these conditions, the system reaches a quasi steady state in which any free metal, M, arriving in the resin layer is instantaneously bound to the resin and the complex arriving in the resin layer is consumed by dissociation, with the resulting free metal binding to the resin. We aim to find an analytical solution for the metal flux, lability degree and concentration profiles corresponding to this steady state. Limiting cases are those corresponding to a negligible dissociation (inert complex) or a sufficiently rapid dissociation so that local equilibrium conditions apply everywhere (fully labile complex). In this last case, the complex fully dissociates at the resin-layer surface, in agreement with the metal concentration being effectively zero at this location. Another limiting case is that of the resin layer being so thin ($r \approx 0$) that metal consumption effectively occurs at a surface.

4.A.1.2 Diffusion-Reaction Conditions in the Resin Layer

With the above conditions, in steady state the diffusion equations for the resin layer explicitly reported in Section 3.A.1 (page 53) can be greatly simplified.

First, there is an effective zero concentration of metal in the resin layer,

$$c_{\mathrm{M}}(0 < x < r) = 0. \tag{4.14}$$

Consequently, the diffusion of complex in the resin layer is described by

$$\frac{\mathrm{d}^2 c_{\mathrm{ML}}}{\mathrm{d}x^2} = \frac{k_{\mathrm{d}}}{D_{\mathrm{ML}}} c_{\mathrm{ML}} = \frac{c_{\mathrm{ML}}}{\lambda_{\mathrm{ML}}^2} \quad \text{for} \quad 0 < \mathrm{x} < \mathrm{r}, \tag{4.15}$$

with

$$\lambda_{\mathrm{ML}} = \sqrt{\frac{D_{\mathrm{ML}}}{k_{\mathrm{d}}}} = \sqrt{\epsilon K'}\mu, \tag{4.16}$$

where λ_{ML} has dimensions of a distance and can be seen as a "penetration parameter" related to the distance required for a complex diffusing into the resin layer to dissociate fully (See Sections 4.3.3 and 4.A.1.7 for a more detailed physical interpretation). The general solution of Eqn 4.15 can be written as

$$c_{\mathrm{ML}}(x \leq r) = Ae^{(x/\lambda_{\mathrm{ML}})} + Be^{(-x/\lambda_{\mathrm{ML}})}, \tag{4.17}$$

where A and B are integration constants that have to fulfil the boundary value problem

$$\left.\frac{\mathrm{d}c_{\mathrm{ML}}}{\mathrm{d}x}\right|_{x=0} = 0 \tag{4.18}$$

and

$$\left.\frac{\mathrm{d}c_{\mathrm{ML}}}{\mathrm{d}x}\right|_{x=r^-} = \left.\frac{\mathrm{d}c_{\mathrm{ML}}}{\mathrm{d}x}\right|_{x=r^+}, \tag{4.19}$$

which implicitly assumes a common complex diffusion coefficient both in the resin and gel layers.

The application of Eqn 4.18 in Eqn 4.17 leads to $A = B$, so that the solution can be rewritten as

$$c_{\mathrm{ML}}(x \leq r) = c_{\mathrm{ML}}(x = 0) \cosh\left(\frac{x}{\lambda_{\mathrm{ML}}}\right). \tag{4.20}$$

Labelling as c_{ML}^r the complex concentration at the frontier between the resin and diffusion layer ($x = r$), Eqn 4.20 becomes

$$c_{\mathrm{ML}}(x \leq r) = c_{\mathrm{ML}}^r \frac{\cosh\left(\frac{x}{\lambda_{\mathrm{ML}}}\right)}{\cosh\left(\frac{r}{\lambda_{\mathrm{ML}}}\right)}. \tag{4.21}$$

The application of Eqn 4.19 requires knowledge of the flux of complex entering the resin layer, calculated from the resin side. From Eqn 4.21, it becomes

$$J_{\mathrm{ML}} = D_{\mathrm{ML}} \left.\frac{\mathrm{d}c_{\mathrm{ML}}}{\mathrm{d}x}\right|_{x=r^-} = D_{\mathrm{ML}} \frac{c^r_{\mathrm{ML}}}{\lambda_{\mathrm{ML}}} \tanh\left(\frac{r}{\lambda_{\mathrm{ML}}}\right) = k_{\mathrm{d}} c^r_{\mathrm{ML}} \lambda_{\mathrm{ML}} \tanh\left(\frac{r}{\lambda_{\mathrm{ML}}}\right). \tag{4.22}$$

4.A.1.3 Diffusion Reaction Conditions in the Gel Layer

In the gel layer, steady-state conditions for M and ML apply

$$0 = D_{\mathrm{M}} \frac{\mathrm{d}^2 c_{\mathrm{M}}}{\mathrm{d}x^2} - k_{\mathrm{a}} c_{\mathrm{M}} c_{\mathrm{L}} + k_{\mathrm{d}} c_{\mathrm{ML}}, \tag{4.23}$$

$$0 = D_{\mathrm{ML}} \frac{\mathrm{d}^2 c_{\mathrm{ML}}}{\mathrm{d}x^2} + k_{\mathrm{a}} c_{\mathrm{M}} c_{\mathrm{L}} - k_{\mathrm{d}} c_{\mathrm{ML}}. \tag{4.24}$$

An equivalent system of equations to that given by Eqns 4.23 and 4.24 is

$$0 = \frac{\mathrm{d}^2}{\mathrm{d}x^2}(D_{\mathrm{M}} c_{\mathrm{M}} + D_{\mathrm{ML}} c_{\mathrm{ML}}), \tag{4.25}$$

$$0 = \frac{\mathrm{d}^2}{\mathrm{d}x^2}(c_{\mathrm{ML}} - K' c_{\mathrm{M}}) - \left(\frac{k_{\mathrm{d}}}{D_{\mathrm{ML}}} + \frac{k'_{\mathrm{a}}}{D_{\mathrm{M}}}\right)(c_{\mathrm{ML}} - K' c_{\mathrm{M}}), \tag{4.26}$$

which has the advantage of allowing the uncoupling of the system. Equation 4.25 is just the addition of Eqns 4.23 and 4.24. Its integration yields

$$D_{\mathrm{M}} c_{\mathrm{M}} + D_{\mathrm{ML}} c_{\mathrm{ML}} = D_{\mathrm{ML}} c^r_{\mathrm{ML}} + \frac{(D_{\mathrm{M}} c^*_{\mathrm{M}} + D_{\mathrm{ML}} c^*_{\mathrm{ML}}) - D_{\mathrm{ML}} c^r_{\mathrm{ML}}}{g}(x - r). \tag{4.27}$$

Equation 4.26 constitutes a closed equation for

$$\phi = c_{\mathrm{ML}} - K' c_{\mathrm{M}}. \tag{4.28}$$

We introduce now a new parameter, m, with dimensions of distance, which could be called a "disequilibration" parameter. It is related to the thickness of the gel layer where M and ML are not in equilibrium and can be seen as an extension of the reaction layer for this particular problem. See Sections 4.3.3 and 4.A.1.8, for a more detailed physical interpretation.

$$\frac{1}{m^2} = \frac{k_{\mathrm{d}}}{D_{\mathrm{ML}}} + \frac{k'_{\mathrm{a}}}{D_{\mathrm{M}}} = \frac{1}{\lambda^2_{\mathrm{ML}}} + \frac{1}{\mu^2} = \frac{1}{\mu^2}\left(\frac{1 + \epsilon K'}{\epsilon K'}\right), \tag{4.29}$$

where μ is the classical definition of reaction layer introduced by Koutecky in planar semi-infinite diffusion [17]:

$$\mu = \sqrt{\frac{D_{\mathrm{M}}}{k'_{\mathrm{a}}}}. \tag{4.30}$$

Thus, Eqn 4.26 can be rewritten as

$$\frac{\mathrm{d}^2\phi}{\mathrm{d}x^2} = \frac{\phi}{m^2}, \tag{4.31}$$

whose general solution is

$$\phi = A\sinh\left(\frac{g+r-x}{m}\right) + B\cosh\left(\frac{g+r-x}{m}\right), \tag{4.32}$$

where A and B are integration constants. The boundary conditions for Eqn 4.31 are given by

$$\phi(x = g + r) = 0 \tag{4.33}$$

and

$$\phi(x = r) = c^r_{\mathrm{ML}}. \tag{4.34}$$

Applying these conditions we obtain $B = 0$ and

$$A = \frac{c^r_{\mathrm{ML}}}{\sinh\dfrac{g}{m}},$$

so that

$$\phi = c^r_{\mathrm{ML}}\frac{\sinh\left(\dfrac{g+r-x}{m}\right)}{\sinh\left(\dfrac{g}{m}\right)}. \tag{4.35}$$

The derivative of ϕ in $x = r$,

$$\left.\frac{\mathrm{d}\phi}{\mathrm{d}x}\right|_{x=r} = -\frac{c^r_{\mathrm{ML}}}{m}\coth\left(\frac{g}{m}\right) = \left.\frac{dc_{\mathrm{ML}}}{dx}\right|_{x=r} - K'\left.\frac{dc_{\mathrm{M}}}{dx}\right|_{x=r}, \tag{4.36}$$

and that of Eqn 4.27,

$$D_{\mathrm{M}}\left.\frac{\mathrm{d}c_{\mathrm{M}}}{\mathrm{d}x}\right|_{x=r} + D_{\mathrm{ML}}\left.\frac{\mathrm{d}c_{\mathrm{ML}}}{\mathrm{d}x}\right|_{x=r} = \frac{(D_{\mathrm{M}}c^*_{\mathrm{M}} + D_{\mathrm{ML}}c^*_{\mathrm{ML}}) - D_{\mathrm{ML}}c^r_{\mathrm{ML}}}{g}, \tag{4.37}$$

allows the flux of ML entering into the resin layer, calculated from the diffusive gel side, to be written as

$$\begin{aligned} J_{\mathrm{ML}} &= D_{\mathrm{ML}}\left.\frac{\mathrm{d}c_{\mathrm{ML}}}{\mathrm{d}x}\right|_{x=r} \\ &= \frac{-D_{\mathrm{ML}}c^r_{\mathrm{ML}}(g/m)\coth(g/m) + \epsilon K'(D_{\mathrm{M}}c^*_{\mathrm{M}} + D_{\mathrm{ML}}c^*_{\mathrm{ML}} - D_{\mathrm{ML}}c^r_{\mathrm{ML}})}{g(1+\epsilon K')}. \end{aligned} \tag{4.38}$$

The continuity of the flux requires the equality of J_{ML} calculated from Eqn 4.22 and 4.38 as stated in Eqn 4.19. The fulfilment of condition 4.19 can then be used to isolate c^r_{ML} so that

$$c^r_{\mathrm{ML}} = \frac{c^*_{\mathrm{ML}}(1+\epsilon K')}{\epsilon K' + \frac{g}{m}\coth\left(\frac{g}{m}\right) + \frac{g}{\lambda_{\mathrm{ML}}}(1+\epsilon K')\tanh\left(\frac{r}{\lambda_{\mathrm{ML}}}\right)}. \tag{4.39}$$

4.A.1.4 Metal Flux

Under steady-state conditions, the metal flux bound to the resin layer, J, is the total metal flux entering the resin layer both as free metal and complex,

$$J = D_{\mathrm{M}}\frac{\mathrm{d}c_{\mathrm{M}}}{\mathrm{d}x}\bigg|_{x=0} + D_{\mathrm{ML}}\frac{\mathrm{d}c_{\mathrm{ML}}}{\mathrm{d}x}\bigg|_{x=0}, \tag{4.40}$$

and due to the linearity of the profile of $D_{\mathrm{M}}c_{\mathrm{M}} + D_{\mathrm{ML}}c_{\mathrm{ML}}$ in the gel layer (as given by Eqn 4.27),

$$J = D_{\mathrm{M}}\frac{c^*_{\mathrm{M}}}{g} + D_{\mathrm{ML}}\frac{c^*_{\mathrm{ML}} - c^r_{\mathrm{ML}}}{g}$$

which, using Eqn 4.39, becomes

$$J = D_{\mathrm{M}}\frac{c^*_{\mathrm{M}}}{g} + D_{\mathrm{ML}}\frac{c^*_{\mathrm{ML}}}{g}\left(1 - \frac{1+\epsilon K'}{\epsilon K' + \frac{g}{m}\coth\left(\frac{g}{m}\right) + \frac{g}{\lambda_{\mathrm{ML}}}(1+\epsilon K')\tanh\left(\frac{r}{\lambda_{\mathrm{ML}}}\right)}\right). \tag{4.41}$$

4.A.1.5 Lability Degree

For a labile case, full dissociation of the complex at the resin-gel interface is reached, $c^r_{\mathrm{ML}} = 0$ and according to Eqn 4.37, the metal flux bound to the resin becomes

$$J_{\mathrm{labile}} = \frac{D_{\mathrm{M}}c^*_{\mathrm{M}}}{g} + \frac{D_{\mathrm{ML}}c^*_{\mathrm{ML}}}{g}. \tag{4.42}$$

In the opposite case, when the complex is inert, it does not contribute at all to the metal flux, $c^r_{\mathrm{ML}} = c^*_{\mathrm{ML}}$ and the metal flux bound to the resin is just due to the diffusion of the free metal present in the system

$$J_{\mathrm{free}} = J_{\mathrm{inert}} = \frac{D_{\mathrm{M}}c^*_{\mathrm{M}}}{g}. \tag{4.43}$$

The lability degree, defined as

$$\xi = \frac{J - J_{\text{free}}}{J_{\text{labile}} - J_{\text{free}}}, \tag{4.44}$$

can, then, be written as

$$\xi = 1 - \frac{c^r_{\text{ML}}}{c^*_{\text{ML}}}, \tag{4.45}$$

or

$$\xi = 1 - \frac{1 + \epsilon K'}{\epsilon K' + \frac{g}{m}\coth\left(\frac{g}{m}\right) + \frac{g}{\lambda_{\text{ML}}}(1 + \epsilon K')\tanh\left(\frac{r}{\lambda_{\text{ML}}}\right)}, \tag{4.46}$$

or

$$\xi = 1 - \frac{1 + \epsilon K'}{\epsilon K' + \frac{g\sqrt{1+\epsilon K'}}{\mu\sqrt{\epsilon K'}}\coth\left(\frac{g\sqrt{1+\epsilon K'}}{\mu\sqrt{\epsilon K'}}\right) + \frac{g}{\mu\sqrt{\epsilon K'}}(1 + \epsilon K')\tanh\left(\frac{r}{\mu\sqrt{\epsilon K'}}\right)}. \tag{4.47}$$

Equation 4.47 allows recovery of $\xi = 1$ or $\xi = 0$ for the labile or inert limits by taking $\mu \to 0$ or $\mu \to \infty$, respectively.

The maximum ξ that can exhibit a complex in a DGT for a given $g \gg m$ will be obtained for a thick enough resin ($r \gg \mu\sqrt{\epsilon K'}$) and is given by

$$\xi = 1 - \frac{1 + \epsilon K'}{\epsilon K' + \frac{g\sqrt{1+\epsilon K'}}{\mu\sqrt{\epsilon K'}} + \frac{g(1+\epsilon K')}{\mu\sqrt{\epsilon K'}}}. \tag{4.48}$$

In the other limit, $r \to 0$, ξ given by 4.47 reverts to the case of ML not penetrating into the resin layer, Eqn 22 in Salvador *et al.* [14].

4.A.1.6 Concentration Profiles

As stated by Eqns 4.14 and 4.21, in the resin layer $c_{\text{M}}(0 < x \leq r) = 0$ and

$$c^r_{\text{ML}} = \frac{c^*_{\text{ML}}(1 + \epsilon K')}{\epsilon K' + \frac{g}{m}\coth\left(\frac{g}{m}\right) + \frac{g}{\lambda_{\text{ML}}}(1 + \epsilon K')\tanh\left(\frac{r}{\lambda_{\text{ML}}}\right)} \times \frac{\cosh\left(\frac{x}{\lambda_{\text{ML}}}\right)}{\cosh\left(\frac{r}{\lambda_{\text{ML}}}\right)}, \tag{4.49}$$

where Eqn 4.39 has been used.

In the gel layer, Eqns 4.27 and 4.35 can be combined to obtain c_{M} and c_{ML} so that

$$c_{\mathrm{M}}(r < x < r + g) = \frac{(c^*_{\mathrm{M}} + \epsilon c^*_{\mathrm{ML}}) - \epsilon c^r_{\mathrm{ML}}}{g(1 + \epsilon K')} - \frac{\epsilon c^r_{\mathrm{ML}} \sinh\left(\dfrac{g + r - x}{m}\right)}{(1 + \epsilon K') \sinh\left(\dfrac{g}{m}\right)}, \quad (4.50)$$

and

$$c_{\mathrm{M}}(r < x < r+g) = \frac{K'(c^*_{\mathrm{M}} + \epsilon c^*_{\mathrm{ML}}) - \epsilon c^r_{\mathrm{ML}}}{g(1 + \epsilon K')} + \frac{\epsilon c^r_{\mathrm{ML}} \sinh\left(\dfrac{g + r - x}{m}\right)}{(1 + \epsilon K') \sinh\left(\dfrac{g}{m}\right)}, \quad (4.51)$$

with c^r_{ML} given by Eqn 4.39.

4.A.1.7 Physical Meaning of the Penetration Parameter λ_{ML}

The complex concentration profile inside the resin layer is given by Eqn 4.21. The derivative of this profile at $x = r$ is then

$$\frac{\mathrm{d}c_{\mathrm{ML}}(x = r)}{\mathrm{d}x} = \frac{c^r_{\mathrm{ML}}}{\lambda_{\mathrm{ML}}} \tanh\left(\frac{r}{\lambda_{\mathrm{ML}}}\right). \quad (4.52)$$

To find an effective distance of penetration of the complex into the resin layer, we can represent the complex profile inside the resin by a straight line that is a tangent to the complex concentration profile where it coincides at $x = r$. The equation for this straight line is

$$c_{\mathrm{ML}}(x) - c_{\mathrm{ML}}(x = r) = \frac{c^r_{\mathrm{ML}}}{\lambda_{\mathrm{ML}}} \tanh\left(\frac{r}{\lambda_{\mathrm{ML}}}\right)(x - r). \quad (4.53)$$

The effective penetration for the complex can be found by just requiring that $c_{\mathrm{ML}}(x)$, as given by Eqn 4.53, is zero. With this condition, and recalling Eqn 4.49 for $c_{\mathrm{ML}}(x = r)$, x becomes

$$x = r - \lambda_{\mathrm{ML}} \coth\left(\frac{r}{\lambda_{\mathrm{ML}}}\right). \quad (4.54)$$

For $r \gg \lambda_{\mathrm{ML}}$, $\coth(r/\lambda_{\mathrm{ML}}) \approx 1$ and, then

$$x = r - \lambda_{\mathrm{ML}},$$

so that, in this case, λ_{ML} is a quantification of the distance of penetration of the complex before falling to zero concentration by dissociation.

4.A.1.8 Physical Meaning of the Disequilibration Parameter m

Inside the gel layer, moving towards decreasing x-values, the concentration profiles of both metal and complex decrease due to the consumption of the metal at the resin phase. At long distances from the resin layer, the dissociation of the complex is sufficiently fast to allow local equilibrium with the metal. However, as the resin-layer is approached, there is a distance where dissociation is not fast enough to reach equilibrium with the metal. In this region, $\phi = c_{\mathrm{ML}} - K'c_{\mathrm{M}}$ starts to increase. Let us obtain the effective thickness of this reaction layer or disequilibration layer. This thickness will be obtained by assuming that ϕ is a straight line that passes through the point $(x = r, \phi(x = r))$ and the "effective" thickness will be given by the distance necessary for ϕ to drop to zero. The slope of this straight line is given by Eqn 4.36:

$$\left.\frac{\mathrm{d}\phi}{\mathrm{d}x}\right|_{x=r} = -\frac{c^r_{\mathrm{ML}}}{m}\coth\left(\frac{g}{m}\right), \tag{4.55}$$

so that the equation for the straight line is

$$\phi - \phi(x = r) = -\frac{c^r_{\mathrm{ML}}}{m}\coth\left(\frac{g}{m}\right)(x - r), \tag{4.56}$$

and, recalling that $\phi(x = r) = c^r_{\mathrm{ML}}$ (see Eqn 4.28), the x-value that corresponds to $\phi = 0$ is

$$x = r + m\tanh\left(\frac{g}{m}\right).$$

Thus, the disequilibration layer in the gel domain has an effective thickness given by $m\tanh(g/m)$. When $g \gg m$, $\tanh(g/m) \approx 1$ and the effective thickness of the disequilibration layer is given by m.

4.A.1.9 Condition for Fully Labile Behaviour when $\epsilon K' \gg 1$

We now focus on the case of interest $\epsilon K' \gg 1$ ($\sqrt{\epsilon K'} \gg 1$) and $g > r$ (typical standard DGT sensor). In general, $\lambda_{\mathrm{ML}} > m$ since $\lambda_{\mathrm{ML}} = \sqrt{1 + \epsilon K'\mu}$ (see Eqn 4.16). Then, if $r > \lambda_{\mathrm{ML}}$, we have $g > r > \lambda_{\mathrm{ML}} > m$, so that $g > m$. Also, when $\epsilon K' \gg 1$, $m \approx \mu$ as can be seen from Eqn 4.29.

Let us apply the condition $r > \lambda_{\mathrm{ML}}$ to Eqn 4.46. If $r > \lambda_{\mathrm{ML}}$ and $g > m$, $\tanh(r/\lambda_{\mathrm{ML}}) \approx 1$ and $\coth(g/m) \approx 1$ so that Eqn 4.46 becomes

$$\xi = 1 - \frac{1}{1 + \dfrac{1}{\epsilon K'}\dfrac{g}{m} + \dfrac{g}{\lambda_{\mathrm{ML}}}}. \tag{4.57}$$

Recalling that $m \approx \mu$ and $\lambda_{\mathrm{ML}} \approx \sqrt{\epsilon K'}\mu$ (see Eqn 4.16), Eqn 4.57 becomes

$$\xi = 1 - \frac{1}{1 + \frac{g}{\lambda_{\mathrm{ML}}}\left(\frac{1}{\epsilon K'} + 1\right)} \approx \frac{1}{1 + \frac{g}{\lambda_{\mathrm{ML}}}} \approx 1 - \frac{\lambda_{\mathrm{ML}}}{g} \approx 1, \tag{4.58}$$

whenever $\sqrt{\epsilon K'} \gg 1$ as assumed above.

Thus, the condition $r > \lambda_{\mathrm{ML}}$ when $\sqrt{\epsilon K'} \gg 1$ and $g > r$ (typical standard DGT sensor) leads to fully labile complexes.

4.A.1.10 Accuracy of the Analytical Expressions for the Metal Flux and Lability Degree

Figures 4.6 and 4.7 show an increase in both the flux received by the resin and the lability degree as the kinetic complexation constants increase. In both figures, analytical results of expressions 4.41 and 4.46 superimpose with the rigorous numerical results (computed with the code detailed in Chapter 2), indicating the accuracy of these approximate analytical expressions.

Figures 4.6 and 4.7 also depict (see discontinuous line) the flux and the lability degree of a complex that is unable to penetrate into the resin layer while the surface of the resin layer acts as a perfect sink for the metal. These values have been computed with Eqns 4.41 and 4.46 using $r = 0$, which coincide with Eqns 14 and 22 of Salvador *et al.* [14] that were developed for a planar voltammetric sensor and an electroinactive complex under diffusion limited conditions. As can be seen in the figures, Eqns 4.41 and 4.46 reproduce with good accuracy the numerical simulation results, indicating that the penetration of the complex into the resin layer increases both the metal flux and the lability degree of the complex. The analytical expressions 4.41 and 4.46 can, then, be used with good accuracy to predict the metal flux or the lability degree of a complex in a DGT sensor whenever the binding of the corresponding metal to the resin is fast enough for the metal concentration in the resin layer to be negligible.

4.A.2 Additional Figures and Tables

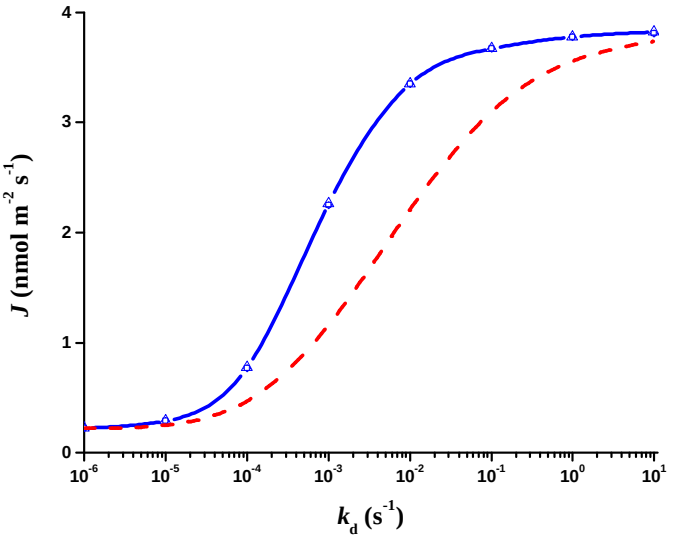

Figure 4.6: Metal flux received by the DGT sensor versus the dissociation constant of the complex (k_d). Markers: values of J obtained by numerical simulation at 4 (□), 7 (△) and 15 (◊) hours (superimposed). Blue continuous line: values obtained from the analytical expression given by Eqn 4.41. Red dashed line: metal flux from Eqn 4.41 with $r = 0$. Remaining parameters: $K = 10^2$ m^3 mol^{-1}, $g = 1.13 \times 10^{-3}$ m, $D_\mathrm{M} = D_\mathrm{M,R} = 6.09 \times 10^{-10}$ m^2 s^{-1}, $D_\mathrm{L} = D_\mathrm{L,R} = 4.26 \times 10^{-10}$ m^2 s^{-1}, $c_\mathrm{TM} = 10^{-2}$ mol m^{-3}, $c_\mathrm{TL} = 0.249$ mol m^{-3}, $k_\mathrm{a,R} = 10^{15}$ m^3 mol^{-1} s^{-1}, $k_\mathrm{d,R}$ s^{-1}, and $c_\mathrm{TR} = 10^{-2}$ mol m^{-3}.

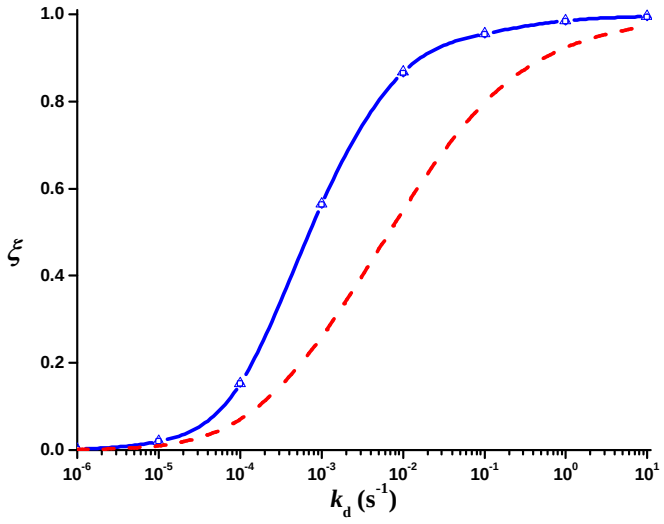

Figure 4.7: Lability degree of a complex in terms versus the dissociation constant of the complex (k_d). Markers: values of ξ obtained by numerical simulation at 4 (□), 7 (△) and 15 (◊) hours (superimposed). Blue continuous line: values obtained from the analytical expression given by Eqn 4.46. Red dashed line: metal flux from 4.46 with $r = 0$. Remaining parameters as in Figure 4.6.

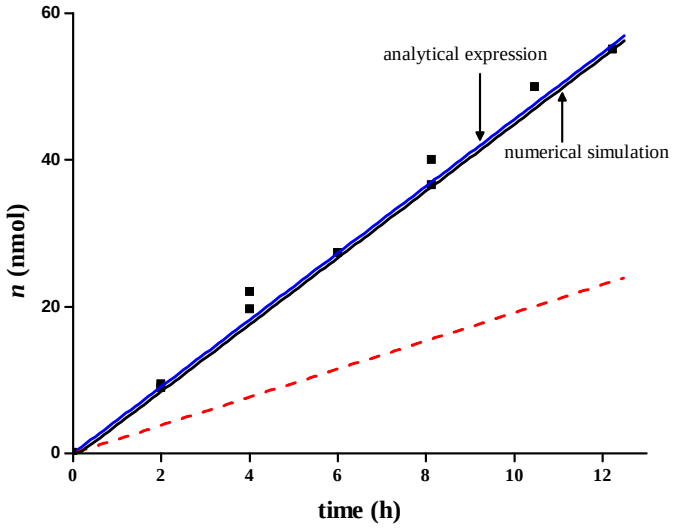

Figure 4.8: Moles of Cd accumulated by DGT in the presence of NTA. Markers: experimental measurements. Black continuous line: theoretical accumulation predicted from numerical simulation when there is penetration of the complex into the resin layer ($r = 4 \times 10^{-4}$ m). Blue continuous line: theoretical accumulation predicted from the approximate analytical expression 4.5 with $r = 4 \times 10^{-4}$ m. Red dashed line: theoretical accumulation predicted from the analytical expression 4.5 with $r = 0$, i.e. the complex is not able to penetrate into the resin. Parameters: total NTA concentration $c_{\mathrm{T,NTA}} = 0.249$ mol m^{-3}; total Cd concentration $c_{\mathrm{TCd}} = 1.08 \times 10^{-2}$ mol m^{-3}; $k_{\mathrm{a}}^{\mathrm{eff}} = 2.58 \times 10^{5}$ mol^{-1} m^3 s^{-1}; $k_{\mathrm{d}} = k_{\mathrm{d}}^{\mathrm{eff}} = 2.76$ s^{-1}; pH $= 7.5$; $I = 0.05$ M and $g = 1.13 \times 10^{-3}$ m. Remaining parameters as in Figure 4.6

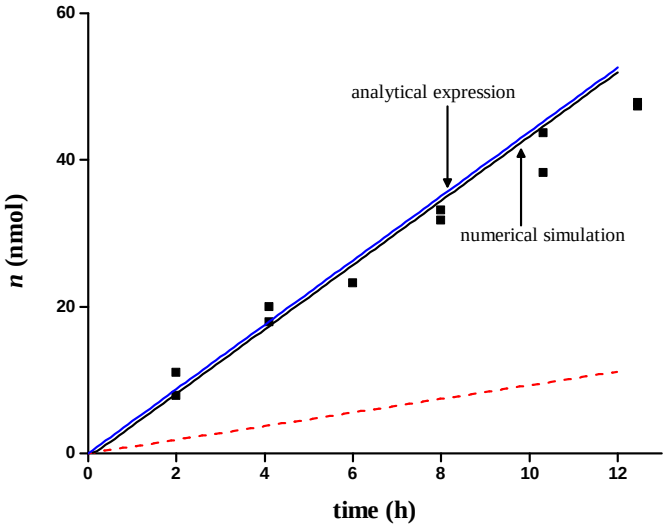

Figure 4.9: Moles of Cd accumulated by DGT in the presence of NTA. Markers: experimental measurements. Black continuous line: theoretical accumulation predicted from numerical simulation when there is penetration of the complex into the resin layer ($r = 4 \times 10^{-4}$ m). Blue continuous line: theoretical accumulation predicted from the approximate analytical expression 4.5 with $r = 4 \times 10^{-4}$ m. Red dashed line: theoretical accumulation predicted from the analytical expression 4.5 with $r = 0$, i.e. the complex is not able to penetrate into the resin. Parameters: total NTA concentration $c_{\mathrm{T,NTA}} = 0.249$ mol m^{-3}; total Cd concentration $c_{\mathrm{TCd}} = 1.8$ mol m^{-3}; $k_{\mathrm{a}}^{\mathrm{eff}} = 2.58 \times 10^5$ mol^{-1} m^3 s^{-1}; $k_{\mathrm{d}} = k_{\mathrm{d}}^{\mathrm{eff}} = 2.76$ s^{-1}; pH = 7.5; $I = 0.05$ M and $g = 1.13 \times 10^{-3}$ m. Remaining parameters as in Figure 4.6

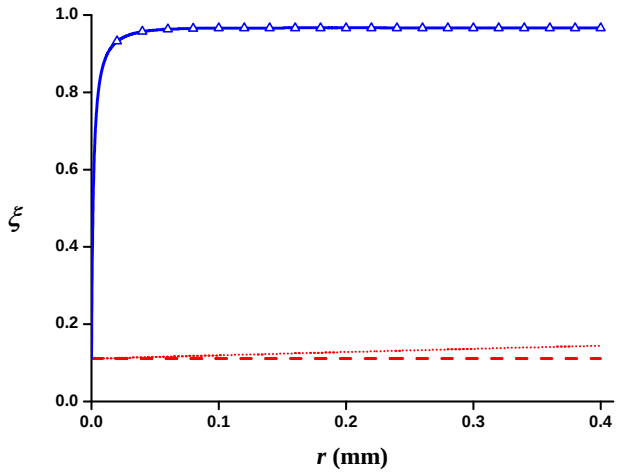

Figure 4.10: Dependence of the lability degree ξ on the thickness of the resin layer. Markers: Blue triangles indicate values from a numerical simulation as described in reference [8]. Blue continuous line depicts the values from the analytical expression 4.11. Red dashed line represents ξ given by Eqn 4.11 with $r = 0$. Red dotted line represents ξ from Eqn 4.11 with thickness of the gel domain given by $g' = g + r$ and no penetration inside the resin. Parameters: $c_{\mathrm{TM}} = 9.96 \times 10^{-3}$ mol m^{-3}; $k_{\mathrm{a}}^{\mathrm{eff}} = 8.77 \times 10^{4}$ m^{3} mol^{-1} s^{-1}; $k_{\mathrm{d}} = k_{\mathrm{d}}^{\mathrm{eff}} = 2.76 \times 10^{-1}$ s^{-1}; pH = 7.03. Remaining parameters as in Figure 4.6.

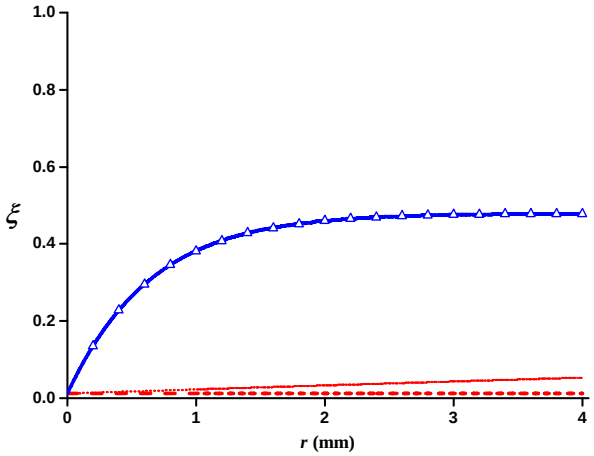

Figure 4.11: Dependence of the lability degree ξ on the thickness of the resin layer. Markers: Blue triangles indicate values from a numerical simulation as described in reference [8]. Blue continuous line depicts the values from the analytical expression 4.11. Red dashed line represents ξ given by Eqn 4.11 with $r = 0$. Red dotted line represents ξ from Eqn 4.11 with thickness of the gel domain given by $g' = g + r$ and no penetration inside the resin. Parameters: $c_{\mathrm{TM}} = 9.96 \times 10^{-3}$ mol m^{-3}; $k_{\mathrm{a}}^{\mathrm{eff}} = 8.77$ m^3 mol^{-1} s^{-1}; $k_{\mathrm{d}} = k_{\mathrm{d}}^{\mathrm{eff}} = 2.76 \times 10^{-4}$ s^{-1}; pH = 7.03. Remaining parameters as in Figure 4.6.

Table 4.1: Theoretical lability degrees of Cd, Co and Ni complexes with NTA for different metal and NTA concentrations and pH values computed with Eqn 4.46. Metal diffusion coefficients in the gel layer have been taken from DGT Research Ltd., http://www.dgtresearch.com. Diffusion coefficients of complexes have been estimated as $0.7 \times D_{\mathrm{M}}$. Speciation has been calculated with Visual MINTEQ using NIST 46.6. Kinetic parameters have been estimated using the Eigen mechanism. Formation of ML_2 and the influence of the protonation processes of the ligand have been considered when necessary.

	$[NTA]_T$ (mol/L)	$[Metal]_T$ (mol/L)	pH	ξ
Cd-NTA	1.0×10^{-3}	1.0×10^{-7}	6	0.99
			9	0.98
	1.0×10^{-4}	1.0×10^{-7}	6	0.99
			9	0.99
	1.0×10^{-4}	1.0×10^{-8}	6	0.99
			9	0.99
	1.0×10^{-3}	1.0×10^{-8}	6	0.99
			9	0.98
Co-NTA	1.0×10^{-3}	1.0×10^{-7}	6	0.82
			9	0.77
	1.0×10^{-4}	1.0×10^{-7}	6	0.83
			9	0.80
	1.0×10^{-4}	1.0×10^{-8}	6	0.83
			9	0.80
	1.0×10^{-3}	1.0×10^{-8}	6	0.82
			9	0.77
Ni-NTA	1.0×10^{-3}	1.0×10^{-7}	6	0.01
			9	0.00
	1.0×10^{-4}	1.0×10^{-7}	6	0.01
			9	0.01
	1.0×10^{-4}	1.0×10^{-8}	6	0.01
			9	0.01
	1.0×10^{-3}	1.0×10^{-8}	6	0.01
			9	0.01

4.A.3 Metal Flux and Lability Degree when the Diffusion Domain Extends into the Solution Phase

4.A.3.1 Metal Flux Received by the DGT Sensor

Let us now consider the particular case in which diffusion proceeds not only inside the gel but also in a water diffusive boundary layer of thickness δ, i.e. bulk conditions are restored beyond the gel phase at $x = r + g + \delta$. Figure 4.12 schematizes the system considered.

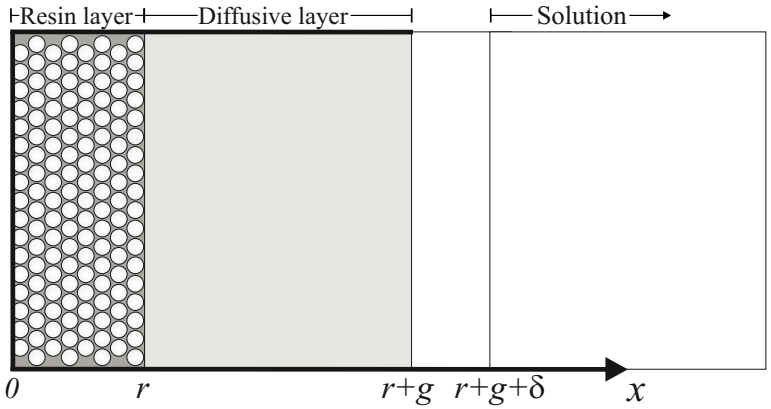

Figure 4.12: Schematic representation of a DGT device considering an additional water diffusive layer of thickness δ.

Let us represent the steady-state concentrations at the gel/water interface as $c_i(x = r + g) = c_i^{r+g}$. At this interface, the concentrations of M and ML and their fluxes must be continuous:

$$c_{\mathrm{M}}((g+r)^-, t) = c_{\mathrm{M}}((g+r)^+, t); \quad c_{\mathrm{ML}}((g+r)^-, t) = c_{\mathrm{ML}}((g+r)^+, t), \tag{4.59}$$

$$\begin{aligned} D_{\mathrm{M}} \left.\frac{\mathrm{d}c_{\mathrm{M}}}{\mathrm{d}x}\right|_{(g+r)^-} &= D_{\mathrm{M,W}} \left.\frac{\mathrm{d}c_{\mathrm{M}}}{\mathrm{d}x}\right|_{(g+r)^+}, \\ D_{\mathrm{ML}} \left.\frac{\mathrm{d}c_{\mathrm{ML}}}{\mathrm{d}x}\right|_{(g+r)^-} &= D_{\mathrm{ML,W}} \left.\frac{\mathrm{d}c_{\mathrm{ML}}}{\mathrm{d}x}\right|_{(g+r)^+}, \end{aligned} \tag{4.60}$$

where $D_{i,\mathrm{W}}$ stands for the diffusion coefficient of species i in the water domain.

Moreover, the flux received by the DGT has been identified with

$$J = D_{\mathrm{M}} \left.\frac{\partial c_{\mathrm{M}}}{\partial x}\right|_r + D_{\mathrm{ML}} \left.\frac{\partial c_{\mathrm{ML}}}{\partial x}\right|_r, \tag{4.61}$$

which, under steady-state conditions is common to all the planes of the DGT considered, so that

$$J = D_{\mathrm{M}}\frac{\mathrm{d}c_{\mathrm{M}}}{\mathrm{d}x}\bigg|_r + D_{\mathrm{ML}}\frac{\mathrm{d}c_{\mathrm{ML}}}{\mathrm{d}x}\bigg|_r = D_{\mathrm{M}}\frac{\mathrm{d}c_{\mathrm{M}}}{\mathrm{d}x}\bigg|_{(g+r)^-} + D_{\mathrm{ML}}\frac{\mathrm{d}c_{\mathrm{ML}}}{\mathrm{d}x}\bigg|_{(g+r)^-} = D_{\mathrm{M}}\frac{\mathrm{d}c_{\mathrm{M}}}{\mathrm{d}x}\bigg|_{(g+r)^+} + D_{\mathrm{ML}}\frac{\mathrm{d}c_{\mathrm{ML}}}{\mathrm{d}x}\bigg|_{(g+r)^+}. \tag{4.62}$$

If we assume that equilibrium conditions are already reached at the gel-water interface,

$$c_{\mathrm{ML}}^{r+g} = K' c_{\mathrm{M}}^{r+g}, \tag{4.63}$$

then the flux in the water phase (where there is equilibrium) can be computed as:

$$J = \frac{D_{\mathrm{M,W}}(c_{\mathrm{M}}^{*} - c_{\mathrm{M}}^{r+g})(1+\epsilon_{\mathrm{W}}K')}{\delta}, \tag{4.64}$$

where

$$\epsilon_{\mathrm{W}} = \frac{D_{\mathrm{ML,W}}}{D_{\mathrm{M,W}}}.$$

The flux in the gel phase can be computed by adapting the equation 4.41 to the boundary conditions 4.59 and 4.60. Thus

$$J = D_{\mathrm{M}}\frac{c_{\mathrm{M}}^{r+g}}{g} + D_{\mathrm{ML}}\frac{c_{\mathrm{ML}}^{r+g}}{g}\left(1 - \frac{1+\epsilon K'}{\epsilon K' + \frac{g}{m}\coth\left(\frac{g}{m}\right) + \frac{g}{\lambda_{\mathrm{ML}}}(1+\epsilon K')\tanh\left(\frac{r}{\lambda_{\mathrm{ML}}}\right)}\right), \tag{4.65}$$

or

$$J = \frac{D_{\mathrm{M,W}}(c_{\mathrm{M}}^{*} - c_{\mathrm{M}}^{r+g})(1+\epsilon_{\mathrm{W}}K'\alpha)}{g}, \tag{4.66}$$

where

$$\alpha = 1 - \frac{1+\epsilon K'}{\epsilon K' + \frac{g}{m}\coth\left(\frac{g}{m}\right) + \frac{g}{\lambda_{\mathrm{ML}}}(1+\epsilon K')\tanh\left(\frac{r}{\lambda_{\mathrm{ML}}}\right)}. \tag{4.67}$$

By isolating the intermediate quantity c_{M}^{r+g} from 4.66 and replacing it into the equality between 4.66 and 4.65, after some algebra one finally obtains:

$$J = \frac{c_{\mathrm{M}}^{*}}{\dfrac{\delta}{D_{\mathrm{M,W}}(1+\epsilon K')} + \dfrac{g}{D_{\mathrm{M}}(1+\epsilon K'\alpha)}}. \tag{4.68}$$

4.A.3.2 Lability Degree

For a labile case, full dissociation of the complex at the resin-gel interface is reached, $c_{\mathrm{ML}}^{r} = 0$ and expression 4.42 for the fully labile flux in the gel phase, can be rewritten as

$$J_{\mathrm{labile}} = \frac{D_{\mathrm{M}} c_{\mathrm{M,lab}}^{r+g}}{g} + \frac{D_{\mathrm{ML}} c_{\mathrm{ML,lab}}^{r+g}}{g}, \tag{4.69}$$

where $c_{\mathrm{M,lab}}^{r+g}$ and $c_{\mathrm{ML,lab}}^{r+g}$ are the metal and complex values at gel-water interface, respectively. This expression must be equal to the labile flux in the water phase,

$$J_{\mathrm{labile}} = \frac{D_{\mathrm{M,W}}(c_{\mathrm{M}}^{*} - c_{\mathrm{M}}^{r+g})(1+\epsilon_{\mathrm{W}} K')}{\delta}. \tag{4.70}$$

Isolating $c_{\mathrm{ML,lab}}^{r+g}$ from 4.69, we obtain for the fully labile flux:

$$J_{\mathrm{labile}} = \frac{D_{\mathrm{M,W}} D_{\mathrm{M}} c_{\mathrm{M}}^{*}(1+\epsilon_{\mathrm{W}} K')(1+\epsilon K')}{\delta D_{\mathrm{M}}(1+\epsilon_{\mathrm{W}} K') + g D_{\mathrm{M,W}}(1+\epsilon K'\alpha)}. \tag{4.71}$$

In the opposite case, when the complex is inert it does not contribute at all to the metal flux, $c_{\mathrm{ML}}^{r} = c_{\mathrm{ML}}^{r+g} = c_{\mathrm{ML}}^{*}$, so the metal flux bound to the resin is just due to the diffusion of the free metal present in the system

$$J_{\mathrm{free}} = J_{\mathrm{inert}} = \frac{D_{\mathrm{M}} c_{\mathrm{ML,lab}}^{r+g}}{g}. \tag{4.72}$$

Analogously to the last case, this flux must be equal to the inert flux in the water phase,

$$J_{\mathrm{free}} = \frac{D_{\mathrm{M,W}}(c_{\mathrm{M}}^{*} - c_{\mathrm{ML,lab}}^{r+g})}{\delta}, \tag{4.73}$$

or

$$J_{\mathrm{free}} = \frac{D_{\mathrm{M,W}} D_{\mathrm{M}} c_{\mathrm{M}}^{*}}{\delta D_{\mathrm{M}} + g D_{\mathrm{M,W}}}. \tag{4.74}$$

The lability degree, defined as

$$\xi = \frac{J - J_{\text{free}}}{J_{\text{labile}} - J_{\text{free}}},$$

can then be written as

$$\xi = \frac{\dfrac{(1+\epsilon K'\alpha)(1+\epsilon_{\text{W}} K')}{\delta D_{\text{M}}(1+\epsilon K'\alpha) + g D_{\text{M,W}}(1+\epsilon_{\text{W}} K')} - \dfrac{1}{\delta D_{\text{M}} + g D_{\text{M,W}}}}{\dfrac{(1+\epsilon K')(1+\epsilon_{\text{W}} K')}{\delta D_{\text{M}}(1+\epsilon K') + g D_{\text{M,W}}(1+\epsilon_{\text{W}} K')} - \dfrac{1}{\delta D_{\text{M}} + g D_{\text{M,W}}}}. \tag{4.75}$$

References

[1] Davison, W. and Zhang, H. In situ speciation measurements of trace components in natural-waters using thin-film gels. *Nature* 367(6463), **1994**: 546–548.

[2] Zhang, H. and Davison, W. Direct in situ measurements of labile inorganically and organically bound metal species in synthetic solutions and natural waters ussing diffusive gradients in thin films. *Analytical Chemistry* 72, **2000**: 4447–4457.

[3] Scally, S., Davison, W. and Zhang, H. In situ measurements of dissociation kinetics and labilities of metals complexes in solution using DGT. *Environmental Science and Technology* 37, **2003**: 1379–1384.

[4] Scally, S., Zhang, H. and Davison, W. Measurements of lead complexation with organic ligands using DGT. *Australian Journal of Chemistry* 57(10), **2004**: 925–930.

[5] Ernstberger, H., Zhang, H., Tye, A., Young, S. and Davison, W. Desorption kinetics of Cd, Zn, and Ni measured in soils by DGT. *Environmental Science and Technology* 39, **2005**: 1591–1597.

[6] Unsworth, E. R., Zhang, H. and Davison, W. Use of diffusive gradients in thin films to measure cadmium speciation in solutions with synthetic and natural ligands: Comparison with model predictions. *Environmental Science and Technology* 39(2), **2005**: 624–630.

[7] Galceran, J., Puy, J., Salvador, J., Cecilia, J. and van Leeuwen, H. Voltammetric lability of metal complexes at spherical microelectrodes with various radii. *Journal of Electroanalytical Chemistry* 505(1-2), **2001**: 85–94.

[8] Mongin, S., Uribe, R., Puy, J., Cecilia, J., Galceran, J., Zhang, H. and Davison, W. Key role of the resin layer thickness in the lability of complexes measured by DGT. *Environmental Science and Technology* 45(11), **2011**: 4869–4875.

[9] Chakrabarti, C., Lu, Y., Gregoire, D., Back, M. and Schroeder, W. Kinetic-studies of metal speciation using chelex cation-exchange resin – Application to cadmium, copper, and lead speciation in river water and snow. *Environmental Science and Technology* 28(11), **1994**: 1957–1967.

[10] Koutechy, J. and Brdicka, R. Fundamental equation for the electrolytic current when depending on the formation rate of the depolariser jointly with diffusion and its polarographic verification. *Collection Czechoslovak Chemical Communication* 12, **1947**: 337–355.

[11] Molina, A., Morales, I. and Lopez-Tenes, M. Chronoamperometric behaviour of a CE process with fast chemical reactions at spherical electrodes and microelectrodes. Comparison with a catalytic reaction. *Electrochemistry Communications* 8(6), **2006**: 1062–1070.

[12] Koutecky, J. and Koryta, J. The general theory of polarographic kinetic currents. *Electrochimica Acta* 3, **1961**: 318–339.

[13] Town, R. M. and van Leeuwen, H. P. Impact of ligand protonation on higher-order metal complexation kinetics in aqueous systems. *Journal of Physical Chemistry A* 112(12), **2008**: 2563–2571.

[14] Salvador, J., Puy, J., Cecilia, J. and Galceran, J. Lability of complexes in steady-state finite planar diffusion. *Journal of Electroanalytical Chemistry* 588(2), **2006**: 303–313.

[15] Wilkinson, K. J. and Buffle, J. *Physicochemical Kinetics and Transport at Chemical-biological Surfaces.* John Wiley, Chichester, UK, **2004**, 445–533.

[16] Pinheiro, J. P., Salvador, J., Companys, E., Galceran, J. and Puy, J. Experimental verification of the metal flux enhancement in a mixture of two metal complexes: the Cd/NTA/glycine and Cd/NTA/citric acid systems. *Physical Chemistry Chemical Physics* 12(5), **2010**: 1131–1138.

[17] Heyrovsky, J. and Kuta, J. *Principles of Polarography.* Academic Press, New York, **1966**.

5

Lability Criteria in Diffusion Gradients in Thin Films

Part of the content of this chapter has been published in:
***Journal of Physical Chemistry A* 116(25), 2012: 6564–6573.**

5.1 Introduction

Diffusive Gradients in Thin films (DGT) is a technique widely used for in situ monitoring a suite of analytes, including metal cations, oxyanions and other inorganic components in waters, sediments and soils [1, 2]. It accumulates solutes in a binding layer after they have diffused through a diffusive layer, usually comprising a hydrogel and a filter membrane (see Figure 5.1). Typically, Chelex 100 resin is used as the binding agent for metal ions [3]. DGT measurements provide information on metal availability [4], and they have also been shown to mimic the uptake of solutes by biota effectively [5].

Various physicochemical phenomena can affect the measurement. For example, metal accumulation is influenced by the presence of ligands whose complexes can partially dissociate within the diffusion layer and consequently contribute to the metal flux. The lability degree allows quantification of this contribution [6–10]. Analytical expressions for the metal flux, the lability degree and the concentration profiles in DGT devices have been recently reported [11] for typical DGT conditions. These expressions have been validated by comparison with both experimental results and numerical simulations, with the latter permitting consideration of a wider range of the

parameter values [12].

A noticeable outcome of this analysis was appreciation of how the metal flux to a DGT sensor in a system that contains complexing ligands may be increased by penetration of complexes into the resin disc. If the system is fully labile the penetration is minimal and DGT measurements can be interpreted using the simple standard theory. However, in some cases where the system is partially labile, this influence of complex penetration on the expected behaviour is dramatic: the system evolves from almost inert (when no penetration is considered) to labile when penetration of the complex into the resin layer is allowed. Penetration of the complex in the resin disc is a plausible hypothesis since the resin disc is made up of resin beads suspended in a gel made up of the same polymer as the diffusive gel disc. It is, then, timely to carefully analyse the processes involved in the accumulation of metal in a DGT device, identifying the key physical parameters and conditions. An informative approach is to consider the lability criteria for the DGT devices. Lability criteria [13–18] are used to decide whether the kinetics of the dissociation or diffusion of the complex is the limiting step in metal accumulation. When dissociation is the rate limiting step, the complex is termed inert or partially labile. Conversely, the complex is called labile when local equilibrium is reached in all the relevant spatial and time scales. Then, diffusion of the complex limits metal accumulation.

Here, lability criteria for the DGT devices are reported and used to appreciate the conditions responsible for the metal flux and lability degree being very dependent on the resin thickness. The characteristics of the transient regime in DGT devices are also considered to clarify further the influence of the resin thickness on the lability of the complex.

5.2 Contribution of Complexes to the Metal Accumulation

A simple system is considered where free metal ion M interacts in solution with a ligand L according to

$$\mathrm{M} + \mathrm{L} \underset{k_\mathrm{d}}{\overset{k_\mathrm{a}}{\rightleftharpoons}} \mathrm{ML}, \tag{5.1}$$

where $K' = Kc_\mathrm{L} = c^*_\mathrm{ML}/c^*_\mathrm{M}$, (superscript * indicates a bulk concentration), k_a and k_d denote the corresponding equilibrium constant and the kinetic association and dissociation constants of the complexation process, respectively.

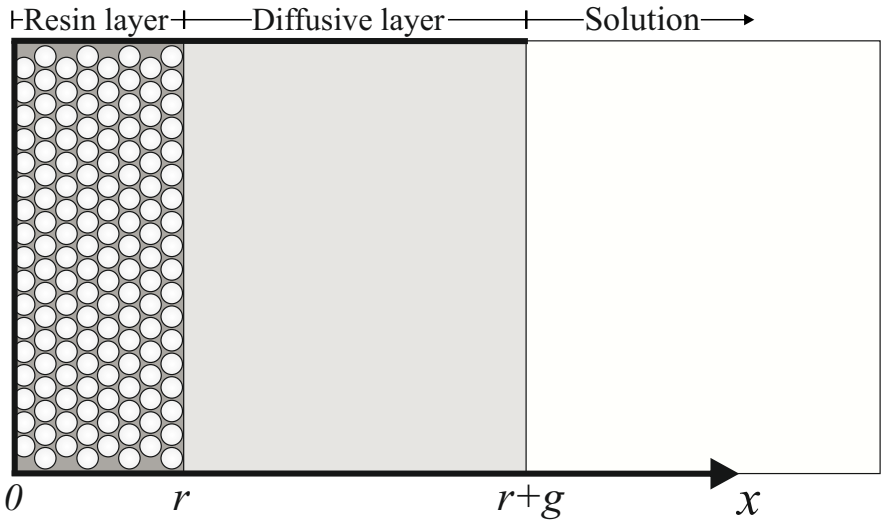

Figure 5.1: DGT Scheme showing the different phases where M, L, and ML can diffuse and react.

Species M, L and ML diffuse in a DGT device through the gel and resin layers (as sketched in Figure 5.1). In the resin layer, only the free metal is fixed according to

$$\mathrm{M} + \mathrm{R} \underset{k_{\mathrm{d,R}}}{\overset{k_{\mathrm{a,R}}}{\rightleftharpoons}} \mathrm{MR}, \tag{5.2}$$

where R labels the binding sites which, as a first approximation, are assumed to be immobile and homogeneously distributed within the resin disc. A numerical solution of the diffusion-reaction equations corresponding to the processes stated above can be reached under very general conditions [12, 19, 20]. This numerical simulation approach is used here to access both the transient and the quasi steady-state regimes and to distinguish different contributions to the accumulation.

When a DGT device is initially deployed in solution, the rate of metal accumulation increases with time. After this transient regime, a (quasi) steady-state is achieved, where metal and complex profiles within the DGT layers are nearly constant with time and metal accumulates linearly with time. An analytical expression (Eqn 5.3) for the steady-state metal flux accumulation, J, in the DGT device can be derived from the following assumptions [11]:

(i) Metal binds so quickly and strongly to the resin sites that the metal concentration inside the resin domain is negligible (as experimentally shown for many systems in [21]).

(ii) Ligand and resin sites are sufficiently in excess to be virtually unaffected by metal concentrations.

(iii) Binding sites in the resin are evenly distributed.

Under this conditions, the steady-state metal flux accumulation can be expressed as (see Chapter 4)

$$J = \frac{D_{\mathrm{M}} c_{\mathrm{M}}^*}{g} + \frac{D_{\mathrm{ML}} c_{\mathrm{ML}}^*}{g} \left[1 - \frac{1 + \epsilon K'}{\epsilon K' + \frac{g}{m} \coth\left(\frac{g}{m}\right) + \frac{g}{\lambda_{\mathrm{ML}}} (1 + \epsilon K') \tanh\left(\frac{r}{\lambda_{\mathrm{ML}}}\right)} \right], \tag{5.3}$$

where D_i and c_i represent, respectively, the diffusion coefficient and concentration of species i, r is the resin thickness and g is the aggregated thickness of diffusive gel plus filter plus diffusive boundary layer (where common diffusion coefficients of solutes are considered). In Eqn 5.4 the disequilibration parameter, m, is related to μ as

$$m = \mu \sqrt{\frac{\epsilon K'}{1 + \epsilon K'}}, \tag{5.4}$$

where μ is the classical definition of a reaction layer developed by Koutecky [22] in planar semi-infinite diffusion and ϵ is the normalized complex diffusion coefficient

$$\mu = \sqrt{\frac{D_{\mathrm{M}}}{k_{\mathrm{a}} c_{\mathrm{L}}^*}}, \tag{5.5}$$

$$\epsilon = \frac{D_{\mathrm{ML}}}{D_{\mathrm{M}}}. \tag{5.6}$$

A complex penetration parameter [11], λ_{ML}, which is related to the thickness of the resin layer that would be necessary for full complex dissociation, is related to m and μ,

$$\lambda_{\mathrm{ML}} = \sqrt{\frac{D_{\mathrm{ML}}}{k_{\mathrm{d}}}} = \sqrt{\epsilon K'} \mu = m \sqrt{1 + \epsilon K'}. \tag{5.7}$$

The lability degree, ξ, is defined as [6, 23]

$$\xi = \frac{J - J_{\mathrm{free}}}{J_{\mathrm{labile}} - J_{\mathrm{free}}}, \tag{5.8}$$

where $J - J_{\text{free}}$ denotes solely the complex contribution to the metal flux. J_{free}, the flux if the complex was totally inert, can be computed for steady state by

$$J_{\text{free}} = \frac{D_{\text{M}} c^*_{\text{M}}}{g}. \tag{5.9}$$

Jlabile, the flux if the complex was totally labile, is given by

$$J_{\text{labile}} = \frac{D_{\text{M}} c^*_{\text{M}}}{g} + \frac{D_{\text{ML}} c^*_{\text{ML}}}{g}. \tag{5.10}$$

Consequently, $J_{\text{labile}} - J_{\text{free}}$ denotes the complex contribution to the metal flux when the complex is fully labile. Then, J at steady state for any lability is given by

$$J_{\text{labile}} = \frac{D_{\text{M}} c^*_{\text{M}}}{g} + \frac{D_{\text{ML}} c^*_{\text{ML}}}{g} \xi. \tag{5.11}$$

The lability degree, ξ, can take values between 0 and 1; $\xi = 1$ means that the system is labile and full dissociation of the complex is reached at $x = r$ (i.e., at the interface between the resin and the gel layers). Conversely, when $\xi = 0$ the system is inert and $c_{\text{ML}}(x = r) = c^*_{\text{ML}}$. It has been shown [11] that the lability degree in a steady-state DGT device can alternatively be expressed as

$$\xi = 1 - \frac{c^r_{\text{ML}}}{c^*_{\text{ML}}}. \tag{5.12}$$

As indicated in the introduction section, the influence of the resin thickness on both the steady-state metal flux and the lability degree could be dramatic. This is the case shown in Figure 5.2, which uses in Eqn 5.3 the parameters of the Cd-NTA system of Mongin *et al.* [12], except k_{d} which has been decreased one order of magnitude. As can be seen, when the resin thickness is increased from $r = 0$ by a few micrometers, the metal flux is increased by a factor of 10 and the lability degree changes from almost 0 to 1. Above 0.02 mm, further increases of r have a minor influence on J or ξ.

The next sections develop qualitative explanations and simple conditions to understand and predict this strong influence of the resin thickness on lability.

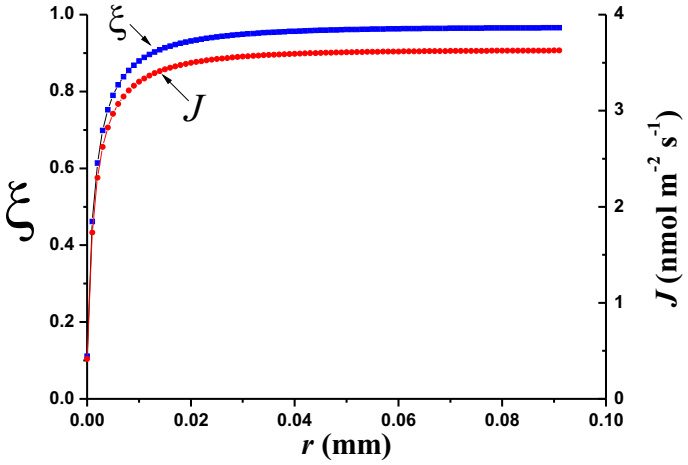

Figure 5.2: Dependence of the lability degree (ξ) (referred to the left ordinate axis) and steady state-metal flux, J, (referred to the right ordinate axis) on the thickness of the resin disc. Parameters correspond to the Cd-NTA system at pH = 7.03, ionic strength $I = 0.05$ M and T= 25 °C: $g = 1.13\times10^{-3}$ m, $D_{\mathrm{M}} = D_{\mathrm{M,R}} = 6.09\times10^{-10}$ m^2 s^{-1}, $D_{\mathrm{L}} = D_{\mathrm{L,R}} = 4.26\times 10^{-10}$ m^2 s^{-1}, $c_{\mathrm{TM}} = 9.96 \times 10^{-3}$ mol m^{-3}, $c_{\mathrm{TL}} = 0.249$ mol m^{-3}, $k_{\mathrm{a}} = 8.77 \times 10^4$ m^3 mol^{-1} s^{-1}, and $k_{\mathrm{d}} = 0.276$ s^{-1}. The standard resin thickness ($r = 4 \times 10^{-4}$ m) lies outside the range shown, in the region of near constant ξ and J.

5.3 The Reaction Layer

When M is consumed in the binding layer, a concentration profile of M is usually induced in the gel layer adjacent to the gel-resin interface. At the same time, the depletion of M induces complex dissociation and establishes a concentration profile of the complex due to its tendency to dissociate in seeking local equilibrium conditions with metal and ligand. The layer where local equilibrium is not reached is the so-called reaction layer, as was classically introduced by the Czech school in the context of chemical-electrochemical processes relevant to voltammetry [24, 25].

Figures 5.3 and 5.4 shows steady-state concentration profiles obtained from numerical simulation, as described in Chapter 2, using the parameters given in Figure 5.2. To illustrate the effect of resin thickness, resin discs that were extremely thin, $r = 4 \times 10^{-8}$ m, (Figure 5.3) and of standard thickness, $r = 4 \times 10^{-4}$ m, (in Figure 5.4) were considered. While the complex profile for the thin resin is almost flat, indicating that the complex dissociation is far from complete, most of the complex has dissociated at the resin-gel interface in the standard resin disc. Accordingly, the system is almost

inert ($\xi = 0.13$) in the DGT device of Figure 5.3, while the same system is almost labile ($\xi = 0.97$, recall Eqn 5.12) in the DGT device of Figure 5.4, in agreement with the results shown in Figure 5.2.

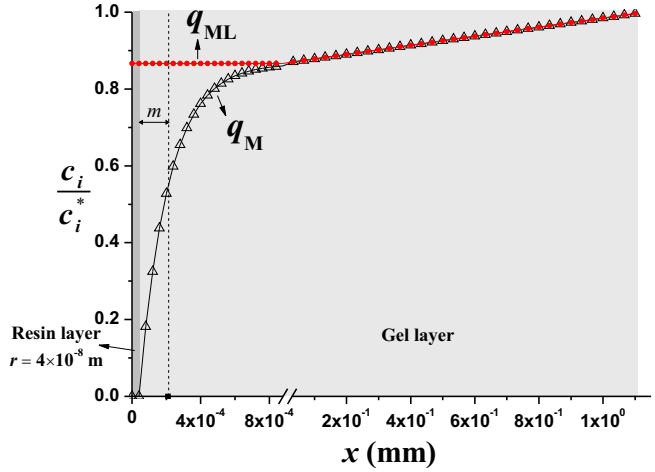

Figure 5.3: Normalized concentration profiles ($q_i = c_i/c_i^*$) of M and ML for resin thickness $r = 4 \times 10^{-8}$. Markers: red circles (ML) and black triangles (M) have been calculated with the numerical simulation described in Chapter 2, with $k_{a,R} = 10^{15}$ m^3 mol^{-1} s^{-1}, $k_{d,R} = 10^{-6}$ s^{-1}, $c_{TR} = 10^{-2}$ mol m^{-3} and $t = 10$ h. The rest of the parameters as in Figure 5.2.

In both Figures 5.3 and 5.4, the normalized profiles of metal and complex, $q_i = c_i/c^*$, with $i =$ M, ML, coincide in a region that approximately extends from the gel-solution interface ($x = r+g$) to $x = r+m\tanh g/m$ (see Chapter 4). The coincidence indicates local equilibrium conditions between M and ML. With the parameters of Figures 5.3 and 5.4, $g \gg m$, $tanhg/m \approx 1$ and $m\tanh g/m$ reduces to m without loss of accuracy. Thus, the reaction layer in the gel solution (the region where there is not equilibrium between M and ML) extends from r to $r+m$. Notice in Eqn 5.4 that m does not depend on r, so that both DGT sensors depicted in Figure 5.3 have a common thickness of the reaction layer in the gel domain, $m = 1.7 \times 10^{-7}$ m. As can be seen in Figure 5.3 and in the inset of Figure 5.4, the normalized complex profile in this region is above the metal one, indicating that net dissociation takes place.

Figures 5.3 and 5.4 (inset) show there is an additional layer inside the resin domain where metal and complex are not in equilibrium. The complexes that can penetrate into the resin gel develop a concentration profile in this layer. Since metal concentration is almost zero in the resin gel, equilib-

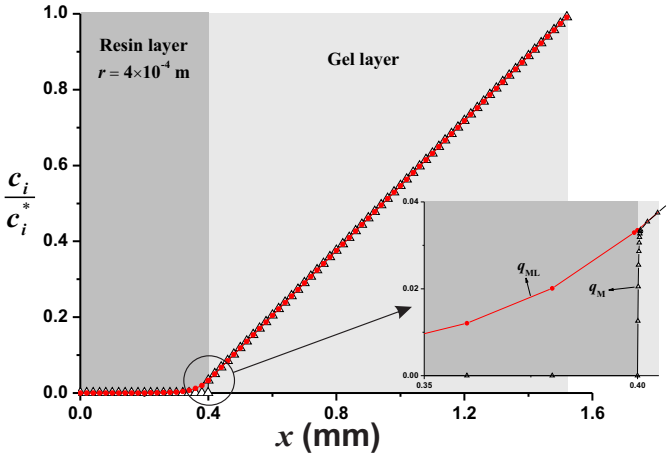

Figure 5.4: Normalized concentration profiles ($q_i = c_i/c_i^*$) of M and ML for resin thickness $r = 4 \times 10^{-4}$. Markers: red circles (ML) and black triangles (M) have been calculated with the numerical simulation described Chapter 2, with ${}^{\circ}kar = 10^{15}$ m^3 mol^{-1} s^{-1}, $k_{\mathrm{d,R}} = 10^{-6}$ s^{-1}, $c_{\mathrm{TR}} = 10^{-2}$ mol m^{-3} and $t = 10$ h. The rest of the parameters as in Figure 5.2.

rium conditions do not apply unless the concentration of the complex is also zero. Accordingly, the reaction layer in DGT devices extends to both sides of the resin gel interface as can be seen in Figures 5.3 and 5.4. This additional domain of the reaction layer in the resin disc is key to the potentially huge influence of the resin thickness on the lability degree, as seen in Figure 5.2. As reported [11], $\lambda_{\mathrm{ML}} \coth r/\lambda_{\mathrm{ML}}$ is the distance from the resin-gel interface for full complex dissociation. This is the thickness of the reaction layer in the resin disc whenever $\lambda_{\mathrm{ML}} \coth(r/\lambda_{\mathrm{ML}}) < r$. Otherwise (when $\lambda_{\mathrm{ML}} \coth(r/\lambda_{\mathrm{ML}}) > r$), the thickness is r. The dependence of this distance on r is illustrated by the cases of Figures 5.3 and 5.4. For $r = 4 \times 10^{-8}$ m, $\lambda_{\mathrm{ML}} \coth(r/\lambda_{\mathrm{ML}}) = 3.38 \times 10^{-2}$ m is thicker than the resin layer and the complex dissociation is incomplete. Conversely, for $r = 4 \times 10^{-4}$ m, $\lambda_{\mathrm{ML}} \coth(r/\lambda_{\mathrm{ML}}) = 3.92 \times 10^{-5}$ m is smaller than the resin thickness, indicating the full dissociation of the complex in the resin domain of this DGT device.

When $r \gg \lambda_{\mathrm{ML}}$, $\coth(r/\lambda_{\mathrm{ML}}) \approx 1$ and the distance for full complex dissociation becomes λ_{ML}, a value independent of r. Under this condition, the lability degree and the metal flux become independent of r, as can be seen from both J and ξ being practically horizontal in the rightmost part of Figure 5.2.

To better appreciate conceptually why this change in r affects the lability so dramatically, lability criteria are discussed in the next section.

5.4 The Lability Criteria

In determining the effect of the physical parameters of DGT on complex lability it is useful to have a means of assessing lability for the steady state situation. Simple inequalities have traditionally been used to decide whether a complex is labile or not, i.e., to assess whether transport or chemical dissociation kinetics is limiting the metal flux [9,26,27]. These inequalities, based on the comparison of the maximum kinetic and diffusive fluxes, are useful for assessing extreme situations. However, their inability to provide fully quantitative evaluations (such as those yielded by the lability degree) of the contribution of partially labile complexes to the metal flux, is a limitation.

If $\epsilon K' \gg 1$, then $D_{\mathrm{M}} c^*_{\mathrm{M}} \ll D_{\mathrm{ML}} c^*_{\mathrm{ML}}$ and the metal flux is due to the dissociating complex both in the gel and resin domains. The layer for net dissociation in the gel domain is given by m, while in the resin domain it is given by λ_{ML}, if $r > \lambda_{\mathrm{ML}} \coth(r/\lambda_{\mathrm{ML}})$, or by r, if $r < \lambda_{\mathrm{ML}} \coth(r/\lambda_{\mathrm{ML}})$. As the maximum complex concentration is c^*_{ML}, the maximum complex contribution to the metal accumulation, denoted as J_{kin}, can be estimated using

$$J_{\mathrm{kin}} = k_{\mathrm{d}} c^*_{\mathrm{ML}} [m + \min(r, \lambda_{\mathrm{ML}})],$$

where "min" represents the minimum.

Disappearance of the complex by dissociation has to be sustained by the supply of ML by diffusion, which maximally is given by $J_{\mathrm{diff}} = D_{\mathrm{ML}} c^*_{\mathrm{ML}}/g$. A comparison between J_{kin} and J_{diff}, provided by the lability parameter, L, is able to identify the rate limiting step in the metal flux,

$$\begin{aligned} L = \frac{J_{\mathrm{kin}}}{J_{\mathrm{diff}}} &= \frac{k_{\mathrm{d}} c^*_{\mathrm{ML}} [m + \min(r, \lambda_{\mathrm{ML}})]}{\dfrac{D_{\mathrm{ML}} c^*_{\mathrm{ML}}}{g}} \\ &= \frac{k_{\mathrm{d}} g [m + \min(r, \lambda_{\mathrm{ML}})]}{D_{\mathrm{ML}} c^*_{\mathrm{ML}}}. \end{aligned} \tag{5.13}$$

The system is labile (diffusion limits the metal flux) when $L \gg 1$ and inert when $L \ll 1$.

Decreasing r can decrease J_{kin}, but has no effect on J_{diff}, (Eqn 5.13). Therefore, use of a thinner resin gel layer will tend to reduce the lability of the complex, in agreement with the decrease of the metal accumulation shown

in Figure 5.2. With the use of Eqn 5.13, conditions are examined in Sections 5.4.1 and 5.4.2 for the dominance of inert behaviour when the resin layer is sufficiently thin and labile behaviour when the resin layer is sufficiently thick.

5.4.1 Thin Resin Case

When $r \to 0$ ($r \ll \lambda_{\mathrm{ML}},\ r \ll m$), J_{kin} reduces to $J_{\mathrm{kin}} = k_{\mathrm{d}} c^*_{\mathrm{ML}} m$ and the lability parameter is given by

$$L = \frac{k_{\mathrm{d}} c^*_{\mathrm{ML}} m}{\frac{D_{\mathrm{ML}} c^*_{\mathrm{ML}}}{g}} = \frac{k_{\mathrm{d}} m g}{D_{\mathrm{ML}}}. \tag{5.14}$$

Thus, a simple condition to have a low lability degree, $L \ll 1$, is

$$m \ll \frac{D_{\mathrm{ML}}}{k_{\mathrm{d}} g}, \tag{5.15}$$

or

$$\frac{g}{\epsilon}\sqrt{\frac{k_{\mathrm{d}}}{K' D_{\mathrm{ML}}}} \ll 1. \tag{5.16}$$

Conversely, under the same conditions of $r \ll m$ (so that $m + \min(r, \lambda_{\mathrm{ML}}) \approx m$), a system is labile when

$$m \gg \frac{D_{\mathrm{ML}}}{k_{\mathrm{d}} g}, \tag{5.17}$$

or

$$\frac{g}{\epsilon}\sqrt{\frac{k_{\mathrm{d}}}{K' D_{\mathrm{ML}}}} \gg 1. \tag{5.18}$$

When inequality 5.18 holds, the system tends to be inert and the kinetic flux, $J_{\mathrm{kin}} = k_{\mathrm{d}} c^*_{\mathrm{ML}} m$, is a good approximation for the actual metal flux, since the complex concentration in the reaction layer can be well described by c^*_{ML} due to the small dissociation of ML. Indeed, for the data of Figure 5.3, $J_{\mathrm{kin}} = 5.78 \times 10^{-10}$ mol m^{-2} s^{-1} is close to the actual flux $J = 5.01 \times 10^{-10}$ mol m^{-2} s^{-1} and lower than $J_{\mathrm{diff}} = 5.01 \times 10^{-10}$ mol m^{-2} s^{-1} (See Table 5.1). Accordingly, $L = J_{\mathrm{kin}}/J_{\mathrm{diff}} = 0.15 < 1$, indicating that the system is non-labile. In this case, L approaches ξ, since J_{kin} and J_{diff} approach respectively J and J_{diff}, while the contribution of J_{free} to J is almost negligible ($J_{\mathrm{free}} = 7.07 \times 10^{-14}$ mol m^{-2} s^{-1}), in agreement with the condition $\epsilon K' = 53131 \gg 1$.

The metal accumulation can be split into the contribution from the complex dissociation inside the resin domain plus the contribution from the transport and dissociation processes in the gel layer. The steady-state metal

Table 5.1: Values of the total steady-state flux J, J_{kin}, J_{diff}, J_{free}, and $L = J_{\text{kin}}/J_{\text{diff}}$ for the two r values of figures 5.3 and 5.4. Common parameters: $\epsilon K' = 53131$ and $m = 1.70 \times 10^{-7}$ m.

r (m)	ξ	L	J	J_{kin}	J_{diff} (mol m^{-2} s^{-1})	J_{free}
4×10^{-8}	0.13	0.15	5.01×10^{-10}	5.78×10^{-10}	3.75×10^{-9}	7.06×10^{-14}
4×10^{-4}	0.96	28.8	3.63×10^{-9}	1.08×10^{-7}	3.75×10^{-9}	7.06×10^{-14}

accumulation flux, J, received by the DGT device can be written as

$$J = D_{\text{M}} \frac{\mathrm{d}c_{\text{M}}}{\mathrm{d}x}\bigg|_r + D_{\text{ML}} \frac{\mathrm{d}c_{\text{ML}}}{\mathrm{d}x}\bigg|_r = J_{\text{M}}(x = r) + J_{\text{ML}}(x = r), \tag{5.19}$$

where the first term of the right-hand side gathers the contribution from the transport and dissociation processes in the gel domain and the second term is just the contribution by the complex dissociation inside the resin domain. When $\epsilon K' \gg 1$, the contribution of the bulk free metal concentration, J_{free}, is negligible and the first term of the right hand side of Eqn 5.19 essentially accounts for the complex dissociation in the gel domain.

Figure 5.5 plots the diffusional flux of both metal and complex along the DGT device: $J_{\text{M}} = D_{\text{M}} \frac{\mathrm{d}c_{\text{M}}(x)}{\mathrm{d}x}$ and $J_{\text{ML}} = D_{\text{ML}} \frac{\mathrm{d}c_{\text{ML}}(x)}{\mathrm{d}x}$. At steady state, $J = J_{\text{M}}(x) + J_{\text{ML}}(x)$ is constant at any spatial position in the gel ($x > r$) and equal to J. For $x \gg r + m$ ($m = 1.70 \times 10^{-7}$ m in Figure 5.5), J_{ML} can be regarded as constant and equal to the total metal flux bound to the resin, J, because in this region the flux due to the free metal, J_{M}, is negligible ($\epsilon K' \gg 1$). This behaviour is also consistent with the linear part of the complex concentration profile seen for most of the region $x > r + m$ in Figure 5.3.

Inside the part of the reaction layer of the gel domain, i.e., for $r < x < r+m$, Figure 5.5 shows that J_{ML} decreases concomitantly with the increase in J_{M}. Within this region, there is net dissociation of ML to render M. At $x = r$, the component $J_{\text{M}}(x = r)$ is still lower than the total metal flux, $J_{\text{M}}(x = r) < J$, since there is still an extra contribution to the total accumulation due to the complex dissociation inside the resin domain. However, this contribution is smaller, the thinner the resin disc.

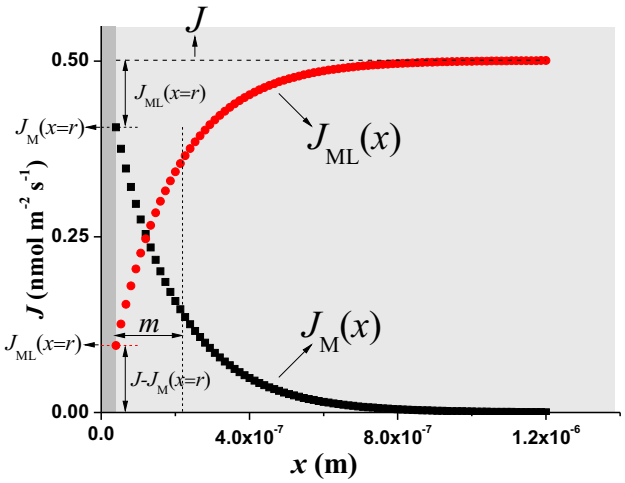

Figure 5.5: Plot of $J_{\mathrm{M}}(x)$ (black squares) and $J_{\mathrm{ML}}(x)$ (red bullets) along the gel domain. Parameters: as in Figure 5.2 with $r = 4 \times 10^{-8}$ m. The vertical dash line indicates the position of $x = r + m$.

5.4.2 Thick Resin Case

As r is increased (but still assuming $r < \lambda_{\mathrm{ML}}$, $r \sim m$), J_{kin} increases as $J_{\mathrm{kin}} = k_{\mathrm{d}} c^*_{\mathrm{ML}}(m + r)$. Further increasing of r leads to $r \gg \lambda_{\mathrm{ML}} \coth(r/\lambda_{\mathrm{ML}})$, in which case the thickness of the reaction layer in the resin domain is given by λ_{ML} and J_{kin} has to be computed using

$$J_{\mathrm{kin}} = k_{\mathrm{d}} c^*_{\mathrm{ML}}(m + r).$$

This applies in the system considered in Figure 5.4, where $r = 4 \times 10^{-4}$ m, representing the standard DGT device. In this case, the lability parameter becomes

$$L = \frac{J_{\mathrm{kin}}}{J_{\mathrm{diff}}} = \frac{k_{\mathrm{d}} g(m + \lambda_{\mathrm{ML}})}{D_{\mathrm{ML}}}, \tag{5.20}$$

which for the parameters of Figure 5.4, yields $L = 29 \gg 1$ indicating that the system is labile. Notice that in this case, the actual flux, $J = 3.63 \times 10^{-9}$ mol m^{-2} s^{-1}, can be approximated by $J_{\mathrm{diff}} = 3.75 \times 10^{-9}$ mol m^{-2} s^{-1} (See Table 5.1).

To sustain this steady-state metal flux, the supply of complex by transport should be higher than in the case where $r = 4 \times 10^{-8}$ m. This can be easily seen by comparing the slope of the normalized profile of the complex ($x > r + m$) in Figures 5.3 and 5.4.

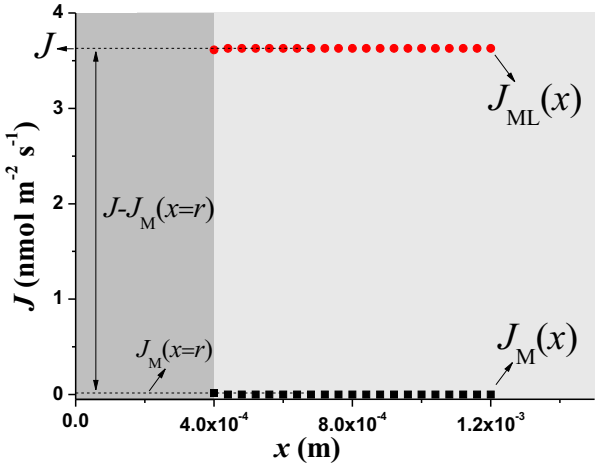

Figure 5.6: Plot of $J_{\mathrm{M}}(x)$ (black squares) and $J_{\mathrm{ML}}(x)$ (red bullets) along the gel domain. Parameters: As in Figure 5.2 with $r = 4 \times 10^{-4}$ m.

To appreciate the contribution of the complex dissociation in the resin domain to the metal accumulation, we first consider the fluxes of metal and complex in the diffusive gel given by Figure 5.6 ($r = 4 \times 10^{-4}$ m). For $x > r + m$, $J_{\mathrm{M}}(x)$ is negligible ($\epsilon K' \gg 1$), while $J \approx J_{\mathrm{ML}} \approx J_{\mathrm{diff}} = D_{\mathrm{ML}} c^*_{\mathrm{ML}}/g$, in agreement with the labile behaviour of the system. When $r < x < r+m$ (the reaction layer in the gel domain), J_{M} increases slightly as r decreases, but this increase is almost negligible compared to the metal flux received by DGT, indicating that, in this case, almost all the metal bound to the resin arises from the complex dissociation inside the resin domain, so $J \approx J_{\mathrm{ML}}(x = r)$. When $r \gg \lambda_{\mathrm{ML}}$, Eqn 5.20 indicates that a complex is labile ($L \gg 1$) when

$$m + \lambda_{\mathrm{ML}} \gg \frac{D_{\mathrm{ML}}}{k_{\mathrm{d}} g}. \tag{5.21}$$

Since for the complexes of interest, $\lambda_{\mathrm{ML}} = m\sqrt{1 + \epsilon K'} \gg m$, condition 5.21 can be rewritten as

$$\frac{1}{g}\sqrt{\frac{D_{\mathrm{ML}}}{k_{\mathrm{d}}}} \ll 1. \tag{5.22}$$

5.4.3 The Transition of Labile Behaviour

The conditions for low and high lability, Eqns 5.15 and 5.22 respectively, can be combined to predict a strong influence of the resin thickness on ξ,

$$m < \frac{D_{\mathrm{ML}}}{k_{\mathrm{d}} g} < \lambda_{\mathrm{ML}}, \tag{5.23}$$

or

$$\sqrt{\frac{D_{\mathrm{M}}}{k'_{\mathrm{a}}}} < \frac{D_{\mathrm{ML}}}{k_{\mathrm{d}} g} < \frac{D_{\mathrm{ML}}}{k_{\mathrm{d}}}. \tag{5.24}$$

The first inequality is consistent with inert behaviour when $r \ll m$, while the second one is consistent with a labile system when $r \gg \lambda_{\mathrm{ML}}$. Summarizing, for thin r, $r \ll m$, diffusional transport of the complex does not provide sufficient time for it to dissociate (while moving from the gel to the back of the resin) and, consequently, its concentration in the gel layer can remain quite high. Its behaviour, then, approaches the inert situation. When r is larger, $r \gg \lambda_{\mathrm{ML}}$, the complex is reduced to zero within the resin domain. It can, therefore, be depleted considerably within the gel layer and it appears much more labile.

5.5 Relevance of these Results for the Practical Use of DGT

Important guidelines for the use and interpretation of DGT can be inferred from the above discussion. Firstly, the lability degree for measurements made using a voltammetric sensor (characterized by no complex penetration into the electrode volume and diffusion layer δ much smaller than g) could be much smaller than the lability for measurements made using a standard DGT device, if the conditions 5.24 apply. This increase of lability for DGT is in small part due to the increase of the diffusion domain (i.e. moving from δ to g). However, the main cause of the increase in the lability degree is the penetration of the complex into the resin domain of DGT, which affects directly the overall (effective) thickness of the reaction layer. A comparison of the increase of the lability degree due to similar increases of either the gel or resin domains is reported in Figure 4.3, page 79.

Secondly it is necessary to consider the typical DGT setup where thicknesses of the DGT resin and gel layers, are of the order of mm (0.4 and 1 mm respectively for the standard device), while m is of the order of 10^{-6} m. Consequently $m \ll r$, unless complexes are extremely inert, in which case they would neither contribute to the flux nor be of interest. For the complexes of interest (i.e. when $\epsilon K' \gg 1$), $m \ll \lambda_{\mathrm{ML}} = m\sqrt{1+\epsilon K'}$ (see definition in Eqn 5.7), indicating that the reaction layer is thicker in the resin than in the gel domain. Gathering both results, it appears that for standard DGT devices, the contribution to the metal accumulation from the complex dissociation in the resin domain is likely to be higher than the contribution from the dissociation in the gel domain (i.e. $k_{\mathrm{d}} c^*_{\mathrm{ML}} m \ll k_{\mathrm{d}} c^*_{\mathrm{ML}} r$ or $k_{\mathrm{d}} c^*_{\mathrm{ML}} m \ll k_{\mathrm{d}} c^*_{\mathrm{ML}} \lambda_{\mathrm{ML}}$), as seen in Section 5.4.2.

This result is extremely important because it indicates that the lability degree is almost independent of the ligand concentration in the DGT measurements. Actually, with increasing ligand concentration the system tends to be more inert, due to the increase of the association rate, but this effect does not apply in the resin domain where free metal is absent. The impact of the ligand concentration is, then, reduced to the impact on the contribution coming from the dissociation in the gel domain, which is typically negligible in comparison to the contribution from the dissociation in the resin domain. Other consequence of the low impact of the ligand concentration on DGT lability could be the absence of mixture effects [10, 28, 29].

5.6 The Transient Regime

Although transient concentration profiles of M, L and ML for DGT have recently been discussed [30,31], the impact of the complex penetration into the resin layer was not considered. Its effect on the transient regime has a practical application, as it influences the minimum deployment times required to allow simple interpretations of DGT measurements.

Transient results were obtained from the numerical solution of the diffusion-reaction equations described in Section 3.A.1 (page 53). Resin and gel domains were assumed to be initially devoid of any metal, while bulk conditions applied at the DBL-solution interface (this is equivalent to including the filter and DBL thickness into g).

5.6.1 Transient Regime: Flux and Concentration Profiles

Figures 5.7 and 5.8 depict $J(t)$, $J_{\mathrm{M}}(x = r, t)$ and $J_{\mathrm{ML}}(x = r, t)$ versus time for the DGT devices referred to in Figures 5.2–5.8. After the few minutes required for the species to reach the resin layer, the metal flux for $r = 4{\times}10^{-4}$ m is higher than for $r = 4 \times 10^{-8}$ m, consistent with the labile behaviour associated with the thicker resin. Additionally, for $r = 4 \times 10^{-8}$ m (Figures 5.3 and 5.7), $J(t)$, $J_{\mathrm{M}}(x = r, t)$ and $J_{\mathrm{ML}}(x = r, t)$ are no longer related by steady-state Eqn 5.19. Instead, $J(t)$ (the rate of metal binding to the resin) is a little lower than $J_{\mathrm{M}}(x = r, t) + J_{\mathrm{ML}}(x = r, t)$, indicating that the flux of complex entering the resin domain per unit time is higher than the flux dissociated within the resin disc. This excess is responsible for the complex accumulation in the resin domain during the transient period, as shown by the time evolution of $J_{\mathrm{M}}(x = r, t) + J_{\mathrm{ML}}(x = r, t) - J(t)$ (Figure 5.7). At the end of the transient period, $c_{\mathrm{ML}}(x = r) \approx 0.87 c^{*}_{\mathrm{ML}}$ (Figure 5.3), in agreement with the non-labile behaviour of the complex in this DGT device with a very thin resin layer. Moreover, $J_{\mathrm{M}}(x = r, t) > J_{\mathrm{ML}}(x = r, t)$, indicating that the main contribution to the bound metal comes from the complex dissociation in the reaction layer located in the gel domain.

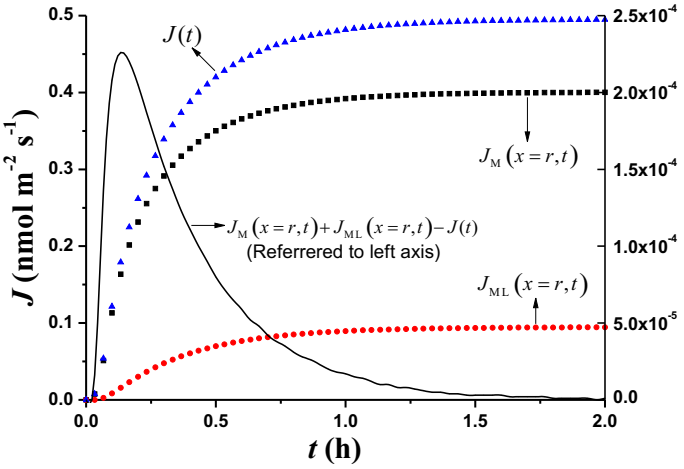

Figure 5.7: Transient fluxes. Markers: triangles: $J(t)$; squares: $J_{\mathrm{M}}(x = r, t)$; bullets: $J_{\mathrm{ML}}(x = r, t)$. Parameters: As in Figure 5.2 with $r = 4\times10^{-8}$ m. $J(t)$, $J_{\mathrm{M}}(x = r, t)$ and $J_{\mathrm{ML}}(x = r, t)$ are referred to the left ordinate axis while $J_{\mathrm{M}}(x = r, t) + J_{\mathrm{ML}}(x = r, t) - J(t)$ is referred to the right ordinate axis.

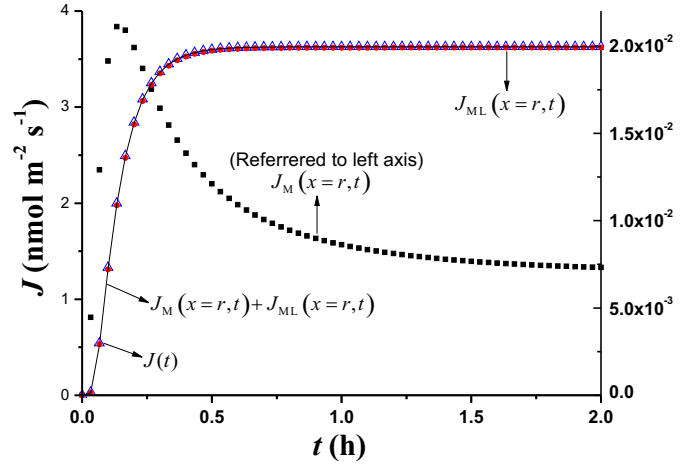

Figure 5.8: Transient fluxes. Markers: triangles: $J(t)$; squares: $J_{\mathrm{M}}(x = r, t)$; bullets: $J_{\mathrm{ML}}(x = r, t)$. Parameters: As in Figure 5.2 with $r = 4\times10^{-4}$ m. $J(t)$, $J_{\mathrm{ML}}(x = r, t)$ and $J_{\mathrm{M}}(x = r, t) + J_{\mathrm{ML}}(x = r, t)$ are referred to the left ordinate axis while $J_{\mathrm{M}}(x = r, t)$ is referred to the right ordinate axis.

In contrast, for $r = 4 \times 10^{-4}$ m (see Figure 5.8), representing a typical commercial DGT device, the system is labile with negligible concentration of the complex in the resin domain at steady state (see Figure 5.4). Accumulation of the complex in the transient regime is then negligible because almost all the complex that enters into the resin dissociates. Figure 5.8 also shows that $J_{\mathrm{M}}(x = r, t) \ll J_{\mathrm{ML}}(x = r, t)$, and $J(t) \approx J_{\mathrm{ML}}(x = r, t)$, indicating that almost all the accumulated metal comes from the dissociation of the complex inside the resin domain, in agreement with the results of Section 5.4.2.

The different behaviour of $J_{\mathrm{M}}(x = r, t)$ seen in Figures 5.7 and 5.8 is further considered by examining the concentration profiles in the transient regime at time = 0.1 h (Figures 5.9 and 5.10). Comparison of Figures 5.4 and 5.10 show that the concentrations of M can transiently exceed the M values reached in steady state. For $k_{\mathrm{d}}t \gg 1$ [15] and $x > r + m$, the profile of M adapts, by complex dissociation, to fulfil equilibrium with the profiles of L and ML, as shown by the profile of Q/K (Eqn 5.25) in Figures 5.9 and 5.10.

$$\frac{Q}{K} = \frac{\left(\dfrac{c_{\mathrm{ML}}}{c_{\mathrm{M}} c_{\mathrm{L}}}\right)}{\left(\dfrac{c^*_{\mathrm{ML}}}{c^*_{\mathrm{M}} c^*_{\mathrm{L}}}\right)} = \frac{\left(\dfrac{c_{\mathrm{ML}}}{c^*_{\mathrm{ML}}}\right)}{\left(\dfrac{c_{\mathrm{M}}}{c^*_{\mathrm{M}}}\right)\left(\dfrac{c_{\mathrm{L}}}{c^*_{\mathrm{L}}}\right)} = \frac{q_{\mathrm{ML}}}{q_{\mathrm{M}} q_{\mathrm{L}}}. \tag{5.25}$$

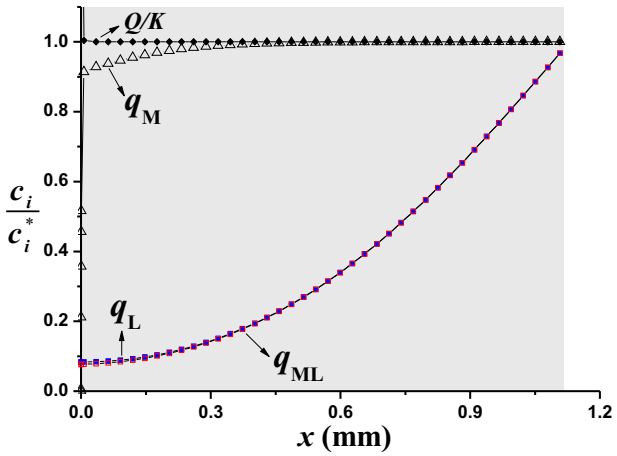

Figure 5.9: Transient normalized profiles ($q_i = c_i/c_i^*$) of c_{M}, c_{ML} and c_{L} at $t = 0.1$ h in a DGT device with resin layer thickness $r = 4 \times 10^{-8}$ m. The rest of parameters as in Figure 5.2. The ratio Q/K (see Eqn 5.25) is also depicted.

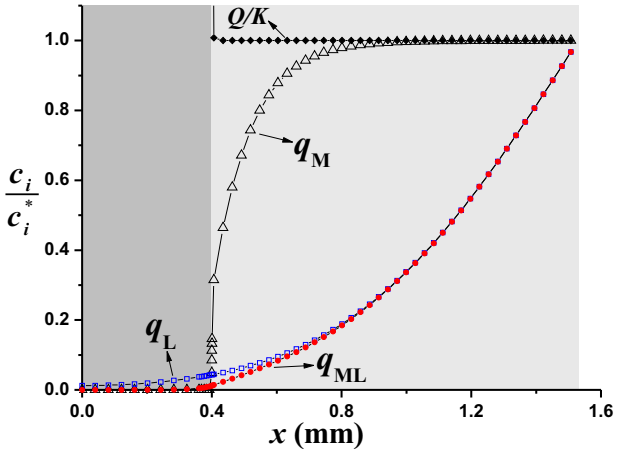

Figure 5.10: Transient normalized profiles ($q_i = c_i/c_i^*$) of c_{M}, c_{ML} and c_{L} at $t = 0.1$ h in a DGT device with resin layer thickness $r = 4 \times 10^{-4}$ m. The rest of parameters as in Figure 5.2. The ratio Q/K (see Eqn 5.25) is also depicted.

Because ML and L share a common diffusion coefficient, the normalized concentration profiles of L and ML, at short times, practically coincide, so that for $x > r + m$,

$$\frac{c_{\mathrm{M}}}{c_{\mathrm{M}}^*} = \frac{\left(\dfrac{c_{\mathrm{ML}}}{c_{\mathrm{ML}}^*}\right)}{\left(\dfrac{c_{\mathrm{L}}}{c_{\mathrm{L}}^*}\right)} \approx 1. \tag{5.26}$$

This implies that the M profile for $r < x < r + m$ is quite steep, which enables J_{M} to increase rapidly at short times. This behaviour can also be seen in Figure 4 of Davison and Zhang's review [31].

As time elapses, the profiles of L and ML depicted in Figure 5.10 (for the labile system) diverge: c_{ML} remains close to zero in the resin, due to dissociation, but the ligand profile increases continuously to eventually achieve a horizontal profile $c_{\mathrm{L}}(x) \approx c_{\mathrm{L}}^*$. In the same time period, c_{M} decreases (as predicted by Eqn 5.26 for increasing c_{L}) to approach the equilibrium conditions of the linear profile seen in Figure 5.4. The decrease in c_{M} leads to the peaked behaviour of $J_{\mathrm{M}}(x = r, t)$ seen in Figure 5.8.

For $r = 4 \times 10^{-8}$, the peaked behaviour of $J_{\mathrm{M}}(x = r, t)$ is not apparent (see Figure 5.7. The initial behaviour of the normalized profiles proceeds as in the case for $r = 4 \times 10^{-4}$ discussed above. However, now, the profiles of both

L and ML increase at the same time, so that Eqn 5.26 no longer requires a decrease of the profile of M.

5.6.2 Time to Reach Quasi Steady-State in the DGT Technique

For practical purposes, we define here the time to approach steady-state, t_{ss}, as the time required for the flux to reach 95% of the steady-state J (operationally, we took the flux corresponding to $t = 10$ h as the steady-state (ss) flux in the results presented below).

Table 5.2 gathers the times to approach steady state in DGT devices with different resin thicknesses. Counterintuitively, t_{ss} decreases as r increases, which would be expected to require more time to establish steady state concentration gradients. This behaviour is due to the different ML profiles reached in steady state as r increases. For large r values ($r = 4 \times 10^{-4}$ m, in Table 5.2), the system is close to labile, and the steady-state complex profile through the diffusive layer increases linearly from virtually zero at the resin gel. Conversely, in the near inert case ($r = 4 \times 10^{-8}$ m), the complex profile is quite flat at the end of the transient period with $c_{ML}(x = r) \approx c^*_{ML}$. This last situation requires a longer time for all the gel domain to be replenished with complex (up to c^*_{ML}).

Table 5.2: t_{ss} (computed by numerical simulation as the time required for the flux being 95% of the steady state flux) and steady-state lability degree (computed with Eqn 5.3) for the system in Figure 5.2 with different thickness of the resin domain.

r (m)	t_{ss} (min)	lability degree ξ at ss
4×10^{-8}	49	0.13
4×10^{-7}	48	0.29
4×10^{-6}	29	0.75
4×10^{-5}	20	0.96
4×10^{-4}	20	0.97

Notice that after a time of 20 min (as computed for t_{ss} in Table 5.2 for $r = 4 \times 10^{-4}$ m), $J_M(x = r, t)$ is still changing markedly, despite $J(t)$ having reached the steady-state value (Figure 5.8). This change does not impact on t_{ss}, because it has been defined with respect to the flux $J(t)$ and the contribution of $J_M(x = r, t)$ to $J(t)$ is less than 5%. As commented at the end of section 5.6.1, the decrease of $J_M(x = r, t)$ is linked to the time required for the ligand concentration to reach the bulk value in all the gel

domain [32], which is consistent with the time required to reach the true steady state.

Table 5.3 shows values of t_{ss} for a standard DGT device ($r = 4 \times 10^{-4}$ m, $g = 1.13 \times 10^{-3}$ m) when the kinetic dissociation constant is varied from low values (yielding an inert complex) to high values (yielding labile behaviour).

Table 5.3: t_{ss} (computed by numerical simulation as the time required for the flux being 95% of the steady state flux) and steady-state lability degree (computed with Eqn 5.3) for the system in Figure 5.2 with different thickness of the resin domain.

$\log(k_d)$	ξ	t_{ss} (h)
-8	0.00	0.25
-7	0.00	0.25
-6	0.00	0.32
-5	0.02	1.11
-4	0.15	1.44
-3	0.57	0.84
-2	0.87	0.42
-1	0.96	0.34
-0	0.99	0.32
1	1.00	0.31
2	1.00	0.32

For the parameters of Table 5.3, t_{ss} reaches a maximum of the order of 1.4 hours for partially labile complexes (lability degree close to 0.15). In agreement with the results reported in Table 5.2, a low lability degree leads to the longest t_{ss} because of the time required for L and ML to be distributed virtually uniformly in all the diffusion domains (gel and resin). As follows from Eq. 4.17 in Crank's book [33], the time required for $c_L(x = 0, t)$ being $0.95c_L^*$ can be estimated by

$$t_{ss} \approx -\frac{4(g+r)^2}{\pi^2 D_L} \ln\left(0.05\frac{\pi}{4}\right). \tag{5.27}$$

Using the data of Table 5.3 the derived values of $t_{ss} \approx 2$h is reasonably close to the value obtained from numerical simulation of 1.44 h for $k_d = 10^{-4}$ s^{-1}. When the system is quasi labile or quasi inert, Eqn 5.27 overestimates the

time to reach the steady-state metal accumulation flux. In the inert regime, the time for replenishing the ML concentration profile has no impact on J because the complex does not contribute to the metal accumulation flux. For the labile regime, there is no replenishment of ML because it dissociates in the gel domain. A better estimation of t_{ss} is, in these cases given by the Einstein-Smoluchowski expression,

$$t_{ss} \approx \frac{g^2}{\pi^2 D} \tag{5.28}$$

Using $D = D_M$ in the inert case and $D = D_M c^*_M / c_{T,M} + D_{ML} c^*_{ML} / c_{T,M}$ in the labile case (this implicitly assumes an excess of ligand) for the data of Table 5.3, Eqn 5.28 provides $t_{ss} \approx 0.19$ h and $t_{ss} \approx 0.26$ h for the inert and labile regimes, respectively. Thus, Eqn 5.27 provides an upper limit of t_{ss} for all cases and a rough estimate for low lability systems, while the Einstein-Smoluchowski expression can be useful for the labile and inert regimes.

Although t_{ss} values reported in Table 5.3 are usually negligible compared to typical deployments of ≥ 1 day, they should be considered in laboratory experiments with model systems.

The Einstein-Smoluchowski approach can be seen as computing the time required for the effective thickness of the diffusion layer (in planar symmetry under diffusion limited conditions) to reach the full diffusion domain. Sometimes, it has been used as a measure of the time scale of the technique, i.e., as the time available for the complex to dissociate. In this way, it can be used to justify the increase of the lability degree of a complex as the time scale of the analytical technique increases [4, 34, 35]. As explained in this work, penetration of complexes into the resin domain should be considered in the estimation of the time scale of the DGT technique, as the high impact of penetration on the lability of complexes is not due to the increase of the overall diffusion domain.

5.7 Conclusions

A particular dynamic feature of the DGT devices stems from the fact that the reaction layer is not only present in the gel domain, but also extends into the resin domain. This special feature was considered in the derivation of lability criteria for DGT (see Eqn 5.13), which were used to understand the large effect of the resin thickness on the lability degree of some complexes. A complex can be almost inert for a thin enough resin layer and become labile when the resin layer is sufficiently thick. Conditions for this behaviour have been reported (see Eqn 5.24).

The penetration of the complexes into the resin domain has a direct impact on the reaction layer, so that the main contribution to the metal accumulation flux for some partially labile complexes comes from the complex dissociation inside the resin domain. This effect rationalises the low impact of the ligand concentration on the lability degree of a complex in the DGT devices.

Penetration of complexes influences the transient behaviour of a system. The time to reach steady state (t_{ss}) was quantified as the time required for the flux of metal bound to the DGT resin layer to be at least 95% of the steady state metal flux . Systems that have complexes with low lability take longer to reach steady state than those with either inert or labile complexes.

References

[1] Warnken, K. W., Zhang, H. and Davison, W. *Passive Sampling Techniques in Environmental Monitoring*, chapter In situ monitoring and dynamic speciation measurements in solution using DGT. Elsevier, Amsterdam, **2007**, 251–278.

[2] Davison, W., Zhang, H. and Warnken, K. W. *Passive Sampling Techniques in Environmental Monitoring*, chapter Theory and applications of DGT measurements in soils and sediments. Elsevier, Amsterdam, **2007**, 353–378.

[3] Warnken, K. W., Zhang, H. and Davison, W. Performance characteristics of suspended particulate reagent-iminodiacetate as a binding agent for diffusive gradients in thin films. *Analytica Chimica Acta* 508(1), **2004**: 41–51.

[4] Van Leeuwen, H., Town, R., Buffle, J., Cleven, R., Davison, W., Puy, J., Van Riemsdijk, W. and Sigg, L. Dynamic speciation analysis and bioavailabilty of metals in aquatic systems. *Environmental Science and Technology* 39(22), **2005**: 8545–8556. Times Cited: 126 Version papier.

[5] Degryse, F., Smolders, E., Zhang, H. and Davison, W. Predicting availability of mineral elements to plants with the DGT technique: a review of experimental data and interpretation by modelling. *Environmental Chemistry* 6(3), **2009**: 198–218.

[6] Galceran, J., Puy, J., Salvador, J., Cecilia, J. and van Leeuwen, H. Voltammetric lability of metal complexes at spherical microelectrodes with various radii. *Journal of Electroanalytical Chemistry* 505(1-2), **2001**: 85–94.

[7] Puy, J., Cecilia, J., Galceran, J., Town, R. and van Leeuwen, H. Voltammetric lability of multiligand complexes: the case of ML2. *Journal of Electroanalytical Chemistry* 571(2), **2004**: 121–132.

[8] Galceran, J., Puy, J., Salvador, J., Cecilia, J., Mas, F. and Garces, J. Lability and mobility effects on mixtures of ligands under steady-state conditions. *Physical Chemistry Chemical Physics* 5(22), **2003**: 5091–5100.

[9] Salvador, J., Puy, J., Cecilia, J. and Galceran, J. Lability of complexes in steady-state finite planar diffusion. *Journal of Electroanalytical Chemistry* 588(2), **2006**: 303–313.

[10] Salvador, J., Garces, J., Galceran, J. and Puy, J. Lability of a mixture of metal complexes under steady-state planar diffusion in a finite domain. *Journal of Physical Chemistry B* 110, **2006**: 13661–13669.

[11] Uribe, R., Mongin, S., Puy, J., Cecilia, J., Galceran, J., Zhang, H. and Davison, W. Contribution of partially labile complexes to the DGT metal flux. *Environmental Science and Technology* 45(12), **2011**: 5317–5322.

[12] Mongin, S., Uribe, R., Puy, J., Cecilia, J., Galceran, J., Zhang, H. and Davison, W. Key role of the resin layer thickness in the lability of complexes measured by DGT. *Environmental Science and Technology* 45(11), **2011**: 4869–4875.

[13] Davison, W. Defining the electroanalyticallly measured species in a natural water sample. *Journal of Electroanalytical Chemistry* 87, **1978**: 395–404.

[14] Whitfield, M. and Turner, D. R. *Chemical Modeling in Aqueous Systems*. American Chemical Society, Washington DC, **1979**, 657–680.

[15] De Jong, H. and Van Leeuwen, H. Voltammetry of metal complex systems with different diffusion coefficients of the species involved. *Journal of Electroanalytical Chemistry* 234, **1987**.

[16] van Leeuwen, H. and Pinheiro, J. Lability criteria for metal complexes in micro-electrode voltammetry. *Journal of Electroanalytical Chemistry* 471(1), **1999**: 55–61.

[17] Buffle, J., Startchev, K. and Galceran, J. Computing steady-state metal flux at microorganism and bioanalogical sensor interfaces in multiligand systems. A reaction layer approximation and its comparison with the rigorous solution. *Physical Chemistry Chemical Physics* 9, **2007**: 2844–2855.

[18] Molina, A., Martinez, F. and Laborda, E. A simple transient approach to dynamic metal speciation: Can independent of time complex

voltammetric lability criteria be used? *Electrochemistry Communications* 11(3), **2009**: 562–567.

[19] Tusseau-Vuillemin, M. H., Gilbin, R. and Taillefert, M. A dynamic numerical model to characterize labile metal complexes collected with diffusion gradient in thin films devices. *Environmental Science and Technology* 37(8), **2003**: 1645–1652.

[20] Lehto, N., Davison, W., Zhang, H. and Tych, W. An evaluation of DGT performance using a dynamic numerical model. *Environmental Science and Technology* 40(20), **2006**: 6368–6376.

[21] Levy, J. L., Zhang, H., Davison, W., Puy, J. and Galceran, J. Assessment of trace metal binding kinetics in the resin phase of diffusive gradients in thin films. *Analytica Chimica Acta* 717, **2012**: 143–150.

[22] Koutechy, J. and Brdicka, R. Fundamental equation for the electrolytic current when depending on the formation rate of the depolariser jointly with diffusion and its polarographic verification. *Collection Czechoslovak Chemical Communication* 12, **1947**: 337–355.

[23] Galceran, J. and Van Leeuwen, H. *Dynamic of Biouptake Processes: the Role of Transport, Adsorption and Internalization*, chapter 4. Wiley, Chichester, UK, **2004**.

[24] Koutecky, J. and Koryta, J. The general theory of polarographic kinetic currents. *Electrochimica Acta* 3, **1961**: 318–339.

[25] van Leeuwen, H., Puy, J., Galceran, J. and Cecilia, J. Evaluation of the Koutecky-Koryta approximation for voltammetric currents generated by metal complex systems with various labilities. *Jjournal of Electroanalytical Chemistry* 526(1-2), **2002**: 10–18.

[26] van Leeuwen, H. Revisited: the conception of lability of metal complexes. *Electroanalysis* 13(10), **2001**: 826–830.

[27] Molina, A., Martinez, F., Laborda, E. and Puy, J. Lability of metal complexes at spherical sensors. Dynamic voltammetric measurements. *Physical Chemistry Chemical Physics* 12(20), **2010**: 5396–5404.

[28] Salvador, J., Garces, J., Companys, E., Cecilia, J., Galceran, J., Puy, J. and Town, R. Ligand mixture effects in metal complex lability. *Journal of Physical Chemistry A* 111, **2007**: 4304–4311.

[29] Pinheiro, J. P., Salvador, J., Companys, E., Galceran, J. and Puy, J. Experimental verification of the metal flux enhancement in a mixture of two metal complexes: the Cd/NTA/glycine and Cd/NTA/citric acid systems. *Physical Chemistry Chemical Physics* 12(5), **2010**: 1131–1138.

[30] van Leeuwen, H. P. Steady-state DGT fluxes of nanoparticulate metal complexes. *Environmental Chemistry* 8(5), **2011**: 525–528.

[31] Davison, W. and Zhang, H. Progress in understanding the use of diffusive gradients in thin films (DGT) – Back to basics. *Environmental Chemistry* 9(1), **2012**: 1–13.

[32] van der Veeken, P. L., Pinheiro, J. P. and van Leeuwen, H. P. Metal speciation by DGT/DET in colloidal complex systems. *Environmental Science and Technology* 42(23), **2008**: 8835–8840.

[33] Crank, J. *The Mathematics of Diffusion.* Clarendon Press, Oxford, **1975**.

[34] Sigg, L., Black, F., Buffle, J., Cao, J., Cleven, R., Davison, W., Galceran, J., Gunkel, P., Kalis, E., Kistler, D., Martin, M., Noël, S., Nur, Y., Odzak, N., Puy, J., Van Riemsdijk, W., Temminghoff, E., Tercier-Waeber, M., Toepperwien, S., Town, R., Unsworth, E., Warnken, K., Weng, L., Xue, H. and Zhang, H. Comparison of analytical techniques for dynamic trace metal speciation in natural freshwaters. *Environmental Science and Technology* 40(6), **2006**: 1934–1941.

[35] Unsworth, E., Warnken, K., Zhang, H., Davison, W., Black, F., Buffle, J., Cao, J., Cleven, R., Galceran, J., Gunkel, P., Kalis, E., Kistler, D., van Leeuwen, H., Martin, M., Noel, S., Nur, Y., Odzak, N., Puy, J., van Riemsdijk, W., Sigg, L., Temminghoff, E., Tercier-Waeber, M., Toepperwien, S., Town, R., Weng, L. and Xue, H. Model predictions of metal speciation in freshwaters compared measurements by in situ techniques. *Environ Sci Technol* 40, **2006**: 1942–1949.

6

Impact of Ionic Strength on Metal Accumulation in DGT

6.1 Introduction

Dynamic speciation is an emerging field that aims to understand, measure and predict the transport and bioavailability of metal ions in natural environments. Natural waters contain a large number of metal cations, small ligands as well as different proportions of dissolved organic matter which compete and interact with metals present in the system modifying its mobility and availability. The uptake of metals in this system is then, in general, a dynamic process since following the internalization process, there is a cascade of interconversion processes which tend to buffer the consumption at the surface of the sensor or living organism [1–6].

Diffusion Gradient in Thin Films (DGT) are simple devices widely used for in situ measuring the availability of most of the metal cations as well as some anions. They are based on the use of a hydrogel which defines a diffusion domain located on top of a binding layer containing a binding agent embedded in the same hydrogel used in the diffusion domain; both discs are mounted in a plastic moulder (see Figure 1.2 on page 5). Recently, some steps in the DGT measurement have been carefully analyzed. Using assemblies of resin discs in the same DGT device, the distribution of the metal bound to the resin disc has been assessed concluding that for most of the cations, at pH $\geq$ 6, the binding is strong and fast so that the resin disc acts as a perfect sink for the metal [7]. In another series of works, the contribution of complexes to the DGT accumulation has been studied [8–10].

It has been concluded that the resin disc plays an active role in the metal accumulation by extending the layer where there is net dissociation of the complex so that in many cases, the main source of metal accumulation is the dissociation of the complex inside the resin domain. Implications of these results for the practical DGT use have been discussed.

Here, in this work, another implication of these results is analyzed: The impact of the ionic strength in the metal accumulation in presence of complexes. Different previous papers have shown that the hydrogel can contain some negatively charged sites [11–14]. At low ionic strength, the charge of the gel domain leads to an electrostatic accumulation of the metal cations on the hydrogel and to metal accumulations on the DGT higher than expected. This influence is only noticeable under low ionic strength and especially when the crosslinker is not well washed. Exhaustive washing and long deployment times tend to reduce this influence [12].

The current understanding of the metal accumulation process in the DGT indicates that the resin disc plays a key role in the metal accumulation. The resin disc is expected to exhibit a high negative charge due to the metal binding sites of the resin embedded in the disc. Thus, while at high ionic strength electrostatic effects of these charged sites are screened by the background electrolyte, at low ionic strength, there will be an additional influence on the metal accumulation from the charge of the resin disc. This influence is expected to be mild for the free metal since its concentration drops to zero at the resin disc surface so that there is no penetration of free metal in the resin disc for almost all the metal cations. However, this influence is expected to be relevant for charged complexes. In this case, if the main source of metal accumulation is the complex dissociation inside the resin disc, attractive or repulsive electrostatic effects of the resin disc over these complexes is expected to strongly modify the metal accumulation. It is the aim of this work to assess the influence of low ionic strengths in the DGT metal accumulation of charged complexes. Nitrilotriacetic acid (NTA) is used as ligand since it tends to form dominant negatively charged complexes with divalent cations [15]. Section 6.2 contains the theoretical framework, Section 6.3 is devoted to the experimental details and Section 6.4 reports the experimental results together with the theoretical fitting. Finally, practical conclusions are reported in Section 6.5.

6.2 Theoretical Framework

Let us consider, in solution, the complexation of a metal M with a ligand L according to the scheme

$$\mathrm{M} + \mathrm{L} \underset{k_\mathrm{d}}{\overset{k_\mathrm{a}}{\rightleftharpoons}} \mathrm{ML}, \tag{6.1}$$

with corresponding equilibrium conditions

$$K = \frac{k_\mathrm{a}}{k_\mathrm{d}} = \frac{c^*_\mathrm{ML}}{c^*_\mathrm{M} c^*_\mathrm{L}}, \tag{6.2}$$

where K, k_a and k_d are respectively the equilibrium, and the association and dissociation rate constants of the complexation process, and c^*_i labels the concentration of species i in the bulk solution.

Although Eqn 6.2 represents a general complexation reaction, in this chapter, the complexation of Ni, Cd and Co with Nitrilotriacetic (NTA) acid will be exemplified. All these divalent cations bind to the NTA^{3-} species giving rise to negatively charged complexes.

Let us consider the following assumptions:

(i) **Perfect sink**. As previously, M, L and ML are considered to diffuse in a domain which comprises the resin layer ($0 < x < r$) and the gel layer ($0 < x < r + g$). We assume that metal concentration drops to zero along the resin gel domain due to its fast and strong binding to the resin sites. Conversely, complex penetrates into the resin gel, where it still dissociates. No direct ternary binding of complex to the resin sites is considered [16]. Thus, complex has to dissociate to allow the metal to be bound to the resin sites. Chelex beads embedded in the gel of the resin disc are used as binding agent. As a first approximation, binding sites are assumed to be evenly distributed in the resin gel [17].

(ii) **DBL**. There is evidence that the diffusion domain extends into the adjoining solution. For deployments in solution, the thickness of this extra layer is called the diffusive boundary layer (DBL) [18]. For the sake of simplicity, the DBL will not be explicitly considered here. Actually, when the difference between diffusion coefficients of a species in the solution and the gel layer is negligible, the existence of the DBL can be accounted for by simply increasing the effective value of g (see Chapter 4). The diffusion coefficients of metal ions in the filter commonly used to cover the gel layer have been shown to be similar to the values in the gel layer. Therefore this layer can also be considered by extending g.

(iii) **Electrostatic effects from the diffusive gel can be neglected. Conversely, electrostatic effects from the resin disc will be relevant**. Chelex uses iminodiacetic acid groups to bind the metals. At common environmental pH, these groups are partially charged so that electrostatic effects will arise at low ionic strength. Concentration of both low and partially labile complexes do not vanish in all the resin domain. Accordingly, concentration of electrically charged in the resin domain will be influenced from these electrostatic effects. In the present case, as complexes are negatively charged, the negative charge of the resin is expected to reduce the accumulation of complex species in the resin domain as the screening effect of the background electrolyte decreases. The diffusive gel can also contain charged groups. Previous results have reported a high affinity but low capacity of binding of metals to the polyacrylamide gels [19]. Yezek *et al* [11], also examined this effect and they did not found important electrostatic effects in a well washed polyacrilamide gel for $I > 0.1$ mM.

However, the charge of the resin domain is expected to be higher than that of the diffusive gel, since the resin gel contains the charges of the polyacrilamide gel plus the charge of the Chelex. In Chapter 5, we have stated that the main way of metal accumulation in a standard DGT device is complex dissociation inside the resin domain. Thus, in systems where the dominant metal species is the complex, if experimental data indicate a strong influence of the ionic strength in the metal accumulation, as in the data reported in this work, this influence should be due to the modification of the main source of metal release. We will then assume that electrostatic effects from the resin gel are in the basis of the ionic strength influence while electrostatic effects from the diffusive disc will be neglected.

(iv) **In both, the resin and gel domains, it is assumed that the electric potential is homogeneous, but there is a potential drop between them. This potential drop is due to the charge of the metal binding sites in the Chelex beads**. This hypothesis means that the background electrolyte ($NaNO_3$) together with the charge of the sites in the resin beads determine the electrostatic potential difference between both phases. Effects of the metal and complex concentration profile on the electrostatic potential are negligible (even at low ionic strength, metal concentrations are negligible with respect to the concentration of the background electrolyte).

(v) **Concentrations at the resin-gel interphase fulfil equilibrium conditions given by the electrostatic potential**. Concentrations at both faces of the resin-gel interphase follow Boltzmann equilibrium derived from the drop of electrostatic potential.

6.2.1 Mathematical Model

Let us denote as Ψ the difference of electrostatic potential between the resin and gel domains. The relationship between Ψ and Π, the Boltzmann factor, for a species of electrical charge equal to -1 is given by

$$\Pi = \frac{c_{\mathrm{ML}}^{r^+}}{c_{\mathrm{ML}}^{r^-}} = \exp\left(-\frac{F\Psi}{RT}\right), \tag{6.3}$$

where $c_{\mathrm{ML}}^{r^+}$ and $c_{\mathrm{ML}}^{r^-}$ stand, respectively, for the complex concentration in the diffusive gel domain and in the resin domain at both sides of the resin/gel interface. Notice that we are using $z = -1$ since the electric charge of the M-NTA complexes is -1. Free metal is not influenced by Donnan effects inside the resin domain since we assume that the resin surface acts as a perfect sink for the metal.

Assuming that the electrostatic potential is given by the charge of the resin beads, which is screened by the background electrolyte ($NaNO_3$) and neglecting the metal effects in this screening, the relationship between the electrostatic potential and the ionic strength (I, taken as the concentration of $NaNO_3$) is given by (see Section 6.A.1 on page 147 for details)

$$\Psi = \frac{RT}{F}\operatorname{arcsinh}\left(-\frac{Q}{2V_r I}\right), \tag{6.4}$$

where Q stands for the electric charge of the resin beads and V_r labels the volume of the resin domain.

With these hypothesis and those stated in Section 6.2, the expression for the metal flux derived in Chapter 4 can be extended to take into account a possible electrostatic effect of the resin. The revised expression becomes:

$$J = \frac{D_{\mathrm{M}} c_{\mathrm{M}}^*}{g} + \frac{D_{\mathrm{ML}} c_{\mathrm{ML}}^*}{g}\left[1 - \frac{\Pi(1+\epsilon K')}{\Pi\epsilon K' + \frac{\Pi g}{m}\coth\left(\frac{g}{m}\right) + \frac{g}{\lambda_{\mathrm{ML}}}(1+\epsilon K')\tanh\left(\frac{r}{\lambda_{\mathrm{ML}}}\right)}\right], \tag{6.5}$$

where all the symbols have the standard meaning (See the Section 6.A.2 for further details, page 148). Notice that no change on the diffusion coefficients between gel and resin domains is assumed, to keep the model as simple as possible.

The lability degree, ξ, is defined as

$$\xi = \frac{J - J_{\mathrm{free}}}{J_{\mathrm{labile}} - J_{\mathrm{free}}}, \tag{6.6}$$

indicating the fraction of the current contribution of the complex to the metal accumulation with respect to the maximum accumulation arisen when dissociation was so fast that metal and complex were in equilibrium along all the diffusive gel domain. Notice that this factor is just the factor between brackets in the right hand side of Eqn 6.5 since $D_{\mathrm{ML}}c_{\mathrm{ML}}/g$ is just the maximum contribution of the complex. Thus, ξ becomes

$$\xi = 1 - \frac{\Pi(1+\epsilon K')}{\Pi\epsilon K' + \dfrac{\Pi g}{m}\coth\left(\dfrac{g}{m}\right) + \dfrac{g}{\lambda_{\mathrm{ML}}}(1+\epsilon K')\tanh\left(\dfrac{r}{\lambda_{\mathrm{ML}}}\right)}. \qquad (6.7)$$

6.3 Experimental Section

6.3.1 Test Solutions

Ultrapure water (Milli-Q, Millipore) was used in all preparations. Metal stock solutions of 1000 mg metal L^{-1} were prepared from nitrate salts (AnalaR, BDH). The stocks were not acidified to allow greater control of pH during solution preparation [20].

Test solutions were prepared with Milli-Q water, to give final concentrations of 0.1, mM $NaNO_3$ (AnalaR, BDH) (i.e., $I = 0.1$, mM) with 0.005 M MOPS (BDH; pH buffer). The pH of the solution was then adjusted to 7 by dropwise addition of 0.1 M NaOH (BDH). Metals were added to solution to give a concentration of 10 μM for Co and Cd and 25 μM for Ni. Stirred solutions were left to equilibrate for 1 to 2 h.

6.3.2 Preparation of DGT Devices

Open-pore polyacrylamide diffusive gels and Chelex resin gels were prepared as documented previously [20] under clean conditions within a Class-100 laminar flow cabinet. Diffusive gels of thickness 0.80 mm were prepared, hydrated in Milli-Q. Previous experiments using similarly treated gels [12] have shown theoretical accumulation of metals from inorganic solution at $I \geq 1$ mM. These results suggest a slight positive charge on the diffusive gels. To minimize this effect, the diffusive gels were well washed until the pH of the wash water was < 7, then conditioned and stored in 0.03 M $NaNO_3$ as described previously [20]. Resin layers (of standard type, regular Chelex) of thickness 0.40 ($\pm$0.01) mm were also made, washed and conditioned. Diffusive and resin gel discs were cut using a 2.4 cm diameter gel cutter.

The devices were assembled in a Class-100 laminar flow cabinet as previously described [20]. Plastic DGT pistons and cap mouldings were pre-cleaned using one 24 h 1% Decon-90 (Decon Laboratories, UK) soak, two 24 h

10% AnalaR HNO_3 soaks, 5 washes in Milli-Q and a final soak in Milli-Q overnight. Resin gel layers were then positioned on the piston. The diffusive gel was placed on top of the resin layer, followed by an acid-washed and Milli-Q rinsed filter membrane (0.45 μm pore size, 0.14 mm thickness, 25 mm diameter, Supor-450 hydrophilic polyethersulfone membrane, Pall Corporation, USA). A total thickness of the diffusive domain of $g = 9.22 \times 10^{-4}$ m which includes the gel and filter thickness was used. Caps were fitted to secure the gels (window of area 2.54 cm^2; effective exposure area $A = 3.14 \times 10^{-4}$ m^2 due to lateral diffusion of metals in the gel [21]). Devices were deployed immediately or stored in plastic bags with 1 mL of 0.03 M $NaNO_3$ to prevent dehydration of the gel layers.

6.3.3 DGT Deployments

DGT devices were deployed at random in a 28-device rack, custom built to fit the 8 L test container. Preliminary tests using this rack showed that any variation in results is not due to position of devices within the rack (5–7% relative standard deviation all positions; 3 tests). In the current tests, devices were deployed for 24 h. Temperature measurements and 1 mL sub-samples of test solution were taken twice. Following deployment, the devices were retrieved, the fitted cap removed, and the resin layers carefully placed into 1.5 mL tubes (pre-rinsed three times with Milli-Q). One mL of 1 M HNO_3 (Aristar, BDH) was added to each tube, and the tubes placed on a shaker for 24 h to allow efficient extraction of the metals from the resin. Samples were diluted 10-fold prior to analysis. From the lowest ionic strength, additional amounts of $NaNO_3$ were added to the container to adjust the ionic strength to 10^{-3}, 10^{-2} and 10^{-1} M, respectively.

6.3.4 ICP-MS

Trace metal analysis was performed using a Thermo Elemental X7 inductively coupled plasma mass spectrometer (ICP-MS) running under the PlasmaLab® software package. A mixed metals stock was used for the preparation of ICP-MS standards (2 g L^{-1} of each trace metal, BDH). Standards were prepared at concentrations of 0.25, 0.5, 1, 2, 5, 10 and 20 μg L^{-1} trace metals. Rh was added as the internal reference (1 μg L^{-1}). Ongoing measurements of a selected standard were made every 20 samples, with a relative standard deviation of repeated measurements of $< 5\%$. Certified reference material SLRS-4 or SLRS-5 (Riverine Water, National Research Council, Canada) was measured routinely at the beginning of sample runs ($n = 2 - 3$). Runs were deemed acceptable where measured values were within one standard deviation of the supplied values.

The mass of metal accumulated on the resin was calculated as follows:

$$M = \frac{c_e(V_e + V_g)}{f_e}, \tag{6.8}$$

where M is the metal accumulated on the resin (ng metal gel^{-1}), c_e is the concentration from ICP-MS measurements of the eluted resin gel (μg L^{-1}), V_e is the volume of eluent, V_g is the volume of the resin gel and f_e is the elution factor, typically 0.8 [20].

Experiments for four different ionic strengths were carry out: $I = 0.1$ mM (A); $I = 1$ mM (B);$I = 10$ mM (C);and $I = 100$ mM (D). Experimental metal accumulations are shown in Table 6.1.

Table 6.1: DGT metal accumulation of Co, Ni and Cd in presence of NTA for four different values of ionic strength (experiments A, B, C and D). Experimental data at 24 h. The theoretical accumulations, i.e., the accumulations expected at 24 h if the M-NTA complexes were fully labile, are also shown. The ratio $D_{\mathrm{MNTA}}/D_{\mathrm{M}} = 0.7$ is assumed.

		Theoretical (nmol)			Experimental (nmol)		
	I(mM)	Co	Ni	Cd	Co	Ni	Cd
A	0.1	108.26	416.53	149.68	23.35	4.91	83.46
B	1	108.26	416.53	149.68	35.36	7.62	92.91
C	10	108.26	416.53	149.68	66.45	20.97	104.16
D	100	108.26	416.53	149.68	78.98	90.5	102.66

6.4 Results and Discussion

A first starting point is the observation that the Cd accumulation in solutions C, D and E (see columns under the experimental accumulation) is very close to 0.7 times the theoretical accumulation of Cd. This is just the factor reported for the ratio $D_{\mathrm{CdNTA}}/D_{\mathrm{Cd}}$ [9, 22]. This means that the Cd-NTA complex is fully labile in experiments C, D and E, so that the Donnan potential of the resin does not affect the accumulation.

A similar behavior is shown by Co. The Co accumulation in experiments D and E is just 0.7 times the theoretical accumulation of Co. This means that the Co-NTA complex is also fully labile in solutions D and E but not in C.

With data of Table 6.1, Ni-NTA is only partially labile under conditions of all the experiments since, even at the highest ionic strength an accumulation close to only a quarter of the theoretical accumulation is found. These results

agree quite well with those reported in Figure 4.5 (Section 4.3.5, page 79). However, experimental results reported in Table 6.1 for Ni indicate higher accumulation than the expectations derived from Figure 4.5 (page 83), based on Eigen values for the kinetic dissociation constant.

6.4.1 Fitting Procedure

6.4.1.1 Kinetic Dissociation Constant of the Ni-NTA from Conditions of Solution D

Assuming no Donnan effects for values of ionic strength $I \geq 0.1$ M [14], electrostatic effects due to the resin charges in solution D can be neglected and $\Pi = 1$ can be used under these conditions. By using $\Pi = 1$ in Eqn 6.5, we can then determine the kinetic dissociation constant for Ni-NTA.

The procedure starts computing the lability degree of each complex in each experiment as the accumulated measured mass divided by 0.7 times the theoretical mass indicated in Table 6.1 (The factor 0.7 is just the value that we are assuming for the ratio $D_{\mathrm{CdNTA}}/D_{\mathrm{Cd}}$),

$$\xi_{\mathrm{exp}} \approx \frac{J}{J_{\mathrm{labile}}} = \frac{\text{accumulated mass with ligand}}{0.7 \times \text{accumulated mass without ligand}}. \tag{6.9}$$

Equation 6.9 indicates that we are neglecting the accumulation due to the free metal. Indeed, we have checked that $\epsilon K' \gg 1$ for all the experiments, for all the complexes at pH 7 and for the whole range of ionic strength values studied. Values of ξ_{exp} are reported in Table 6.2 for the different experiments.

Table 6.2: Lability degree of M-NTA complexes (M = Co, Ni, Cd) computed by Eqn 6.9 using data from Table 6.1

	ξ_{exp} *		
I (mM)	Co	Ni	Cd
0.1	0.31	0.02	0.80
1	0.47	0.03	0.89
10	0.88	0.07	0.99
100	0.95	0.31	0.98

* $D_{\mathrm{ML}} = 0.7 D_{\mathrm{M}}$

We can use the lability degree of the Ni-NTA complex at experiment D to obtain the corresponding k_{d} value. In particular, recalling that

$$m = \frac{\lambda_{\mathrm{ML}}}{\sqrt{1 + eKp}}, \tag{6.10}$$

and using $g = 9.22 \times 10^{-4}$ as reported in the experimental section, and $K' = 2.47 \times 104$ M^{-1} given by Visual MINTEQ, Eqn 6.7 can be solved to obtain λ_{ML} using, in the leftmost hand side, the experimental value ξ_{exp} from Table 6.2. Afterwards, k_d can be computed from

$$k_d = \frac{D_{ML}^2}{\lambda_{ML}}, \tag{6.11}$$

using $D_{ML} = 0.7 D_M$. The resulting kinetic dissociation rate constant for Ni is $k_d = 5.81 \times 10^{-4}$ s^{-1}.

Here we have supposed that the kinetic dissociation rate constant (k_d) do not change with the ionic strength. Actually, we have seen that the strong dependence of K and k_a on the ionic strength is almost canceled when we compute k_d as

$$k_d = \frac{k_a}{K}. \tag{6.12}$$

A further discussion on this assumption in given in Section 6.A.3, page 153.

6.4.1.2 Fitting of the Boltzmann Factors, Π, at each Ionic Strength

Once k_d of the Ni-NTA is known, Π values can be computed by fitting the experimentally measured lability degree at the different ionic strengths using Eqn 6.7. Π values thus obtained hold for all the metals, since they are only dependent on the charge of the resin and the ionic strength. Resulting values are gathered in Table 6.3. With the Π values reported in Table 6.3, a unique

Table 6.3: Boltzmann factors (Π) for M-NTA complexes (M = Co, Ni, Cd) for different values of ionic strength. Values obtained from fitting of Eqn 6.7 with data of Table 6.2. The table also shows the ratio Q/V_r (the density of charge of the Chelex, see Eqn 6.13) and the Donnan potential computed by Eqn 6.4.

	I (mM)	Π	Ψ (mV)	Q/V_r
A	0.1	32.49	90	5.10×10^{-3}
B	1	19.12	80	1.35×10^{-2}
C	10	6.08	50	6.04×10^{-2}
D	100	1.00	0	0

kinetic dissociation constant for each M-NTA complex can be computed using Eqn 6.7 and experiment B. This experiment is used since both Co-NTA and Cd-NTA are non labile at this ionic strength so that the lability degree is dependent on the kinetic dissociation constant. The resulting k_d-values are reported in Table 6.4. These values can be compared with the expected values using Eigen ideas which are also reported in Table 6.4. The

Table 6.4: Kinetic dissociation rate constants for M-NTA complexes (M = Co, Ni, Cd). The values are obtained from Eqn 6.7 using the lability values reported in Table 6.2. The k_d values calculated by using Eigen ideas are reported in the last column.

	k_d Values	
	fitted	using Eigen ideas
Ni-NTA	5.81×10^{-4}	7.77×10^{-6}
Co-NTA	6.55×10^{-2}	7.38×10^{-3}
Cd-NTA	2.90×10^{0}	4.19×10^{0}

k_d values recovered for Cd are not far away from Eigen expectations, but some differences are obtained for Co and Ni. Part of this deviation could be due to a difference between the diffusion coefficient of ML in the gel and resin domains, which we are currently taken as equal.

We can try to check the accuracy of these fittings by plotting the experimental mass accumulation together with the predicted mass from Eqn 6.5 with k_d given in Table 6.4 and Π given in Table 6.3 for all the ionic strength values. Figures 6.1 to 6.3 show these results for the different metals.

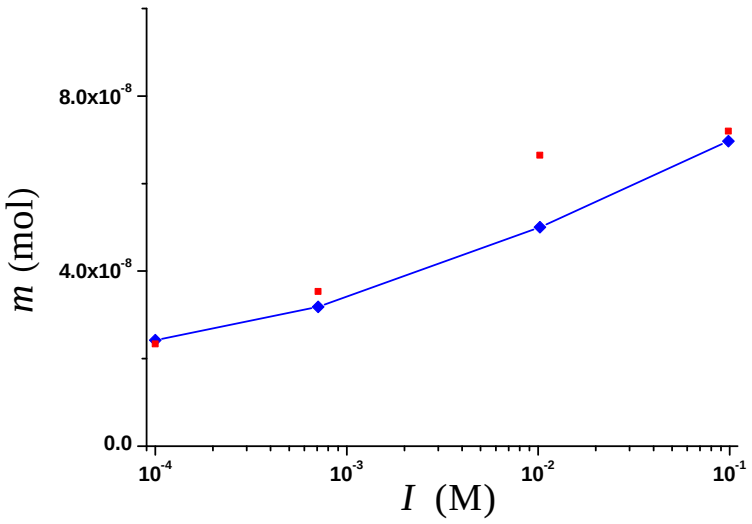

Figure 6.1: Accumulated mass of Co in front of ionic strength. Blue line plus diamond: values computed by Eqn 6.5 using fitted values of Tables 6.3 and 6.4. Red squares: experimental accumulation reported in Table 6.1.

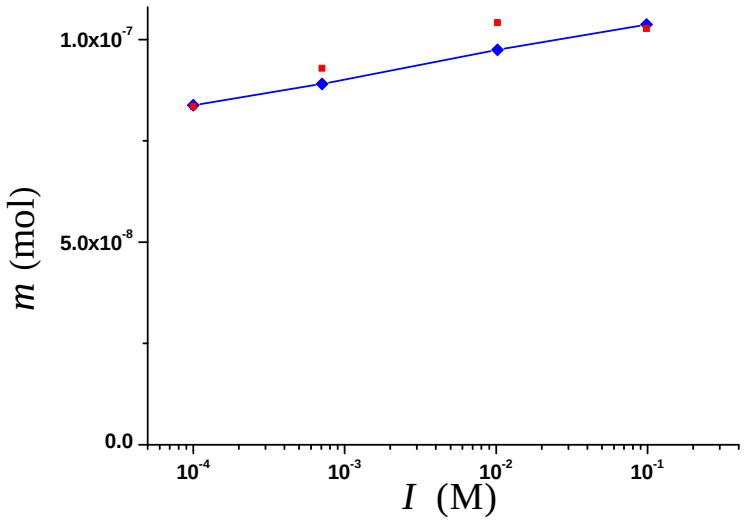

Figure 6.2: Accumulated mass of Cd in front of ionic strength. Blue line plus diamond: values computed by Eqn 6.5 using fitted values of Tables 6.3 and 6.4. Red squares: experimental accumulation reported in Table 6.1.

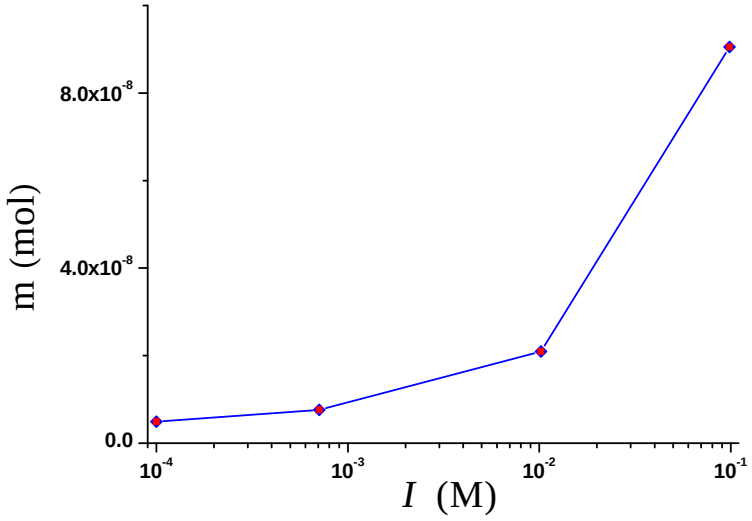

Figure 6.3: Accumulated mass of Ni in front of ionic strength. Blue line plus diamond: values computed by Eqn 6.5 using fitted values of Tables 6.3 and 6.4. Red squares: experimental accumulation reported in Table 6.1.

A quite nice agreement between calculated and experimental mass accumulation for all the metals and experiments is shown.

Values of Π reported in Table 6.3 deserve further comments: for the lowest ionic strength, the concentration of M-NTA at the resin side of the resin/gel interface is 32 times lower than the corresponding concentration at the gel part. This is a quite important electrostatic effect which cannot be neglected in the interpretation of DGT metal accumulations at low ionic strengths. Donnan factors of this order have been found for proton accumulations at the Donnan volume of humic acids [23]. Also, factors of the order of 10^3 are found between the concentration of divalent metals in the Donnan phase with respect to the bulk solution in the metal titration of Humic Acids.

A graphical explanation of the resin effect on the complex concentration profile is found in Figure 6.4 which depicts the concentration profiles of Ni (blue markers) and Ni-NTA (red markers) at pH = 7 and $I = 10^{-2}$ M. Notice the drop of the Ni-NTA profile at $x = r$, the resin gel interface. The ratio between the concentrations at both sides of the interface is just the factor Π whose value is Π = 6.08 as indicated in Table 6.3. This effect is derived from the electrostatic repulsion between the negative charge of both the resin and the Ni-NTA species.

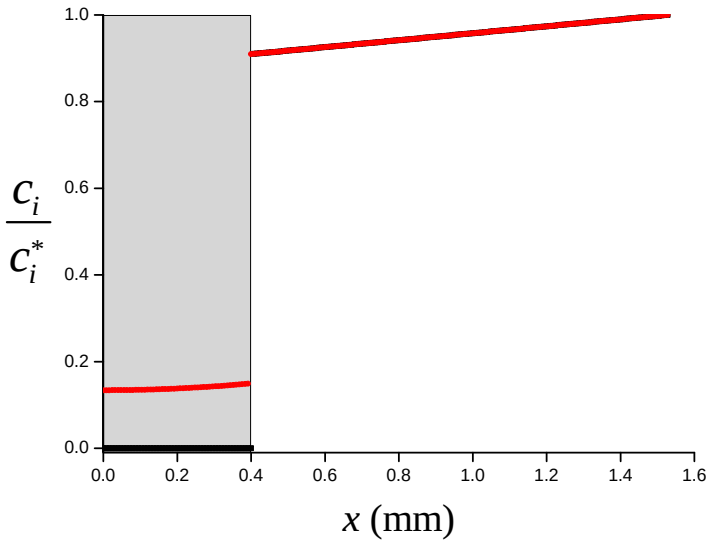

Figure 6.4: Normalized concentration profiles of Ni (Black line) and Ni-NTA (red line) for $I = 1 \times 10^{-2}$ M (Π = 6.08). The profile was computed by Eqn 6.7 using data of Tables 6.3 and 6.4.

A final step is the calculation of the charge of the resin in each experiment. Combining Eqns 6.3 and 6.4 we have

$$\ln \pi = \operatorname{arcsinh}\left(-\frac{Q}{2V_r I}\right), \tag{6.13}$$

from which the density of charge of the chelex, Q/V_r, can be determined at each ionic strength. Results are reported in the last column of Table 6.3.

6.5 Conclusions

Donnan effects are relevant to understand the metal accumulations at low ionic strength media especially for partially labile complexes. The main influence of Donnan effects arise from the deprotonated groups of the resin beads. As this charge is negative, the main effect is a exclusion of the negatively charged complexes. No important effects are expected for free metals, since they get bound just at the resin-gel interface.

A model that considers Donnan potentials derived from the resin charges and the screening of the background electrolyte is here developed under equilibrium conditions for the resin/gel interface. Expressions for metal flux accumulation and lability degree are reported.

Electrostatic potentials of the order of 100 mV arise in the standard resin domain made up with Chelex at pH = 7 and $I = 0.1$ mM. The corresponding Donnan factors can be read in Table 6.3. Notice that these values can be used for any DGT experiment at pH = 7, whenever the mass of Chelex in the resin disc is the standard one as used in the present work. Obviously, complexes with charge z need to correct the Boltzmann factor as Π^z.

Expressions here reported for the metal flux and lability degree are able to quantitatively reproduce the metal accumulations for Cd, Co and Ni-NTA complexes in the ionic strength range $I = 0.1$, to $I = 100$ mM.

6.A Supporting Information

6.A.1 Relationship Between the Electrostatic Potential and the Ionic Strength

Let us denote c_i^r and c_i^g as the concentration of specie i in the resin and in the gel phase, respectively. As we used $NaNO_3$ as background electrolyte, the relationship between concentration expressed in 6.3 can be read as

$$\frac{c^g_{NO_3^-}}{c^r_{NO_3^-}} = \exp\left(-\frac{F\Psi}{RT}\right), \tag{6.14}$$

$$\frac{c^g_{Na^+}}{c^r_{Na^+}} = \exp\left(+\frac{F\Psi}{RT}\right). \tag{6.15}$$

Additionally, the electroneutrality conditions read

$$c^g_{NO_3^-} + c^g_{Na^+} = 0, \tag{6.16}$$

in the gel phase, and

$$c^r_{NO_3^-} + c^r_{Na^+} + \frac{Q}{V_r} = 0. \tag{6.17}$$

in the resin phase, where Q stands for the electric charge of the resin beads and V_r labels the volume of the resin domain.

By Using $c^g_{NO_3^-} = -c^g_{Na^+}$ (from Eqn 6.16, and expressions 6.14 and 6.15, we can rewrite 6.17 as

$$c^g_{NO_3^-}\left(e^{\left(\frac{F\Psi}{RT}\right)} - e^{\left(-\frac{F\Psi}{RT}\right)}\right) = -\frac{Q}{V_r}, \tag{6.18}$$

or

$$\sinh\left(\frac{F\Psi}{RT}\right) = -\frac{Q}{2V_r c^g_{NO_3^-}}. \tag{6.19}$$

On the other side, the ionic strength can be computed as

$$I = \sum_i \frac{1}{2} c_i z_i^2 = \frac{1}{2} c^g_{NO_3^-} + \frac{1}{2} c^g_{Na^+} = c^g_{NO_3^-}. \tag{6.20}$$

Then, isolating Ψ from 6.19, we can express the electrostatic potential as a function of the ionic strength,

$$\Psi = \frac{RT}{F}\,\mathrm{arcsinh}\left(-\frac{Q}{2V_r I}\right). \tag{6.21}$$

6.A.2 Steady State Approximate Analytical Solution for the Metal Flux and Lability Degree

6.A.2.1 The Model

Here we used the same model and assumptions used in Section 4.A (Chapter 4, page 84). The mathematical formulation is the same except that here we assume a difference of electrostatic potential between the resin and gel domains. Then, the relationship between concentration of complex inside and outside the resin-gel surface gives the new boundary condition at $x = r$,

$$\Pi = \frac{c_{\mathrm{ML}}^{r^+}}{c_{\mathrm{ML}}^{r^-}}, \tag{6.22}$$

where Π, is the Boltzmann factor, and $c_{\mathrm{ML}}^{r^-}$ and $c_{\mathrm{ML}}^{r^+}$ are respectively, the concentration at both left and right sides of the frontier of resin-gel interface. In this model, free metal is not influenced by Donnan effects inside the resin domain, since we assume that the resin surface acts as a perfect sink for the metal.

6.A.2.2 Diffusion-Reaction Conditions in the Resin Layer

With the above conditions, in steady state the diffusion equations for the resin layer explicitly reported in Section 3.A.1 (page 53) can be greatly simplified.

First, there is an effective zero concentration of metal in the resin layer,

$$c_{\mathrm{M}}(0 < x < r) = 0. \tag{6.23}$$

Consequently, the diffusion of complex in the resin layer is described by

$$\frac{\mathrm{d}^2 c_{\mathrm{ML}}}{\mathrm{d}x^2} = \frac{k_{\mathrm{d}}}{D_{\mathrm{ML,R}}} c_{\mathrm{ML}} = \frac{c_{\mathrm{ML}}}{\lambda_{\mathrm{ML}}^2} \quad \text{for} \quad 0 < \mathrm{x} < \mathrm{r}, \tag{6.24}$$

with

$$\lambda_{\mathrm{ML}} = \sqrt{\frac{D_{\mathrm{ML,R}}}{k_{\mathrm{d}}}} = \sqrt{\epsilon K'}\mu, \tag{6.25}$$

where λ_{ML} has dimensions of a distance and can be seen as a "penetration parameter" related to the distance required for a complex diffusing into the resin layer to dissociate fully (See Sections 4.3.3 and 4.A.1.7 for a more detailed physical interpretation). The general solution of Eqn 6.24 can be written as

$$c_{\mathrm{ML}}(x \leq r) = Ae^{(x/\lambda_{\mathrm{ML}})} + Be^{(-x/\lambda_{\mathrm{ML}})}, \tag{6.26}$$

where A and B are integration constants that have to fulfil the boundary value problem

$$\left.\frac{\mathrm{d}c_{\mathrm{ML}}}{\mathrm{d}x}\right|_{x=0} = 0 \tag{6.27}$$

and

$$D_{\mathrm{ML,R}} \left.\frac{\mathrm{d}c_{\mathrm{ML}}}{\mathrm{d}x}\right|_{x=r^-} = D_{\mathrm{ML}} \left.\frac{\mathrm{d}c_{\mathrm{ML}}}{\mathrm{d}x}\right|_{x=r^+}, \tag{6.28}$$

The application of Eqn 6.27 in Eqn 6.26 leads to $A = B$, so that the solution can be rewritten as

$$c_{\mathrm{ML}}(x \leq r) = c_{\mathrm{ML}}(x = 0) \cosh\left(\frac{x}{\lambda_{\mathrm{ML}}}\right). \tag{6.29}$$

Labelling as $c_{\mathrm{ML}}^{r^-}$ the complex concentration at the frontier between the resin and diffusion layer ($x = r$),

$$c_{\mathrm{ML}}^{r^-} = c_{\mathrm{ML}}(x = r^-) = c_{\mathrm{ML}}(x = 0) \cosh\left(\frac{r}{\lambda_{\mathrm{ML}}}\right), \tag{6.30}$$

the complex concentration profile inside the resin layer becomes

$$c_{\mathrm{ML}}(x \leq r) = c_{\mathrm{ML}}^{r^-} \frac{\cosh\left(\frac{x}{\lambda_{\mathrm{ML}}}\right)}{\cosh\left(\frac{r}{\lambda_{\mathrm{ML}}}\right)}. \tag{6.31}$$

The application of Eqn 6.28 requires knowledge of the flux of complex entering the resin layer calculated from the resin side. From Eqn 6.31, it becomes

$$J_{\mathrm{ML}} = D_{\mathrm{ML,R}} \left.\frac{\mathrm{d}c_{\mathrm{ML}}}{\mathrm{d}x}\right|_{x=r^-} = D_{\mathrm{ML,R}} \frac{c_{\mathrm{ML}}^{r^-}}{\lambda_{\mathrm{ML}}} \tanh\left(\frac{r}{\lambda_{\mathrm{ML}}}\right) = k_{\mathrm{d}} c_{\mathrm{ML}}^{r^-} \lambda_{\mathrm{ML}} \tanh\left(\frac{r}{\lambda_{\mathrm{ML}}}\right) \tag{6.32}$$

6.A.2.3 Diffusion-Reaction Conditions in the Gel Layer

In the gel layer, steady state conditions for M and ML apply

$$0 = D_{\mathrm{M}} \frac{\mathrm{d}^2 c_{\mathrm{M}}}{\mathrm{d}x^2} - k_{\mathrm{a}} c_{\mathrm{M}} c_{\mathrm{L}} + k_{\mathrm{d}} c_{\mathrm{ML}}, \tag{6.33}$$

$$0 = D_{\mathrm{ML}} \frac{\mathrm{d}^2 c_{\mathrm{ML}}}{\mathrm{d}x^2} + k_{\mathrm{a}} c_{\mathrm{M}} c_{\mathrm{L}} - k_{\mathrm{d}} c_{\mathrm{ML}}. \tag{6.34}$$

An equivalent system of equations to that given by Eqns 6.33 and 6.34 is

$$0 = \frac{\mathrm{d}^2}{\mathrm{d}x^2}(D_{\mathrm{M}}c_{\mathrm{M}} + D_{\mathrm{ML}}c_{\mathrm{ML}}), \tag{6.35}$$

$$0 = \frac{\mathrm{d}^2}{\mathrm{d}x^2}(c_{\mathrm{ML}} - K'c_{\mathrm{M}}) - \left(\frac{k_{\mathrm{d}}}{D_{\mathrm{ML}}} + \frac{k'_{\mathrm{a}}}{D_{\mathrm{M}}}\right)(c_{\mathrm{ML}} - K'c_{\mathrm{M}}), \tag{6.36}$$

which has the advantage of allowing the uncoupling of the system.

Eqn 6.35 is just the addition of Eqns 6.33 and 6.34. Its integration yields

$$D_{\mathrm{M}}c_{\mathrm{M}} + D_{\mathrm{ML}}c_{\mathrm{ML}} = D_{\mathrm{ML}}c^r_{\mathrm{ML}} + \frac{(D_{\mathrm{M}}c^*_{\mathrm{M}} + D_{\mathrm{ML}}c^*_{\mathrm{ML}}) - D_{\mathrm{ML}}c^r_{\mathrm{ML}}}{g}(x - r). \tag{6.37}$$

Eqn 6.36 constitutes a closed equation for

$$\phi = c_{\mathrm{ML}} - K'c_{\mathrm{M}}. \tag{6.38}$$

Recalling that m (see 4.3.3 for a detailed physical interpretation) can be written as

$$\frac{1}{m^2} = \frac{1}{\mu^2}\left(\frac{1 + \epsilon K'}{\epsilon K'}\right), \tag{6.39}$$

where μ is the classical definition of reaction layer introduced by Koutecky in planar semi-infinite diffusion [24],

$$\mu = \sqrt{\frac{D_{\mathrm{M}}}{k'_{\mathrm{a}}}}, \tag{6.40}$$

Eqn 6.36 can be rewritten as

$$\frac{\mathrm{d}^2\phi}{\mathrm{d}x^2} = \frac{\phi}{m^2}, \tag{6.41}$$

whose general solution is

$$\phi = A\sinh\left(\frac{g + r - x}{m}\right) + B\cosh\left(\frac{g + r - x}{m}\right), \tag{6.42}$$

where A and B are integration constants. The boundary conditions for Eqn 6.41 are given by

$$\phi(x = g + r) = 0 \tag{6.43}$$

and

$$\phi(x = r) = c^r_{\mathrm{ML}}. \tag{6.44}$$

Applying these conditions we obtain $B = 0$ and

$$A = \frac{c_{\mathrm{ML}}^{r^+}}{\sinh \dfrac{g}{m}},$$

so that

$$\phi = c_{\mathrm{ML}}^{r^+} \frac{\sinh\left(\dfrac{g + r - x}{m}\right)}{\sinh\left(\dfrac{g}{m}\right)}. \tag{6.45}$$

The derivative of ϕ in $x = r$

$$\left.\frac{\mathrm{d}\phi}{\mathrm{d}x}\right|_{x=r^+} = -\frac{c_{\mathrm{ML}}^{r^+}}{m} \coth\left(\frac{g}{m}\right) = \left.\frac{\mathrm{d}c_{\mathrm{ML}}}{\mathrm{d}x}\right|_{x=r^+} - K' \left.\frac{\mathrm{d}c_{\mathrm{M}}}{\mathrm{d}x}\right|_{x=r^+}, \tag{6.46}$$

and that of Eqn 6.37

$$D_{\mathrm{M}} \left.\frac{\mathrm{d}c_{\mathrm{M}}}{\mathrm{d}x}\right|_{x=r^+} + D_{\mathrm{ML}} \left.\frac{\mathrm{d}c_{\mathrm{ML}}}{\mathrm{d}x}\right|_{x=r^+} = \frac{(D_{\mathrm{M}} c_{\mathrm{M}}^* + D_{\mathrm{ML}} c_{\mathrm{ML}}^*) - D_{\mathrm{ML}} c_{\mathrm{ML}}^{r^+}}{g}, \tag{6.47}$$

allows the flux of ML entering into the resin layer, calculated from the diffusive gel side, to be written as

$$\begin{aligned} J_{\mathrm{ML}} &= D_{\mathrm{ML}} \left.\frac{\mathrm{d}c_{\mathrm{ML}}}{\mathrm{d}x}\right|_{x=r^+} \\ &= \frac{-D_{\mathrm{ML}} c_{\mathrm{ML}}^{r^+} (g/m) \coth(g/m) + \epsilon K' (D_{\mathrm{M}} c_{\mathrm{M}}^* + D_{\mathrm{ML}} c_{\mathrm{ML}}^* - D_{\mathrm{ML}} c_{\mathrm{ML}}^{r^+})}{g(1 + \epsilon K')}. \end{aligned} \tag{6.48}$$

The continuity of the flux requires the equality of J_{ML} calculated from Eqn 6.48 and from 6.32 (as stated in Eqn 6.28). The fulfilment of condition 6.28 can then be used to isolate $c_{\mathrm{ML}}^{r^+}$ so that

$$c_{\mathrm{ML}}^{r^+} = \frac{\Pi c_{\mathrm{ML}}^* (1 + \epsilon K')}{\Pi \epsilon K' + \Pi \dfrac{g}{m} \coth\left(\dfrac{g}{m}\right) + \dfrac{g}{\lambda_{\mathrm{ML}}} \dfrac{D_{\mathrm{ML,R}}}{D_{\mathrm{ML}}} (1 + \epsilon K') \tanh\left(\dfrac{r}{\lambda_{\mathrm{ML}}}\right)}. \tag{6.49}$$

6.A.2.4 Metal Flux

Under steady state conditions, the metal flux bound to the resin layer, J, is the total metal flux entering the resin layer both as free metal and complex,

$$J = D_{\mathrm{M}} \frac{\mathrm{d}c_{\mathrm{M}}}{\mathrm{d}x}\bigg|_{x=0} + D_{\mathrm{ML}} \frac{\mathrm{d}c_{\mathrm{ML}}}{\mathrm{d}x}\bigg|_{x=0}, \tag{6.50}$$

and due to the linearity of the profile of $D_{\mathrm{M}}c_{\mathrm{M}} + D_{\mathrm{ML}}c_{\mathrm{ML}}$ in the gel layer (as given by Eqn 6.37),

$$J = D_{\mathrm{M}} \frac{c^*_{\mathrm{M}}}{g} + D_{\mathrm{ML}} \frac{c^*_{\mathrm{ML}} - c^{r^+}_{\mathrm{ML}}}{g},$$

which, using Eqn 6.49, becomes

$$J = D_{\mathrm{M}} \frac{c^*_{\mathrm{M}}}{g} + D_{\mathrm{ML}} \frac{c^*_{\mathrm{ML}}}{g} \left(1 - \frac{\Pi(1+\epsilon K')}{\Pi\epsilon K' + \Pi \dfrac{g}{m} \coth\left(\dfrac{g}{m}\right) + \dfrac{g}{\lambda_{\mathrm{ML}}} \dfrac{D_{\mathrm{ML,R}}}{D_{\mathrm{ML}}} (1+\epsilon K') \tanh\left(\dfrac{r}{\lambda_{\mathrm{ML}}}\right)} \right) \tag{6.51}$$

6.A.2.5 Lability Degree

For a labile case, full dissociation of the complex at the resin-gel interface is reached, $c^r_{\mathrm{ML}} = 0$ and according to Eqn 6.47, the metal flux bound to the resin becomes

$$J_{\mathrm{labile}} = \frac{D_{\mathrm{M}} c^*_{\mathrm{M}}}{g} + \frac{D_{\mathrm{ML}} c^*_{\mathrm{ML}}}{g}. \tag{6.52}$$

In the opposite case, when the complex is inert, it does not contribute at all to the metal flux, $c^r_{\mathrm{ML}} = c^*_{\mathrm{ML}}$ and the metal flux bound to the resin is just due to the diffusion of the free metal present in the system

$$J_{\mathrm{free}} = J_{\mathrm{inert}} = \frac{D_{\mathrm{M}} c^*_{\mathrm{M}}}{g}. \tag{6.53}$$

The lability degree, defined as

$$\xi = \frac{J - J_{\mathrm{free}}}{J_{\mathrm{labile}} - J_{\mathrm{free}}}, \tag{6.54}$$

can, then, be written as

$$\xi = 1 - \frac{c_{\mathrm{ML}}^{r+}}{c_{\mathrm{ML}}^{*}}, \tag{6.55}$$

or

$$\xi = 1 - \frac{\Pi(1+\epsilon K')}{\Pi\epsilon K' + \Pi\dfrac{g}{m}\coth\left(\dfrac{g}{m}\right) + \dfrac{g}{\lambda_{\mathrm{ML}}}\dfrac{D_{\mathrm{ML,R}}}{D_{\mathrm{ML}}}(1+\epsilon K')\tanh\left(\dfrac{r}{\lambda_{\mathrm{ML}}}\right)}. \tag{6.56}$$

6.A.3 Dependence of k_{d} on the Ionic Strength

The ionic strength could impacts on the predicted metal accumulation via changes in parameters such as K, k_{a} and k_{d}. Here we are interested in knowing how this parameters change with ionic strength (I).

First, We know that

$$k_{\mathrm{d}} = \frac{k_{\mathrm{a}}}{K}. \tag{6.57}$$

Following Eigen ideas, k_{a} can be estimate by

$$k_{\mathrm{a}} = K^{\mathrm{os}} k_{\mathrm{w}}, \tag{6.58}$$

where K^{os} and k_{w} stand, respectively, for the stability constant of the outer sphere ML complex and the dehydration rate constant of M. The k_{w} values are reported in the literature and K^{os}-values could be estimated using the electrostatic model

$$K^{\mathrm{os}} = \frac{4\pi}{3} N_{\mathrm{AV}} a^3 \exp\left(-\frac{U(a)}{k_{\mathrm{B}}T}\right), \tag{6.59}$$

where

$$U(a) = \frac{z_{\mathrm{M}} z_{\mathrm{L}} e^2}{4\pi\varepsilon_0\varepsilon a}\left(1 - \frac{\kappa a}{1+\kappa a}\right), \tag{6.60}$$

and

$$\kappa = \sqrt{\frac{2N_{\mathrm{AV}}e^2 I}{\varepsilon_0\varepsilon k_{\mathrm{B}}T}}. \tag{6.61}$$

On the other hand, the complexation constant (K) at a given ionic strength is related the thermodynamic complexation constant, K^{th}, by

$$K^{\mathrm{th}} = K\frac{\gamma_{\mathrm{ML}}}{\gamma_{\mathrm{M}}\gamma_{\mathrm{L}}}, \tag{6.62}$$

where γ_i labels the activity coefficient of species i.

Using Davies expression for the activity coefficients,

$$\gamma_i = -0.51 z_i^2 \left(\frac{\sqrt{I}}{1+\sqrt{I}} - 0.3I \right), \tag{6.63}$$

we have

$$\begin{aligned} K &= K^{\mathrm{th}} \frac{\gamma_{\mathrm{M}} \gamma_{\mathrm{L}}}{\gamma_{\mathrm{ML}}} \\ &= \frac{\left(-0.51 z_{\mathrm{M}}^2 \left(\frac{\sqrt{I}}{1+\sqrt{I}} - 0.3I \right) \right) \left(-0.51 z_{\mathrm{L}}^2 \left(\frac{\sqrt{I}}{1+\sqrt{I}} - 0.3I \right) \right)}{-0.51 z_i^2 \left(\frac{\sqrt{I}}{1+\sqrt{I}} - 0.3I \right)}. \end{aligned} \tag{6.64}$$

As the validity of the Davies equation is expected up to $I = 0.5$ M, Eqns 6.64 and 6.58 can be used in 6.57 to study the dependence of k_{d} on I

Figures 6.5, 6.6 and 6.7 show k_{d} as a function of I for Ni, Co and Cd respectively, in the range of the experimental values of ionic strength used here.

As the small changes of k_{d} values shown in Figures 6.5, 6.6 and 6.7 do not produce appreciable changes in the calculus of lability degree by Eqn 6.7 (see Figures 6.8, 6.9 and 6.10), in a first approximation we used a fixed value of k_{d} for the whole range of ionic strength values.

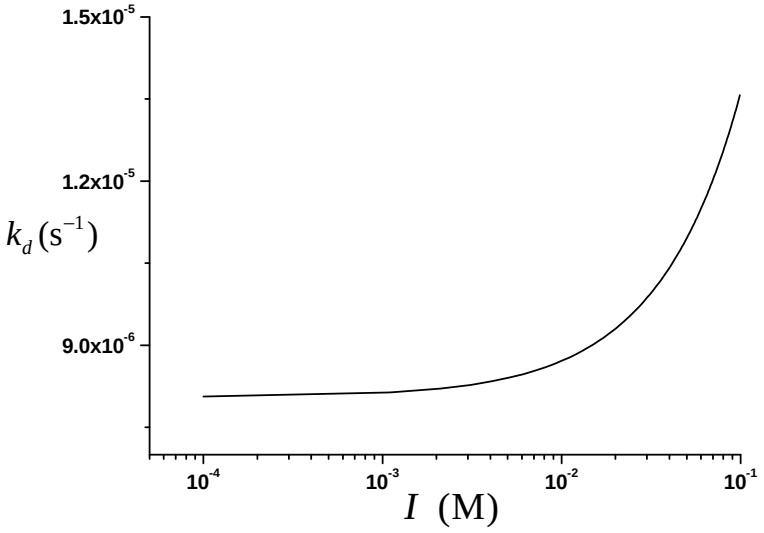

Figure 6.5: Kinetic dissociation rate constant (k_{d}) of Ni-NTA as a function ionic strength.

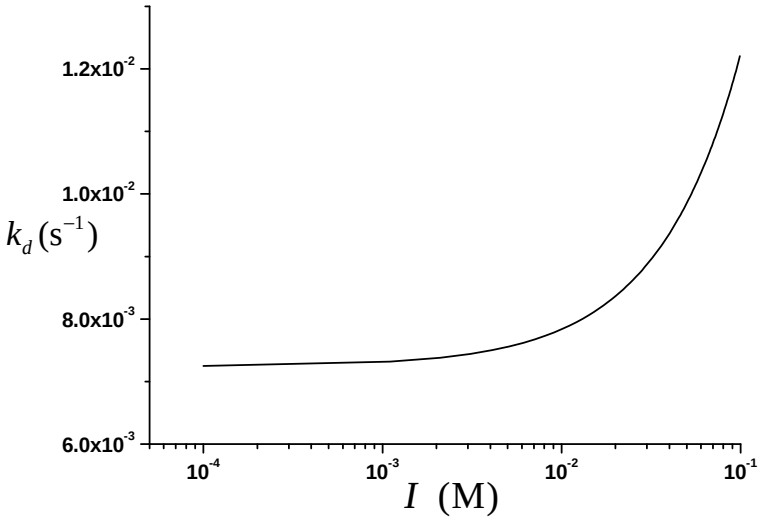

Figure 6.6: Kinetic dissociation rate constant (k_{d}) of Co-NTA as a function ionic strength.

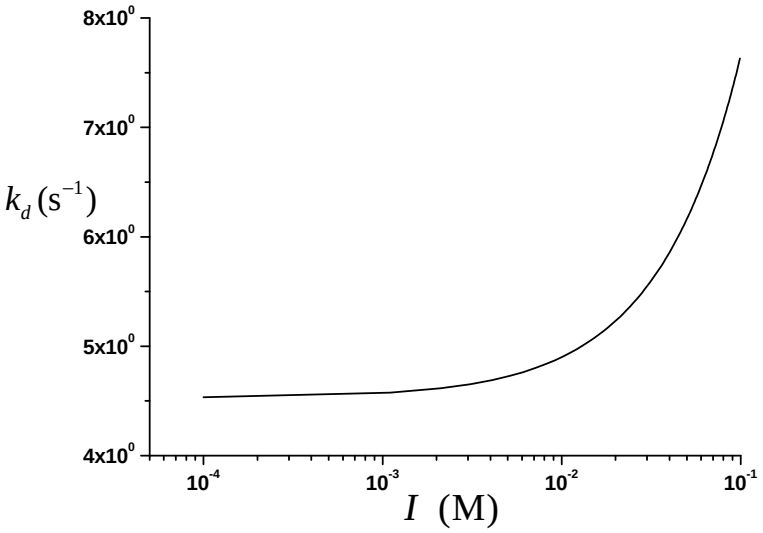

Figure 6.7: Kinetic dissociation rate constant (k_d) of Cd-NTA as a function ionic strength.

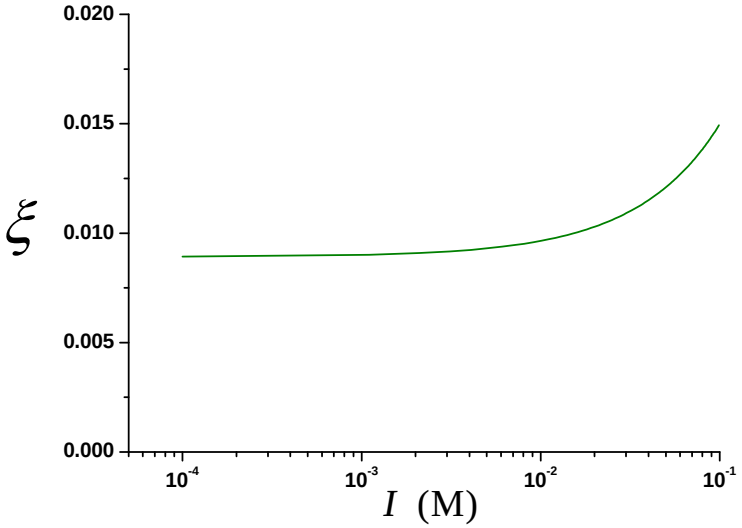

Figure 6.8: Lability degree (ξ) of Ni-NTA as a function ionic strength.

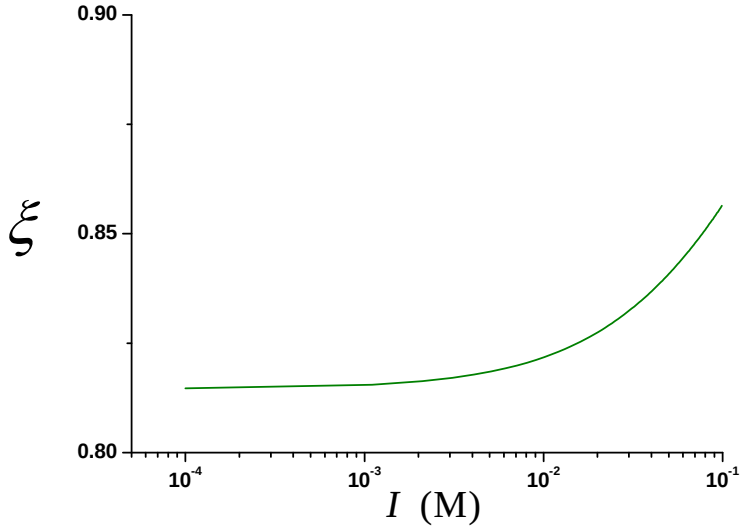

Figure 6.9: Lability degree (ξ) of Co-NTA as a function ionic strength.

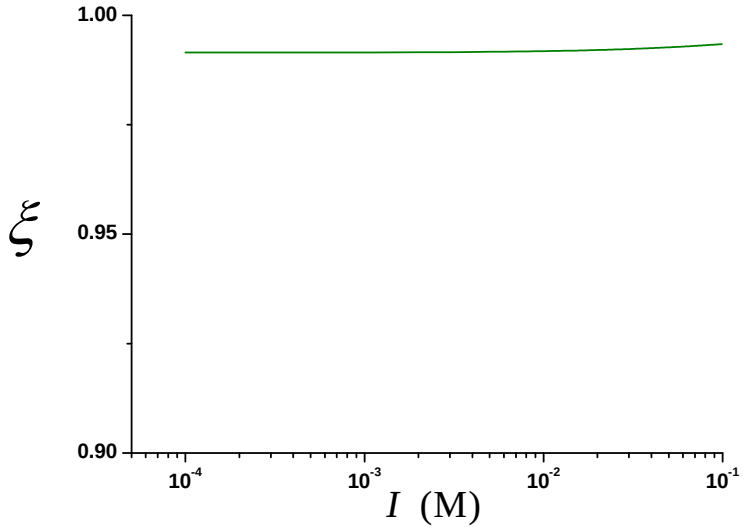

Figure 6.10: Lability degree (ξ) of Cd-NTA as a function ionic strength.

References

[1] Buffle, J. and Horvai, G. *In situ Monitoring of Aquatic Systems: Chemical Analysis and Speciation*, volume 6. John Wiley and Sons, Chichester, UK, **2000**.

[2] Fasfous, I. I., Yapici, T., Murimboh, J., Hassan, I., Chakrabarti, C., Back, M., Lean, D. and Gregoire, D. Kinetics of trace metal competition in the freshwater environment: Some fundamental characteristics. *Eenvironmental Science and Technology* 38(19), **2004**: 4979–4986.

[3] Galceran, J. and van Leeuwen, H. P. *IUPAC Series on Analytical and Physical Chemistry of Environmental Systems*, chapter Physicochemical kinetics and transport at chemical-biological surfaces. John Wiley, **2004**, 147–203.

[4] Buffle, J. *Complexation Reactions in Aquatic Systems. An Analytical Approach.* Chichester, UK, **1988**.

[5] Salvador, J., Puy, J., Cecilia, J. and Galceran, J. Lability of complexes in steady-state finite planar diffusion. *Journal of Electroanalytical Chemistry* 588(2), **2006**: 303–313.

[6] Salvador, J., Puy, J., Galceran, J., J., Cecilia, J., Town, R. and van Leeuwen, H. Lability criteria for successive metal complexes in steady-state planar diffusion. *Journal of Physical Chemistry B* 110(2), **2006**: 891–899.

[7] Levy, J., Zhang, H., Davison, W., Puy, J. and Galceran, J. Assessment of trace metal binding kinetics in the resin phase of diffusive gradients in thin films. *Analytica Chimica Acta* 717, **2012**: 143–150.

[8] Uribe, R., Mongin, S., Puy, J., Cecilia, J., Galceran, J., Zhang, H. and Davison, W. Contribution of partially labile complexes to the DGT metal flux. *Environmental Science and Technology* 45(12), **2011**: 5317–5322.

[9] Mongin, S., Uribe, R., Puy, J., Cecilia, J., Galceran, J., Zhang, H. and Davison, W. Key role of the resin layer thickness in the lability of complexes measured by DGT. *Environmental Science and Technology* 45(11), **2011**: 4869–4875.

[10] Puy, J., Uribe, R., Mongin, S., Galceran, J., Cecilia, J., Levy, J., Zhang, H. and Davison, W. Lability criteria in diffusive gradients in thin films. *The Journal of Physical Chemistry A* **2012**.

[11] Yezek, L. and van Leeuwen, H. Donnan effects in the steady-state diffusion of metal ions through charged thin films. *Langmuir* 21(23), **2005**: 10342–10347.

[12] Warnken, K., Zhang, H. and Davison, W. Trace metal measurements in low ionic strength synthetic solutions by diffusive gradients in thin films. *Analytical Chemistry* 77, **2005**: 5440–5446.

[13] Yezek, L., van der Veeken, P. and van Leeuwen, H. Donnan effects in metal speciation analysis by DET/DGT. *Environmental Science and Technology* 42(24), **2008**: 9250–9254.

[14] Golmohamadi, M., Davis, T. and Wilkinson, K. Diffusion and partitioning of cations in an agarose hydrogel. *Journal of Physical Chemistry A* 116(25), **2012**: 6505–6510.

[15] Diaz, J., Sanchis, J., Chekmeneva, E., Arino, C. and Esteban, M. Non-linear multivariate curve resolution analysis of voltammetric pH titrations. *Analyst* 135(7), **2010**: 1653–1662.

[16] Chakrabarti, C., Lu, Y., Gregoire, D., Back, M. and Schroeder, W. Kinetic-studies of metal speciation using chelex cation-exchange resin – Application to cadmium, copper, and lead speciation in river water and snow. *Environmental Science and Technology* 28(11), **1994**: 1957–1967.

[17] Zhang, H. and Davison, W. Direct in situ measurements of labile inorganically and organically bound metal species in synthetic solutions and natural waters ussing diffusive gradients in thin films. *Analytical Chemistry* 72, **2000**: 4447–4457.

[18] Warnken, K., Davison, W., Zhang, H., Galceran, J. and Puy, J. In situ measurements of metal complex exchange kinetics in freshwater. *Environmental Science and Technology* 41(9), **2007**: 3179–3185.

[19] Garmo, O. A., Davison, W. and Zhang, H. Interactions of trace metals with hydrogels and filter membranes used in DET and DGT techniques. *Environmental Science and Technology* 42(15), **2008**: 5682–5687.

[20] Davison, W., Fones, G., Harper, M., Teasdale, P. and Zhang, H. *In Situ Moniring Aquatic Systems: Chemical Analysis and Speciation*, chapter Dialysis, DET and DGT: In situ diffusional techniques for studying water, sediments and soils. Wiley, New York, **2000**, 495–570.

[21] Davison, W. and Zhang, H. Progress in understanding the use of diffusive gradients in thin films (DGT) – Back to basics. *Environmental Chemistry* 9(1), **2012**: 1–13.

[22] Unsworth, E. R., Zhang, H. and Davison, W. Use of diffusive gradients in thin films to measure cadmium speciation in solutions with synthetic and natural ligands: Comparison with model predictions. *Environmental Science and Technology* 39(2), **2005**: 624–630.

[23] Koopal, L., Saito, T., Pinheiro, J. and van Riemsdijk, W. Ion binding to natural organic matter: General considerations and the NICA-Donnan model. *Colloids and Surfaces A: Physicochemical and Engineering Aspects* 265(1-3), **2005**: 40–54.

[24] Heyrovsky, J. and Kuta, J. *Principles of Polarography.* Academic Press, New York, **1966**.

7

Mixture Effect

7.1 Introduction

Generally, a mixture of different kind of ligands, particles, colloids, and so forth, is the common situation encountered by a metal in natural aquatic ecosystem [1–4]. In those systems, the metal flux toward a consuming interface, for example, an analytical sensor or an accumulating organism, results from the coupled diffusion and kinetics of interconversion between the metal M and the various species in the medium. As we have seen in previous sections, the prediction of the processes that control the metal flux is embodied in the concept of lability.

Until now, few papers [5–9] have given some consideration to the effect of the mixture, that is, the change in the lability degree of a complex in a mixture with respect to the lability degree of the same complex in a single ligand system (with the same bulk concentrations than in mixture). Actually, for DGT devices, considering complex penetration into resin, there are no previous studies about the mixture effect.

In Chapter 5 we have stated that for standard DGT devices, in which complex can penetrate the resin layer, the mixture effect could be small in comparison to voltammetric measurements. This statement is based on the fact that the main contribution to total DGT flux comes from complex dissociation inside the resin, where no mixture effects are present because the absence of free metal concentration.

In this chapter we discuss the mixture effect in detailed way, aiming to quantify it in a system with a mixture of ligands.

7.2 Contribution of Complexes to the Metal Flux in DGT

When a DGT device is deployed in solution, the rate of metal accumulation increases with time. After this transient regime, a (quasi) steady-state is achieved where all metal (both, as free or as complex) entering into the resin gets bound linearly with time. In a system containing one metal M and a single ligand L, the rate of metal accumulation in this (quasi) steady-state can be expressed by

$$J = \frac{D_{\mathrm{M}} c^*_{\mathrm{M}}}{g} + \frac{D_{\mathrm{ML}} c^*_{\mathrm{ML}}}{g}\xi, \tag{7.1}$$

where, in case of ligand excess (i.e. $\epsilon K' \gg 1$),

$$\xi = 1 - \frac{\Pi(1+\epsilon K')}{\Pi\epsilon K' + \dfrac{\Pi g}{m}\coth\left(\dfrac{g}{m}\right) + \dfrac{g}{\lambda_{\mathrm{ML}}}(1+\epsilon K')\tanh\left(\dfrac{r}{\lambda_{\mathrm{ML}}}\right)}. \tag{7.2}$$

Similarly, in steady state, the metal accumulation in a DGT device can be seen as the sum of two different contributions,

$$J = D_{\mathrm{M}}\frac{\mathrm{d}c_{\mathrm{M}}}{\mathrm{d}x}\bigg|_{x=r} + D_{\mathrm{ML}}\frac{\mathrm{d}c_{\mathrm{ML}}}{\mathrm{d}x}\bigg|_{x=r} = J_{\mathrm{M}}(x=r) + J_{\mathrm{ML}}(x=r), \tag{7.3}$$

where $J_{\mathrm{M}}(x=r)$ is the flux contribution coming from free metal transport and complex dissociation in the diffusive gel, and $J_{\mathrm{ML}}(x=r)$ is the one coming from net complex dissociation inside the resin.

In a system with excess of ligand, i.e. $\epsilon K' \gg 1$, ($J_{\mathrm{free}} \approx 0$) profiles of c_{M} and c_{ML} are known [10] so Eqn 7.3 can be used to evaluate separately the contribution of complex to the flux both inside and outside of resin layer. Figure 7.1 (using similar parameters to those of Cd-NTA experimental system of Mongin *et al* [11]) shows the complex contribution to the flux by dissociation in a DGT sensor both inside the resin layer, $J_{\mathrm{ML}}(x=r)$, and inside the gel layer, $J_{\mathrm{M}}(x=r) - J_{\mathrm{free}}$, against different values of the lability degree (yielded by varying the kinetic dissociation constant from low values, inert complex, to high values, labile behavior), for two values of ionic strength (panels a and b) and for two different K values.

Let us focus initially on panel (a) of Figure 7.1 (where $I \geq 0.1$ M). For almost all the kinetic range (even at very low values of lability in leftmost side), $J_{\mathrm{ML}}(x=r) > J_{\mathrm{M}}(x=r)$, indicating that in a measure with a standard DGT sensor, the main contribution to the flux comes from complex dissociation inside resin, independently of the K value. The behavior at the highest lability values ($\xi \sim 1$ at rightmost side of Figure 7.1a) deserves an additional comment: when the complex concentration on the resin-gel interface is zero

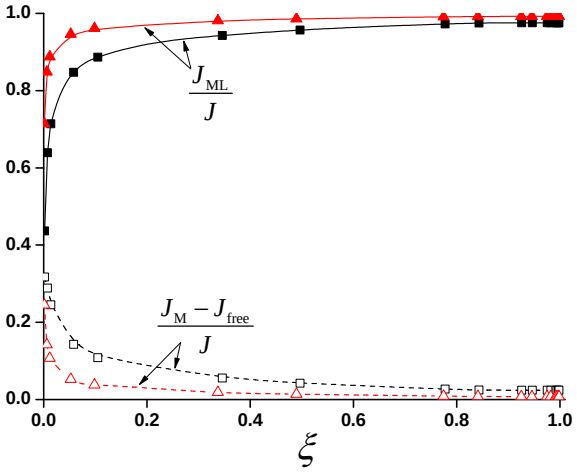

(a) $\Pi = 1$

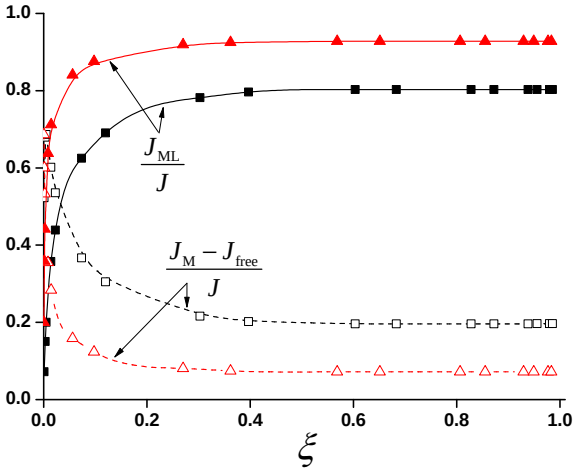

(b) $\Pi = 10$

Figure 7.1: Complex contribution to DGT flux by dissociation both inside the gel and inside the resin, as a function of lability degree computed by Eqn 7.2. Empty markers plus dashed line: normalized values of complex flux dissociated inside the gel layer, $(J_M - J_{free})/J$. Filled markers plus continuous line: normalized values of complex flux dissociated inside the resin layer, $(J_{ML})/J$. (a) Values for $\Pi = 1$. (b) Values for $\Pi = 10$. Each panel shows two different values of K: squares, $K = 10^4$ mol^{-1} m^3; triangles, $K = 10^4$ mol^{-1} m^3. The other parameters correspond to the Cd-NTA system reported in Mongin *et al.* [11] at pH = 7.03 and $T = 25$ °C: $r = 4 \times 10^{-4}$ m; $g = 1.13 \times 10^{-3}$ m; $D_M = D_{M,R} = 6.09 \times 10^{-10}$ m^2 s^{-1}; $D_L = D_{L,R} = 4.26 \times 10^{-10}$ m^2 s^{-1}; $c_{TM} = 10^{-2}$ mol m^{-3}; $c_{TL} = 0.249$ mol m^{-3}.

($\xi = 1 - c^r_{\mathrm{ML}}/c^*_{\mathrm{ML}}$), the complex contribution comes from dissociation at the $x = r$ surface, i.e., still inside the resin!

As stated before, changes in ligand concentration induce changes in metal association rate, but this effect does not apply inside the resin domain, because there, metal concentration is null. These results could indicate that the complex lability degree and, therefore, the rate of accumulated mass, are practically independent of the ligand concentration present in a DGT measurement. In order to evaluate deeply this hypothesis, in the next section we study the dependence of lability degree and the metal flux on the ligand concentration.

On the other hand, for low values of ionic strength (see panel b of Figure 7.1), due to Donnan effects, there is a decrease on the concentration values of negative partially labile complexes inside the resin domain (as sketched in Figure 6.4, page 145) and, consequently, the contribution to the flux coming from complex dissociation inside the resin decreases. Therefore, the flux coming from complex dissociation inside the gel is more important, and since it is dependent on the ligand concentration, the mixture effect in this system could be appreciable. From here on, our analysis will be focused on systems in which $I \geq 0.1$ M, i.e. $\Pi = 1$ or on systems with positive charged complexes (see Chapter 6).

7.3 Dependence of the Lability Degree and Metal Flux on Ligand Concentration

In case of ligand excess ($\epsilon K' \gg 1$) the impact of ligand concentration on the lability degree and metal flux in a DGT could be studied using Eqn 7.2. Figure 7.2 shows the dependence of the lability degree on the total ligand concentration in a DGT sensor (blue line) and in a voltammetric device ($r = 0$, red dashed line). The Figure 7.2 confirms that, because most of the flux received by the DGT device comes from dissociation inside resin, the lability is almost unaffected by the ligand concentration.

If there is no ligand excess, equation 7.2 is no longer valid. However, the system can be studied with the rigorous numerical solution detailed in Chapter 2. Figure 7.3a and 7.3b show the dependence of lability degree on the total ligand concentration, in a DGT sensor and in a voltammetric device ($r = 0$), respectively. In both panels continuous line depicts the lability degree calculated by Eqn 7.2 and markers show the lability degree obtained from the rigorous numerical solution detailed in Chapter 2.

Figures 7.3a and 7.3b show that for ligand excess conditions, Eqn 7.2 repro-

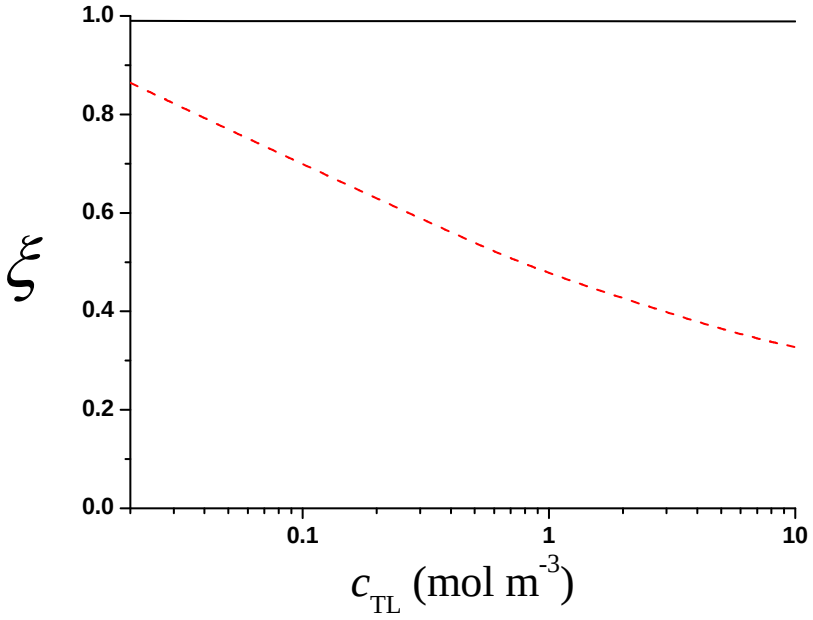

Figure 7.2: Lability degree (in a system with one metal and a single ligand) as a function of total ligand concentration for a standard DGT device (blue line, $r = 4 \times 10^{-4}$ m) and a voltammetric sensor (red dashed line, $r = 0$). Parameters: $k_a = 8.77 \times 10^4$ m^3 mol^{-1} s^{-1}, and $k_d = 2.76$ s^{-1} Other parameters as in Figure 7.1.

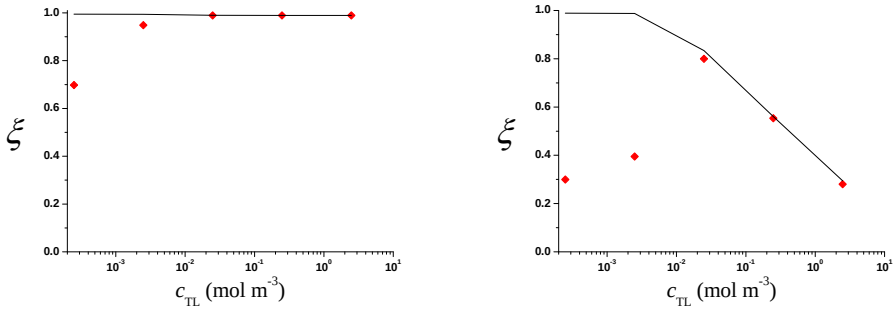

(a) DGT sensor, $r = 4 \times 10^{-4}$ m **(b)** Voltammetric sensor, $r = 0$

Figure 7.3: Lability degree as a function of total ligand concentration. Panel (a): for a DGT sensor. Panel (b): for a voltammetric sensor. Continuous line: lability degree calculated by Eqn 7.2 with $\Pi = 1$. Markers: lability degree obtained from the rigorous numerical solution detailed in Chapter 2. Parameters: $k_a = 8.77 \times 10^4$ mol^{-1} m^3 s^{-1}, and $k_d = 2.76$ s^{-1} The rest of parameters as in Figure 7.1.

duces the results obtained by numerical simulation. However, for low values of $c_{\mathrm{T,L}}$ compared to $c_{\mathrm{T,M}}$, Eqn 7.2 predicts a constant value of ξ, distant from values of numerical solution. As we stated above, the validity of Eqn 7.2 requires the fulfillment of condition $\epsilon K' \gg 1$. This last condition suggests that the ligand concentration will be approximately constant and equal to its bulk value, c^*_{L}, inside both gel and resin domains. However, when there is not ligand excess, the complex dissociation inside the DGT contributes to increase the amount of ligand above c^*_{L} (see Figure 7.4). This increase of the ligand concentration inside the resin has no impact over the lability degree because there, the metal concentration is null. However, a ligand concentration greater than c^*_{L} in the gel layer, produces an increase in the association rate, which in turn yield a raise of the complex profile and consequently, a decreasing on the lability degree (remind that $\xi = 1 - c^r_{\mathrm{ML}}/c^*_{\mathrm{ML}}$).

Nevertheless, despite of noticeable influence of ligand concentration on the lability degree shown for low values of $c_{\mathrm{T,L}}$ on left side of Figure 7.3, it is important to note that for these values, the condition $c_{\mathrm{T,L}} \ll c_{\mathrm{T,M}}$ implies $c^*_{\mathrm{ML}} \ll c^*_{\mathrm{M}}$ and suggests that most of the flux is transported in form of J_{free}. Thus, the error due to the use equation 7.1 in computing the total metal flux is negligible, although the complex contribution analytically calculated is far different from the value obtained by numerical simulation, as depicted in Figure 7.3. To visualize this, Figure 7.5 shows the dependence of total metal flux on the total ligand concentration. Continuous line depicts the flux calculated by Eqn 7.1 and markers show the flux obtained from the rigorous numerical solution.

These results indicate that, in a system with one metal and a single ligand, the metal flux measured by a DGT sensor is almost independent of both the constant equilibrium K and the ligand concentration, as indicate by the approximate expression 4.13 derived in Chapter 4, page 71. Therefore, this suggests that flux measurements by DGT devices in a system with a mixture of ligands, could be few influenced by the mixture effect because of key role of the resin. In next section we analyse this hypothesis.

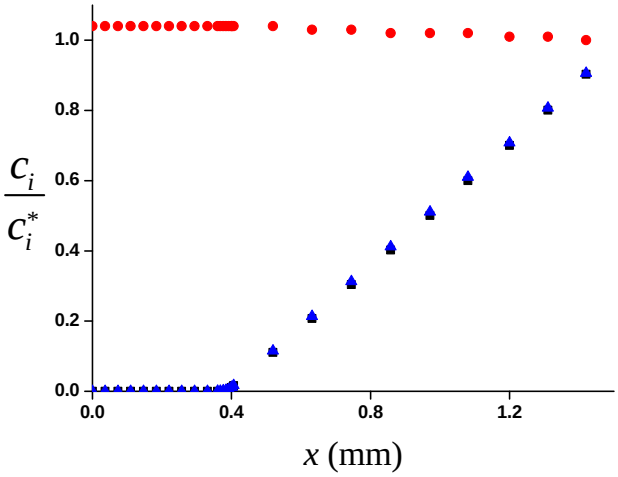

(a) $c_{\mathrm{T,L}} = 2.49 \times 10^{-1}$ mol m^{-3}

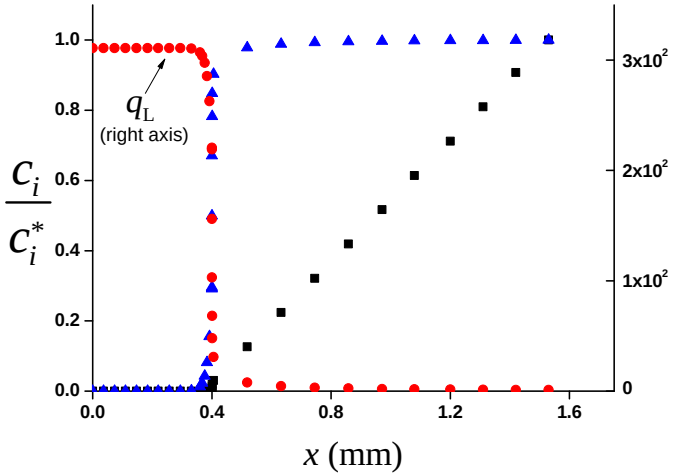

(b) $c_{\mathrm{T,L}} = 2.49 \times 10^{-4}$ mol m^{-3}

Figure 7.4: Normalized M, L and ML steady-state concentration profiles in DGT, for two different values of $c_{\mathrm{T,L}}$. Markers: squares (M), bullets (L), and triangles (ML), have been calculate with numerical simulation describe in Chapter 2. Panel (a): Profiles for $c_{\mathrm{T,L}} = 2.49 \times 10^{-1}$ mol m^{-3}. Panel (b): Profiles for $c_{\mathrm{T,L}} = 2.49 \times 10^{-4}$ mol m^{-3}.. The rest of parameters as in Figure 7.1. The profiles are normalized to theirs bulk values ($q_i = c_i/c_i^*$).

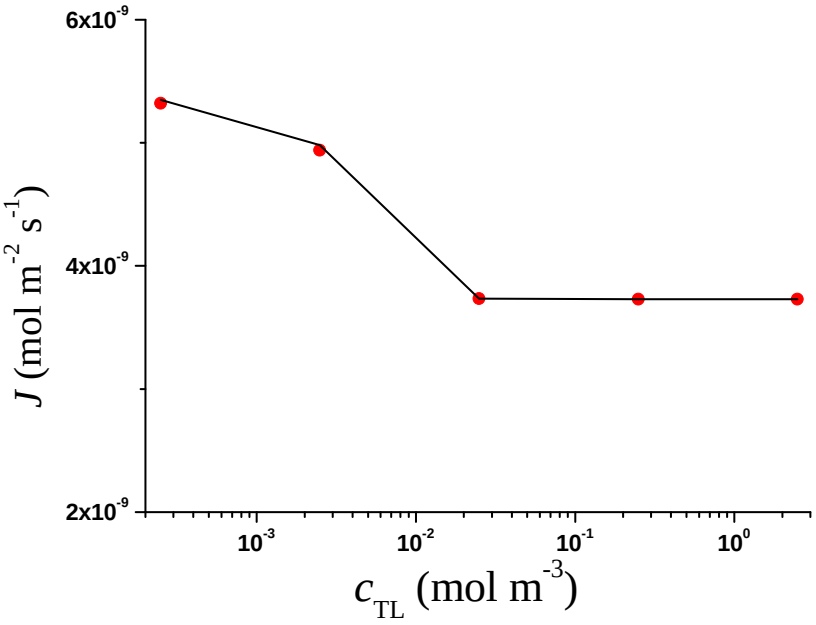

Figure 7.5: Total metal flux as a function of total ligand concentration. Continuous line: flux calculated by Eqn 7.1. Markers: flux obtained from the rigorous numerical solution detailed in Chapter 2. Parameters as in Figure 7.3a.

7.4 Mixture Effect

Let us consider an analytical sensor or an accumulating organism in an aquatic ecosystem, which can act as a consuming surface for a given metal complex, ML, present in the medium. As we have seen in Chapter 4 the concept of complex lability involves the diffusion and kinetics of interconversion between M and the ligand, L. If a mixture of other ligands is added to this medium, the lability degree of the first metal complex could be modified. This modification (named the mixture effect) is consequence of the coupling of association and dissociation processes of all of the complexes according to the competitive complexation reaction scheme (as we will see in Section 7.4.1).

Here we studied the impact of adding new ligands (with the simplest stoichiometric relationship), to a system with just one metal complex, on the lability degree and the flux measured by a DGT sensor.

7.4.1 Theoretical Framework

Let us consider in solution a mixture of h independent ligands ^{1}L, ^{2}L,..., ^{h}L, which can bind a metal ion M according to the scheme

$$\mathrm{M} + {}^{i}\mathrm{L} \underset{k_{\mathrm{d},i}}{\overset{k_{\mathrm{a},i}}{\rightleftharpoons}} \mathrm{M}^{i}\mathrm{L}, \tag{7.4}$$

where $k_{\mathrm{a},i}$ and $k_{\mathrm{d},i}$ are, respectively, the association and dissociation kinetic constants for the complexation process of M by ^{i}L. The corresponding equilibrium conditions read

$$K_i = \frac{k_{\mathrm{a},i}}{k_{\mathrm{d},i}} = \frac{c^*_{\mathrm{M}^i\mathrm{L}}}{c^*_{\mathrm{M}} c^*_{i_{\mathrm{L}}}}, \tag{7.5}$$

where K_i is the equilibrium constant and c_i^* labels the concentration of species i in the bulk solution.

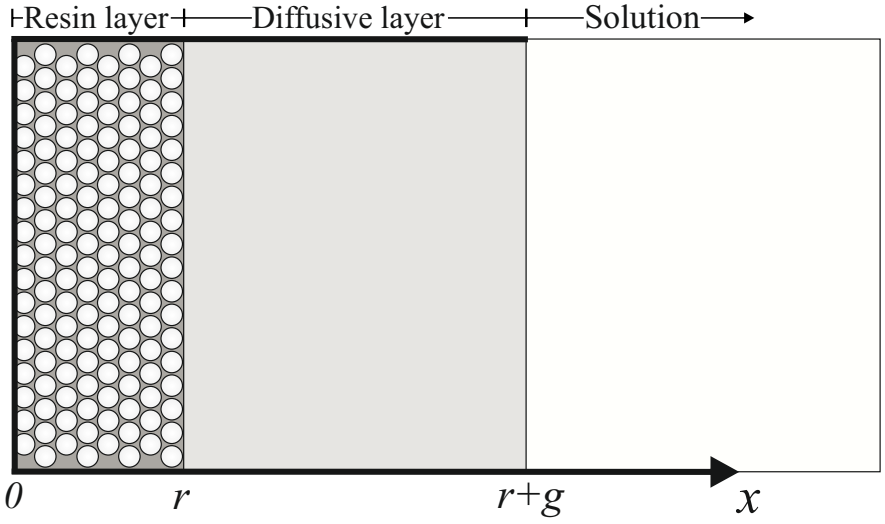

Figure 7.6: Schematic representation of a DGT device.

When a DGT is deployed in this solution, the species diffuse throw the gel toward the binding resin (Figure 7.6). If the resin acts as a perfect sink and diffusion is the only relevant transport mechanism, the balance equations

for metal and complex in steady state conditions read,

$$c_{\mathrm{M}}(x) = 0 \quad \text{for} \quad 0 < x \leq r, \tag{7.6}$$

$$D_{\mathrm{M}} \frac{\mathrm{d}^2 c_{\mathrm{M}}}{\mathrm{d}x^2} + \sum_{i=1}^{h} k_{\mathrm{d},i} c_{\mathrm{M}^i\mathrm{L}} - \sum_{i=1}^{h} k_{\mathrm{a},i} c_{\mathrm{M}} c_{i_{\mathrm{L}}} = 0 \quad \text{for} \quad r < x < r + g, \tag{7.7}$$

$$D_{\mathrm{M}^i\mathrm{L}} \frac{\mathrm{d}^2 c_{\mathrm{M}^i\mathrm{L}}}{\mathrm{d}x^2} - \sum_{i=1}^{h} k_{\mathrm{d},i} c_{\mathrm{M}^i\mathrm{L}} + \sum_{i=1}^{h} k_{\mathrm{a},i} c_{\mathrm{M}} c_{i_{\mathrm{L}}} = 0 \quad \text{for} \quad r < x < r + g. \tag{7.8}$$

The boundary conditions for $x = r + g$ are

$$\begin{aligned} c_{\mathrm{M}}(x = r + g) &= c^*_{\mathrm{M}}, \\ c_{\mathrm{M}^i\mathrm{L}}(x = r + g) &= c^*_{\mathrm{M}^i\mathrm{L}}, \end{aligned} \tag{7.9}$$

and for $x = r$

$$\begin{aligned} c_{\mathrm{M}}(x = r) &= c^r_{\mathrm{M}} = 0, \\ c_{\mathrm{M}^i\mathrm{L}}(x = r) &= c^r_{\mathrm{M}^i\mathrm{L}}. \end{aligned} \tag{7.10}$$

7.4.1.1 Flux and lability degree

In steady state, all flux passing throw the surface $x = r$ gets bound to the resin. Then, it can be obtained by the sum of metal plus each complex contribution,

$$J = D_{\mathrm{M}} \frac{\mathrm{d}c_{\mathrm{M}}}{\mathrm{d}x}\bigg|_r + \sum_{i=1}^{h} D_{\mathrm{M}^i\mathrm{L}} \frac{\mathrm{d}c_{\mathrm{M}^i\mathrm{L}}}{\mathrm{d}x}\bigg|_r . \tag{7.11}$$

On the other hand, by adding all the diffusion equations given in 7.7 and 7.8, we obtain

$$\frac{\mathrm{d}^2 c_{\mathrm{M}}}{\mathrm{d}x} \left(D_{\mathrm{M}} c_{\mathrm{M}} + \sum_{i=1}^{h} D_{\mathrm{M}^i\mathrm{L}} c_{\mathrm{M}^i\mathrm{L}} \right) = 0, \tag{7.12}$$

or

$$D_{\mathrm{M}} c_{\mathrm{M}} + \sum_{i=1}^{h} D_{\mathrm{M}^i\mathrm{L}} c_{\mathrm{M}^i\mathrm{L}} = Ax + B \quad \text{for} \quad r < x < r + g. \tag{7.13}$$

Solving this system alongside with boundary conditions 7.9 and 7.10 and applying Eqn 7.11 the total metal flux can be rewritten,

$$J = \frac{D_{\mathrm{M}} c^*_{\mathrm{M}}}{g} + \sum_{i=1}^{h} \left[\frac{D_{\mathrm{ML}} c^*_{\mathrm{ML}}}{g} \left(1 - \frac{c^r_{\mathrm{M}^i\mathrm{L}}}{c^*_{\mathrm{M}^i\mathrm{L}}} \right) \right]. \tag{7.14}$$

In the first term of the right hand side of Eqn 7.14, we recognize J_{free} for this system. The second term indicates the increase of the metal flux due to the presence of the complexes in the system; this can be labeled J_{complex},

$$J_{\text{complex}} = \sum_{i=1}^{h} \left[\frac{D_{\text{ML}} c^*_{\text{ML}}}{g} \left(1 - \frac{c^r_{\text{M}^i\text{L}}}{c^*_{\text{M}^i\text{L}}} \right) \right] = \sum_{i=1}^{h} J_{\text{complex},i}. \tag{7.15}$$

As $0 < 1 - c^r_{\text{M}^i\text{L}}/c^*_{\text{M}^i\text{L}} < 1$ Eqn 7.15 evidences that the maximum kinetic contribution to the flux that a given M^iL complex can achieve, is just its maximum purely diffusive flux (reached when $c^r_{\text{M}^i\text{L}} = 0$), $J_{\text{diff},i} = D_{\text{M}^i\text{L}} c^*_{\text{M}^i\text{L}}/g$. So, we can define the particular degree of lability of the complex M^iL by

$$\xi_i = \frac{J_{\text{complex},i}}{J_{\text{diff},i}} = 1 - \frac{c^r_{\text{M}^i\text{L}}}{c^*_{\text{M}^i\text{L}}}. \tag{7.16}$$

Then, the global degree of lability of the system becomes

$$\xi = \frac{J - J_{\text{free}}}{J_{\text{labile}} - J_{\text{free}}} = \frac{J - \frac{D_{\text{M}} c^*_{\text{M}}}{g}}{\sum_{i=1}^{h} \frac{D_{\text{M}^i\text{L}} c^*_{\text{M}^i\text{L}}}{g}} = \sum_{i=1}^{h} \frac{J_{\text{diff},i}}{\sum_{i=1}^{h} J_{\text{diff},i}} \xi_i. \tag{7.17}$$

Thus, the global lability degree is a weighted average of the lability degrees for each of the different complexes present in the mixture with weighting factors dependent on the particular diffusion coefficients and on the respective abundances in the bulk solution, that is, on the fraction of the maximum diffusive flux of M^iL, $J_{\text{diff},i}$, over the total maximum diffusive flux of all complexes.

It is important to note that Eqn 7.17 is valid even without ligand excess. However, the rigorous computation of ξ_i requires knowledge of $c^r_{\text{M}^i\text{L}}$ which follows from the solution of the system of differential Eqns 7.7 and 7.8, corresponding to the transport and reaction processes in the mixture. For a general mixture case, this system can be solved with the rigorous numerically simulation described in Chapter 2. Results for a system with a mixture of two ligands are discussed in next sections.

7.5 Mixture Effect in a System With Two Ligands

As we focus our interest on complexes in an aquatic medium, we will assume Eigen and Tamm mechanism [12,13] so that the kinetic association constant for a given metal is only dependent on the charge of the ligand. Therefore, we assume that $k_{\text{a},1} = k_{\text{a},2}$, i.e., the ligands share a common value for the stability constant of the respective outersphere complex with the metal (a common charge of the ligands and a fixed ionic strength are required).

7.5.1 Impact of Mixture on Complexes Lability Degree

When the composition of a mixture is changed, bulk complex concentrations change according to the equilibrium conditions assumed in Eqns 7.5 and 7.9. New values of J and ξ_i then arise depending on the composition. Here, to assess the pure mixture effect, we compare the lability degree of each complex in the mixture (ξ_i), with the corresponding in a single ligand system with the same bulk metal and complex concentration than in the mixture, $\xi_i^{h=1}$. From now on, we use the results obtained with the rigorous numerical simulation described in Chapter 2, to study the mixture effect.

Table 7.1 shows the general parameters used for these calculations. It is important to note that the lability degree of both complexes was chosen neither completely labile nor totally inert in order to better appreciate changes.

Table 7.1: General parameters used for numerical calculations. Other common Parameters: $r = 4 \times 10^{-4}$ m; $g = 1.13 \times 10^{-3}$ m; $k_{\mathrm{a,R}} = 10^{15}$ m^3 mol^{-1} s^{-1}; $k_{\mathrm{d,R}} = 10^{-6}$ s^{-1} and $c_{\mathrm{T,R}} = 5 \times 10^2$ mol m^{-3}.

Complex	k_{d} (s^{-1})	D_{M} (m^2 $^{-1}$)	$D_{\mathrm{L}} = D_{\mathrm{ML}}$ (m^2 s^{-1})
M^{1}L	1×10^{-2}	6.09×10^{-10}	4.26×10^{-10}
M^{2}L	1×10^{-4}	6.09×10^{-10}	4.26×10^{-10}

Figure 7.7 shows ξ, ξ_i and $\xi_i^{h=1}$ as a function of total ligand concentration $c_{\mathrm{T,^1L}}$ and $c_{\mathrm{T,^2L}}$ (panels a and b, respectively). In each panel, the concentration of the non-added ligand is kept constant.

In order to analyse this behaviour let us focus, initially, on a fixed $c_{\mathrm{T,^2L}}$ value in panel (b) of Figure 7.7. For instance, for $c_{\mathrm{T,^2L}} = 0.1$ mol m^{-3}, the lability degree of M^{1}L complex in the mixture, ξ_1 (circled point at Figure 7.7b), is lower than its value in a single ligand system, $\xi_1^{h=1}$. For this point, the M^{1}L and M^{2}L profiles in a single ligand system are depicted in Figure 7.8. As it can be seen, both complexes are in equilibrium with free metal in the gel domain beyond the thickness of the respective reaction layer.

Let us assume that we have initially a solution with just M^{1}L complex present. When we add M^{2}L to this solution, there is a "competition" in trying to reach the equilibrium with free metal. The M^{2}L complex starts to dissociate contributing to raise the free metal concentration profile inside the gel layer. This increasing of metal yields, in turn, an increase of M^{1}L profile in looking for its own equilibrium (see Figure 7.9a). The result is a decrease of ξ_1 with respect to $\xi_1^{h=1}$.

Notice that instead of dissociation of $c_{\mathrm{M^1L}}$ until equilibrium with the new

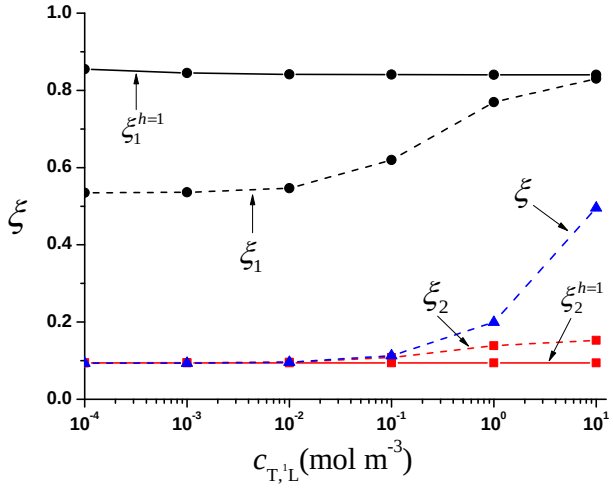

(a) $c_{\mathrm{T},^2\mathrm{L}} = 1 \times 10^{-1}$ mol m^{-3}

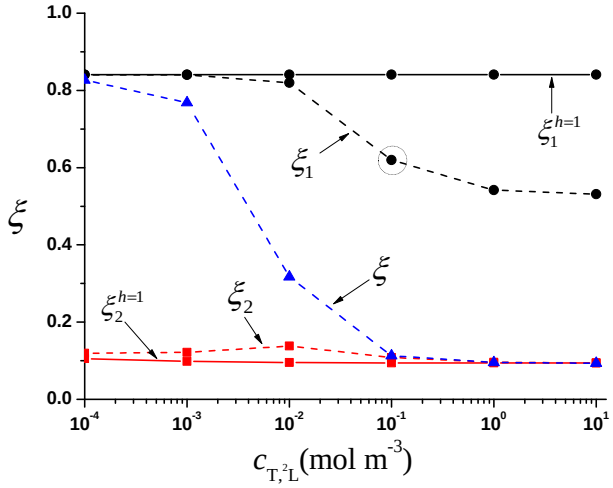

(b) $c_{\mathrm{T},^1\mathrm{L}} = 1 \times 10^{-1}$ mol m^{-3}

Figure 7.7: Global lability degree of the system as a function of total concentration of ligand (ξ, blue dashed line plus triangles), lability degree of complex M^1L in the mixture (ξ_1, black dashed line plus bullets) and lability degree of complex M^2L in the mixture (ξ_2, red dashed line plus squares). Additionally, the figure includes the lability degree of complexes in a single ligand system, $\xi_1^{h=1}$ (bullets plus black continuous line) and $\xi_2^{h=1}$ (squares plus red continuous line). Parameters: $k_{\mathrm{a},1} = k_{\mathrm{a},2} = 1 \times 10^4$ m^3 mol^{-1} s^{-1}, $c_{\mathrm{T,M}} = 1 \times 10^{-2}$ mol m^{-3}; others parameters as in Table 7.11. For panel (a) $c_{\mathrm{T},^2\mathrm{L}} = 1 \times 10^{-1}$ mol m^{-3} and for panel (b) $c_{\mathrm{T},^1\mathrm{L}} = 1 \times 10^{-1}$ mol m^{-3}. In each panel, the concentration of the non-added ligand is kept constant.

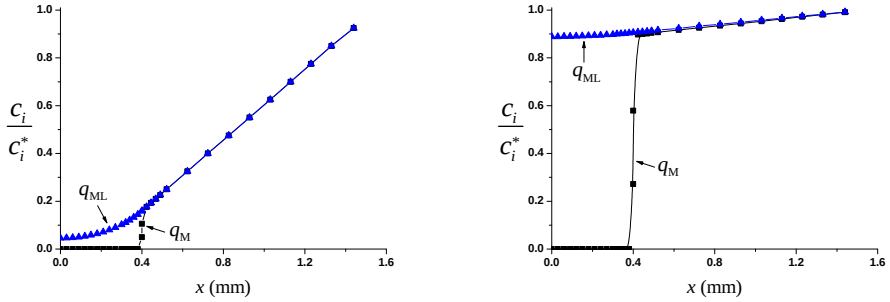

(a) M+^{1}L system. **(b)** M+^{2}L system.

Figure 7.8: Normalized steady-state concentration profiles ($q_i = c_i/c_i^*$) of M (■) and ML (▲) for two different systems. Panel (a): single ligand M+^{1}L system with $c_{T,^1L} = 1 \times 10^{-1}$ mol m^{-3}. Panel (b): single ligand M+^{2}L system with $c_{T,^2L} = 1 \times 10^{-1}$ mol m^{-3}. The rest of parameters as in Table 7.1.

metal concentration at each spatial position, the M^{1}L complex overpasses the dissociation corresponding to the equilibrium beyond the reaction layer thickness in the gel domain. Accordingly, the M^{1}L complex is not in equilibrium with free metal M in this region. Instead, a net association of ^{1}L arises see (Figure 7.9b).

This behaviour can be understood if we recall that $k_{d,1} \gg k_{d,2}$ so that the time scale for dissociation of M^{1}L complex, is shorter than for M^{2}L. Thus, dissociation of M^{1}L starts and reach (quasi) equilibrium before M^{2}L dissociates. Dissociation of M^{2}L produces a new free metal which tends then to associate with ^{1}L to yield M^{1}L.

Here, It is important to notice that any of the previous work has noticed this effect. Therefore, the results of the reaction layer approximation developed for mixtures of ligands in voltammetric sensors [14] do not consider this phenomenon. Additional work is required to evaluate the importance of this effect in developing a reaction layer approximation for mixtures of ligands in DGT.

If the amount of M^{2}L added is greater (rightmost side of Figure 7.7b) the lost of lability degree of M^{1}L complex increases. Indeed, in this zone the main complex is M^{2}L, so, even a small dissociation of M^{2}L could contribute to appreciably raise the free metal concentration profile inside the gel layer.

On the other hand, for lower values of $c_{T,^2L}$, the amount of M^{1}L is enough to reach the equilibrium with metal (see Figure 7.10). Under these conditions, the decreasing in M profile, induces a decrease (a small one because its

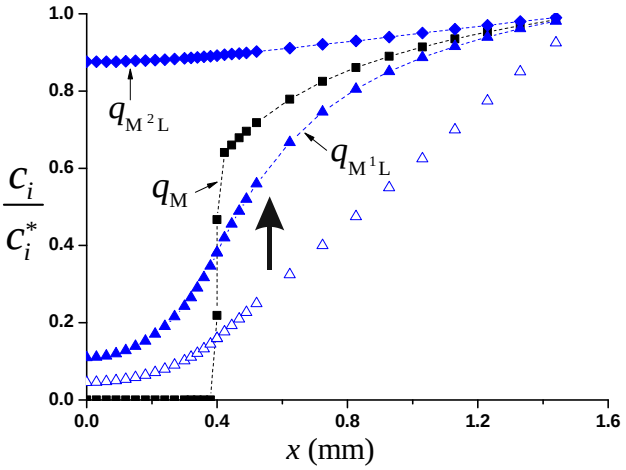

(a) Normalized concentration profiles

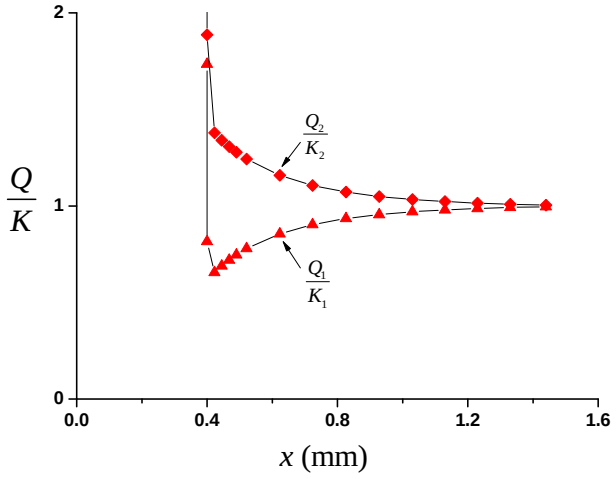

(b) Ratios Q_1/K_1 and Q_2/K_2

Figure 7.9: Panel (a): Normalized steady-state concentration profiles ($q_i = c_i/c_i^*$) of M (squares), M^1L (triangles) and M^2L (diamonds) for $M+^1L+^2L$ system. The figure also shows the M^1L profile (empty triangles) for the $M+^1L$ single ligand system. Panel (b): Ratios Q_1/K_1 and Q_2/K_2 for $M+^1L+^2L$ system depicted in panel (a). Parameters as in Figure 7.8.

inertness) in M^2L profile and, therefore, ξ_2 increase with respect to his value at not mixed system.

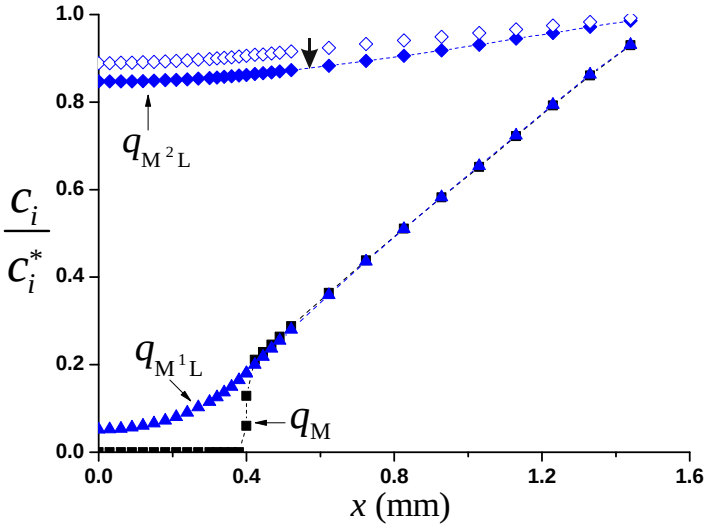

Figure 7.10: Normalized steady-state concentration profiles ($q_i = c_i/c_i^*$) of M (squares), M^1L (triangles) and M^2L (diamonds) for $M+^1L+^2L$ system. The figure also shows the M^2L profile (empty diamonds) for the $M+^2L$ single ligand system. Parameters: $c_{T,^1L} = 1 \times 10^{-1}$ mol m^{-3} and $c_{T,^2L} = 1 \times 10^{-2}$ mol m^{-3}. The rest of parameters as in Figure 7.8.

The case for Figure 7.7a, where we have increased the total concentration of ligand ^1L, can be explained in analogous way.

7.5.2 Impact of Mixture on Metal Flux

To study the impact of the mixture effect on the metal flux, we compare the real metal flux in the mixture, J (see Eqn 7.14), with a hypothetical flux $J^{h=1}$, computed assuming that the lability degree of complexes in the mixture was the corresponding to the single ligand system, keeping the same $c^*_{i_L}$ and $c^*_{M^{i}L}$ values than in the mixture,

$$J^{h=1} = J_{\text{free}} + \frac{D_{M^1L} c^*_{M^1L}}{g} \xi_1^{h=1} + \frac{D_{M^2L} c^*_{M^2L}}{g} \xi_2^{h=1}, \tag{7.18}$$

Panels (a) and (b) of Figure 7.11 show both fluxes J, and $J^{h=1}$ (Eqn 7.18), for the same system depicted in Figures 7.7a and 7.7b, respectively. Apart

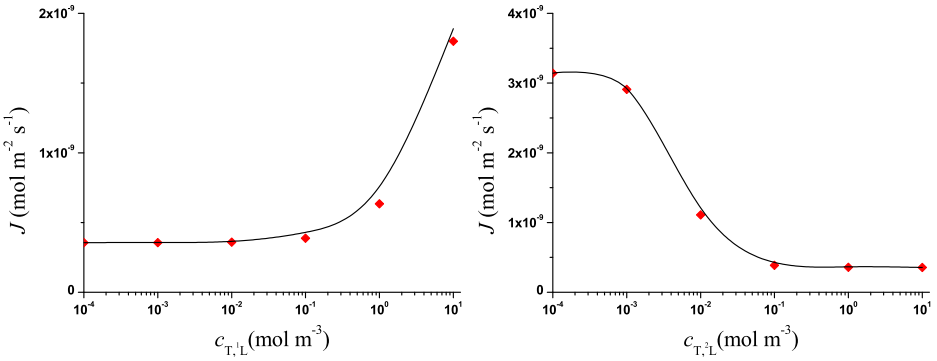

(a) $c_{\mathrm{T},^2\mathrm{L}} = 1 \times 10^{-1}$ mol m^{-3} **(b)** $c_{\mathrm{T},^1\mathrm{L}} = 1 \times 10^{-1}$ mol m^{-3}

Figure 7.11: Total metal flux J (continuous line) in the M+^{1}L+^{2}L system. Panel (a): J as a function of $c_{\mathrm{T},^1\mathrm{L}}$. Panel (b): J as a function of $c_{\mathrm{T},^2\mathrm{L}}$. Both panels also show, in markers, the hypothetical flux $J^{h=1}$ (Eqn 7.18). In each panel, the concentration of the non-added ligand is kept constant. Parameters as in Figure 7.7.

from electrochemical measures (i.e. without complex penetration), where mixture effect can cause changes in flux of the order of around 40% [9], in a DGT sensor those effects are lowered. Indeed, as we mention before, the main contribution to the flux in a DGT device comes from complex dissociation inside the resin (where there is no mixture effect because the null metal concentration), so the impact of the mixture effect on the total metal flux must be lower.

In order to quantify the mixture effect in DGT, contour plots of $(J-J^{h=1})/J$ provide an adequate tool for explore it. For a typical range of K_1 and $k_{\mathrm{d},1}$ values, Figure 7.12a shows contour plots of $(J-J^{h=1})/J$ for a fixed value of $c_{\mathrm{T},^1\mathrm{L}}$ and $c_{\mathrm{T},^2\mathrm{L}}$, keeping constant the relationship between kinetic constants shown in Table 7.1 (i.e. for $k_{\mathrm{d},1} = 10^2 k_{\mathrm{d},2}$). For the wide range of used parameters, Figure 7.12a shows a maximum of around 10% in the mixture effect, a value close to experimental error, and far from values obtained with voltammetric devices (where $r = 0$)

We could even get a less mixture effect by increasing the thickness of resin layer (experimentally this can be done by simple use of two o more contiguous resin layer). Actually, Increasing the resin thickness we increase the proportion of complex dissociated inside, where there is no mixture effect. Figure 7.12b shows a contour plots of $(J-J^{h=1})/J$ for the same parameters that in Figure 7.12a except for $r = 8 \times 10^4$ m, a twice value of the standard resin layer thickness.

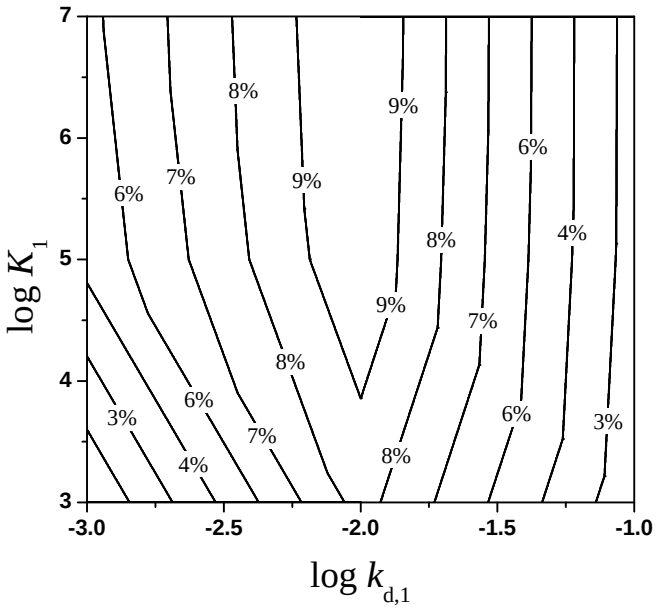

(a) $r = 4 \times 10^{-4}$ m

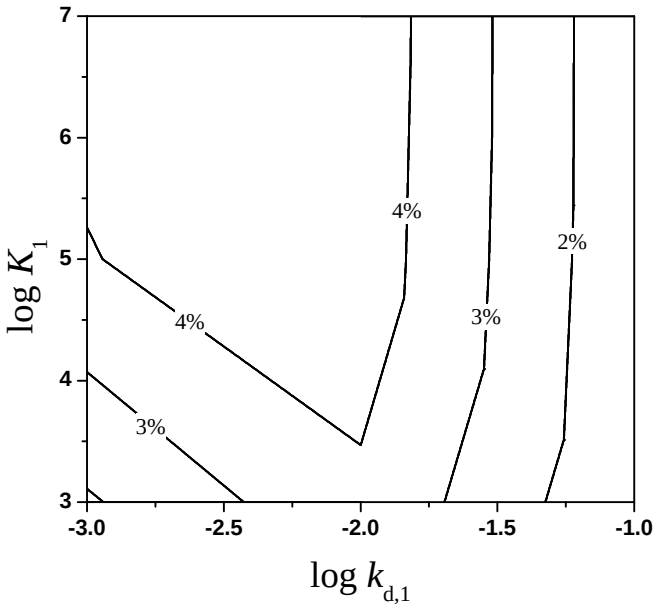

(b) $r = 8 \times 10^{-4}$ m

Figure 7.12: Contour plots of $(J - J^{h=1})/J$ for a fixed values of $c_{\mathrm{T},^1\mathrm{L}} = 1 \times 10^{-1}$ mol m^{-3} and $c_{\mathrm{T},^2\mathrm{L}} 1 \times 10^{-1}$ mol m^{-3}, keeping constant the relationship between kinetic constants shown in Table 7.1 (i.e. for $k_{\mathrm{d},1} = 10^2 k_{\mathrm{d},2}$). In Panel (a): $r = 4 \times 10^{-4}$ m; in panel (b): $r = 8 \times 10^{-4}$ m. The rest of parameters as in caption of Table 7.1.

7.6 Conclusions

We recall that Eqn 7.2 was derived for excess ligand condition in a system with a metal in presence of a single ligand. However, we have shown that for no excess conditions, the error due to use equation 7.1 in compute the total metal flux in a DGT device is negligible.

On the other hand, in a mixture of complexes, the lability degree can be compute analytically with Eqn 7.17. In Eqn 7.17 the lability degree of each complex, ξ_i, depends on the interaction with the rest of complexes in solution, so, the rigorous computation of ξ_i requires the solution of corresponding transport and reaction processes in the mixture. Here, we have seen that using $\xi_i^{h=1}$ (the lability degree of each complex, calculated by Eqn 7.2 in a single ligand system with the same bulk metal and complex concentration than in the mixture) in Eqn 7.17, the differences in the DGT measured flux, i.e. the mixture effect, are lesser than 10% or even smaller if we increase the resin thickness.

The reduced mixture effect can be explained if we recall that in a system with a partially labile complex, the addition of a more labile complex leads to an increase in the lability degree of the first one. On the contrary, the addition of a less labile one leads to a decrease of the lability degree of the initial complex. As a result, the impact on the increasing (or decreasing) in the flux on the first complex is (in part) compensated by the decreasing (or increasing) in the flux of the added complex.

As we have seen in previous chapters the lability degree of a complex, in a single system is not an intrinsic property of the complex, but a property dependent of the experimental sensor used for its measurement. Additionally, in a mixture of many complexes the lability is influenced by the concentration of the rest of complexes present in the solution. Nevertheless, the reduced mixture effect in measures with DGT devices, would facilitate the interpretation of experimental data and could help in the understanding of interaction of metal with different ligands.

References

[1] Buffle, J. and Horvai, G. *In situ Monitoring of Aquatic Systems: Chemical Analysis and Speciation*, volume 6. John Wiley and Sons, Chichester, UK, **2000**.

[2] Fasfous, I. I., Yapici, T., Murimboh, J., Hassan, I., Chakrabarti, C., Back, M., Lean, D. and Gregoire, D. Kinetics of trace metal competition in the freshwater environment: Some fundamental characteristics. *Eenvironmental Science and Technology* 38(19), **2004**: 4979–4986.

[3] Galceran, J. and van Leeuwen, H. P. *IUPAC Series on Analytical and Physical Chemistry of Environmental Systems*, chapter Physicochemical kinetics and transport at chemical-biological surfaces. John Wiley, **2004**, 147–203.

[4] Buffle, J. *Complexation Reactions in Aquatic Systems. An Analytical Approach*. Chichester, UK, **1988**.

[5] Turner, D. and Whitfield, M. Reversible electrodeposition of trace-metal ions from multi-ligand systems.1. Theory. *Journal of Electroanalytical Chemistry* 103(1), **1979**: 43–60.

[6] Turyan, Y. Equations of a polarographic kinetic wave and the limiting current in the presence of depolarizers in the bulk of the solution and their parallel electroreduction. *Soviet Electrochemistry* 20(4), **1984**: 428–435.

[7] van Leeuwen, H., Cleven, R. and Buffle, J. Voltammetric techniques for complexation measurements in natural aquatic media - Role of the size of macromolecular ligands and dissociation kinetics of complexes. *Pure and Applied Chemistry* 61(2), **1989**: 255–274.

[8] Salvador, J., Garces, J., Galceran, J. and Puy, J. Lability of a mixture of metal complexes under steady-state planar diffusion in a finite domain. *Journal of Physical Chemistry B* 110, **2006**: 13661–13669.

[9] Salvador, J., Garces, J., Companys, E., Cecilia, J., Galceran, J., Puy, J. and Town, R. Ligand mixture effects in metal complex lability. *Journal of Physical Chemistry A* 111, **2007**: 4304–4311.

[10] Uribe, R., Mongin, S., Puy, J., Cecilia, J., Galceran, J., Zhang, H. and Davison, W. Contribution of partially labile complexes to the DGT metal flux. *Environmental Science and Technology* 45(12), **2011**: 5317–5322.

[11] Mongin, S., Uribe, R., Puy, J., Cecilia, J., Galceran, J., Zhang, H. and Davison, W. Key role of the resin layer thickness in the lability of complexes measured by DGT. *Environmental Science and Technology* 45(11), **2011**: 4869–4875.

[12] Morel, F. *Principles of Aquatic Chemistry.* John Wiley, New York, **1993**.

[13] van Leeuwen, H. and Town, R. Stripping chronopotentiometry at scanned deposition potential (SSCP). Part 4. The kinetic current regime. *Journal of Electroanalytical Chemistry* 561(1-2), **2004**: 67–74.

[14] Zhang, Z. and Buffle, J. Interfacial metal flux in ligand mixtures. 1. The revisited reaction layer approximation: Theory and examples of applications. *Journal of Physical Chemistry A* 113(24), **2009**: 6562–6571.

8

Lability Degree of Metal Fulvic Acid Complexes

8.1 Introduction

The circulation and the toxic or nutritional impacts of trace metals in the environment are strongly dependent on its complexation with natural organic matter (NOM) present in the aquatic media and soils, because the resulting distribution of species affects the (bio)availability of the element [1]. So, novel methods to quantify the speciation and to reach a deeper understanding of the characteristics of such complexation are of interest.

Given that NOM is a mixture of a large number of different molecules, complexation with NOM is heterogeneous [2], not only because of the different functional groups, but also due to the interactions of the group with different chemical environments. Accordingly, the binding affinity between metal and NOM decreases as the metal concentration increases. Actually, at low metal concentrations only the strongest binding sites will be occupied while increasing the metal concentration lower affinity sites become increasingly occupied. Additionally, in the binding process there is a competition between proton and metal for –at least– some of the sites. All these issues are addressed by advanced isotherms such as NICA (nonideal competitive adsorption) isotherm [3].

Alternatively to a description by isotherms, it proves useful to justify NOM binding data via the distribution, either continuous or discrete, of sites with different affinities. This distribution is known as the affinity spectrum. In this approach, the global coverage is seen as a weighted sum of coverages

of sets of sites with common affinity. In the simplest version, the coverage dependence (with free metal ion concentration) for each set is described by a Langmuirian isotherm. For systems with competing cations, the affinity spectrum becomes multidimensional. However, there are important limitations to its straightforward application. For instance, the concept of multidimensional affinity spectrum cannot be used when metal and proton do not share the same complexation sites (as in the case of proton simple binding an metal chelate complexation).

A less restrictive formalism relies on the concept of conditional affinity spectrum (CAS) [4]. CAS is always monodimensional and characterizes the affinity distribution for a given ion while fixing the concentrations of all other ions.

In this chapter we try to give an answer to an old question: Which is the lability degree of metal complexed to NOM? Although some attempts have recently been reported [5], the question is still open. The theoretical framework developed in previous chapters, together with previous tools developed by this research group [4, 6–8], allow us to suggest an interesting and new way to answer this question: Using the concept of CAS, metal bound to NOM can be seen as metal bound binding to a mixture of ligands with different concentrations and different affinities. Additionally, Eigen ideas are applied to derive the distribution of kinetic dissociation constants associate to the CAS. This distribution is called the *Conditional Kinetic Spectrum* (CKS). This spectrum is used to characterize the kinetics of the metal binding to humic (HA) or fulvic (FA) acids. A discretization of the CAS and CKS allows to transform the heterogeneity of the humic or fulvic acids into a mixture of multiple ligands of given affinities and kinetic constants. Then, the formalism and results shown in Chapter 7 can be used to assess the lability degree of the system.

This chapter is organized as follows: In Section 8.2 there is a revision of the concept of CAS. In particular, the analytical expression for the CAS underlying NICA isotherm is reported. In addition to the metal specifically bound to NOM through the formation of a true chemical bound, there is also a metal accumulation from electrostatic forces close to the negatively charged NOM. This is referred to as territorial or electrostatic binding. The description of the electrostatic binding with the Donnan model is also included in this section. The main interest of using NICA-Donnan model stands from the fact that a very simple analytical expression for the CAS is available, as well as from the fact that generic NICA-Donnan parameters for the binding of many cations to fulvic and humic acids are available in literature [9]. Once these concepts have been introduced, the concept of site occupation distribution function (SODF) is reviewed since this concept will

lead (after discretization) to the computation of the concentrations of the free and complexed sites of the mixture of ligands equivalent (in terms of binding properties) to the fulvic or humic acids.

Section 8.3 is devoted to the application of Eigen ideas to this system in order to derive the kinetic dissociation constant of each complex in the mixture.

Section 8.4 describes the calculation of the global lability degree of the mixture by applying the numerical simulation tool developed in Chapter 2. Together with the numerical results obtained from discretization of the CAS corresponding to the FA, analytical expressions developed in Chapter 7 are also used to predict the approximate global lability degree of the FA complexes. Influence of pH on these results is also reported.

8.2 Theoretical Background

8.2.1 The Binding Curve

Different analytical techniques like potentiometry, spectroscopy or membrane techniques, have been used to determine the free metal concentration in equilibrium with a given total metal concentration added to a system that contains a macromolecule. This knowledge allows an operational definition of the formal species bound metal (c_{ML}) and ligand (c_{L}) as

$$c_{\mathrm{ML}} = c_{\mathrm{T,M}} - c_{\mathrm{M}} \tag{8.1}$$

and

$$c_{\mathrm{L}} = c_{\mathrm{T,L}} - c_{\mathrm{ML}}. \tag{8.2}$$

Experimental titration results are gathered in the so-called binding curve, θ versus $\log c_{\mathrm{M}}$ (see Figure 8.1), where

$$\theta = \frac{c_{\mathrm{ML}}}{c_{\mathrm{T,L}}}. \tag{8.3}$$

The binding curve represents the fraction of bound ligand as a function of free metal concentration present in the system.

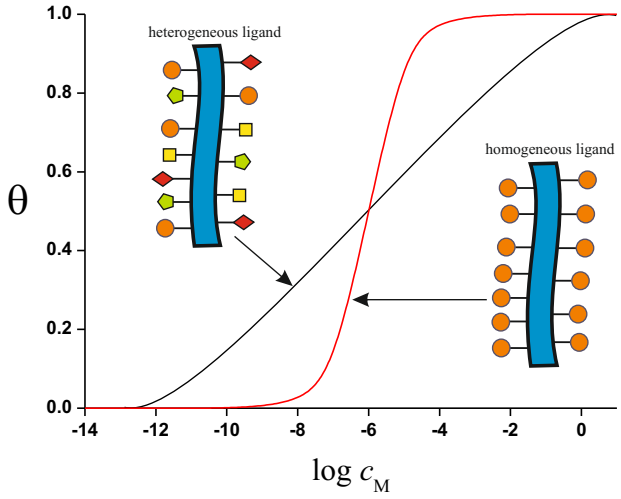

Figure 8.1: Typical binding curves. Red line stands for a homogeneous ligand while black line corresponds to a heterogeneous one. The figure also shows an schematic representation of homogeneous and heterogeneous ligands.

8.2.2 The Affinity Spectrum

In the simplest case, when all binding sites in a macromolecule have the same affinity (homogeneous ligand, red line in Figure 8.1) the coverage as a function of metal concentration may be described by a Langmuirian isotherm,

$$\theta = \frac{K c_M}{1 + K c_M}. \tag{8.4}$$

However, natural organic matter appears to be chemically heterogeneous. The intrinsic heterogeneity of a ligand derives from the presence of reactive groups which differ in their intrinsic affinities for a complexing species (as is the case of humic/fulvic acid). In those cases, a way to describe heterogeneity consists in assuming that the macromolecular coverage, θ, could be interpreted as a (discrete or continuous) superposition of a set of local isotherms, $f(c_M, K_i)$, each one corresponding to a binding site, weighted by his probability of occurrence, the affinity spectrum $p(K)$ [10, 11]. Thus, the coverage can be written as

$$\theta(c_M) = \sum_i p_i(K_i)\theta_i(c_M) = \sum_i p_i(K_i) f(c_M, K_i), \tag{8.5}$$

in a discrete form, or by

$$\theta(c_{\mathrm{M}}) = \int_0^{\infty} p(K) f(c_{\mathrm{M}}, K) \mathrm{d}K, \tag{8.6}$$

in a continuous form.

Equation 8.6 is not the most general relationship because it assumes that all binding sites have the same local isotherm and that they do not interact. Moreover, although the local equilibrium process could be assayed in terms of other isotherms, the simplest assumption is to postulate a set of non interacting sites. So, restricting the kernel of the integral in Eqn 8.6 to a Langmuir isotherm, the coverage can be written as:

$$\theta(c_{\mathrm{M}}) = \int_0^{\infty} p(K) \frac{K c_{\mathrm{M}}}{1 + K c_{\mathrm{M}}} \mathrm{dK}. \tag{8.7}$$

Usually, the affinity spectrum is given in terms of $\log K$, which is proportional to the binding free energy. Thus, equation 8.7 can be rewritten as

$$\theta(c_{\mathrm{M}}) = \int_{-\infty}^{\infty} p(\log K) \frac{K c_{\mathrm{M}}}{1 + K c_{\mathrm{M}}} \mathrm{d}(\log \mathrm{K}). \tag{8.8}$$

Given some experimental data of $\theta(c_{\mathrm{M}})$, through semianalytical and numerical procedures, the integral Eqn 8.8 can be solved to obtain the affinity spectrum $p(\log K)$ [11–14]. Alternatively to numerical methods, in 1948 Sips [15] reported an analytical method to solve Eqn 8.8 once $\theta(c_{\mathrm{M}})$ values are fitted to an analytical isotherm. According to Sips

$$p(\log K) = \frac{\ln(10)}{\pi} \, \mathrm{Im}[\theta(c_{\mathrm{M}} = -1/K)], \tag{8.9}$$

where Im stands for the imaginary part.

8.2.3 Multicomponent Systems and the Conditional Affinity Spectrum (CAS)

In going from single component binding to multicomponent binding, several factors have to be considered. For humic substances for instance, it is logical to assume that the active sites for protons are also involved in the binding of other cations. That is to say, all specifically bound cations, including the proton, could compete for the same sites. Competition is taken into account in a binding model by considering that the reference sites can be occupied by different ions, and this will affect both the local and the overall binding equation.

Let us assume that the adsorption process can be viewed as binding to independent sites, each of which obeys the Langmuir isotherm with a given

affinity. A straightforward generalization of the affinity spectrum methodology to multicomponent systems relies on the definition of a multidimensional affinity spectrum [16–18],

$$\theta_i(c_1, c_2, \ldots, c_n) = \int_{-\infty}^{\infty}\int_{-\infty}^{\infty}\cdots\int_{-\infty}^{\infty} p(x_1, x_2, \ldots, x_n) \times \frac{K_i c_i}{1 + \sum_{j=1}^{n} K_j c_j} dx_1 dx_2 \cdots dx_n, \tag{8.10}$$

where c_i and K_i represent, respectively, the concentration and the binding stability constant for component i, and $x_i = \log K_i$. If a particular functional form for the affinity spectrum is suggested, the integrals appearing in 8.10 can, in principle, be performed and a binding isotherm can be obtained [16, 17, 19].

On the other hand, sometimes one could be interested in the inverse problem: the finding of the affinity spectrum embedded in a suitable binding isotherm. For monocomponent systems, the inverse problem was analytically solved by Sips in his classical analysis of binding to heterogeneous surfaces [15]. Numerical regularization techniques have also been successfully applied to solve the inverse problem from experimental binding data [20, 21]. For multicomponent systems, the n-dimensional nature of the integrals appearing in Eqn 8.10 complicates the interpretation of the binding isotherms in terms of an underlying affinity spectrum. However, there is an alternative and complementary approach to the study of multicomponent adsorption. If we restrict to a fixed concentration of all competing cations in Eqn 8.10 except one, e.g., ion i, then the competitive isotherm becomes monocomponent and the corresponding affinity spectrum, $p(\log K_i'; c_{m\neq i} = \text{cnt})$, is defined from

$$\theta_i(c_i) = \int_{-\infty}^{\infty} p(\log K_i'; c_{m\neq i} = \text{cnt}) \frac{K_i' c_i}{1 + K_i' c_i} d(\log K_i'), \tag{8.11}$$

where K_i' labels the effective or conditional affinity "seen" by ion i, and $p(\log K_i'; c_{m\neq i} = \text{cnt})$ indicates the relative abundance of available sites having this affinity. From now on, $p(\log K_i'; c_{m\neq i} = \text{cnt})$ will be denoted as the *Conditional Affinity Spectrum* (CAS).

The advantage of the restriction $c_m = \text{cnt}$ for all $m \neq i$ is that it allows us to obtain the CAS by applying the inversion formula for monocomponent isotherms given by Eqn 8.9 [15, 22].

In the next section we will obtain the CAS for a mixture of competitive ions in presence of a heterogeneous ligand (like humic or fulvic acid), using a NICA isotherm to describe the binding coverage.

8.2.4 CAS in a Mixture of Competing Ions

Since acid-base ionisable groups participate in the binding sites of NOM, two components have been recognized in the binding energy: one of electrostatic origin, giving rise to the electrostatic binding, and a second chemical component responsible for the specific binding [2].

Here we use the NICA-Donnan model, in which the specific binding (intrinsic interactions) is described by the NICA model and the non-specific binding (electrostatic interactions) is described by the Donnan model. the NICA-Donnan model has been extensively applied to heterogeneous complexation, yielding satisfactory results in modeling the binding and in predicting the effect of the ionic strength and the competition between several ions present in the medium, largely by potentiometric techniques [23–26] but also by voltammetry [25, 27].

8.2.4.1 The NICA Isotherm. Specific Binding

The NICA (Non Ideal Competitive Adsorption) isotherm is widely used to describe the competitive binding of metal ions to natural organic matter in environmental chemistry. The monomodal form of the NICA equation reads [28]

$$\theta_i = \frac{Q_i}{Q_{\max i}} = \frac{\left(\tilde{K}_i c_i\right)^{n_i}}{\sum_j \left(\tilde{K}_j c_j\right)^{n_j}} \frac{\left(\sum_j \left(\tilde{K}_j c_j\right)^{n_j}\right)^p}{1 + \left(\sum_j \left(\tilde{K}_j c_j\right)^{n_j}\right)^p}, \tag{8.12}$$

where Q_i is the total amount of the component i bound to the humic acid in mol kg^{-1}; $Q_{\max i}$ is the total number of sites able to bound the species i, in mol kg^{-1}; $\tilde{K}_j$ is related to the average affinity constant for the component j in absence of other competing cations, and c_j is the concentration of component j in mol L^{-1}. The various summations are over all j components (including i). This includes the proton and the metal ions present. Parameters n_k ($0 < n_k \leq 1$) are related to the ion specific non-ideality; the smaller the value of n, the greater the non-ideality. Parameter p ($0 < p \leq 1$) represents the intrinsic heterogeneity of the ligand and is common to all components; the smaller value of p, the greater the heterogeneity. Notice that when only one ion is present in the system NICA isotherm reduces to the Langmuir-Freundlich isotherm, which helps in recognizing the physical meaning of parameters $\tilde{K}_j$ and of the product $n_j p$

Since proton titration curves of humic matter (fulvic or humic acid) often show a double wave shape [29], NICA isotherm is usually written as a bi-

modal (carboxylic and phenolic sites) distribution when applied to these kind of ligands:

$$\begin{aligned} Q_i = Q_{\max i,1} \frac{\left(\tilde{K}_{i,1} c_i\right)^{n_{i,1}}}{\sum\limits_j \left(\tilde{K}_{j,1} c_j\right)^{n_{j,1}}} \frac{\left(\sum\limits_j \left(\tilde{K}_{j,1} c_j\right)^{n_{j,1}}\right)^{p_1}}{1 + \left(\sum\limits_j \left(\tilde{K}_{j,1} c_j\right)^{n_{j,1}}\right)^{p_1}} \\ + Q_{\max i,2} \frac{\left(\tilde{K}_{i,2} c_i\right)^{n_{i,2}}}{\sum\limits_j \left(\tilde{K}_{j,2} c_j\right)^{n_{j,2}}} \frac{\left(\sum\limits_j \left(\tilde{K}_{j,2} c_j\right)^{n_{j,2}}\right)^{p_2}}{1 + \left(\sum\limits_j \left(\tilde{K}_{j,2} c_j\right)^{n_{j,2}}\right)^{p_2}}, \end{aligned} \tag{8.13}$$

where the subscripts 1 and 2 refer to the carboxylic and phenolic type of the distribution respectively. Assuming monodentate binding to all the sites i.e., one cation per site, for a mixture of specifically-bound divalent cations the net charge of the humic substances, q, is given by the charge contribution from the various surfaces species of the two modes by

$$q = q_1 + q_2, \tag{8.14}$$

with

$$\begin{aligned} q_1 &= -Q_{\max i,1} + Q_{\mathrm{H},1} + 2 \sum Q_{\mathrm{M}_j 1}, \\ q_2 &= -Q_{\max i,2} + Q_{\mathrm{H},2} + 2 \sum Q_{\mathrm{M}_j 2}, \end{aligned} \tag{8.15}$$

where $Q_{\max i}$ stands for the total number of acid-base sites present in the humic macromolecule (each unoccupied site is assumed to have a charge -1), Q_{H} is the number of protonated sites and $\sum Q_{\mathrm{M}_j}$ is the number of bound divalent metals.

The net charge of the macromolecule (q) gives rise to a local electrostatic potential, which tends both to attract oppositely charged ions and to exclude coions.

8.2.4.2 The Donnan Model. Electrostatic Binding

Among many others [30–33], the Donnan model has been used to account for the electrostatic binding in NOM.

In the Donnan approach the polyelectrolyte is considered to behave as an electrically neutral gel phase having a particular volume, V_{D}, throughout

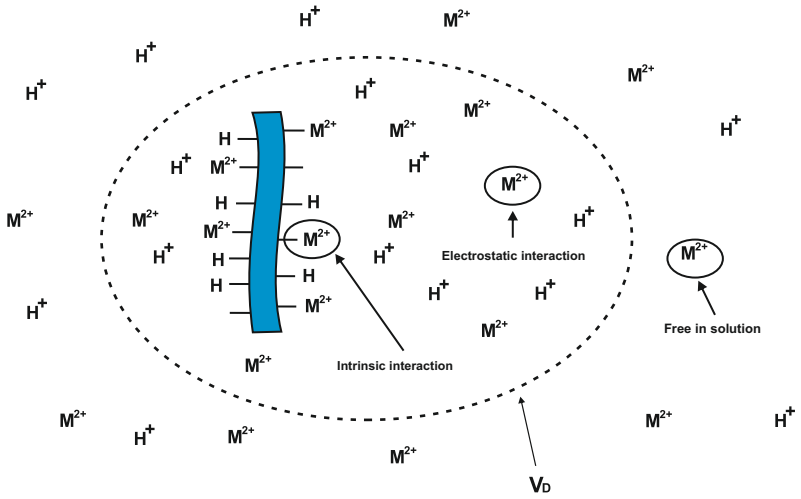

Figure 8.2: Schematic representation of intrinsic and electrostatic interactions in a humic substance molecule.

which there is a uniform averaged electrostatic potential known as the Donnan potential, Ψ^{D}, with respect to the uniform zero potential of the solution phase (see Figure 8.2).

In the simplest Donnan model it is assumed that all of the charge on the humic particle, q, is completely neutralized by attraction of counter-ions and exclusion of co-ions within the Donnan volume, V_{D}. This leads to the basic equation of charge neutrality given by

$$\frac{q}{V_{\mathrm{D}}} + \sum_j z_j (c_{\mathrm{D},j} - c_j) = 0, \tag{8.16}$$

where q is the net charge of humic substances (eq g^{-1} or eq mol^{-1}), V_{D} is the volume of the Donnan solution phase (L kg^{-1}, see Figure 8.2 for a schematic representation of V_{D}), $c_{\mathrm{D},j}$ are the molar concentrations of the various cations and anions present in the Donnan phase, c_j are the concentrations in the bulk solution and z_j are their charges, including the sign.

Inside this scheme, the concentrations in the Donnan phase ($c_{\mathrm{D},j}$) are related to bulk concentrations (c_j) by a Boltzmann factor as

$$c_{\mathrm{D},j} = \chi^{z_j} c_j, \tag{8.17}$$

where χ, the Boltzmann factor, is linked to the uniform Donnan potential (Ψ^{D}) by

$$\chi = \exp\left(-\frac{F\Psi^{\mathrm{D}}}{RT}\right), \tag{8.18}$$

where F is the Faraday constant, R is the gas constant and T is the absolute temperature.

A critical aspect of this model is how the Donnan volume depends on changes in solution chemistry. Benedetti *et al.* [34] discussed this point in some detail and concluded that the most influential parameter is the ionic strength (i.e., the effect of the pH or the macromolecule charge on the volume is neglected). The variation of Donnan volume with ionic strength, I, for various humic substances is assumed to follow the empirical relation [34]

$$\log V_{\mathrm{D}} = b(1 - \log I) - 1, \tag{8.19}$$

where the coefficient b varies with the type of humic substance. For instance, for a humic acid, $b \approx 0.43$ [35].

Koopal *et al.* [36] advice the use of the empirical Donnan volume relation suggested by Benedetti *et al.*, because this model does not need information on the size of the macromolecule and/or the molar mass. As a result, the model is independent of the type of ion that binds, which is favorable for its use in the case of multi-component ion binding.

When the Donnan model for the electrostatics applies, NICA isotherm can be combined with electrostatic interactions by introducing (in Eqn 8.13) the concentration of species at the neighborhood of binding site ($c_{\mathrm{D},j}$) instead of using the bulk concentration c_j. Knowing the Donnan volume, the total concentrations of all ions present, and the appropriated NICA isotherm parameters, it is possible to solve Eqns 8.13–8.17 to obtain the Boltzmann factor and therefore, the concentrations and the potential in the Donnan phase.

As a result, we obtain the NICA-Donnan model in which the specific binding (intrinsic interactions) is described by the NICA model and the non-specific binding (electrostatic interactions) is described by the Donnan model. As we have pointed before, the convenience of using The NICA-Donnan model comes from the fact that the set of parameters (needed in Eqn 8.13) to describe the binding of many cations to humic or fulvic acids are independent of the solution composition (concentration of background salt and pH) and they are also available from the literature. Likewise, as shown in the next section, analytical expression for the CAS underlying a NICA isotherm has been already derived.

8.2.4.3 CAS Underlying NICA Isotherm in a Mixture of Competing Ions

Replacing the coverage described in the NICA-Donnan model (Eqn 8.13) in Eqn 8.9 give us $p(\log K_i'; c_{m\neq i} = \mathrm{cnt})$, the conditional affinity spectrum

which reads [8]

$$p(\log K'_i; c_{m\neq i}) = \frac{\ln 10}{\pi}\left(\frac{1}{\dfrac{n_{i,1}}{n_{\mathrm{H},1}}Q_{\max \mathrm{H},1} + \dfrac{n_{i,2}}{n_{\mathrm{H},2}}Q_{\max \mathrm{H},2}}\right)$$
$$\times \sum_{j=1}^{2}\left(\frac{n_{i,j}}{n_{\mathrm{H,j}}}Q_{\max \mathrm{H,j}}\frac{\left(\tilde{K}_{i,j}/{K'}_i\right)^{n_{i,j}} M_{i,j}^{p_j-1}}{1 + M_{i,j}^{2p_j} + 2M_{i,j}^{p_j}\cos\left(p_j\phi_{i,j}\right)}\left[\sin\left(\pi n_{i,j} - \left(1-p_j\right)\phi_{i,j}\right)\right.\right.$$
$$\left.\left. + M_{i,j}^{p_j}\sin\left(\pi n_{i,j} - \phi_{i,j}\right)\right]\right), \tag{8.20}$$

where

$$M_{i,j}(K'_i; c_{\mathrm{H}}, c_{m\neq i}) = \left[\left\{\left(\tilde{K}_{H,j}c_{\mathrm{H}}\right)^{n_{\mathrm{H,j}}} + \sum_{m\neq i}\left(\tilde{K}_{m,j}c_m\right)^{n_{m,j}}\right.\right.$$
$$\left.\left. + \left(\tilde{K}_{i,j}/{K'}_i\right)^{n_{i,j}}\cos\left(\pi n_{i,j}\right)\right\}^2 + \left\{\left(\tilde{K}_{m,j}c_m\right)^{n_{m,j}}\right\}^2\right]^{1/2}, \tag{8.21}$$

and

$$\cos\left(\pi\phi_{i,j}\right) = \left(\tilde{K}_{H,j}c_{\mathrm{H}}\right)^{n_{\mathrm{H,j}}} + \sum_{m\neq i}\left(\tilde{K}_{m,j}c_m\right)^{n_{m,j}} + \left(\tilde{K}_{i,j}/{K'}_i\right)^{n_{i,j}}\cos\left(\pi n_{i,j}\right). \tag{8.22}$$

Equation 8.20 constitutes a general explicit expression for the CAS underlying NICA isotherm in a complex mixture of cations.

Using the set of generic NICA-Donnan parameters reported in literature [9] and gathered in Table 8.3 of the Supporting Information (page 207), Figure 8.3 shows the effective (conditional) Pb ion binding affinity spectra of a generic fulvic acid for different values of pH.

In Figure 8.3 the shift of the CAS towards lower affinities reflects a significant competition effect. That is, the sites with high affinity for the Pb also display a high affinity for proton, which indicates a large correlation between the binding energies of both cations.

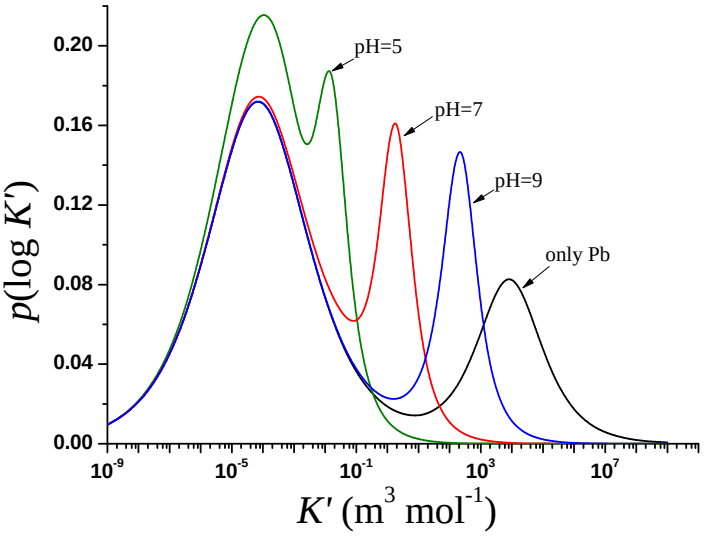

Figure 8.3: Effect of competitive proton on the effective Pb specific binding affinity spectra of a generic fulvic acid. Each line correspond to different values of pH. Parameters: NICA-Donnan parameters from Milne *et al.* [9]; $c_{\mathrm{T,Pb}} = 2,5 \times 10^{-8}$ M, and $c_{\mathrm{T,FA}} = 30$ mg L^{-1}.

8.2.5 CAS as a Function of Total Binding Energy

As the concentrations c_i used in this model in Eqns 8.13 and 8.20 are the values in the Donnan phase ($c_{\mathrm{D},i}$), the NICA-Donnan isotherm and the CAS underlying it, account only for the intrinsic (chemical) binding, i.e., the binding energies free of electrostatic contribution. So, affinity spectra in Figure 8.3 depict only the distribution of chemical energies involved in the cation binding to the fulvic ligand.

The distribution of total binding energy experienced by the ion can be assessed by adding the corresponding electrostatic contribution to each chemical affinity $\log K_i'$. Using Eqn 8.18 the energy shift can be read as,

$$\log K_i = \log K_i'(\mathrm{sb}) + \frac{2F\Psi^{\mathrm{D}}}{RT}\,, \tag{8.23}$$

where (sb) refers to specific binding and K_i (without prime) stands for the effective (conditional) total equilibrium constant. Notice that Eqn 8.23 is only true when the binding of the probe ion do no alter the Donnan potential, e.i., when the metal concentration is low enough, in comparison to the background electrolyte so that the Donnan potential is almost determined by the background salt.

As a result of 8.23, when we plot the CAS as a function of the total binding energy there is a shift towards higher affinities. In this shift, $p(\log K_i)$ has been used as the density of probability of the total affinity $\log K_i' + 2F\Psi^{\mathrm{D}}/RT$ (for divalent binding cations). Thus:

$$p(\log K_i) = p(\log K_i'), \tag{8.24}$$

where K_i and K_i' are related by Eqn 8.23. Figure 8.4 shows the CAS shift for Pb at pH = 9.

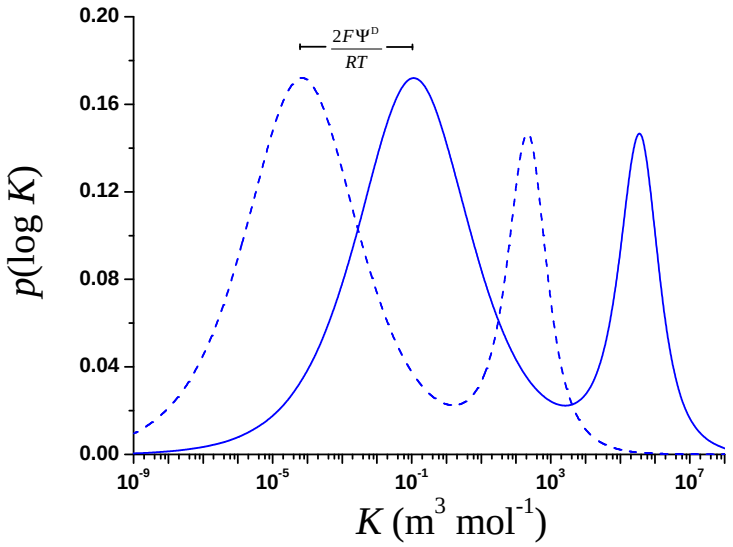

Figure 8.4: Effective Pb binding affinity spectra of a generic fulvic acid at pH = 9. Dashed line: CAS as a function of specific (chemical) binding energy. Continuous line: CAS as a function of total binding energy (see Eqn 8.23). Parameter as in Figure 8.3.

8.2.6 Site Occupation Distribution Function

As CAS provides the relative amount of binding sites of each affinity that are available for a given ion irrespective of its concentration, the distribution of occupied sites (or Site Occupation Distribution Function, SODF) at the actual concentration of ion i, can be easily calculated as

$$p_{\mathrm{occ}}(\log K_i; c_{m\neq i} = \mathrm{cnt}) = p(\log K_i; c_{m\neq i} = \mathrm{cnt}) \frac{K_i c_i}{1 + K_i c_i}. \tag{8.25}$$

This distribution at some Pb concentrations is depicted together with the CAS, at a fixed pH value, in Figure 8.5.

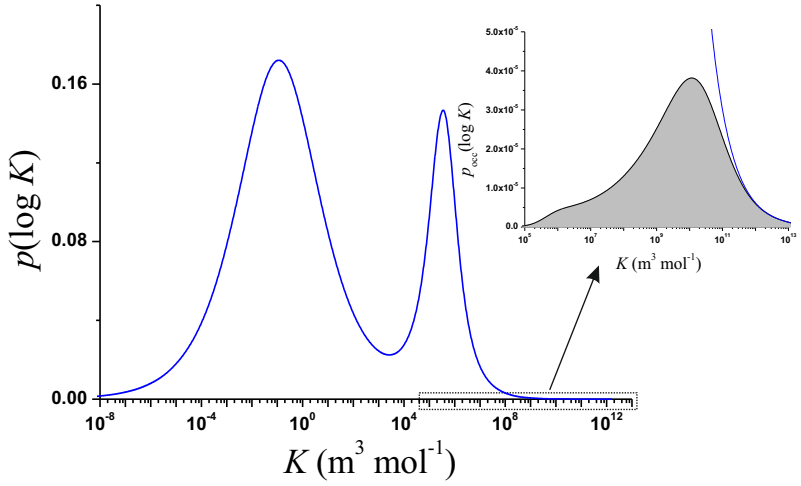

Figure 8.5: Effective Pb binding affinity spectra of a generic fulvic acid as a function of total binding energy (blue line). The shadow area in the inside shows the Site Occupation Distribution Function (SODF) for Pb. Parameters as in figure 8.3 for pH = 9.

8.3 Conditional Kinetic Spectrum (CKS)

If the CAS for a specific ion is discretized into a finite number of values of $\log K$, each resultant part can be seen as a ligand with a binding affinity $\log K_i$, separate to the next one ($\log K_{i+1}$) by a constant interval $\Delta \log K$. This system is analogous to the system composed by an ion in presence of a mixture of ligands with different affinities and the same diffusion coefficient.

8.3.1 Complex and Total Ligand Concentration

As the coverage represents the fraction of occupied sites ($\theta = c_{\mathrm{ML}}/c_{\mathrm{T,L}}$), a discretized form of Eqn 8.11 could be used to calculate the complex concentration ($c_{\mathrm{M}^i\mathrm{L}}$) associated at each ^{i}L ligand (with affinity $\log K_i$),

$$c_{\mathrm{M}^i\mathrm{L}} = p(\log K_i)\frac{K_i c_{\mathrm{M}}}{1 + K_i c_{\mathrm{M}}}\Delta(\log K)c_{\mathrm{T,L}}. \tag{8.26}$$

In a similar way the total ligand concentration associated at each ^{i}L ligand can be computed as

$$c_{\mathrm{T},^i\mathrm{L}} = p(\log K_i)\Delta(\log K)c_{\mathrm{T,L}}. \tag{8.27}$$

Figure 8.6 depicts an schematic representation of $c_{\mathrm{M}^{i}\mathrm{L}}$ and $c_{\mathrm{T},^{i}\mathrm{L}}$ for the CAS depicted in Figure 8.5

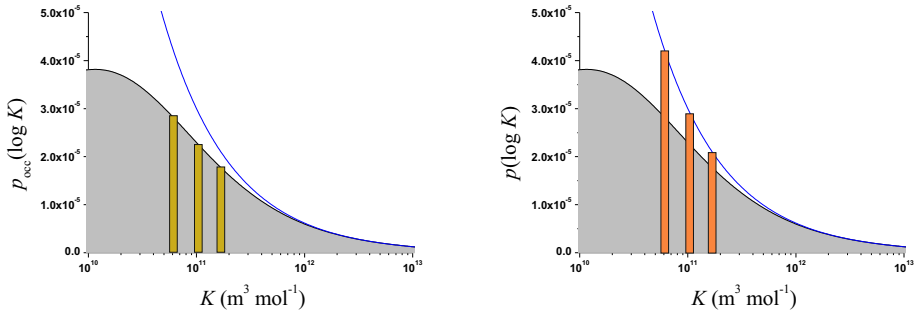

(a) $c_{\mathrm{M}^{i}\mathrm{L}}$ **(b)** $c_{\mathrm{T},^{i}\mathrm{L}}$

Figure 8.6: Schematics representation (in a discretized CAS) of $p_{occ} = p(\log K)Kc_{\mathrm{M}}/(1+Kc_{\mathrm{M}})$ and $p(\log K)$, which are proportional to $c_{\mathrm{M}^{i}\mathrm{L}}$ and $c_{\mathrm{T},^{i}\mathrm{L}}$, respectively.

8.3.2 Kinetic Constants

Eigen mechanism has been widely used to describe the kinetics of metal ion complexation in aqueous systems [37]. It is composed of two essential steps: the formation of a precursor outer-sphere complex, followed by the release of water from the inner sphere of the metal ion to form a coordination bond with the ligand; these steps are schematized in Eqn 8.28. The major importance of the basic Eigen scheme is that it allows the estimation of the rate of complex formation from the nature of the metal and the charge/size of the ligand, irrespective of the chemical nature of the latter. This greatly facilitates theoretical prediction of rate constants of environmental processes involved with dissociation of metal complexes.

The two basic steps in the Eigen scheme of complex formation between an aqueous metal ion, $\mathrm{M(H_2O)_6}^{2+}$, and a ligand L^{-} are

$$\begin{aligned} \mathrm{M(H_2O)_6}^{2+} + \mathrm{L}^{-} &\underset{k_{\mathrm{d}}^{\mathrm{os}}}{\overset{k_{\mathrm{a}}^{\mathrm{os}}}{\rightleftharpoons}} \mathrm{M(H_2O)_6 \bullet L}^{+} \\ \mathrm{M(H_2O)_6 \bullet L}^{+} &\underset{k_{\mathrm{d}}^{\mathrm{is}}}{\overset{k_{\mathrm{a}}^{\mathrm{is}}}{\rightleftharpoons}} \mathrm{M(H_2O)_5L}^{+} + \mathrm{H_2O} \end{aligned} \tag{8.28}$$

where $k_{\mathrm{a}}^{\mathrm{os}}$ and $k_{\mathrm{d}}^{\mathrm{os}}$ are the association and dissociation rate constants for the outer-sphere complex ($\mathrm{M(H_2O)_6 \bullet L}^{+}$), and $k_{\mathrm{a}}^{\mathrm{is}}$ and $k_{\mathrm{d}}^{\mathrm{is}}$ are the association

and dissociation rate constants for the inner-sphere complex $M(H_2O)_5L^+$ $+H_2O$. The rate-limiting step for inner-sphere complex formation from $M(H_2O)_6 \bullet L^+$, is the elimination of a water molecule from the inner hydration shell of ${M(H_2O)_6}^{2+}$. Its rate constant k_a^{is} is usually denoted as k_w.

According to Eigen ideas, in the stationary state of the overall complex formation process, the outer-sphere complex concentration can be taken as essentially time-independent. Then the overall rate constant, k_a, for inner-sphere complex formation from ${M(H_2O)_6}^{2+}$ and L^- is given by [38]

$$k_a = \frac{k_a^{os} k_w}{k_d^{os} + k_w}, \tag{8.29}$$

where k_w stands for the dehydration rate constant for the metal ion. According to the Fuoss theory k_a^{os} and k_d^{os} are given by

$$k_a^{os} = 4\pi N_{av} a (D_M + D_L) \frac{U^{os}}{\exp(U^{os} + 1)}, \tag{8.30}$$

and

$$k_d^{os} = \frac{3(D_M + D_L)}{a^2} \frac{U^{os} \exp(U^{os})}{\exp(U^{os} + 1)}, \tag{8.31}$$

where U^{os} is the dimensionless electrostatic pair interaction energy, a is the charge center-to-center distance of closets approach between ion and ligand, and D_M and D_L are the diffusion coefficients of metal and ligand respectively.

Recently, extensions of the Eigen mechanism to ligands with multi-point charges, surfaces or colloids have been reported [38, 39]. Here, as we are using the NICA-Donann parameters for the binding, we will use the Donnan potential there derived for the computation of U^{os} to be consistent.

By using the Donnan model, we have implicitly considered that the (constant) electrostatic interaction potential Ψ^D accounts for the electrostatic part of the binding to the macromolecule. Under this condition, the electrostatic pair interaction energy should be calculated as

$$U^{os} = \frac{z_M F \Psi^D}{RT} = \ln \frac{c_{D,M}}{c_M}. \tag{8.32}$$

Under this scheme, all the ${}^iL$ ligands share the same k_a value given by Eqns 8.29 to 8.32.

Once we have computed the common k_a, the set of kinetic dissociation rate constants, $k_{d,i}$, associated to the binding of metal and ligand could be obtained with

$$k_{d,i} = \frac{k_a}{K_i}, \tag{8.33}$$

where K_i stands for the total equilibrium constant of metal-^{i}L binding.

8.3.3 Conditional Kinetic Spectrum

For a fixed value of the association rate constant, k_a, we can introduce the *Conditional Kinetic Spectrum* (CKS), which represents the CAS as a function of the kinetic dissociation rate constant, k_d. In general, we have

$$\left|p(\log K)\mathrm{d}(\log K)\right| = \left|p(\log k_\mathrm{d})\mathrm{d}(\log k_\mathrm{d})\right|. \tag{8.34}$$

Using the relationship $K = k_\mathrm{a}/k_\mathrm{d}$, Eqn 8.34 can be rewritten as

$$\left|p(\log K)\mathrm{d}(\log K)\right| = \left|p(\log K)\mathrm{d}\left(\log \frac{k_\mathrm{a}}{k_\mathrm{d}}\right)\right| \tag{8.35}$$

$$= \left|p(\log K)\mathrm{d}(\log k_\mathrm{a} - \log k_\mathrm{d})\right|. \tag{8.36}$$

Now, for a fixed k_a value it holds

$$\left|p(\log K)\mathrm{d}(-\log k_\mathrm{d})\right| = \left|p(\log k_\mathrm{d})\mathrm{d}(\log k_\mathrm{d})\right|, \tag{8.37}$$

or

$$p(\log K) = p(\log k_\mathrm{d}). \tag{8.38}$$

Using the result of Eqn 8.38, the expression 8.20 can also be used for compute the CAS as a function of k_d, that is, the CKS. Figure 8.7 shows the CKS and the SODF associate to the CAS depicted in Figure 8.4.

Up to now we have transformed the heterogeneity of HA/FA into a mixture of ligands with well specified concentration and kinetic constant values. From now on, we will focus on the calculation of the lability degree of this system.

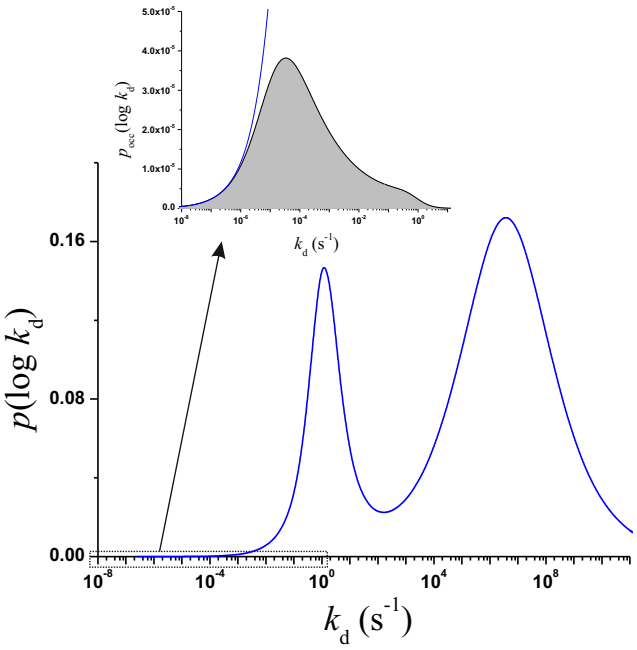

Figure 8.7: Conditional Kinetic Spectrum and Site Occupation Distribution Function associated to the CAS depicted in Figure 8.4. Others parameters: $k_a = 4.25 \times 10^5$ m^3 mol^{-1} s^{-1} (using $a = 1 \times 10^{-9}$ m in Eqn 8.29); $D_M = 8.03 \times 10^{-10}$ m^2 s^{-1} and $D_{M^iL} = 2.41 \times 10^{-10}$ m^2 s^{-1}.

8.4 Evaluation of the Lability Degree in the Pb–FA system for Different pH Values.

8.4.1 Numerical Evaluation

We now consider a system composed by a 30 mg L^{-1} of fulvic acid[1], and a total Pb concentration of 2.5×10^{-8} mol L^{-1} at ionic strength $I = 0.1$ M. The speciation distribution (concentrations of free and complexed metal, and concentrations in Donnan phase) in this system at different pH values, have been obtained from Visual MINTEQ. Results are reported in Table 8.1. NICA-Donnan parameters used in this speciation calculation are those reported by Milne *et al.* [9].

It is important to notice that for the range of pH values considered, almost all the metal is complexed to fulvic acid, so the amount of free and territorially Pb bound (last two columns on Table 8.1) are negligible.

[1]To express $c_{T,FA}$ in units of mol L^{-1} we use the relationship $Q_{\max i,j} = Q_{\max H,j}(n_{i,j}/n_{H,j})$, which have been introduced to keep the thermodynamic consistence of NICA Model [23]. Thus $c_{T,FA\,i}$ (mol L^{-1}) $= [Q_{\max i,1} + Q_{\max i,2}]c_{T,FA\,i}$ (kg L^{-1}).

Table 8.1: Values of free and complex metal concentration in a solution containing 30 mg L^{-1} of fulvic acid and a total Pb concentration of 2.5×10^{-8} mol L^{-1} at ionic strength $I = 0.1$ M. $c_{M^iL}(1)$ and $c_{M^iL}(2)$ refer to the complex associated to carboxylic and phenolic sites respectively, while $c_{M^iL}(T)$ stands for the total complex concentration (carboxylic plus phenolic). The last column contain the Donnan concentrations of Pb related to the total volume. The values reported in this table have been obtained with Visual MINTEQ.

pH	$c_{M^iL}(1)$	$c_{M^iL}(2)$	$c_{M^iL}(T)$ (mol L^{-1})	c_i	$c_{D,i}$
5	7.91×10^{-9}	1.62×10^{-8}	2.41×10^{-8}	5.71×10^{-10}	2.30×10^{-11}
7	2.54×10^{-9}	2.25×10^{-8}	2.5×10^{-8}	4.66×10^{-12}	3.15×10^{-15}
9	5.71×10^{-10}	2.44×10^{-8}	2.5×10^{-8}	3.78×10^{-14}	3.15×10^{-15}

From the concentrations and parameters of Table 8.1 we evaluate the CAS and the CKS of this fulvic acid seen by Pb.

For different values of $\Delta \log K$ we discretized the CAS and the CKS. Details of these calculations, the set of data obtained from discretizations and the parameters used for them, are consigned in Section 8.A.1.

Using the data obtained from discretizations (see Tables 8.5, 8.6, 8.7 and 8.8 in Section 8.A.1, pages 211–218), the global lability degree can be computed by the rigorous numerical simulation described in Chapter 2. Table 8.2 shows the values obtained from numerical solutions for four different discretizations. Special care has been devoted to check the independence of the numerical evaluation of the lability degree on the thickness of the discretization grid. Obviously, we expect that decreasing the thickness of the grid, numerical results will tend to the result of the continuous distribution of affinities representing the binding properties of the FA, but we would also like to check that numerical results are out of influence of mixture effects due to the discretization used. This independence of the lability degree reported in Table 8.2 on the discretization used, suggests that the numerical evaluations can be considered a good estimation of the lability degree of the Pb-FA complex.

It is important to note that for a given metal concentration, not all affinity values ($\log K$ or $\log k_d$) of the CAS are involved in the binding. Indeed, when we discretize, just the set of ligands with affinities lying under the SODF, i.e., the set of ligands with $c_{M^iL} \neq 0$, are involved in the lability degree evaluation (shadow data in Tables 8.5, 8.6, 8.7 and 8.8). Low affinity ligands are not occupied and, accordingly, they can not contribute to the release of metal.

Table 8.2: Lability degree of Pb–FA system as measured with a standard DGT. Values obtained form numerical simulation for four different $\Delta \log K$ values: ξ^a, for $\Delta \log K = 0.64$; ξ^b, for $\Delta \log K = 0.6$; ξ^c, for $\Delta \log K = 0.3$; and ξ^d, for $\Delta \log K = 0.2$. The last column shows the analytical lability degree computed by Eqns 8.39 and 8.41. Parameters indicated in Tables 8.5, 8.6, 8.7 and 8.8

pH	ξ^a	ξ^b	ξ^c	ξ^d	ξ analytical
5	0.94	0.94	0.94	0.94	0.98
7	0.78	0.78	0.78	0.78	0.79
9	0.33	0.33	0.33	0.33	0.30

8.4.2 Analytical Evaluation

As we have stated, once the CKS has been discretized, the resultant system can be considered as a metal in presence of a mixture of ligands with different affinities, so the lability degree may also be computed analytically (as indicated in Chapter 7) by

$$\xi = \sum_{i=1}^{h} \frac{J_{\text{diff},i}}{\sum_{i=1}^{h} J_{\text{diff},i}} \xi_i, \tag{8.39}$$

where $J_{\text{diff},i}$ and ξ_i are, respectively, the diffusive flux and the lability degree associated to the M^iL complex. In a measure with a standard DGT, $J_{\text{diff},i}$ is given by (see Section 7.4)

$$J_{\text{diff},i} = \frac{D_{\text{M}^i\text{L}} c^*_{\text{M}^i\text{L}}}{g}, \tag{8.40}$$

and ξ_i can be computed with the approximated equation

$$\xi_i = 1 - \frac{1 + \epsilon K_i'}{\epsilon K_i' + \frac{g}{m} \coth\left(\frac{g}{m}\right) + \frac{g}{\lambda_{\text{M}^i\text{L}}}(1 + \epsilon K_i') \tanh\left(\frac{r}{\lambda_{\text{M}^i\text{L}}}\right)}. \tag{8.41}$$

The resulting lability degree from the analytical evaluation through Eqn 8.39 is included in the last column of Table 8.2. As can be seen, a good agreement between the numerical and analytical evaluation of ξ is found. This agreement gives confidence to the results found and points out the ability of using the simple Eqn 8.39 in the computation of the lability degree of metal complexes with heterogeneous ligands, avoiding the use of numerical simulations methods.

Figure 8.8 shows (for data of table 8.1) the discretized SODFs as a function of k_{d}. Each panel additionally shows the corresponding values of the coverage and analytical lability degree ξ_i (calculated by Eqn 8.41).

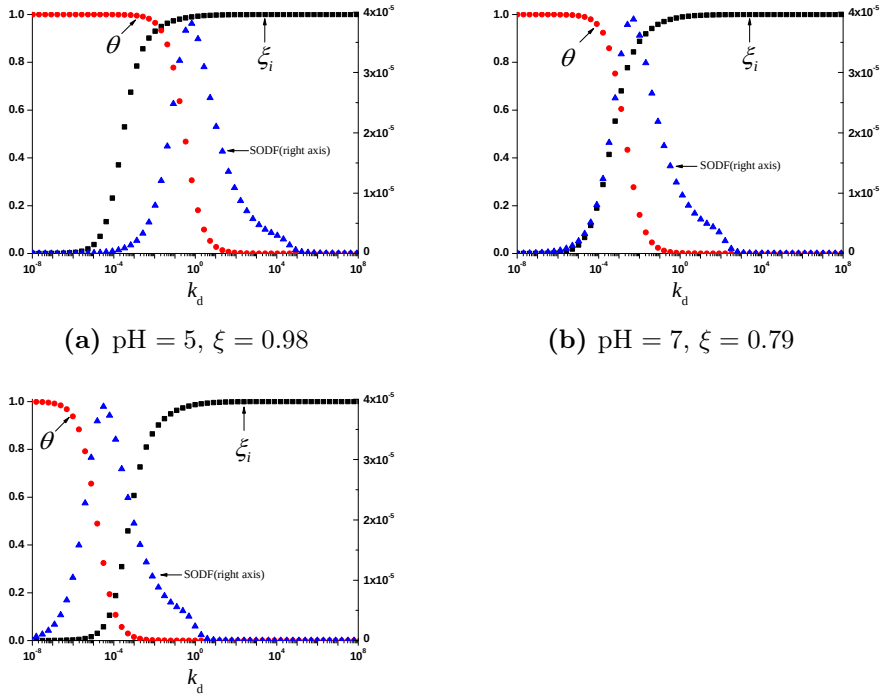

(a) pH $= 5$, $\xi = 0.98$

(b) pH $= 7$, $\xi = 0.79$

(c) pH $= 9$, $\xi = 0.30$

Figure 8.8: Discretized SODF as a function of k_{d}. Each panel additionally depicts the corresponding values of coverage and lability degree. The values of global lability degree computed by Eqn 8.39 are indicated at each label.

At the lowest values of pH depicted in Figure 8.8 (i.e. the highest proton concentration, panel a) the conditional affinity of the sites for Pb is low due to the exchange work. Thus the corresponding k_{d} of these sites is high enough to make most of the occupied sites labile. As the global lability degree calculated by Eqn 8.39 is a weighted average of the lability degrees of each one of the different $\mathrm{M}^i\mathrm{L}$ complexes present in the mixture, the panel (a) shows the higher global lability degree of the set. As the proton concentration decreases, sites show a higher values of conditional affinities K (lower values of k_{d}) for Pb. As a result the SODF shifts towards higher K (lower k_{d}) values yielding to a decrease in the global lability value.

8.5 Conclusions

Based on the CAS methodology, we have introduced here the *Conditional Kinetic Spectrum* for the description of metal-macromolecular binding in multicomponent systems. The discretization of the CAS and CKS distributions has allowed us to transform the problem of the lability of a metal complex with a heterogeneous ligand, into the problem of the lability degree of a mixture of ligands with different affinities and kinetic dissociation constants sharing a common diffusion coefficient. Concentrations of complex and ligands in this mixture have been evaluate from the Site Occupation Distribution Function.

Finally, the lability degree has been obtained for the case of Pb-FA complex at different pH values, from both numerical simulation and analytical expressions for the lability degree of a mixture. The agreement between both results indicates the successful use of a simple analytical expression. According to the results of this chapter Pb-FA complexes are expected to be labile at pH = 5 while they are quite inert ($\xi = 0.3$) at pH = 9, when this property is measured with the standard configuration of DGT devices.

8.A Supporting Information

8.A.1 Discretized Pb-FA CKS Data

For the Pb-FA system, we compute the CAS (using Eqn 8.20), as a function of the total energy, with parameters consigned in Table 8.3 and concentrations reported in Table 8.4.

Table 8.3: Parameters used for computing the CAS in the Pb-FA system. These values correspond to those reported by Milne *et al.* [9].

Parameter	Value
$n_{\mathrm{Pb},1}$	0.6
$n_{\mathrm{Pb},2}$	0.69
$n_{\mathrm{H},1}$	0.66
$n_{\mathrm{H},2}$	0.76
$\log(\tilde{K}_{\mathrm{Pb},1})$	-1.16
$\log(\tilde{K}_{\mathrm{Pb},2})$	6.92
$\log(\tilde{K}_{\mathrm{H},1})$	2.34
$\log(\tilde{K}_{\mathrm{H},2})$	8.60
p_1	0.59
p_2	0.7
$Q_{\max \mathrm{H},1}$ [a]	5.88
$Q_{\max \mathrm{H},2}$ [a]	1.86
V_{D} [b]	0.7

[a] (mol kg^{-1})
[b] (L kg^{-1})

Once the CAS is obtained, we discretized it into a finite number of values of $\log K$. As we have stated, each resultant part can be seen as a ligand with a binding affinity $\log K_i$, separate to the next ligand (with affinity $(\log K_{i+1})$) by a constant interval $\Delta \log K$. In order to compute (numerically or analytically) the lability degree we need to know the kinetic rate constants and the concentrations of the species associated to each ligand. Here we report a detailed calculation of all the parameters corresponding to a particular ligand (or site of macromolecule) ${}^{i}\mathrm{L}$, characterized by a binding affinity $\log K_i$.

The CAS of the system described in Tables 8.3 and 8.4 can be computed

Table 8.4: Values of Pb free and Donnan concentrations in a solution containing 30 mg L^{-1} of fulvic acid and a total Pb concentration of 2.5×10^{-8} mol L^{-1} at ionic strength $I = 0.1$ M. The last column contain the Donnan concentrations of Pb related to the Donnan volume. The values have been obtained with Visual MINTEQ.

pH	c_i (mol L^{-1})	$c_{D,i}$ (mol L^{-1})
5	5.71×10^{-10}	5.55×10^{-7}
7	4.66×10^{-12}	7.66×10^{-9}
9	3.78×10^{-14}	7.61×10^{-11}

with Eqn 8.20. Table 8.5 contains the $p(\log K)$ values corresponding to the discretized Pb-FA CAS for $\Delta \log K = 0.64$ at pH = 7. The corresponding $k_{d,i}$ values are calculate with Eqn 8.33 (as is explained below) and they are also reported in Table 8.5. Let us focus, for instance, on the calculation of the $k_{d,i}$ corresponding to $K = 6.54 \times 10^5$ m^3 mol^{-1} (green shadow row on Table 8.5). As explained in Section 8.3.1, the total ligand concentration associated at each ^{i}L ligand can be computed with Eqn 8.27. With $c_{T,FA} = 30$ mg L^{-1}, $c_{T,Pb} = 2.5 \times 10^{-8}$ mol L^{-1} and $I = 0.1$ M, for the ligand corresponding to $K = 6.54 \times 10^5$ m^3 mol^{-1}, the total ligand concentration will be

$$c_{T,^iL} = p(\log K_i)\Delta(\log K)c_{T,L} = 5.26 \times 10^{-4} \text{ mol m}^{-3}. \tag{8.42}$$

Likewise, the complex concentration (c_{M^iL}) associated to ^{i}L ligand (with affinity $\log K_i$), can be calculate using Eqn 8.26. With $c_{T,FA} = 30$ mg L^{-1}, $c_{T,Pb} = 2.5 \times 10^{-8}$ mol L^{-1} and $I = 0.1$ M, for $K = 6.54 \times 10^5$ m^3 mol^{-1}, the complex concentration will be

$$c_{M^iL} = p(\log K_i)\frac{K_i c_M}{1 + K_i c_M}\Delta(\log K)c_{T,L} = 1.60 \times 10^{-6} \text{ mol m}^{-3}. \tag{8.43}$$

Finally, in order to obtain the kinetic constant associate to each ligand, we need to compute the electrostatic interaction energy between the metal cation and the FA. This energy, within the Donnan model, is given by

$$U^{os} = \ln \frac{c_{D,M}}{c_M} = 3.22\,. \tag{8.44}$$

where c_M and $c_{D,M}$ have been taken from Table 8.4.

With this U^{os} value (at pH = 7), we can obtain the kinetic association rate constant as:

$$k_a = \frac{k_a^{os} k_w}{k_d^{os} + k_w} = 4.25 \text{ m}^3 \text{ mol}^{-1} \text{ s}^{-1}, \tag{8.45}$$

where we have used Eqns 8.30 and 8.31 with $D_{\mathrm{M}} = 8.03 \times 10^{-10}$ m^2 s^{-1}, $D_{\mathrm{ML}} = 0.3 D_{\mathrm{M}} = 2.41 \times 10^{-10}$ m^2 s^{-1}, $a = 1 \times 10^{-9}$ m and $k_{\mathrm{w}} = 7 \times 10^{9}$ s^{-1}. The corresponding kinetic dissociation rate constant will be

$$k_{\mathrm{d}} = \frac{k_{\mathrm{a}}}{K} = 6.49 \times 10^{-1} \text{ s}^{-1}. \tag{8.46}$$

Finally, the lability degree associate to the ligand can be computed analytically as

$$\xi_i = 1 - \frac{1 + \epsilon K_i'}{\epsilon K_i' + \dfrac{g}{m} \coth\left(\dfrac{g}{m}\right) + \dfrac{g}{\lambda_{\mathrm{M}^i\mathrm{L}}}(1 + \epsilon K_i') \tanh\left(\dfrac{r}{\lambda_{\mathrm{M}^i\mathrm{L}}}\right)} = 0.99\,. \tag{8.47}$$

Once we have characterized all the set of ligands obtained after discretization, the global lability degree of the Pb-FA system can be computed both numerically (by rigorous simulation described in Chapter 2) or analytically (using Eqn 8.39). Results are gathered in Table 8.2.

The complete set of data obtained from CKS discretizations of Pb-FA system at pH = 7 and the parameters used for them, are consigned in the next tables. In order to check the consistence of reported data we have verified that $\sum_i c_{\mathrm{T},{}^i\mathrm{L}} - c_{{}^i\mathrm{L}} = c_{\mathrm{M}^i\mathrm{L}} = 2.5 \times 10^{-8}$ mol L^{-1} as reported in Table 8.4.

Table 8.5: Discretized values of CKS for Pb-FA system ($\Delta \log K = 0.64$). The shadow data correspond to the set used for numerical calculation (14 ligands). Parameters: $c_{\mathrm{T,Pb}} = 2.5 \times 10^{-8}$ M; $c_{\mathrm{T,FA}} = 30$ mg L^{-1}; $I = 0.1$ M; pH = 7; $k_{\mathrm{a}} = 4.25 \times 10^{5}$ m^3 mol^{-1} s^{-1} (using $a = 1 \times 10^{-9}$ m in Eqn 8.29); for ξ_i evaluation(Eqn 8.39) $D_{\mathrm{M}} = 8.03 \times 10^{-10}$ m^2 s^{-1} and $D_{\mathrm{M}^i\mathrm{L}} = 2.41 \times 10^{-10}$ m^2 s^{-1}.

K (m^3 mol^{-1})	k_{d} (s^{-1})	$p(\log K)$	θ_i	SODF	$c_{\mathrm{T},^i\mathrm{L}}$ (mol m^{-3})	$c_{^i\mathrm{L}}$ (mol m^{-3})	ξ_i
1.64E+12	2.58E-07	1.75E-07	1.00E+00	1.75E-07	2.36E-08	3.08E-12	9.41E-04
3.77E+11	1.13E-06	4.69E-07	9.99E-01	4.69E-07	6.33E-08	3.61E-11	4.09E-03
8.63E+10	4.93E-06	1.26E-06	9.98E-01	1.26E-06	1.71E-07	4.24E-10	1.74E-02
1.98E+10	2.15E-05	3.42E-06	9.89E-01	3.38E-06	4.61E-07	4.96E-09	6.67E-02
4.53E+09	9.38E-05	9.25E-06	9.55E-01	8.83E-06	1.25E-06	5.65E-08	1.93E-01
1.04E+09	4.10E-04	2.51E-05	8.29E-01	2.08E-05	3.39E-06	5.81E-07	4.47E-01
2.38E+08	1.79E-03	6.83E-05	5.25E-01	3.59E-05	9.22E-06	4.38E-06	7.24E-01
5.44E+07	7.81E-03	1.86E-04	2.02E-01	3.77E-05	2.52E-05	2.01E-05	8.69E-01
1.25E+07	3.41E-02	5.09E-04	5.49E-02	2.80E-05	6.88E-05	6.50E-05	9.35E-01
2.86E+06	1.49E-01	1.40E-03	1.31E-02	1.84E-05	1.89E-04	1.87E-04	9.68E-01
6.54E+05	6.49E-01	3.89E-03	3.04E-03	1.18E-05	5.26E-04	5.24E-04	9.85E-01
1.50E+05	2.83E+00	1.11E-02	6.98E-04	7.78E-06	1.51E-03	1.50E-03	9.93E-01
3.43E+04	1.24E+01	3.42E-02	1.60E-04	5.48E-06	4.62E-03	4.62E-03	9.97E-01
7.87E+03	5.40E+01	1.12E-01	3.67E-05	4.12E-06	1.52E-02	1.52E-02	9.98E-01
1.80E+03	2.36E+02	1.56E-01	8.40E-06	1.31E-06	2.10E-02	2.10E-02	9.99E-01
4.13E+02	1.03E+03	7.24E-02	1.92E-06	1.39E-07	9.77E-03	9.77E-03	1.00E+00
9.46E+01	4.49E+03	6.18E-02	4.41E-07	2.72E-08	8.35E-03	8.35E-03	1.00E+00
⋮	⋮	⋮	⋮	⋮	⋮	⋮	⋮

Continued on next page

Table 8.5 – continued from previous page

K (m^3 mol^{-1})	k_d (s^{-1})	$p(\log K)$	θ_i	SODF	c_{T,i_L} (mol m^{-3})	c_{i_L} (mol m^{-3})	ξ_i
4.53E-215	9.38E+219	1.43E-76	2.11E-223	3.013E-299	1.93E-77	1.93E-77	1.00E+00

Table 8.6: Discretized values of CKS for Pb-FA system ($\Delta \log K = 0.6$). The shadow data correspond to the set used for numerical calculation (17 ligands). Parameters: $c_{\mathrm{T,Pb}} = 2.5 \times 10^{-8}$ M; $c_{\mathrm{T,FA}} = 30$ mg L^{-1}; $I = 0.1$ M; pH = 7; $k_{\mathrm{a}} = 4.25 \times 10^{5}$ m^3 mol^{-1} s^{-1} (using $a = 1 \times 10^{-9}$ m in Eqn 8.29); for ξ_i evaluation(Eqn 8.39) $D_{\mathrm{M}} = 8.03 \times 10^{-10}$ m^2 s^{-1} and $D_{\mathrm{M}^i\mathrm{L}} = 2.41 \times 10^{-10}$ m^2 s^{-1}.

K (m^3 mol^{-1})	k_{d} (s^{-1})	$p(\log K)$	θ_i	SODF	$c_{\mathrm{T},^i\mathrm{L}}$ (mol m^{-3})	$c_{^i\mathrm{L}}$ (mol m^{-3})	ξ_i
4.13E+11	1.03E-06	5.58E-08	9.99E-01	4.41E-07	5.58E-08	3.61E-11	3.73E-03
1.04E+11	4.10E-06	1.41E-07	9.98E-01	1.11E-06	1.41E-07	4.24E-10	1.46E-02
2.61E+10	1.63E-05	3.59E-07	9.92E-01	2.81E-06	3.59E-07	4.96E-09	5.30E-02
6.54E+09	6.49E-05	9.13E-07	9.68E-01	6.98E-06	9.13E-07	5.65E-08	1.52E-01
1.64E+09	2.58E-04	2.33E-06	8.85E-01	1.63E-05	2.33E-06	5.81E-07	3.56E-01
4.13E+08	1.03E-03	5.94E-06	6.58E-01	3.09E-05	5.94E-06	4.38E-06	6.33E-01
1.04E+08	4.10E-03	1.52E-05	3.26E-01	3.91E-05	1.52E-05	2.01E-05	8.21E-01
2.61E+07	1.63E-02	3.90E-05	1.08E-01	3.33E-05	3.90E-05	6.50E-05	9.08E-01
6.54E+06	6.49E-02	1.00E-04	2.96E-02	2.34E-05	1.00E-04	1.87E-04	9.52E-01
1.64E+06	2.58E-01	2.60E-04	7.60E-03	1.56E-05	2.60E-04	5.24E-04	9.76E-01
4.13E+05	1.03E+00	6.82E-04	1.92E-03	1.03E-05	6.82E-04	1.50E-03	9.88E-01
1.04E+05	4.10E+00	1.85E-03	4.83E-04	7.07E-06	1.85E-03	4.62E-03	9.94E-01
2.61E+04	1.63E+01	5.41E-03	1.21E-04	5.19E-06	5.41E-03	1.52E-02	9.97E-01
6.54E+03	6.49E+01	1.62E-02	3.05E-05	3.90E-06	1.62E-02	2.10E-02	9.99E-01
1.64E+03	2.58E+02	1.89E-02	7.66E-06	1.14E-06	1.89E-02	9.77E-03	9.99E-01
4.13E+02	1.03E+03	9.16E-03	1.92E-06	1.39E-07	9.16E-03	8.35E-03	1.00E+00
1.04E+02	4.10E+03	7.77E-03	4.83E-07	2.97E-08	7.77E-03	1.05E-02	1.00E+00
2.61E+01	1.63E+04	9.49E-03	1.21E-07	9.10E-09	9.49E-03	1.45E-02	1.00E+00
6.54E+00	6.49E+04	1.01E-01	3.05E-08	6.49E+04	1.28E-02	1.28E-02	1.00E+00

Continued on next page

Table 8.6 – continued from previous page

K (m^3 mol^{-1})	k_d (s^{-1})	$p(\log K)$	θ_i	SODF	$c_{T,^iL}$ (mol m^{-3})	$c_{^iL}$ (mol m^{-3})	ξ_i
1.64E+00	2.58E+05	1.35E-01	7.66E-09	2.58E+05	1.70E-02	1.70E-02	1.00E+00
⋮	⋮	⋮	⋮	⋮	⋮	⋮	⋮
6.54E-201	6.49E+205	1.43E-76	3.05E-209	4.48E-280	1.86E-72	1.86E-72	1.00E+00

Table 8.7: Discretized values of CKS for Pb-FA system ($\Delta \log K = 0.3$). The shadow data correspond to the set used for numerical calculation (27 ligands). Parameters: $c_{\mathrm{T,Pb}} = 2.5 \times 10^{-8}$ M; $c_{\mathrm{T,FA}} = 30$ mg L^{-1}; $I = 0.1$ M; pH = 7; $k_{\mathrm{a}} = 4.25 \times 10^{5}$ m^3 mol^{-1} s^{-1} (using $a = 1 \times 10^{-9}$ m in Eqn 8.29); for ξ_i evaluation(Eqn 8.39) $D_{\mathrm{M}} = 8.03 \times 10^{-10}$ m^2 s^{-1} and $D_{\mathrm{M}^i\mathrm{L}} = 2.41 \times 10^{-10}$ m^2 s^{-1}.

K (m^3 mol^{-1})	k_{d} (s^{-1})	$p(\log K)$	θ_i	SODF	$c_{\mathrm{T},^i\mathrm{L}}$ (mol m^{-3})	$c_{^i\mathrm{L}}$ (mol m^{-3})	ξ_i
1.64E+12	2.58E-07	1.74E-07	1.00E+00	1.7401E-07	1.10E-08	1.44E-12	9.41E-04
8.24E+11	5.16E-07	2.76E-07	1.00E+00	2.7642E-07	1.75E-08	4.56E-12	1.87E-03
4.13E+11	1.03E-06	4.40E-07	9.99E-01	4.3933E-07	2.78E-08	1.45E-11	3.73E-03
2.07E+11	2.05E-06	6.99E-07	9.99E-01	6.9851E-07	4.43E-08	4.59E-11	7.41E-03
1.04E+11	4.10E-06	1.11E-06	9.98E-01	1.1107E-06	7.05E-08	1.46E-10	1.46E-02
5.20E+10	8.17E-06	1.77E-06	9.96E-01	1.7653E-06	1.12E-07	4.61E-10	2.86E-02
2.61E+10	1.63E-05	2.82E-06	9.92E-01	2.8017E-06	1.79E-07	1.46E-09	5.43E-02
1.31E+10	3.25E-05	4.50E-06	9.84E-01	4.431E-06	2.85E-07	4.61E-09	9.79E-02
6.54E+09	6.49E-05	7.18E-06	9.68E-01	6.9566E-06	4.55E-07	1.44E-08	1.63E-01
3.28E+09	1.30E-04	1.15E-05	9.39E-01	1.0763E-05	7.26E-07	4.46E-08	2.52E-01
1.64E+09	2.58E-04	1.83E-05	8.85E-01	1.6197E-05	1.16E-06	1.34E-07	3.70E-01
8.24E+08	5.16E-04	2.93E-05	7.93E-01	2.3208E-05	1.85E-06	3.83E-07	5.07E-01
4.13E+08	1.03E-03	4.68E-05	6.58E-01	3.0766E-05	2.96E-06	1.01E-06	6.41E-01
2.07E+08	2.05E-03	7.48E-05	4.91E-01	3.6704E-05	4.73E-06	2.41E-06	7.49E-01
1.04E+08	4.10E-03	1.20E-04	3.26E-01	3.8975E-05	7.57E-06	5.11E-06	8.24E-01
5.20E+07	8.17E-03	1.92E-04	1.95E-01	3.7338E-05	1.21E-05	9.76E-06	8.75E-01
2.61E+07	1.63E-02	3.07E-04	1.08E-01	3.3205E-05	1.94E-05	1.73E-05	9.10E-01
1.31E+07	3.25E-02	4.92E-04	5.73E-02	2.8202E-05	3.11E-05	2.93E-05	9.35E-01
6.54E+06	6.49E-02	7.89E-04	2.96E-02	2.3351E-05	5.00E-05	4.85E-05	9.53E-01

Continued on next page

Table 8.7 – continued from previous page

K (m^3 mol^{-1})	k_d (s^{-1})	$p(\log K)$	θ_i	SODF	$c_{T,^iL}$ (mol m^{-3})	$c_{^iL}$ (mol m^{-3})	ξ_i
3.28E+06	1.30E-01	1.27E-03	1.51E-02	1.9092E-05	8.03E-05	7.91E-05	9.67E-01
1.64E+06	2.58E-01	2.04E-03	7.60E-03	1.553E-05	1.29E-04	1.28E-04	9.77E-01
8.24E+05	5.16E-01	3.30E-03	3.82E-03	1.2629E-05	2.09E-04	2.08E-04	9.83E-01
4.13E+05	1.03E+00	5.37E-03	1.92E-03	1.0303E-05	3.40E-04	3.39E-04	9.88E-01
2.07E+05	2.05E+00	8.79E-03	9.63E-04	8.466E-06	5.56E-04	5.56E-04	9.92E-01
1.04E+05	4.10E+00	1.46E-02	4.83E-04	7.0399E-06	9.23E-04	9.22E-04	9.94E-01
5.20E+04	8.17E+00	2.46E-02	2.42E-04	5.9604E-06	1.56E-03	1.56E-03	9.96E-01
2.61E+04	1.63E+01	4.26E-02	1.21E-04	5.1682E-06	2.70E-03	2.70E-03	9.97E-01
1.31E+04	3.25E+01	7.51E-02	6.08E-05	4.5672E-06	4.75E-03	4.75E-03	9.98E-01
6.54E+03	6.49E+01	1.27E-01	3.05E-05	3.8842E-06	8.07E-03	8.07E-03	9.99E-01
3.28E+03	1.30E+02	1.71E-01	1.53E-05	2.6141E-06	1.08E-02	1.08E-02	9.99E-01
1.64E+03	2.58E+02	1.49E-01	7.66E-06	1.1404E-06	9.43E-03	9.43E-03	9.99E-01
8.24E+02	5.16E+02	1.01E-01	3.84E-06	3.8776E-07	6.40E-03	6.40E-03	1.00E+00
4.13E+02	1.03E+03	7.22E-02	1.92E-06	1.3884E-07	4.57E-03	4.57E-03	1.00E+00
⋮	⋮	⋮	⋮	⋮	⋮	⋮	⋮
1.04E-94	4.10E+99	5.7849E-34	4.83E-103	2.795E-136	3.66E-35	3.66E-35	1.00E+00

Table 8.8: Discretized values of CKS for Pb-FA system ($\Delta \log K = 0.2$). The shadow data correspond to the set used for numerical calculation (40 ligands). Parameters: $c_{\mathrm{T,Pb}} = 2.5 \times 10^{-8}$ M; $c_{\mathrm{T,FA}} = 30$ mg L^{-1}; $I = 0.1$ M; pH = 7; $k_{\mathrm{a}} = 4.25 \times 10^{5}$ m^3 mol^{-1} s^{-1} (using $a = 1 \times 10^{-9}$ m in Eqn 8.29); for ξ_i evaluation(Eqn 8.39) $D_{\mathrm{M}} = 8.03 \times 10^{-10}$ m^2 s^{-1} and $D_{\mathrm{M}^i\mathrm{L}} = 2.41 \times 10^{-10}$ m^2 s^{-1}.

K (m^3 mol^{-1})	k_{d} (s^{-1})	$p(\log K)$	θ_i	SODF	$c_{\mathrm{T},{}^i\mathrm{L}}$ (mol m^{-3})	$c_{{}^i\mathrm{L}}$ (mol m^{-3})	ξ_i
1.64E+12	2.58E-07	1.74E-07	1.00E+00	1.7401E-07	7.35E-09	9.59E-13	9.41E-04
1.04E+12	4.10E-07	2.3694E-07	1.00E+00	2.3689E-07	1.00E-08	2.07E-12	1.49E-03
6.54E+11	6.49E-07	3.2268E-07	1.00E+00	3.2257E-07	1.36E-08	4.47E-12	2.36E-03
4.13E+11	1.03E-06	4.3956E-07	9.99E-01	4.3933E-07	1.86E-08	9.64E-12	3.73E-03
2.61E+11	1.63E-06	5.9895E-07	9.99E-01	5.9846E-07	2.53E-08	2.08E-11	5.90E-03
1.64E+11	2.58E-06	8.1637E-07	9.99E-01	8.153E-07	3.45E-08	4.49E-11	9.31E-03
1.04E+11	4.10E-06	1.113E-06	9.98E-01	1.1107E-06	4.70E-08	9.70E-11	1.47E-02
6.54E+10	6.49E-06	1.5178E-06	9.97E-01	1.5128E-06	6.41E-08	2.09E-10	2.30E-02
4.13E+10	1.03E-05	2.0704E-06	9.95E-01	2.0596E-06	8.74E-08	4.52E-10	3.57E-02
2.61E+10	1.63E-05	2.8248E-06	9.92E-01	2.8017E-06	1.19E-07	9.74E-10	5.48E-02
1.64E+10	2.58E-05	3.855E-06	9.87E-01	3.8053E-06	1.63E-07	2.10E-09	8.24E-02
1.04E+10	4.10E-05	5.2622E-06	9.80E-01	5.1555E-06	2.22E-07	4.50E-09	1.20E-01
6.54E+09	6.49E-05	7.1848E-06	9.68E-01	6.9566E-06	3.03E-07	9.63E-09	1.69E-01
4.13E+09	1.03E-04	9.812E-06	9.51E-01	9.3271E-06	4.14E-07	2.05E-08	2.28E-01
2.61E+09	1.63E-04	1.3403E-05	9.24E-01	1.2383E-05	5.66E-07	4.31E-08	2.98E-01
1.64E+09	2.58E-04	1.8311E-05	8.85E-01	1.6197E-05	7.73E-07	8.93E-08	3.79E-01
1.04E+09	4.10E-04	2.5023E-05	8.29E-01	2.0733E-05	1.06E-06	1.81E-07	4.69E-01
6.54E+08	6.49E-04	3.4203E-05	7.53E-01	2.5755E-05	1.44E-06	3.57E-07	5.60E-01
4.13E+08	1.03E-03	4.6759E-05	6.58E-01	3.0766E-05	1.97E-06	6.75E-07	6.46E-01

Continued on next page

Table 8.8 – continued from previous page

K (m^3 mol^{-1})	k_d (s^{-1})	$p(\log K)$	θ_i	SODF	c_{T,i_L} (mol m^{-3})	c_{i_L} (mol m^{-3})	ξ_i
2.61E+08	1.63E-03	6.3939E-05	5.48E-01	3.5057E-05	2.70E-06	1.22E-06	7.20E-01
1.64E+08	2.58E-03	8.745E-05	4.34E-01	3.7927E-05	3.69E-06	2.09E-06	7.80E-01
1.04E+08	4.10E-03	0.00011963	3.26E-01	3.8975E-05	5.05E-06	3.40E-06	8.27E-01
6.54E+07	6.49E-03	0.0001637	2.34E-01	3.8249E-05	6.91E-06	5.29E-06	8.62E-01
4.13E+07	1.03E-02	0.00022406	1.61E-01	3.6149E-05	9.46E-06	7.93E-06	8.89E-01
2.61E+07	1.63E-02	0.00030677	1.08E-01	3.3205E-05	1.29E-05	1.15E-05	9.11E-01
1.64E+07	2.58E-02	0.00042016	7.11E-02	2.9889E-05	1.77E-05	1.65E-05	9.28E-01
1.04E+07	4.10E-02	0.00057571	4.61E-02	2.6537E-05	2.43E-05	2.32E-05	9.43E-01
6.54E+06	6.49E-02	0.00078925	2.96E-02	2.3351E-05	3.33E-05	3.23E-05	9.54E-01
4.13E+06	1.03E-01	0.00108272	1.89E-02	2.0435E-05	4.57E-05	4.48E-05	9.64E-01
2.61E+06	1.63E-01	0.00148659	1.20E-02	1.7828E-05	6.27E-05	6.20E-05	9.71E-01
1.64E+06	2.58E-01	0.0020434	7.60E-03	1.553E-05	8.62E-05	8.56E-05	9.77E-01
1.04E+06	4.10E-01	0.00281296	4.81E-03	1.3527E-05	1.19E-04	1.18E-04	9.82E-01
6.54E+05	6.49E-01	0.00388002	3.04E-03	1.1794E-05	1.64E-04	1.63E-04	9.86E-01
4.13E+05	1.03E+00	0.00536612	1.92E-03	1.0303E-05	2.26E-04	2.26E-04	9.89E-01
2.61E+05	1.63E+00	0.0074479	1.21E-03	9.0292E-06	3.14E-04	3.14E-04	9.91E-01
1.64E+05	2.58E+00	0.01038656	7.65E-04	7.9485E-06	4.38E-04	4.38E-04	9.93E-01
1.04E+05	4.10E+00	0.01457586	4.83E-04	7.0399E-06	6.15E-04	6.15E-04	9.94E-01
6.54E+04	6.49E+00	0.02062133	3.05E-04	6.2853E-06	8.70E-04	8.70E-04	9.96E-01
4.13E+04	1.03E+01	0.02946796	1.92E-04	5.6677E-06	1.24E-03	1.24E-03	9.97E-01
2.61E+04	1.63E+01	0.04258458	1.21E-04	5.1682E-06	1.80E-03	1.80E-03	9.97E-01
1.64E+04	2.58E+01	0.06211859	7.66E-05	4.757E-06	2.62E-03	2.62E-03	9.98E-01

Continued on next page

Table 8.8 – continued from previous page

K (m^3 mol^{-1})	k_d (s^{-1})	$p(\log K)$	θ_i	SODF	c_{T,i_L} (mol m^{-3})	c_{i_L} (mol m^{-3})	ξ_i
1.04E+04	4.10E+01	0.09047974	4.83E-05	4.3719E-06	3.82E-03	3.82E-03	9.98E-01
6.54E+03	6.49E+01	0.12740151	3.05E-05	3.8842E-06	5.38E-03	5.38E-03	9.99E-01
4.13E+03	1.03E+02	0.16199687	1.92E-05	3.1163E-06	6.84E-03	6.84E-03	9.99E-01
⋮	⋮	⋮	⋮	⋮	⋮	⋮	⋮
2.61E-59	1.63E+64	1.9674E-21	1.21E-67	2.388E-88	8.30E-23	8.30E-23	1.00E+00

References

[1] Ruzic, I. Trace metal complexation at heterogeneous binding sites in aquatic systems. *Marine Chemistry* 53, **1996**: 1 – 15.

[2] Buffle, J. *Complexation Reactions in Aquatic Systems. An Analytical Approach*. Chichester, UK, **1988**.

[3] Benedetti, M., Milne, C., Kinniburgh, D., Vanriemsdijk, W. and Koopal, L. Metal-ion binding to humic substances - Application of the nonideal competitive adsorption model. *Environmental Science and Technology* 29(2), **1995**: 446–457.

[4] Garces, J., Mas, F. and Puy, J. Conditional equilibrium constants in multicomponent heterogeneous adsorption: The conditional affinity spectrum. *Journal of Chemical Physics* 124(4), **2006**: 044710.

[5] Town, R., Duval, J., Buffle, J. and van Leeuwen, H. Chemodynamics of metal complexation by natural soft colloids: Cu(II) binding by humic acid. *Journal of Physical Chemistry A* 116(25, SI), **2012**: 6489–6496.

[6] Puy, J., Galceran, J., Huidobro, C., Companys, E., Samper, N., Garces, J. and Mas, F. Conditional affinity spectra of Pb^{2+} – Humic acid complexation from data obtained with AGNES. *Environmental Science and Technology* 42(24), **2008**: 9289–9295.

[7] Puy, J., Huidobro, C., David, C., Rey-Castro, C., Salvador, J., Companys, E., Garces, J., Galceran, J., Cecilia, J. and Mas, F. Conditional affinity spectra underlying NICA isotherm. *Colloids and Surfaces A: Physicochemical and Engineering Aspects* 347(1-3), **2009**: 156–166.

[8] Rey-Castro, C., Mongin, S., Huidobro, C., David, C., Salvador, J., Garces, J., Galceran, J., Mas, F. and Puy, J. Effective affinity distribution for the binding of metal ions to a generic fulvic acid in natural waters. *Environmental Science and Technology* 43(19), **2009**: 7184–7191.

[9] Milne, C., Kinniburgh, D., van Riemsdijk, W. and Tipping, E. Generic NICA-Donnan model parameters for metal-ion binding by humic substances. *Environmental Science and Technology* 37(5), **2003**: 958–971.

[10] Garces, J., Mas, F., Puy, J., Galceran, J. and Salvador, J. Use of activity coefficients for bound and free sites to describe metal-macromolecule complexation. *Journal of the Chemical Society-Faraday Transactions* 94(18), **1998**: 2783–2794.

[11] van Riemsdijk, W. and Koopal, L. K. *Environmental Particles*. Lewis, Boca Raton, **1992**.

[12] Dewit, J., van Riemsdijk, W. and Koopal, L. Proton binding to humic substances.1. Electrostatic effects. *Environmental Science and Technology* 27(10), **1993**: 2005–2014.

[13] Nederlof, M., Dewit, J., van Rriemsdijk, W. and Koopal, L. Determination of proton affinity distribution for humic subtances. *Environmental Science and Technology* 27(5), **1993**: 846–856.

[14] Nederlof, M., Van Rriemsdijk, W. and Koopal, L. Determination of adsorption affinity distributions - A general framework for methods related to local isotherm approximations. *Journal of Colloid and Interface Science* 135(2), **1990**: 410–426.

[15] Sips, R. On the structure of a catalyst surface. *Journal of Chemical Physics* 16(5), **1948**: 490–495.

[16] Nieszporek, K. and Rudzinski, W. On the enthalpic effects accompanying the mixed-gas adsorption on heterogeneous solid surfaces: A theoretical description based on the integral equation approach. *Colloids and Surfaces A: Physicochemical and Engineering Aspects* 196(1), **2002**: 51–61.

[17] Rusch, U., Borkovec, M., Daicic, J. and van Riemsdijk, W. Interpretation of competitive adsorption isotherms in terms of affinity distributions. *Journal of Colloid and Interface Science* 191(1), **1997**: 247–255.

[18] Moon, H. and Tien, C. Adsorption of gas-mixtures on adsorbents with heterogeneous surfaces. *Chemical Engineering Science* 43(11), **1988**: 2967–2980.

[19] Rudzinski, W., Nieszporek, K., Moon, H. and Rhee, H. On the theoretical origin and applicability of the potential - theory approach to predict mixed - gas adsorption on solid - surfaces from single - gas

adsorption - isotherms. *Chemical Engineering Science* 50(16), **1995**: 2641–2660.

[20] Cernik, M., Borkovec, M. and Westall, J. Affinity distribution description of competitive ion binding to heterogeneous materials. *Langmuir* 12(25), **1996**: 6127–6137.

[21] Garces, J. L., Mas, F. and Puy, J. Application of maximum entropy formalism in the determination of the affinity spectrum in macromolecular complexation. *Environmental Science and Technology* 32(4), **1998**: 539–548.

[22] Koper, G. J. M. and Borkovec, M. Exact affinity distributions for linear polyampholytes and polyelectrolytes. *Journal of Chemical Physics* 104(11), **1996**: 4204–4213.

[23] Kinniburgh, D., van Riemsdijk, W., Koopal, L., Borkovec, M., Benedetti, M. and Avena, M. Ion binding to natural organic matter: Competition, heterogeneity, stoichiometry and thermodynamic consistency. *Colloids and Surfaces A: Physicochemical and Engineering Aspects* 151(1-2), **1999**: 147–166.

[24] Pinheiro, J. P., Mota, A. M. and Benedetti, M. F. Effect of aluminum competition on lead and cadmium binding to humic acids at variable ionic strength. *Environmental Science and Technology* 34(24), **2000**: 5137–5143.

[25] Pinheiro, J. P., Mota, A. M. and Benedetti, M. F. Lead and calcium binding to fulvic acids: Salt effect and competition. *Environmental Science and Technology* 33(19), **1999**: 3398–3404.

[26] Christl, I., Milne, C. J., Kinniburgh, D. G. and Kretzschmar, R. Relating ion binding by fulvic and humic acids to chemical composition and molecular size. 2. Metal binding. *Environmental Science and Technology* 35(12), **2001**: 2512–2517.

[27] Berbel, F., Diaz-Cruz, J., Arino, C., Esteban, M., Mas, F., Garces, J. and Puy, J. Voltammetric analysis of heterogeneity in metal ion binding by humics. *Environmental Science and Technology* 35(6), **2001**: 1097–1102.

[28] Koopal, L., van Rriemsdijk, W., Dewit, J. and Benedetti, M. Analytical isotherm equations for multicomponent adsorption to heterogeneous surfaces. *Journal of Colloid and Interface Science* 166(1), **1994**: 51–60.

[29] Milne, C., Kinniburgh, D., Dewit, J., van Riemsdijk, W. H. and Koopal, L. Analysis of metal-ion binding by a peat humic-acid using a simple electrostatic model. *Journal of Colloid and Interface Science* 175(2), **1995**: 448–460.

[30] Anderson, C. and Record, M. Ion distributions around DNA and other cylindrical polyions - Theoretical descriptions and physical implications. *Annual Review of Biophysics and Biophysical Chemistry* 19, **1990**: 423–465.

[31] Sharp, K. and Honig, B. Electrostatic interactions in macromolecules - Theory and applications. *Annual Review of Biophysics and Biophysical Chemistry* 19, **1990**: 301–332.

[32] Asakura, S., Imai, N. and Oosawa, F. Theory of mechanochemical systems. *Journal of Polymer Science* 13(71), **1954**: 499–510.

[33] Katchalsky, A., Alexandrowicz, Z. and Kedem, O. *Chemical Physics of Ionic Solutions*. John Wiley and Sons, **1996**.

[34] Benedetti, M. F., van Riemsdik, W. H. and Koopal, L. K. Humic substances considered as a heterogeneous Donnan gel phase. *Environmental Science and Technology* 30(6), **1996**: 1805–1813.

[35] Kinniburgh, D. G., Milne, C. J., Benedetti, M. F., Pinheiro, J. P., Filius, J., Koopal, L. K. and VanRiemsdijk, W. H. Metal ion binding by humic acid: Application of the nica-donnan model. *Environmental Science and Technology* 30(5), **1996**: 1687–1698. Times Cited: 186.

[36] Koopal, L., Saito, T., Pinheiro, J. and van Riemsdijk, W. Ion binding to natural organic matter: General considerations and the NICA-Donnan model. *Colloids and Surfaces A: Physicochemical and Engineering Aspects* 265(1-3), **2005**: 40–54.

[37] Eigen, M. and Tamm, K. Fast elementary steps in chemical reaction mechanisms. *Pure and Applied Chemistry* 6, **1963**: 97–115.

[38] van Leeuwen, H. P. and Buffle, J. Chemodynamics of aquatic metal complexes: From small ligands to colloids. *Environmental Science and Technology* 43(19), **2009**: 7175–7183.

[39] van Leeuwen, H., Town, R. and Buffle, J. Impact of ligand protonation on eigen-type metal complexation kinetics in aqueous systems. *Journal of Physical Chemistry A* 111(11), **2007**: 2115–2121.

Conclusions

Understanding bioavailability is key to the assessment of the potential toxicity or nutritional properties of trace metals and their compounds in natural media. With this work, we have attempted to contribute to improve the analytical capability of DGT devices for determining the bioavailability of trace metals in natural waters. The main results obtained are quoted below.

- For complexes that are able to diffuse into the resin disc of a DGT device, the thickness of the resin layer has a huge influence on their lability degree. If the free metal concentration is negligible inside the resin layer, the dissociation of the complexes which penetrate into the resin layer adds to the measured metal and dramatically increases the lability degree. Accordingly, expressions for the lability degree deduced in the context of voltammetric techniques are, in general, inapplicable to the DGT measurements, as they neglect the complex penetration inside the resin layer.

- Experimental results for the Cd-NTA system obtained at different pH and NTA concentrations were consistent with fully labile behaviour. These results were accurately simulated using a dynamic numerical model that included penetration of complexes into the resin layer. On the contrary, when complexes were supposed to be excluded from the resin layer, the simulated accumulations were substantially lower than measured.

- DGT can be expected to measure a greater proportion of the metal in a natural water than previously thought, because most metal complexes can be expected to be labile. Field measurements support this conclusion. In situ measurements of Zn, Cu and Mn by DGT agree well with total filterable concentrations for a wide range of waters. Lower DGT values for Cu and Ni at low concentrations have been attributed to the partial lability of their complexes with humic substances, consistent with the very strong complexes with Cu and the known slow dissociation of Ni complexes. The consistently higher concentrations of Cu in natural waters measured by DGT compared to voltammetry

probably reflects the increased lability associated with the resin layer, rather than simply reflecting a larger dissociation region given by the diffusive layer.

- For ligand excess conditions ($\epsilon K' \gg 1$), we have reported new analytical expressions for the flux and the lability degree of complexes in DGT. The good agreement between experimental DGT measurements on the Cd-NTA system and predictions made using those analytical equations, provides confidence in their use more for predicting metal accumulated by DGT and the associated lability. Further measurements in the presence of other metals and ligands are required to provide more exhaustive validation. This new understanding represents an important step in the direction of quantitative interpretation of in situ DGT measurements in natural waters.

- A particular dynamic feature of the DGT devices stems from the fact that the reaction layer is not only present in the gel domain, but also extends into the resin domain. This special feature was considered in the derivation of lability criteria for DGT (see Eqn 5.13), which were used to understand the large effect of the resin thickness on the lability degree of some complexes. A complex can be almost inert for a thin enough resin layer and become labile when the resin layer is sufficiently thick. Conditions for this behaviour have been reported (see Eqn 5.24).

- The penetration of the complexes into the resin domain has a direct impact on the reaction layer, so that the main contribution to the metal accumulation flux for some partially labile complexes comes from the complex dissociation inside the resin domain. This effect rationalises the low impact of the ligand concentration on the lability degree of a complex in the DGT devices.

- Penetration of complexes influences the transient behaviour of a system. The time to reach steady state were quantified as the time required for the flux of metal bound to the DGT resin layer to be at least 95% of the steady state metal flux (t_{ss}). Systems that have complexes with low lability take longer to reach steady state than those with either inert or labile complexes.

- Donnan effects are relevant to understand the metal accumulations at low ionic strength media especially for partially labile complexes. The main influence of Donnan effects arise from the deprotonated groups of the resin beads. As this charge is negative, the main effect is a exclusion of the negatively charged complexes. No important effects are expected for free metals, since they get bound just at the resin-gel interface.

- A model that considers Donnan potentials derived from the resin charges and the screening of the background electrolyte is here developed under equilibrium conditions for the resin/gel interface. Expressions for metal flux accumulation and lability degree are reported.

- Expressions here reported for the metal flux and lability degree are able to quantitatively reproduce the metal accumulations for Cd, Co and Ni - NTA complexes in the ionic strength range $I = 0.1$, to $I = 100$ mM.

- In a system with one metal and a single ligand, the metal flux measured by a DGT sensor is almost independent of both the constant equilibrium K and the ligand concentration, as indicate by the approximate expression 4.13. Therefore, this suggests that flux measurements by DGT devices in a system with a mixture of ligands, could be few influenced by the mixture effect because of key role of the resin.

- In general, in a system with a mixture of complexes the lability of each complex is influenced by the concentration of the rest complexes present in the solution. However, as in DGT the main contribution to the flux comes from complex dissociation inside the resin (where there is no influence due to the presence of others ligands, because of free metal absence), the mixture effects are lesser than 10% or even smaller if we increase the resin thickness.

- Consequently, the reduced mixture effect in measures with DGT devices, would facilitate the interpretation of experimental data and could help in the understanding of interaction of metal with different ligands.

- Based on the CAS methodology, here we have introduced the *Conditional Kinetic Spectrum* for the description of metal-macromolecular binding in multicomponent systems. Even though here we have used the CKS methodology to study the Pb-FA system, it is important to recall that this methodology can be applied to a wide variety of mixture of competing ion systems.

- Additional to the the inherent interest of the results obtained with the CKS methodology, we highlight its applicability to the description and understanding of metal–humic/fulvic matter interactions.